

Aus dem Biomedizinischen Centrum
Lehrstuhl für Molekularbiologie
der Ludwig-Maximilians-Universität München

Vorstand: Prof. Dr. rer. nat. Peter B. Becker



Dissection of
Nucleosome Positioning and Spacing Mechanisms
in Saccharomyces cerevisiae

Dissertation

zum Erwerb des Doktorgrades der Naturwissenschaften

an der Medizinischen Fakultät

der Ludwig-Maximilians-Universität zu München

vorgelegt von

Ashish Kumar Singh

aus Lucknow, Indien

2020

Mit Genehmigung der Medizinischen Fakultät
der Universität München

Betreuer: Prof. Dr. rer. nat. Peter B. Becker

Zweitgutachter(in): Prof. Dr. rer. nat. Karl-Peter Hopfner

Dekan: Prof. Dr. med. dent. Reinhard Hickel

Tag der mündlichen Prüfung: 15.04.2021



LUDWIG-
MAXIMILIANS-
UNIVERSITÄT
MÜNCHEN

Promotionsbüro
Medizinische Fakultät



Affidavit

SINGH, ASHISH KUMAR

I hereby declare, that the submitted thesis entitled:

Dissection of nucleosome positioning and spacing mechanisms in *Saccharomyces cerevisiae*

is my own work. I have only used the sources indicated and have not made unauthorized use of services of a third party. Where the work of others has been quoted or reproduced, the source is always given.

I further declare that the submitted thesis or parts thereof have not been presented as part of an examination degree to any other university.

Munich, 19.04.2021

Ashish Kumar Singh

PREFACE

The following research article and review originating from this thesis are in revision currently:

Ashish Kumar Singh, Tamas Schauer[†], Lena Pfaller[†], Tobias Straub, Felix Mueller-Planitz. The biogenesis and function of nucleosome arrays. *Nature Communications*, in revision.
[†] co-second authors.

Ashish Kumar Singh, Felix Mueller-Planitz. Nucleosome positioning and spacing: from mechanism to function. *Journal of Molecular Biology*, in revision. (Review)

Published manuscript:

Johanna Ludwigsen, Sabrina Pfennig, **Ashish K Singh**, Christina Schindler, Nadine Harrer, Ignasi Forne, Martin Zacharias, Felix Mueller-Planitz. Concerted regulation of ISWI by an autoinhibitory domain and the H4 N-terminal tail. *eLife* 2017; 6:e21477. DOI: 10.7554/eLife.21477.

Remaining results presented in this thesis will be published in (at least) one additional publication.

TABLE OF CONTENTS

I.	LIST OF ABBREVIATIONS.....	I
II.	ABSTRACT.....	IV
III.	ZUSAMMENFASSUNG.....	VI
IV.	LIST OF FIGURES.....	VIII
1.	INTRODUCTION.....	1
1.1	Concepts: Nucleosome occupancy, positioning, phasing and spacing.....	2
1.2	Factors determining phased regular array formation.....	5
1.2.1	DNA sequence and histone octamer.....	5
1.2.2	Transcription.....	6
1.2.3	ATP-dependent nucleosome remodelers.....	8
1.2.4	Non-histone DNA binding factors.....	10
1.2.5	Histone and DNA modifications.....	11
1.2.6	Histone variants and linker histones.....	12
1.2.7	Statistical positioning and clamping.....	12
1.3	Functions of nucleosome arrays.....	13
1.3.1	Chromatin fiber folding.....	13
1.3.2	Regular arrays may promote long-range interaction.....	14
1.3.3	Regular arrays prevent intragenic cryptic transcription.....	15
1.3.4	Nucleosome spacing in regulating enzyme activity.....	16
1.4	Aims of this thesis.....	16
2.	RESULTS.....	17
2.1	Chapter 1: The biogenesis and function of nucleosome arrays.....	17
2.1.1	Background.....	18
2.1.2	An improved MNase-Seq protocol to map nucleosome position.....	19
2.1.3	High histone density and nucleosome remodelers cooperate to generate regular nucleosome arrays.....	21
2.1.4	Transcription destroys the nucleosome array regularity.....	24
2.1.5	The INO80 remodeler is an <i>in vivo</i> nucleosome spacing factor.....	28
2.1.6	Spacing remodelers generate nucleosome arrays at replication origins.....	32
2.1.7	The Arp8, but not the Nhp10, module regulates NRL in the INO80 spacing remodeler.....	34
2.1.8	INO80 positions the +1-nucleosome in a H2A.Z-independent manner.....	42
2.1.9	The DNA sequence contributes to NRL determination.....	44
2.1.10	Regular nucleosome arrays protect the genome from genotoxic stress.....	47
2.1.11	Spacing remodelers and array regularity modulate Pol II progression.....	50
2.1.12	Discussion (related to this chapter).....	53
2.2	Chapter 2: Functional dissection of the ISW2 nucleosome remodeler.....	58
2.2.1	Background.....	58
2.2.2	Deletion of the N-terminus of Itc1 has no effect on cell growth.....	59
2.2.3	Deletion of the N-terminus of Itc1 leads to enhanced shmoo formation.....	60

2.2.4	Itc1 lacking its N-terminus shows downstream shift in the +1-nucleosome	61
2.2.5	Deletion of the N-terminus of Itc1 leads to global nucleosome re-organization....	63
2.2.6	ISW2 resolves dinucleosomes at specific genes.....	65
2.2.7	ISW2-dependent genome-wide cell-type specific nucleosome architecture.....	66
2.2.8	Interactome of the ISW2 nucleosome remodeler.....	69
2.2.9	ISW2 interacts with RNA <i>in vivo</i>	70
2.2.10	Discussion (related to this chapter)	71
2.3	Chapter 3: Mechanistic dissection of the ISW1 nucleosome remodeler	74
2.3.1	Background.....	74
2.3.2	A galactose-inducible expression library to study ISW1 remodeling.....	75
2.3.3	The N-terminus of Isw1 is important for ISW1 remodeler function <i>in vivo</i>	78
2.3.4	The AutoN motif is dispensable for ISW1 nucleosome spacing <i>in vivo</i>	80
2.3.5	The NegC motif is important for ISW1 function <i>in vivo</i>	81
2.3.6	The Isw1 ATPase domain may be able to slide nucleosomes <i>in vivo</i>	83
2.3.7	The Isw1 ATPase subunit may slide nucleosomes without accessory subunits.....	84
2.3.8	Discussion (related to this chapter)	85
3.	GENERAL DISCUSSION AND OUTLOOK.....	88
3.1	Interplay of transcription and spacing remodelers towards nucleosome organization.....	89
3.2	Spacing mechanism in yeast.....	90
3.3	Mechanistic dissection of ISWI and Chd1 remodelers <i>in vivo</i>	90
3.4	Role of nucleosome spacing in genome 3D-folding.....	91
3.5	Mechanistic dissection of nucleosome organization in higher organisms.....	91
3.6	Single-molecule and single-cell techniques.....	91
4.	MATERIALS AND METHODS.....	93
4.1	Materials.....	93
4.1.1	Yeast and bacterial strains.....	93
4.1.2	Oligonucleotides sequences.....	104
4.1.3	Plasmids.....	109
4.1.4	Enzymes and Kits.....	111
4.1.5	Antibodies.....	111
4.1.6	Sources of chemicals and consumables.....	112
4.1.7	Buffers and solutions.....	114
4.1.8	Yeast media.....	114
4.2	Methods.....	115
4.2.1	Yeast strain generation.....	115
4.2.1.1	Gene deletion or tagging via direct transformation.....	115
4.2.1.2	Yeast tetrad dissection and synthetic lethality test.....	115
4.2.2	Cloning via Gibson assembly.....	116
4.2.3	MNase-Seq.....	116
4.2.3.1	Yeast nuclei preparation.....	116
4.2.3.2	MNase digestion.....	117
4.2.3.3	DNA isolation and MNase-Seq library preparation.....	117
4.2.4	ATAC-Seq	118

4.2.5	NET-Seq.....	118
4.2.6	Immunoprecipitation-Mass Spectrometry.....	120
4.2.7	General methods.....	120
4.2.7.1	Polymerase Chain Reaction.....	120
4.2.7.2	Restriction digestion.....	121
4.2.7.3	Yeast genomic DNA isolation and colony PCR.....	121
4.2.7.4	Plasmid isolation from <i>E. coli</i> and <i>S. cerevisiae</i>	122
4.2.7.5	<i>E. coli</i> transformation.....	122
4.2.7.6	<i>S. cerevisiae</i> transformation.....	122
4.2.7.7	Electrophoretic separation of DNA using agarose gel.....	122
4.2.7.8	SDS-PAGE.....	123
4.2.7.9	Western blot.....	123
4.2.7.10	Growth assay.....	123
4.2.7.11	DNA damage assay.....	124
4.2.7.12	Ectopic recombination assay.....	124
4.2.7.13	Yeast growth conditions.....	125
4.2.7.14	Antibody generation against Isw1 and Isw2 proteins.....	125
4.2.7.15	Yeast GFP live-cell microscopy.....	125
4.2.7.16	<i>In vivo</i> UV-crosslink and TAP-immunoprecipitation.....	125
4.2.8	Bioinformatic methods.....	126
4.2.8.1	Demultiplexing, mapping and coverage vectors.....	126
4.2.8.2	Composite plot and heatmap generation.....	127
4.2.8.3	Nucleosome repeat length and array regularity calculations.....	127
4.2.8.4	ATAC-Seq analysis.....	127
4.2.8.5	NET-Seq analysis.....	128
4.2.8.6	ChIP-Seq analysis.....	128
4.2.8.7	DANPOS +1-nucleosome fuzziness analysis.....	128
4.2.8.8	Statistical positioning simulation.....	129
4.2.8.9	Nucleosome affinity prediction using nuCpos.....	129
4.2.8.10	Published nucleosome positioning sequences score.....	129
4.2.8.11	Published datasets analysis.....	129
4.2.8.12	Correlations of nucleosome array regularity to published datasets...	130
4.2.8.13	Dinucleosome occupancy analysis using bamR.....	130
5.	BIBLIOGRAPHY.....	131
6.	APPENDIX.....	156
6.1	List of genes responding at the +1-nucleosome in the ISW2 remodeler mutants.....	156
6.2	List of genes responding in cell-type specific or ISW2 dependent manner.....	159
6.3	List of proteins identified from ISW2-TAP immunoprecipitation.....	160
6.4	List of plasmids with galactose-inducible promoters.....	167
6.5	List of antibodies generated against Isw1.....	168
7.	ACKNOWLEDGMENTS.....	169

I. LIST OF ABBREVIATIONS

A	Adenine
ABF1	ARS-binding factor one
ACF	ATP-utilizing chromatin assembly and remodeling factor
ACS	ARS1 consensus sequence
AcidicN	Acidic region in the N-terminus of ISWI
Arp	Actin related protein
ARS	Autonomously Replicating Sequence
ATAC	Assay for Transposase-Accessible Chromatin
ATP	Adenosine triphosphate
AutoN	N-terminal autoinhibitory motif in ISWI
bp	base pair(s)
C	Cytosine
Chd1	Chromodomain-helicase-DNA-binding protein one
ChIP	Chromatin immunoprecipitation
CHRAC	Chromatin accessibility Complex
DDT	DNA binding homeobox and different transcription factors
DNA	Deoxyribonucleic Acid
DNase I	Deoxyribonuclease I
dNTP	Deoxyribonucleotide triphosphate
ds	double strand
DTT	Dithiothreitol
<i>E. coli</i>	<i>Escherichia coli</i>
EDTA	Ethylenediaminetetraacetic acid
Fun30	Function Unknown Now
G	Guanine
GRF	General Regulatory Factor
H1	Histone H1
H2A	Histone H2A
H2A.Z	Histone variant H2A.Z
H2B	Histone H2B
H3	Histone H3
H4	Histone H4
HD	Histone depletion
HSA	Helicase/SANT-associated
HP1	Heterochromatin protein one
HSS	HAND-SANT-SLIDE
Ies	Ino Eighty Subunit
Ino80	INOsitol requiring
Ioc	Iswi one complex
IP	Immunoprecipitation

ISWI	Imitation switch
Itc1	Imitation switch two complex
kb	kilobase
kDa	kilodalton
l	liter
ml	milliliter
mM	millimolar
Mat	Mating-type
MMS	Methyl methanesulfonate
MNase	Micrococcal nuclease
MS	Mass spectrometry
N-terminus	Amino-terminus
NET	Nascent elongation transcript
NegC	C-terminal autoinhibitory domain in ISWI
NFR	Nucleosome free region
Nhp10	Non-histone protein ten
NPS	Nucleosome positioning sequence
NRL	Nucleosome repeat length
NTR	N-terminal region
OD	Optical density
ORC	Origin recognition complex
ppHSA	Post-post-helicase-SANT-associated
PAGE	Polyacrylamide gel electrophoresis
PCR	Polymerase chain reaction
PIC	Pre-initiation complex
PMSF	Phenylmethylsulfonyl fluoride
Pol II	RNA polymerase II
PTM	Post translational modification
REB1	RNA polymerase I enhancer binding protein one
RNA	Ribonucleic acid
Rpb	RNA polymerase B
RSC	Remodel the structure of chromatin
RVB	RuvB-like
SANT domain	SWI3, ADA2, N-CoR and TFIIB domain
<i>S. cerevisiae</i>	<i>Saccharomyces cerevisiae</i>
<i>S. pombe</i>	<i>Schizosaccharomyces pombe</i>
SDS	Sodium dodecyl sulfate
Seq	Sequencing
SHL	Superhelical Location
SLIDE	SANT-like domain
Snf2	Sucrose non-fermenting two
Spo11	SPOrulation eleven

SWI/SNF	SWItch/Sucrose non-fermenting
T	Thymine
TAP	Tandem affinity purification
TCA	Trichloroacetic acid
TEV	Tobacco etch virus
TF	Transcription factor
TFA	Trifluoroacetic acid
TKO	Triple knock out
Top2	Topoisomerase two
TSS	Transcription start site
TTS	Transcription termination site
Ume6	Unscheduled meiotic gene expression six
UV	Ultraviolet
v/v	volume/volume
w/v	weight/volume
WAC	WSTF/ACF1/CBP146 domain
WT	Wild type
μl	microliter

II. ABSTRACT

Eukaryotic genomes are packaged as chromatin that contains an ever-repeating succession of nucleosomes like beads-on-a-string. Nucleosomes, together with linker histones, promote packaging of genome into higher-order chromatin structure. Nucleosomes regulate access to the underlying DNA as well as all nuclear processes, including transcription, replication, and double-strand break repair. Defects in these processes lead to genome instability and diseases. Therefore, it is essential to understand the fundamental mechanisms which regulate nucleosome organization.

Nucleosomes attain a stereotypical organization near major regulatory sites in the genome. At these regions, a nucleosome-free region is followed by well-positioned nucleosomes which are phased to a known genomic point, such as transcription start sites in *S. cerevisiae* and at CCCTC-binding sites in higher organisms. The average distance between these nucleosomes, called nucleosome repeat length (NRL), is surprisingly constant and lead to a regular nucleosome array. How this primary structure of chromatin is established is not completely clear. Several nuclear factors, like transcription, ATP-dependent nucleosome remodelers, barrier factors and DNA sequence are known to contribute to this process. Many of these factors act in a redundant manner in the cell. Therefore, it is difficult to understand the mechanism behind regular arrays and the role of individual factor towards it.

In this thesis, we employed the baker's yeast (*S. cerevisiae*) to dissect the mechanism of regular array formation. We made use of a yeast strain lacking bona fide spacing remodelers of the ISWI- and CHD- families to cleanly dissect the role of cellular factors and function of regular arrays. In chapter 2.1, we show that the RNA Pol II-dependent transcription destroys regular nucleosome arrays and overrides effects of the spacing remodelers. By inhibiting transcription in cells, we identify residual spacing activity and assign it to the INO80 nucleosome remodeler. Several orthogonal approaches establish INO80 as a bona fide spacing remodeler *in vivo*. We dissected the spacing mechanism of INO80 and show that the Arp8 module determines NRL by INO80, while the Nhp10 module is dispensable.

We determine the interplay of histone amounts and remodelers to show that the spacing remodelers critically depend on high histone density to establish the WT-like nucleosome array. ISWI and Chd1 remodelers possess "clamping" activity to establish regular arrays, but this activity is rather weak *in vivo*. Finally, we find that the DNA sequence co-determines NRL in most part of the genome and spacing remodelers override DNA sequence-influenced extremely short- or long- NRLs in the genome. We show that the regular arrays established by the spacing remodelers protect the genome from genotoxic stress such as DNA damage and ectopic recombination, and regulate chromatin accessibility in the gene body. We propose

a four-step model for the establishment of regular nucleosome arrays and suggest that it has evolved to regulate as well as to protect the genome.

In chapter 2.2 and 2.3, we investigated the regulatory mechanism of the ISW1 and ISW2 spacing remodelers *in vivo*. We find that ISW2 requires the N-terminus of its accessory subunit Itc1 to position and space nucleosomes. Unlike ISW1 and Chd1, ISW2 resolves dinucleosomes in the gene body. We present a genome-wide cell-type specific nucleosome architecture analysis and dissect the role of ISW2 in this process. Lastly, we investigated the role of individual domains and subunits in the ISW1 remodeler towards nucleosome positioning and spacing. We show that ISW1 depends on the N-terminus and NegC motif within its ATPase subunit for nucleosome positioning. Surprisingly, the AutoN motif is not required for ISW1 spacing mechanism.

Overall, this study establishes a unifying model of the biogenesis of regular nucleosome arrays and provides a basis for future investigation of the interplay of transcription and spacing remodelers towards establishing the primary structure of chromatin.

III. ZUSAMMENFASSUNG

Eukaryotische Genome sind verpackt in Chromatin, das aus einer sich immer wiederholenden Abfolge von Nukleosomen besteht. Zusammen mit den Linker-Histonen unterstützen die Nukleosomen die Faltung des Genoms in übergeordnete Chromatin-Strukturen. Nukleosomen regulieren den Zugang zur DNA. Sie beeinflussen damit viele Prozesse im Zellkern, inklusive Transkription, Replikation und DNA-Doppelstrang Reparatur. Fehler in diesen Prozessen führen zu Genominstabilität und Krankheiten. Infolgedessen ist es essentiell die zugrundeliegenden Mechanismen, welche die Nukleosom-Organisation regulieren, zu verstehen.

Nukleosomen nehmen eine stereotypische Organisation im Genom ein. Insbesondere an regulatorisch wichtigen Stellen befindet sich eine nukleosom-freie Region. Diese Stellen können Transkriptionsstartstellen in *S. cerevisiae* oder CCCTC-Bindungsstellen in höheren Organismen sein. Benachbart dazu befinden sich eine Reihe gut positionierter Nukleosomen. Die durchschnittliche Distanz zwischen diesen Nukleosomen wird als „nucleosome repeat length“ (NRL) bezeichnet. Sie ist überraschend konstant und führt zu einem regelmäßigem ‚*nucleosome array*‘. Jedoch ist nicht bekannt wie diese primäre Chromatinstruktur etabliert wird. Verschiedene Faktoren, wie Transkription, ATP-abhängige Nukleosome ‚Remodeling‘ Enzyme, Barrierefaktoren und DNA Sequenzen sind dafür bekannt, in diesem Prozess mitzuwirken. Viele dieser Faktoren haben redundante oder antagonistische Aktivitäten innerhalb der Zelle. Deshalb ist es schwierig, die Mechanismen Rolle jedes einzelnen Faktors zu verstehen.

In dieser Arbeit verwendeten wir die Bäckerhefe (*Saccharomyces cerevisiae*) um die Mechanismen der Bildung sehr regelmäßig angeordneter Nukleosom-‚Arrays‘ zu analysieren. Wir nutzen dabei einen Hefestamm, dem Nukleosom ‚Remodeling‘ Enzyme der ISWI- und CHD-Familie fehlen, um die Rolle anderer zellulärer Faktoren zu analysieren. In Kapitel 2.1 zeigen wir, dass die von der RNA Polymerase II-abhängige Transkription die Nukleosom ‚Arrays‘ zerstört und damit die Arbeit von ISWI und CHD-‚Remodeling‘ Enzymen entgegenläuft. Durch Hemmung der Transkription konnten wir eine weitere Aktivität identifizieren, die Nukleosomen ‚Remodeler‘ INO80 zuordnen. Wir analysierten den Mechanismus von INO80 und zeigten, dass INO80 das Arp8 Modul nutzt, um eine präferierte NRL einzustellen. Das Nhp10 Modul auf der anderen Seite ist hierfür entbehrlich.

Indem wir die Histonmenge *in vivo* reduzierten, zeigten wir, dass ‚Remodeler‘ eine hohe Histon Dichte benötigen, um ein Nukleosom ‚Array‘ herzustellen. ISWI- und CHD1- ‚Remodeler‘ besitzen sogenannte „clamping“-Aktivitäten, die an dieser Aktivität beteiligt sind. Unsere Daten zeigen jedoch, dass diese Aktivität sehr schwach ist *in vivo*. Schließlich haben

wir herausgefunden, dass die DNA Sequenzen die NRL teilweise mitfestlegen, und dass ‚Remodeler‘ diese Information jedoch übergehen können. Wir zeigen, dass durch Nukleosom ‚Arrays‘ nicht regelmäßig angeordneten Nukleosomen die Zellen vor genotoxischem Stress wie DNA Schäden, homologe Rekombination und Transposition beschützen. Wir schlagen ein vier-Stufen Modell für die Errichtung von Nukleosom ‚Arrays‘ vor und legen nahe, dass ‚Arrays‘ nicht nur für die Regulierung sondern auch für den Schutz des Genoms evolvierten.

In Kapitel 2 und 3 untersuchten wir die Remodeler ISW1 und ISW2, um deren Regulierung *in vivo* zu verstehen. Wir haben herausgefunden, dass ISW2 den N-Terminus seiner zusätzlichen Untereinheit Itc1 benötigt, um Nukleosomen zu positionieren. Im Gegensatz zu ISW1 und CHD1 löst ISW2 Dinukleosomen auf. Wir präsentieren eine genomweite Analyse der Nukleosomenarchitektur in zwei Zelltypen und analysierten die Rolle von ISW2 in der Etablierung der Zelltypen. Zuletzt untersuchten wir die Rolle der individuellen Domänen und Untereinheiten des ISW1 ‚Remodeler‘. Wir zeigen, dass der ISW1 Remodeler seinen N-Terminus und das NegC Motiv für seine Aktivität benötigt. Überraschenderweise ist das AutoN Motiv nicht nötig für die regelmäßige Anordnung von Nukleosomen durch ISW1.

Diese Studie etabliert ein vereinheitlichtes Modell für die Biogenese von Nukleosom ‚Arrays‘ und bildet die Grundlage für zukünftige Untersuchungen des Zusammenspiels von Transkription und Remodeling Enzymen.

IV. LIST OF FIGURES

1.1	Nucleosome positioning and occupancy concepts.....	3
1.2	Nucleosome phasing repeat length and array regularity concepts.....	4
1.3	Phased regular arrays in yeast.....	5
1.4	Domain organization of the ATPase subunits of four families of nucleosome remodelers.....	8
1.5	Functions of regular nucleosome arrays.....	15
2.1	An improved MNase-Seq protocol to map nucleosomes.....	20
2.2	The improved MNase-Seq protocol provides highly consistent nucleosome maps....	21
2.3	Galactose-inducible system to deplete histones in <i>S. cerevisiae</i>	23
2.4	ISWI and Chd1 remodelers require high histone density to generate WT-like nucleosome arrays.....	24
2.5	Transcription destroys the nucleosome landscape.....	25
2.6	Pol II depletion increases NRL and array regularity in WT cells.....	27
2.7	INO80 is a nucleosome spacing factor <i>in vivo</i>	29
2.8	INO80 contributes to NRL and array regularity in TKO cells.....	30
2.9	INO80 contributes to NRL and array regularity in WT and Pol II depleted cells.....	31
2.10	Spacing remodelers generate nucleosome arrays at replication origins.....	33
2.11	The Nhp10 module in the INO80 remodeler has a negligible role in nucleosome organization <i>in vivo</i>	35
2.12	The N-terminus of the Ino80 ATPase has a negligible role in nucleosome organization <i>in vivo</i>	37
2.13	The Arp8 module determines NRL in the INO80 complex.....	38
2.14	The les6 subunit has an essential role in INO80 dependent nucleosome organization and cell growth.....	40
2.15	The les2 subunit in the INO80 complex is dispensable for cell growth and array regularity.....	41
2.16	INO80 positions the +1-nucleosome independent of the histone variant H2A.Z.....	43
2.17	The DNA sequence contributes to NRL determination catalyzed by spacing remodelers.....	45
2.18	Nucleosome remodelers override DNA sequence influenced NRL.....	46
2.19	Regular nucleosome arrays protect the genome from DNA damage and ectopic recombination.....	49
2.20	Regular nucleosome arrays protect the genome from transposon integration and regulate chromatin accessibility.....	50
2.21	Nucleosome arrays modulate transcription elongation and prevent cryptic TSSs.....	52
2.22	Cells lacking the N-terminus of Itc1 show no growth defect, in conflict with published result.....	60
2.23	Loss of the N-terminus of Itc1 enhances aberrant shmoo-like morphology compared to <i>isw2Δ</i> and <i>itc1Δ</i> cells.....	61

2.24	The ISW2 remodeler lacking the N-terminus of Itc1 is defective in the +1- nucleosome positioning.....	62
2.25	ISW2 remodeler lacking the N-terminus of Itc1 shows similar +1-shift at most genes..	63
2.26	The ISW2 remodeler lacking the N-terminus of Itc1 is defective in nucleosome spacing.....	64
2.27	The ISW2 remodeler resolves dinucleosomes in the gene body of specific genes.....	65
2.28	The ISW2 remodeler contributes to array regularity in the gene body of specific genes.....	68
2.29	Gene Ontology (GO) analysis of the ISW2 interactome.....	70
2.30	ISW2 complex interacts with RNA <i>in vivo</i>	71
2.31	An inducible expression library to modulate Isw1 levels <i>in vivo</i>	76
2.32	Nucleosome array formation by ectopically expressed Isw1 under a promoter library.....	77
2.33	Comparison of NRL and array regularity distributions for cells expressing Isw1 ATPase under a promoter library.....	78
2.34	The N-terminus of Isw1 is required for the ISW1 remodeler function.....	79
2.35	The AutoN mutant ISW1 establishes more regular arrays than the WT ISW1 remodeler.....	81
2.36	The NegC motif is required for ISW1 function <i>in vivo</i>	82
2.37	The Isw1 ATPase domain may slide nucleosomes <i>in vivo</i>	83
2.38	The Isw1 ATPase can slide nucleosomes without Ioc subunits <i>in vivo</i>	85
3.1	A modified four step model for generation of phased regular arrays.....	89

1. INTRODUCTION

The genome of eukaryotic cells is packaged into chromatin via a hierarchical nature of folding ranging from single nucleosomes to compact mitotic chromosomes. At the heart of eukaryotic genome organization is the nucleosome which affects most processes occurring on the DNA. Thus, it is important to understand how cells regulate the organization of chromatin at the nucleosome level.

In this introduction, I will focus on the mechanisms regulating the primary structure of chromatin, specifically nucleosome positioning, phasing and spacing which collectively leads to a regular chromatin organization known as nucleosome arrays. I will describe the current understanding of cis- and trans- factors which contribute to the promoter-associated regular nucleosome arrays in the baker's yeast and arrays outside of the promoter region in yeast and higher eukaryotes. In the end, I will discuss the functional relevance of nucleosome arrays and provide examples of how nucleosome spacing and regular arrays may contribute to various cellular functions.

The following text forms the basis of a review article to be published in the special issue on "Multiscale chromatin organization in space and time" in the Journal of Molecular Biology.

The contribution of the co-authors is as follows:

Felix Mueller-Planitz helped during conceptualization of this text and provided comments.

The genome of most eukaryotes is coated with the fundamental unit of chromatin called nucleosomes. The nucleosome consists of a histone octamer composed of two copies of the canonical histones (H2A, H2B, H3 and H4) and 145-147 bp of DNA wrapped around the histone octamer (Luger et al., 1997). Nucleosomes are connected with the linker DNA, whose length can vary within a single cell, between cell types and diverse organisms (Berkowitz and Riggs, 1981; Pearson et al., 1984). Nucleosomes, together with linker histones, are folded and compacted into higher-order chromatin structures *in vivo* (Fyodorov et al., 2018).

Nucleosomes are known to mediate genome regulation via multiple mechanisms. Nucleosomes physically occlude transcription factors from their binding motifs and, thereby inhibit transcription. They may also potentiate transcription and chromatin opening by site-specific exposure of protein binding motifs (Kornberg and Lorch, 2020; Michael et al., 2020; Nagai et al., 2017). Histones can be post-translationally modified or exchanged with histone variants, like H3.3 and H2A.Z. This dynamic nature of nucleosomes regulates both binding and activity of the chromatin factors (Lawrence et al., 2016). Histones are also mutated in several tumors where they affect the function of chromatin enzymes, thus altering chromatin structure (Nacev et al., 2019). Therefore, it is essential to understand the fundamental mechanisms that govern nucleosome organization and how it affects cellular functions.

At the primary level, chromatin is organized as ever repeating and equally spaced beads-on-a-string structure, called nucleosome arrays (Baldi et al., 2020). In yeast and higher organisms, these nucleosome arrays are mostly aligned relative to a fixed point in the genome. Below, I will discuss the mechanisms determining this primary structure of chromatin, with special emphasis on nucleosome spacing and arrays. I will then summarize our current understanding of the possible functions of regularly spaced nucleosome arrays.

1.1 Concepts: Nucleosome occupancy, positioning, phasing and spacing

Nucleosome organization is generally described for measurements performed on cell population using techniques like MNase-Seq and ATAC-Seq (Buenrostro et al., 2013; Yuan et al., 2005). Recent advancements have provided single-cell and single-molecule nucleosome maps (Baldi et al., 2018b; Lai et al., 2018; Shipony et al., 2020; Stergachis et al., 2020; Wang et al., 2019b). I will, thus, introduce the basic concepts in nucleosome organization from the perspective of a single cell and of a cell population.

Nucleosome positioning is generally referred to as the translational position of the nucleosome along a DNA sequence. It is a property of the cell population and often represented by the central base pair that coincides with the nucleosome dyad. If a nucleosome occupies the same base pair in all cells in a population, it is described as a perfectly positioned nucleosome. On the other hand, a non-positioned nucleosome will occur at all possible genomic positions with equal frequency in a cell population (Struhl and Segal, 2013). In reality, nucleosome positions are a continuum between these two extreme scenarios and often described as a well-positioned or a fuzzy nucleosome (Figure 1.1A). Lower eukaryotes like yeast tend to have most nucleosomes well-positioned while higher eukaryotes have more fuzzy nucleosomes (Valouev et al., 2011; Yuan et al., 2005).

Nucleosome position can also be described as the orientation of DNA relative to the histone octamer, termed as rotational positioning. Genomic DNA sequence has a distinctive ~10 bp periodicity of AA/TT/AT or GC dinucleotides which are preferred in the minor or major groove of the nucleosome, respectively (Satchwell et al., 1986). This helical periodicity enhances positioning of the nucleosome, as exemplified by the synthetic Widom 601 sequence known to harbor high helical periodicity (Lowary and Widom, 1998). *In vivo*, nucleosomes which are translationally shifted by ~10 bp have the same rotational positioning (Brogaard et al., 2012; Chereji et al., 2018; Moyle-Heyrman et al., 2013; Voong et al., 2016).

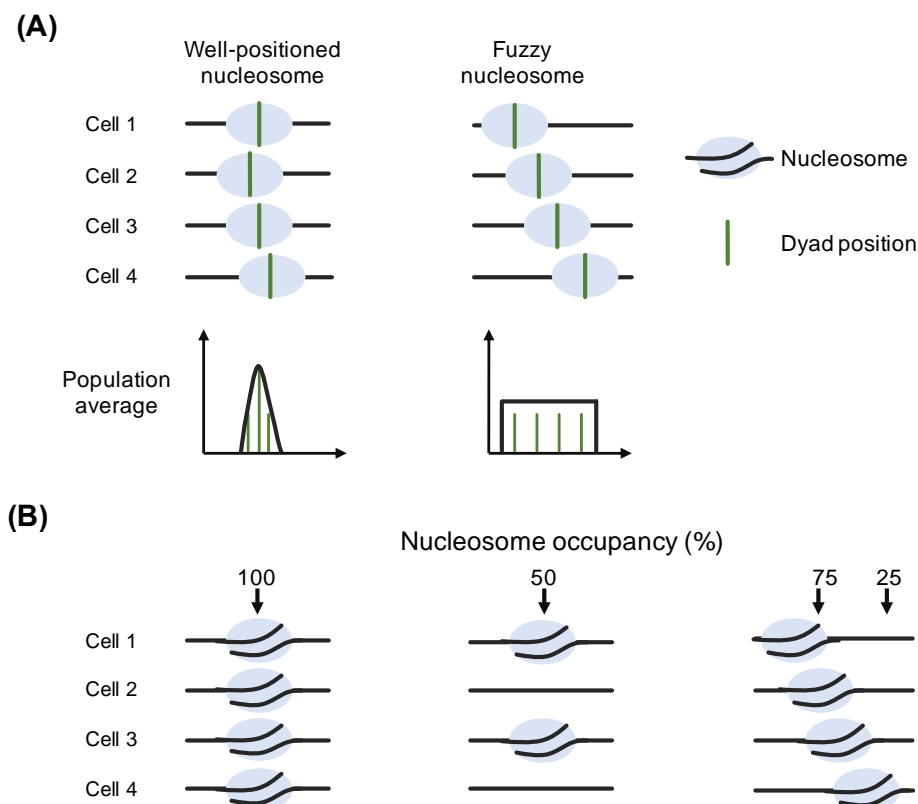


Figure 1.1. Nucleosome positioning and occupancy concepts. (A) The precise position of the nucleosome core particle in the cell population with respect to the DNA sequence is described as nucleosome positioning. When nucleosomes occupy similar position in all cells, it is considered a well-positioned nucleosome. On the other hand, a completely fuzzy nucleosome will occupy all possible genomic locations with equal frequency in cells. **(B)** Nucleosome occupancy is defined as how often a base pair is occupied by any nucleosome in the cell population. (Singh and Mueller-Planitz, unpublished).

Another metric that describes nucleosome organization is occupancy. In a cell, a base pair is either occupied or not by a nucleosome. For a perfectly positioned nucleosome in the genome, it is the fraction of cells which have a nucleosome at the given DNA sequence. Since nucleosomes are never perfectly positioned, nucleosome occupancy is generally described as “the probability for a given base pair to be part of any nucleosome core” (Lieleg et al., 2015b) in a cell population (Figure 1.1B). With the advent of single-molecule techniques, nucleosome occupancy can now also be measured for a gene or a stretch of DNA molecule.

This gene-averaged metric recently revealed largely uniform occupancy (~90%) for known nucleosome positions in the yeast genome (Oberbeckmann et al., 2019).

In cells, the nucleosome core is followed by free linker DNA. The distance between two adjacent nucleosomes is defined as linker length (edge-to-edge distance) or nucleosome spacing (dyad-to-dyad distance) (Lieleg et al., 2015b). Linker length is sometimes also used to describe the length of free DNA on a mononucleosome DNA *in vitro*. To describe an array of nucleosomes, nucleosome repeat length (NRL) and array regularity terms are employed. Both NRL and array regularity measurements require at least three or four nucleosomes and are, in principle, a property a single chromatin fiber in a cell. Due to lack of single-molecule and single-cell techniques in the past, both measurements are performed on the nucleosome signal derived from the cell population. Regardless, when adjacent nucleosomes have similar linker lengths between them, they are considered to have high array regularity and one can confidently measure the average NRL in these arrays. Nucleosome arrays can have high array regularity regardless of the exact NRL. Conversely, arrays with a given NRL can have high or low array regularity. When the linker length between adjacent nucleosomes differ dramatically, array is considered irregular and has an undefined NRL (Figure 1.2).

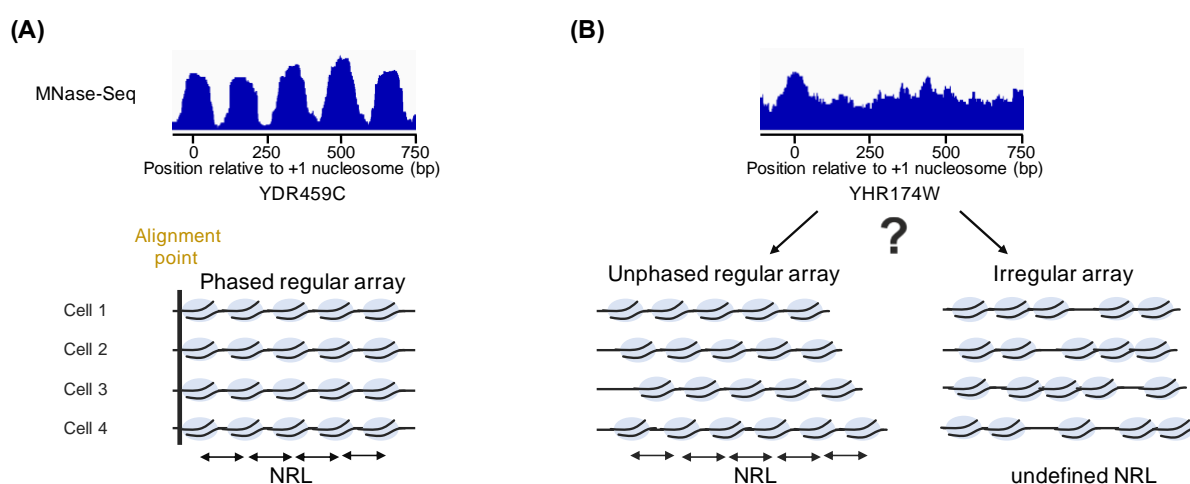


Figure 1.2. Nucleosome phasing, repeat length and array regularity concepts. (A) Phasing is defined for a nucleosome array relative to an alignment point in the genome, for example transcription start sites and CTCF binding sites. When nucleosomes in an array occupy similar positions in the cell population, they are known as phased array. When nucleosomes in a phased array have similar linker lengths between nucleosomes, they are called phased regular array. The average distance between these nucleosomes is called nucleosome repeat length (NRL). (B) Few genes in *S. cerevisiae* have no defined nucleosome signal in the gene body and their promoter region is covered with nucleosomes. These genes can possess either unphased but regular arrays (right) or have irregular arrays with no defined NRL (left). Nucleosome dyads derived from MNase-Seq experiment in WT cells are extended by 100 bp to show nucleosome footprint. (Singh and Mueller-Planitz, unpublished).

Regular nucleosome arrays are usually aligned relative to a fixed point in the genome, resulting in nucleosome phasing. Phasing is a property of nucleosomes in a cell population and found at known alignment points in the genome, like transcription start sites or CCCTC-binding factor (CTCF) sites. Phasing arises when nucleosomes are similarly positioned across a cell population. These nucleosomes can have high or low array regularity. Below, I define

phased nucleosomes which have high array regularity as “phased regular arrays” (Figures 1.2 and 1.3). These phased regular arrays constitute the dominant nucleosome organization in yeast (Figure 1.3) and at several sequence-specific factor binding sites in higher organisms (Baldi et al., 2018a; Wang et al., 2012; Yuan et al., 2005).

1.2 Factors determining phased regular array formation

Several factors are known to contribute towards establishing phased regular arrays *in vivo* (Figure 1.3). I will discuss the contributions of known factors, including transcription, nucleosome remodelers, DNA sequence, barrier factors and histone amounts in the context of promoter regions where these mechanisms are best understood. I will also highlight the interplay among these factors towards determining nucleosome organization. Lastly, I discuss formation of regular arrays at regions other than promoters in the genome.

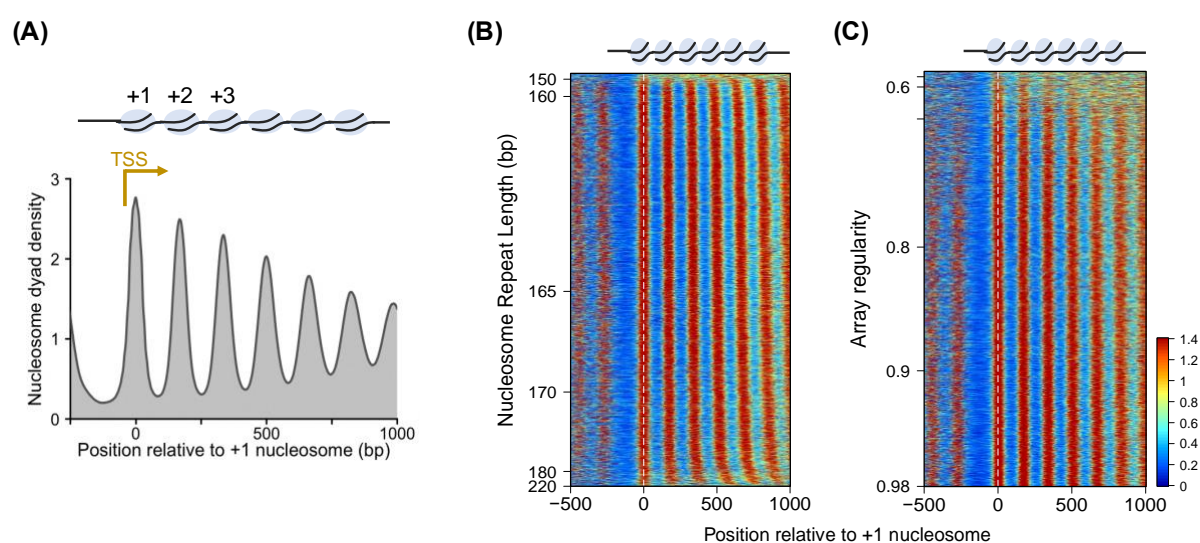


Figure 1.3. Phased regular arrays in yeast. (A) Nucleosomes are aligned relative to transcription start site (TSS) in the *S. cerevisiae* genome. Nucleosome organization is often represented composite plots showing average nucleosome dyad signal from all genes in a cell and of all cells in the population. Nucleosomes are labelled as +1, +2, +3 in the gene body. (B, C) Heatmaps are employed to show nucleosome organization in individual genes where genes are sorted by a defined measure, like NRL or array regularity. Most genes in the *S. cerevisiae* genome attain NRL between 160 and 180 bp. Nucleosome array regularity is a measure of how consistently nucleosomes are equally spaced in an array. As shown in (C), nucleosome arrays have varying degree of array regularity. NRL and array regularity is determined by cross-correlating MNase-Seq signal in each gene with an ideal Gaussian pattern (Ocampo et al., 2016), (Singh and Mueller-Planitz, unpublished).

1.2.1 DNA sequence and histone octamer

The histone octamer is bound by 147 bp DNA which requires energetically unfavorable bending of DNA. This bending energy is compensated by multiple ionic and hydrogen bonds formed between histones and DNA in the nucleosome. The ~10 bp helical periodicity of certain dinucleotides favor bending of the DNA and support nucleosome formation and stability (Satchwell et al., 1986). Dinucleotides, like AA/TT/TA, are favored in the minor groove of DNA when facing the histone octamer. Other dinucleotides, like CC/GG/GC, are preferred in the

major groove of DNA when towards the histone octamer (Drew and Travers, 1985). These dinucleotide periodicities are found in multiple organisms including archaea, yeast, *Drosophila* and mammals, suggesting a conserved role across species (Brogaard et al., 2012; Herzel et al., 1998; Ioshikhes et al., 1996; Johnson et al., 2006; Mavrigh et al., 2008b; Voong et al., 2016; Wedel et al., 2017). Indeed, increasing AA/TT/AA periodicity stabilizes nucleosomes *in vivo* and decreases gene expression (Small et al., 2014).

In contrast to the nucleosome favoring dinucleotides, stretches of poly(dA:dT) and poly(dG:dC) sequences are intrinsically stiff and inhibit nucleosome formation *in vitro* and *in vivo* (Iyer and Struhl, 1995; Rhodes, 1979; Simpson and Kunzler, 1979). These sequences are particularly enriched at the nucleosome-free regions (NFRs) where they contribute to nucleosome depletion (Sekinger et al., 2005; Tsankov et al., 2011; Yuan et al., 2005). Importantly, the poly(dA:dT) sequences are not the only determinants of nucleosome-free regions as the salt gradient dialyzed chromatin have less pronounced nucleosome depletion than the cellular chromatin (Zhang et al., 2011). Indeed, nucleosome remodelers enhance nucleosome depletion at the NFRs, likely by destabilizing or evicting “fragile” nucleosomes formed over these elements (Krietenstein et al., 2016; Kubik et al., 2015).

On a mechanistic level, DNA sequence can influence nucleosome remodeling activity of most families (Rippe et al., 2007). For example, poly(dA:dT) tracts and GC rich motifs stimulate RSC activity (Krietenstein et al., 2016; Kubik et al., 2018; Lorch et al., 2014), DNA sequence at SHL2 affects sliding by Chd1 (Winger and Bowman, 2017) and G/C runs stimulate H2A.Z deposition by SWR1 (Sun et al., 2020). DNA sequence/shape features near promoters also direct nucleosome positioning by the INO80 remodeler (Krietenstein et al., 2016). DNA sequence, especially dinucleotide periodicity, help determine the local position of nucleosomes remodeled by ACF (Partensky and Narlikar, 2009).

Histone octamer: As discussed above, the role of DNA sequence in nucleosome organization is extensively studied. On the other hand, how histone identity influences nucleosome organization is less well understood. A recent study provided insights into this question using a humanized yeast generated by replacing the yeast histones with the human histones. Humanized yeasts show higher nucleosome occupancy, delayed chromatin remodeling and lower gene expression due to less accessible NFRs (Truong and Boeke, 2017). This suggests that the histone octamer has a role in nucleosome organization, and chromatin factors may have evolved in response to fine changes in the histone sequence and nucleosome structure. Consistent with this notion, among the most diverged histones of disease-related organisms, like *Plasmodium* and *Leishmania*, show lower nucleosome stability and varied DNA sequence preference than nucleosomes from human and other model eukaryotes (Dacher et al., 2019; Silberhorn et al., 2016). Mutations in several histone octamer epitopes are found in cancer which affects nucleosome structure and stability. Mutations in the H2A-H2B acidic patch may even diminish nucleosome sliding and chromatin compaction (Arimura et al., 2018; Dao et al., 2019; Nacev et al., 2019).

1.2.2 Transcription

Transcription activity of the gene correlates with the nucleosome organization at the promoter region and in the gene body. Actively transcribed genes show a stereotypical organization in the form of a nucleosome-free region at the promoter, well-positioned +1-nucleosome and phased regular array in the gene body. On the other hand, inactive genes have no clear NFR as promoter regions are mostly covered with nucleosomes. These arrays can also be regular but are not phased relative to a genomic location. Due to lack of phasing in these genes, ensemble measurements initially revealed irregular arrays, which were recently resolved at the level of a chromatin fiber by Array-Seq, single-molecule and single-cell methods (Baldi et al., 2018b; Lai et al., 2018; Wang et al., 2019b).

Using YAC (yeast artificial chromosome) transfer experiments in diverged yeasts, it was proposed that the transcription machinery establishes promoter architecture, +1 positioning and phased regular array formation, possibly in conjunction with the nucleosome remodelers and histone chaperones (Hughes et al., 2012). Basal transcription factors, in co-operation with the pre-initiation complex, may help establish the precise position of the +1-nucleosome (Struhl and Segal, 2013; Zhang et al., 2009). Transcription elongation is suggested to play a role in establishing regular arrays behind the replication fork (Vasseur et al., 2016).

Interestingly, the NFR, +1-nucleosome position and regular nucleosome arrays can be reconstituted to a decent extent in the absence of transcription, suggesting transcription is not an absolute requirement for nucleosome organization (Krietenstein et al., 2016; Zhang et al., 2011). In accord with this, nucleosome arrays are generated independently of Pol II binding and transcription during genome activation of Zebrafish (Zhang et al., 2014). It has also been argued that the half time of genic transcription is longer than the re-establishment time of nucleosome positioning behind the replication fork, suggesting that the nucleosome organization kinetics and establishment is independent of transcription (Fennessy and Owen-Hughes, 2016). Taken together, the importance of transcription towards regular nucleosome arrays formation is unclear.

In *S. cerevisiae*, highly transcribed genes are known to possess less regular arrays than the rest of the genome. This suggests that transcription may destroy regular arrays. Induction of gene expression of certain genes under stress conditions is also shown to decrease array regularity (Cole et al., 2011; Cui et al., 2012). The array destroying activity of RNA Pol II may also be present in higher eukaryotes. In *Drosophila*, the higher the transcription strength of genes, the lower the array regularity (Baldi et al., 2018b; Gilchrist et al., 2010). Transcription is also shown to be important for re-establishment of chromatin accessibility behind the replication fork which may arise from its disrupting activity (Stewart-Morgan et al., 2019).

Lastly, transcription can also modulate NRL in the nucleosome array. Transcribed genes tend to have shorter NRL than genomic average and silent genes possess longer NRL. Similarly, active cell lines have, on average, shorter NRL than dormant cells (Baldi et al., 2018b; De Ambrosis et al., 1987; Gottschling et al., 1983; Ocampo et al., 2016; Valouev et al., 2011). In line with transcription affecting NRL in the genome, Pol II depletion in *S. cerevisiae* leads to longer NRL. This suggests that the act of transcription decreases NRL, likely via a retrograde

movement of nucleosomes during Pol II passage through the DNA (Tramantano et al., 2016; Weiner et al., 2010).

1.2.3 ATP-dependent nucleosome remodelers

The nucleosome remodelers play an essential role in nucleosome organization. They largely belong to four families as classified by their ATPase subunit: SWI/SNF, ISWI, CHD and INO80 (Figure 1.4) (Flaus et al., 2006). These remodelers can perform varied activities including nucleosome sliding, spacing, eviction and switching canonical histones with histone variants. Despite these varied activities, all remodelers contain a central ATPase motor which performs many fundamental aspects of nucleosome remodeling (Clapier and Cairns, 2012; Liu et al., 2015; McKnight et al., 2011; Mueller-Planitz et al., 2013b). Together with the central ATPase module, remodelers contain several domains and accessory subunits which may regulate the ATPase domain and, thus, help determine the outcome of each remodeler family (Figure 1.4) (Clapier et al., 2017; Mueller-Planitz et al., 2013a).

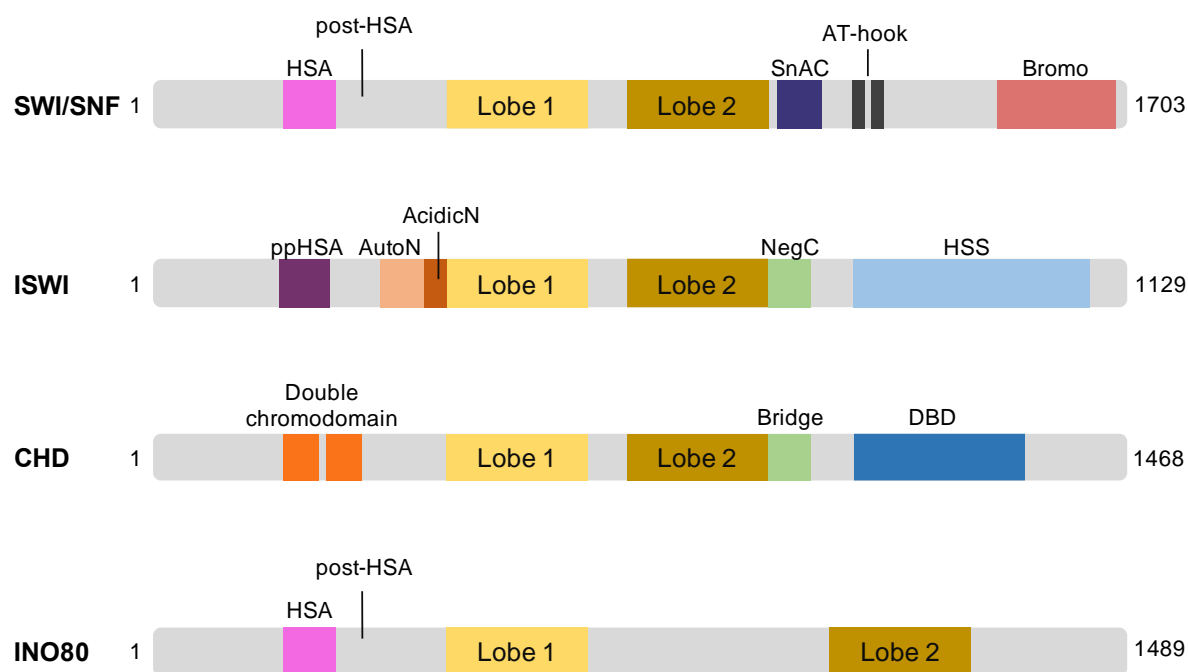


Figure 1.4: Domain organization of the ATPase subunits of four families of nucleosome remodelers. The ATPase subunit of all remodelers families possess two RecA-like lobes, called Lobe 1 and Lobe 2. Two lobes are separated by a small or large insertion (as in INO80 family). Additional motifs and domains in each family are highlighted. Figure is adapted from (Clapier et al., 2017). Numbers indicate total number of amino acids in Snf2, Isw1, Chd1 and Ino80 ATPase subunits from *S. cerevisiae*.

In *S. cerevisiae*, the SWI/SNF family is represented by the SWI/SNF and RSC remodelers. They are mostly recruited to promoter region where they slide nucleosomes away from the promoter region or even evict nucleosomes (Kubik et al., 2019). Consistently, depletion of RSC is known to shift the +1-nucleosome and the phased regular array towards the NFR in a genome-wide manner. The +1 shift occludes the TATA-box binding protein (TBP) region in

the promoter, thus inhibiting gene expression (Ganguli et al., 2014; Kubik et al., 2018). RSC is activated by GC rich motif and dA:dT tracts present in the yeast promoters and slide nucleosomes in a directional manner (Krietenstein et al., 2016; Kubik et al., 2015; Kubik et al., 2018; Lorch et al., 2014). The mechanistic basis of RSC activation by these sequences, and how RSC couples sequence readout to nucleosome sliding and/or eviction is not clear. In contrast to RSC, the SWI/SNF remodeler works majorly at highly expressed and stress-responsive genes (Rawal et al., 2018).

The ISW1a, ISW1b, ISW2 and Chd1 remodelers represent the ISWI- and CHD- families in *S. cerevisiae*. Except for ISW1b, all other ISWI and Chd1 remodelers slide nucleosomes to the center of DNA (Stockdale et al., 2006). This nucleosome centering activity is considered a hallmark of nucleosome spacing activity. *In vitro* reconstitution studies showed that ISW1a, ISW2 and Chd1 can generate regular arrays when incubated with salt gradient dialyzed chromatin (Krietenstein et al., 2016; Vary et al., 2003). Consistently, deletion of *ISW1*, *ISW2* and *CHD1* drastically decreases regular nucleosome arrays in the gene body (Gkikopoulos et al., 2011; Ocampo et al., 2016). ISWI- and Chd1- families of remodelers are also required for *in vitro* chromatin assembly where they catalyze regular array formation (Ito et al., 1997; Lusser et al., 2005). In line with this, *S. cerevisiae* lacking these remodelers have longer NRL and less regular arrays on the newly replicated DNA, suggesting faulty nucleosome assembly (Vasseur et al., 2016; Yadav and Whitehouse, 2016).

Recent genomic studies have investigated the role of ISWI- and CHD- remodelers in higher organisms. Extracts from *Drosophila* embryos lacking Acf1, a signature subunit of the ACF complex, generate less regular nucleosome arrays during *in vitro* chromatin assembly. These mutant embryos also have decreased levels of regular arrays than the WT embryos *in vivo* (Fyodorov et al., 2004; Scacchetti et al., 2018). In line with this, SNF2H remodeler, a homologue of ISWI in higher organisms, is required for nucleosome positioning and spacing in mouse embryonic stem (ES) cells (Barisic et al., 2019; Wiechens et al., 2016). Furthermore, loss of ISWI remodeler decreases the NRL in yeast and *Drosophila* (Baldi et al., 2018a; Ocampo et al., 2016). On the other hand, its loss in mouse ES cells increases the NRL (Barisic et al., 2019). In contrast to yeast, CHD- family of remodelers do not have a significant contribution in higher organisms (Skene et al., 2014; Wiechens et al., 2016). Thus, different species may use ISWI- and CHD- remodelers distinctly.

Lastly, the INO80/SWR1 family of remodelers are majorly known for regulating H2A.Z dynamics. SWR1 exchanges H2A with H2A.Z, while INO80 catalyzes the reverse reaction (Brahma et al., 2017; Mizuguchi et al., 2004; Papamichos-Chronakis et al., 2011). Besides, INO80 remodeler can position the +1-nucleosome and space tri-nucleosomes *in vitro* (Krietenstein et al., 2016; Udugama et al., 2011). INO80 also generates longer NRL than ISWI and Chd1 remodelers during *in vitro* chromatin assembly (Azmi et al., 2017). Cells lacking INO80 show decreased NRL, suggesting INO80 contributes to longer repeat length *in vivo* (van Bakel et al., 2013; Yen et al., 2012).

How spacing remodelers of three families space nucleosomes is still unclear. These remodelers take cues from the available linker DNA to establish regular arrays. Two

mechanisms, namely allosteric and protein ruler, are proposed to explain the spacing mechanism of remodelers. In the allosteric model, nucleosome remodelers sense the linker length and preferentially slide nucleosomes towards the longer linker (Yang et al., 2006). The protein ruler model suggests that the remodeler simultaneously contacts two neighboring nucleosomes, and thereby establishes similar linker length between nucleosomes (Lieleg et al., 2015a; Yamada et al., 2011).

Several epitopes in the histone octamer and nucleosome remodelers have been suggested to regulate nucleosome spacing. Initial studies demonstrated that the accessory domains and subunits, e.g. the HSS domain, the Itc1/Acf1 subunit in the ISWI remodeler, contribute towards spacing (Clapier et al., 2002; Dang et al., 2006; Eberharter et al., 2001; Hota et al., 2013; Kagalwala et al., 2004). Multiple FRET and gel-based studies then showed an elegant interplay among several domains in the remodeler with the H4-tail, H2A-H2B acidic patch and the linker DNA to regulate linker length sensing and nucleosome sliding, which in turn determine nucleosome spacing (Clapier and Cairns, 2012; Dao et al., 2019; Gamarra et al., 2018; Hwang et al., 2014; Leonard and Narlikar, 2015; Levendosky and Bowman, 2019; Ludwigsen et al., 2017; Nodelman et al., 2017). Recently, the linker length sensing by the INO80 remodeler has garnered interest. *In vitro* studies suggested that two modules in the INO80 complex, namely Nhp10 and Arp8, may contribute to this process (Brahma et al., 2018; Knoll et al., 2018; Zhou et al., 2018).

1.2.4 Non-histone DNA binding factors

Multiple sequence-specific DNA binding proteins act as a barrier for regular arrays at a defined genomic location. In *S. cerevisiae*, these barriers include general regulatory factors (GRFs) like Reb1, Abf1, Rap1, Cbf1 which bind in promoters, origin recognition complex (ORC) near replication origins and Pol III transcription factor (TFIIIB-TFIIIC) at the tRNA genes (Lieleg et al., 2015b; Nagarajavel et al., 2013). Depletion of GRFs shifts nucleosome arrays towards the GRF binding sites. GRF binding in the promoter region also inhibits ectopic transcription initiation near their binding sites (Challal et al., 2018; Hartley and Madhani, 2009; Kubik et al., 2015; Kubik et al., 2018; Wu et al., 2018).

GRFs may work together with the nucleosome remodelers to clear promoter region from nucleosomes and position the +1-nucleosome. They can also physically interact with the nucleosome remodelers, especially RSC, which may contribute to specific recruitment of remodelers near promoters (Gavin et al., 2002; Wu et al., 2018). The RSC remodeler is also known to slide or even evict nucleosomes which may facilitate GRF binding in the NFR (Brahma and Henikoff, 2019; Kubik et al., 2015; Kubik et al., 2018; Mivelaz et al., 2020). GRFs may also collaborate with the ISWI and Chd1 remodelers to generate regular arrays close to their binding sites (Krietenstein et al., 2016; Oberbeckmann et al., 2020). Consistent with this, GRFs have been proposed to direct spacing remodelers behind the replication fork to re-establish phased nucleosome arrays (Yadav and Whitehouse, 2016).

In *S. cerevisiae*, nucleosomes are organized into regular arrays near the origins of replication. These regions are nucleosome depleted due to their AT-rich nature and harbor a sequence

motif. Origin recognition complex (ORC) binds this sequence motif and acts as a barrier for phased regular arrays. Depletion of ORC shifts nucleosome arrays towards the ORC binding site (Berbenetz et al., 2010; Eaton et al., 2010). Nucleosome organization near ORC binding sites has been suggested to play a role in the timely initiation of replication (Lipford and Bell, 2001). In line with this, early replicating origins have more regular arrays than the late origins (Deniz et al., 2016; Soriano et al., 2014).

Transcription and nucleosome remodelers also play a role in nucleosome organization at replication origins in yeast. Pervasive transcription near replication origins is suggested to modulate replication origin activity. Origins with high levels of transcription have lower licensing efficiency and are late replicating (Candelli et al., 2018; Gros et al., 2015; Soudet et al., 2018). Nucleosome remodelers of the ISWI- and INO80- families are enriched near the replication origins and promote replication of the late origins (Vincent et al., 2008). Whether ISWI and INO80 remodelers promote replication by generating regular remains to be determined. In line with this notion, these remodelers were shown to promote replication of a chromatin substrate *in vitro* (Azmi et al., 2017; Kurat et al., 2017).

Lastly, phased regular arrays are also present near transcription factor binding sites in higher organisms. Recently, regular arrays were found near su(HW) and Phaser binding sites in *Drosophila* (Baldi et al., 2018a). CTCF and many other transcription factors (TFs) binding sites also harbor phased regular arrays in mammals (Barozzi et al., 2014; Fu et al., 2008; Wang et al., 2012). CTCF binding was shown to correlate with NRL and regular arrays. The higher the bound CTCF, the lower the NRL and the higher the array regularity (Clarkson et al., 2019; Owens et al., 2019). TFs may even have unique repeat lengths near their binding sites (Clarkson et al., 2019). Phased regular arrays near TF binding sites are largely established by the ISWI remodeler in *Drosophila* and higher organisms (Baldi et al., 2018a; Barisic et al., 2019; Wiechens et al., 2016).

1.2.5 Histone and DNA modifications

Histones are post-translationally modified predominantly in the N-terminal tails, but also within the globular domain. These modifications can affect nucleosome stability, chromatin folding, binding as well as enzymatic activity of several chromatin factors (Lawrence et al., 2016).

Histone post-translational modifications (PTMs) can play a role in the recruitment of nucleosome remodelers near specific regions in the genome. For example, ISW1b complex is recruited to gene bodies via H3K36me3 (Maltby et al., 2012; Smolle et al., 2012) and the human Chd1 binds H3K4me3 (Sims et al., 2005). Lysine tetra-acetylation in the H3-tail enhances SWI/SNF and RSC binding to nucleosomes (Chatterjee et al., 2011).

Histone PTMs can also modulate nucleosome sliding. Yeast ISW2 and Chd1 remodelers are inhibited by H4 acetylation (Ferreira et al., 2007), while H2B ubiquitylation stimulates Chd1 (Levendosky et al., 2016; Sundaramoorthy et al., 2018). H3, but not H4, tail acetylation modulates activity of the SWI/SNF and RSC remodelers (Carey et al., 2006; Chatterjee et al., 2011; Lorch et al., 2018). Deposition of the histone variant H2A.Z by the SWR1 remodeler is stimulated by H2A and H4 acetylation (Altaf et al., 2010; Kusch et al., 2004). Recently, a high

throughput study showed how ISWI activity is affected by several histone modifications (Dann et al., 2017).

DNA methylation affects nucleosome positioning in diverse eukaryotes. CpG sites in the linker DNA are methylated in higher organisms. CpG methylation negatively affects nucleosome formation, thus excluding nucleosomes from the linker DNA (Huff and Zilberman, 2014; Kelly et al., 2012). Similar to CpG methylation, N6-methyladenine (6mA) also disfavors nucleosome formation which is overridden by the ACF remodeler (Beh et al., 2019). In contrast to 6mA and CpG methylation, 5-formylcytosine is shown to promote nucleosome occupancy (Raiber et al., 2018).

1.2.6 Histone variants and linker histones

Histone variants are incorporated mostly in a replication-independent manner at certain regions in the genome. They are involved in several genomic processes encompassing transcription, centromere identity, DNA damage response and repair, and chromatin packaging (Bonisch and Hake, 2012; Talbert and Henikoff, 2010). Nucleosomes harboring both H2A.Z and H3.3 variants or only H2A.Bbd are less stable than nucleosomes with canonical histones (Bao et al., 2004; Henikoff et al., 2009; Jin and Felsenfeld, 2007). The histone variants H2A.Z and H2A.Bbd can also affect folding of the chromatin fiber (Fan et al., 2002; Fan et al., 2004; Zhou et al., 2007).

Incorporation of histone variants can stimulate nucleosome remodeler activity. Nucleosome sliding by ISWI and INO80 and nucleosome disassembly by RSC is enhanced by H2A.Z *in vitro* (Brahma et al., 2017; Cakiroglu et al., 2019; Goldman et al., 2010). *In vivo*, however, H2A.Z does not appear to have a genome-wide role in nucleosome organization. Cells lacking H2A.Z or the SWR1 remodeler has no effect on nucleosome organization in *S. cerevisiae* (Hartley and Madhani, 2009; Tramantano et al., 2016). Nevertheless, H2A.Z appears to have a role in nucleosome positioning particularly at the stress-inducible genes (Gevry et al., 2009; Guillemette et al., 2005).

The linker histone H1 is an important player in genome compaction, NRL determination, and higher-order chromosome structure. It simultaneously binds to the entry and exit linker DNA on the nucleosome (Woodcock et al., 2006). *S. cerevisiae* expresses a single linker histone named Hho1. It is deposited sparsely in the chromatin, which may explain its negligible role in nucleosome organization and NRL determination. (Hughes and Rando, 2015; Patterton et al., 1998; Puig et al., 1999). In contrast to yeast, higher organisms express up to 11 variants of H1 and have a critical role in NRL determination (Hergeth and Schneider, 2015). Addition of histone H1 during *in vitro* chromatin assembly leads to a gradual increase in NRL, suggesting linker histones determine NRL (Blank and Becker, 1995). Consistently, depletion of linker histones *in vivo* leads to a decrease in NRL (Fan et al., 2003; Fan et al., 2005). Linker histone subtypes may even differ in the NRL generated by them, suggesting H1 subtypes affect chromatin organization distinctly (Oberg et al., 2012).

1.2.7 Statistical positioning and clamping

Nucleosome arrays aligned to a given location in the genome are suggested to emanate from pure statistical theory (Kornberg and Stryer, 1988). This theory is analogous to a can of tennis balls. A single tennis ball can occupy multiple positions, but an increasing number of balls limits the number of possible positions in the can. Similarly, nucleosomes are packed against a barrier which leads to higher nucleosome positioning near the barrier and a continuous decay away from the barrier (Fedor et al., 1988). Multiple studies have suggested that the statistical positioning theory can largely describe the regular arrays present near genic promoters without any other cellular factors discussed above (Mavrich et al., 2008a; Milani et al., 2009; Mobius and Gerland, 2010; Mobius et al., 2013; Rube and Song, 2014; Yuan et al., 2005).

A critical test for this model is reducing the number of nucleosomes which predicts that the NRL would gradually increase with a decrease in nucleosomes. On the contrary, several studies found little support to an increase in repeat length when histone amounts were lowered (Celona et al., 2011; Gossett and Lieb, 2012; Hu et al., 2014; van Bakel et al., 2013; Zhang et al., 2011). Even a 50% reduction in histone amounts has largely unchanged NRL. Importantly, these studies were performed either *in vivo* or using whole-cell extracts. Chromatin factors, like remodelers, present in these experiments may have overridden the nucleosome arrays generated by pure statistical theory. Indeed, an “active packaging” and “clamping” mechanism has been proposed which may contribute to the unchanged NRL upon reduced histone density. ISWI and Chd1 remodelers are suggested to act as a “clamp” which may establish constant NRL independent of histone density (Lieleg et al., 2015a; Zhang et al., 2011).

1.3 Functions of nucleosome arrays

Until now, I have discussed different mechanisms which contribute to nucleosome array formation. The function of these arrays is not completely clear. Assembly of histone octamers over the genomic DNA is essential to neutralize the negative charge of the DNA. Monovalent salt and linker histone further help in charge neutralization. During salt gradient dialysis, nucleosomes are assembled into irregular arrays with extremely small NRL (Noll et al., 1980; Steinmetz et al., 1978). This tight nucleosome assembly with short NRL enhances charge neutralization and packaging of the genomic DNA, and is, thus, affected by salt concentration (Blank and Becker, 1995). While irregular arrays with small NRL can explain dense packaging of genome during salt gradient dialysis, it cannot readily demonstrate the utility of regular nucleosome arrays and even so of different NRLs found *in vivo*. I will now discuss the importance of regularly spaced nucleosome arrays and highlight specific examples related to it.

1.3.1 Chromatin fiber folding

Genomic DNA is folded into higher-order structures in the form of chromatin. Nucleosome arrays are known to greatly increase genome packaging and 3D-folding and have been studied extensively in the past decades. Early studies using nuclei isolated from dormant cells and *in vitro* reconstituted chromatin revealed 30-nm wide structures, suggesting chromatin

may fold into such secondary structures called 30-nm fibers. These structures are shown to largely exist in two forms: “one-start” solenoid and “two-start” zigzag. More studies seemed to support the zigzag model than the solenoid model (Dorigo et al., 2004; Finch and Klug, 1976; Langmore and Paulson, 1983; Robinson et al., 2006; Schalch et al., 2005; Song et al., 2014; Woodcock et al., 1984).

While these 30-nm structures definitely exist *in vitro*, their *in vivo* existence has long been debated. In recent years, multiple studies employing diverse microscopy and sequencing-based techniques could find very little evidence for 30-nm like structures, arguing against a continuously folded chromatin fiber in cells (Eltsov et al., 2008; Hsieh et al., 2015; Nishino et al., 2012; Ou et al., 2017; Ricci et al., 2015; Risca et al., 2017). Imaging of nucleosomes in single cells shows variable clusters formed of 2-8 nucleosomes. Differentiated cells and heterochromatic regions show larger clusters than embryonic stem cells and euchromatin. Despite these strong evidences against 30-nm structures, sequencing-based methods find slight enrichment of interactions between N and N+2 nucleosomes, indicative of zigzag structures (Hsieh et al., 2015; Risca et al., 2017). These interactions are enriched in heterochromatin, suggesting different regions in the genome are folded distinctly.

A recent study suggests that nucleosome arrays may form globular structures with interdigitated nucleosome fibers that appear to be like a melted polymer (Maeshima et al., 2016). Another study elegantly demonstrated that these globular structures have the potential to undergo liquid-liquid phase separation (LLPS). Surprisingly, the linker histones and the NRL in the chromatin fiber regulates phase separation potential of these globular structures (Figure 1.5A, B) (Gibson et al., 2019).

While super-resolution microscopy and high-throughput sequencing methods provide important insights into genome folding, these datasets currently lack the resolution to distinguish linker lengths and array regularity in a chromatin fiber. Thus, it remains largely unclear how heterogeneity in chromatin fibers affect folding *in vivo*. *In vitro* reconstituted chromatin with defined NRL provides important insights into this. Arrays with short NRL (170 bp) form compact fibers independent of histone H1. On the other hand, arrays with long NRL (200 bp) fold less compactly and require H1 for maximum compaction. Folding of shorter NRL arrays tend to be more sensitive to a small variation in linker lengths (2 or 4 bp) than arrays with longer NRLs. Moreover, linker length quantitation can affect fiber folding in arrays with shorter NRL. Arrays with 167 bp NRL (10n fiber) form compact structures, while 172 bp NRL (10n + 5 fiber) fail to do so, suggesting 10n+5 fibers are open and more accessible (Correll et al., 2012; Routh et al., 2008). Consistent with these results, actively transcribed regions have shorter NRL and show less structured chromatin than heterochromatin (Risca et al., 2017; Schones et al., 2008; Valouev et al., 2011). This is also in line with disrupting nature of transcription and is supported by the Micro-C experiments showing transcription anti-correlates with fiber compaction (Hsieh et al., 2015).

1.3.2 Regular arrays may promote long-range interaction

Active enhancers in the mammalian genomes are flanked by regular arrays. The functional relevance of these arrays, if any, is unclear. *In vitro* results suggested that the NRL can regulate enhancer-promoter communication (EPC) of genomic domains. Nucleosome arrays with longer NRL display a higher level of EPC than the arrays with shorter NRL, suggesting that the nucleosome fiber flexibility contributes to contacts between genomic regions (Nizovtseva et al., 2017; Rubtsov et al., 2006). Certain transcription factors, like ESRRB, are preferentially retained on the chromatin during mitosis. These retained TFs lead to regular array formation and may have a role in the establishment of interphase-like genome folding after mitosis (Festuccia et al., 2019; Owens et al., 2019).

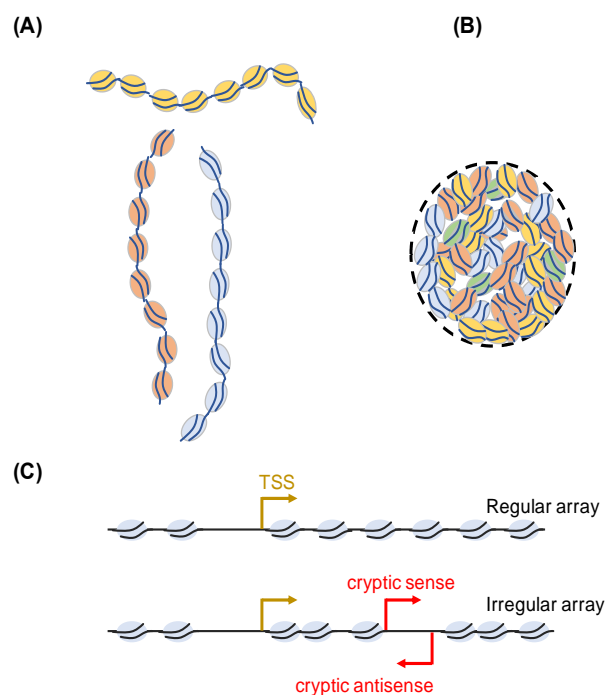


Figure 1.5: Functions of regular nucleosome arrays. (A) Under low salt conditions, nucleosome arrays are fully soluble and form an extended 10 nm fiber. (B) At high concentrations of salt and nucleosome array, nucleosome arrays have a potential to form interdigitated globular structures and undergo liquid-liquid phase separation. (C) Irregular nucleosome arrays may lead to accessible DNA which can allow assembly of transcription initiation machinery at these sites. Regular nucleosome arrays generated by spacing remodelers occlude cryptic TSSs in the gene body. (Singh and Mueller-Planitz, unpublished).

1.3.3 Regular arrays prevent intragenic cryptic transcription

In *S. cerevisiae*, the coding regions are covered with regular nucleosome arrays. Cells lacking ISWI and Chd1 remodelers show higher cryptic sense and antisense transcription frequency in the gene body (Smolle et al., 2012). Similarly, *S. pombe* cells lacking spacing remodelers Hrp1 and Hrp3 show cryptic antisense transcription (Figure 1.5C) (Hennig et al., 2012; Pointner et al., 2012; Shim et al., 2012). Defective chromatin architecture in cells lacking histone chaperones Spt6 and Spt16 or due to reduced histone density also show increased antisense transcription (Doris et al., 2018; Kaplan et al., 2003; Murawska et al., 2020; van Bakel et al., 2013). These results suggest that the lack of proper nucleosome assembly and

organization increases cryptic transcription in the gene body. The occasional exposure of DNA from irregular spacing in these cells may provide access to the transcription machinery.

1.3.4 Nucleosome spacing in regulating enzyme activity

Nucleosomes are a common substrate for most chromatin enzymes. Several structural and biochemical studies suggest that the linker length between nucleosomes can act as a regulatory mechanism for some chromatin factors. The DNA maintenance methyltransferase, for example, has an increased activity on dinucleosomes with 30 bp linker length, and lower activity with other linker lengths (Stoddard et al., 2019). The PRC1-EZH2 histone methyltransferase also prefers certain linker length (40 bp) (Lee et al., 2018). Rpd3 histone deacetylase is also sensitive to linker length between nucleosomes. It has been suggested that ISWI and Chd1 remodelers generate an ideal linker length for Rpd3 activity which promotes repression of cryptic transcription in the gene body (Lee et al., 2013; Smolle et al., 2012).

1.4 Aims of this thesis

Previous studies have suggested the mechanism behind the establishment of promoter architecture and regular nucleosome arrays in the gene body (Hughes et al., 2012; Krietenstein et al., 2016). Transcription initiation and elongation steps, together with spacing remodelers of the ISWI- and CHD- families, are proposed to establish phased regular arrays. As discussed above, regular arrays can also be established independent of transcription via statistical positioning. Therefore, the role of transcription, and if and how it cooperates with nucleosome remodelers has remained unclear. The role of the INO80 spacing remodeler in regular nucleosome array formation is also not known. Furthermore, the interplay of histone density and spacing remodelers towards establishing regular arrays is not clear yet. Lastly, the *in vivo* mechanism and regulation of NRL determination by ISW1, ISW2 and INO80 remodelers is completely known.

To answer these questions, I employed a yeast strain lacking nucleosome remodelers of ISWI- and CHD- families to massively reduce redundancy of remodelers. Using this system, I dissected the mechanism behind the biogenesis of regular arrays as well as the regulatory mechanism of the spacing remodelers from ISWI and INO80 families. In chapter 2.1, I investigated how phased regular arrays are established in *S. cerevisiae* and show the role of cellular factors, including transcription, spacing remodelers, histone density and DNA sequence in this process. I also provide evidence for function of regular arrays beyond the well-known function of packaging of the genome. In chapter 2.2 and 2.3, I studied the spacing mechanism of the ISW1 and ISW2 remodelers, and how individual domains and motifs within these remodelers regulate NRL established by them.

2. RESULTS

2.1 Chapter 1: The biogenesis and function of nucleosome arrays

Results presented in this chapter are from a manuscript which is currently under revision. A large part of this chapter is taken directly from initial versions of the manuscript which was written by me.

The contributions of the co-authors are as follows:

Dr. Tamas Schauer provided initial MNase-Seq and ATAC-Seq data analysis pipelines and provided constant feedback during other analyses in this chapter.

Lena Pfaller contributed to histones and Pol II depletion strains in the TKO background and performed wet-lab experiments related to MNase-Seq together with me.

Dr. Tobias Straub initially adapted NRL calculation scripts (obtained from Dr. Razvan Chereji and Dr. David J. Clark, NIH) from MATLAB into R.

Prof. Dr. Felix Mueller-Planitz conceived the project and performed simulation related to histone depletion in section 2.1.3.

I designed and performed all other experiments and analyses presented in this chapter.

2.1.1 Background

Chromatin has a characteristic organization at the major regulatory sites in the genome, for example, at genic promoters and CTCF binding sites (Fu et al., 2008; Lai and Pugh, 2017; Yuan et al., 2005). Nucleosomes arrange as regular arrays in which the average distance between nucleosomes, known as nucleosome repeat length (NRL), is constant (Baldi et al., 2020). These regular arrays are aligned against the transcription start site (TSS) near genic promoters. The functional importance of nucleosome organization near promoters is well understood (Almer and Horz, 1986; Kubik et al., 2019; Weber et al., 2014). On the contrary, despite strict conservation, the biological function of regular arrays is poorly understood (Lohr et al., 1977; Noll, 1974).

Nucleosome remodelers play an essential role in establishing regular arrays. Deletion of known spacing remodelers from the ISWI- and CHD- families in *S. cerevisiae* disrupts phased regular arrays near promoters (Gkikopoulos et al., 2011; Ocampo et al., 2016). *In vitro*, ISWI, Chd1 and INO80 remodelers can sense the extranucleosomal linker DNA and generate a constant linker length between nucleosomes (Stockdale et al., 2006; Udugama et al., 2011; Yang et al., 2006). *In vivo*, on the other hand, only ISWI and Chd1 are proposed to establish the NRL. The role of INO80 remodeler in this process is unclear (Ocampo et al., 2016).

In principle, phased regular arrays can be established independent of spacing remodelers through statistical positioning. This model suggests that nucleosomes are well-positioned close to a barrier and declines further from the barrier (Kornberg and Stryer, 1988; Mavrich et al., 2008a; Mobius and Gerland, 2010). An important test of this model is decreasing the total number of nucleosomes upon which the NRL should increase. Previous studies showed that NRL is unchanged upon ~50% decrease in nucleosomes (Celona et al., 2011; Gossett and Lieb, 2012; van Bakel et al., 2013; Zhang et al., 2011), in contrast to the predictions from the statistical model. It is possible that the spacing remodelers of the ISWI- and CHD- families may have overridden the nucleosome organization established by pure statistical principles.

Transcription machinery, together with the preinitiation complex, is suggested to play an important role in the generation of NFR and positioning of the +1-nucleosome. Transcription elongation is proposed to help establish nucleosome array by recruiting remodelers of the ISWI- and CHD- families (Hughes et al., 2012; Struhl and Segal, 2013; Vasseur et al., 2016; Zhang et al., 2009). *In vitro* reconstitution of nucleosome arrays using cell extracts lacking transcriptional activity do not reach *in vivo* like arrays (Krietenstein et al., 2016; Zhang et al., 2011), further supporting the idea that transcription contributes towards establishing nucleosome arrays.

It is conceivable that the phased regular arrays are established by massive cooperation between transcription and nucleosome remodelers with input from barrier proteins and DNA sequence. The roles of individual factors are usually studied *in vivo* by removing one factor in the context of other factors. The inherent redundancy among these factors may conceal their actual role, thus limiting our understanding of how nucleosomes are organized *in vivo* and the contribution of individual factors towards it. Here, we employ a yeast strain lacking remodelers of the ISWI- and CHD- families (*isw1Δ, isw2Δ, chd1Δ*; TKO) (Tsukiyama et al., 1999) to

massively reduce this functional redundancy. We use this system to dissect the biogenesis of regular arrays and their functions *in vivo*.

2.1.2 An improved MNase-Seq protocol to map nucleosome position

A major technique used in this thesis is micrococcal nuclease (MNase) digestion of yeast nuclei followed by paired-end sequencing of the released DNA fragments (Almer and Horz, 1986; Chereji and Clark, 2018; Kent et al., 2011; Wal and Pugh, 2012). MNase is an exo- and endo- nuclease which preferentially cuts in unprotected DNA, e.g. in linker DNA, and releases nucleosomes from chromatin (Dingwall et al., 1981; Horz and Altenburger, 1981; Noll, 1974). Paired-end sequencing of the released fragments allows deducing both ends of DNA from sequencing reads (Cole et al., 2011; Henikoff et al., 2011). By mapping sequenced DNA to the reference genome, one can deduce the position and center of nucleosomes in the genome with near base-pair resolution.

The classical way of performing MNase-Seq is a titration of MNase such that an ideal digestion pattern represents 80% mononucleosome and 20% di-nucleosome in agarose gel electrophoresis (Chereji et al., 2019; Chereji et al., 2016; Mieczkowski et al., 2016; Weiner et al., 2010). The mononucleosome fragment (~150 bp) is then isolated from an agarose gel and sequenced using high-throughput paired-end sequencing (Figure 2.1A). We initially performed MNase-Seq in wild type (WT) cells using this method. While visualizing the nucleosome distribution of WT cells in the genome browser, we noticed an uneven distribution of nucleosome fragments as judged by variable amplitude of nucleosomes (Figure 2.1B). This was most apparent in the gene body with regions lacking nucleosomes entirely. Furthermore, this pattern was independent of MNase digestion degree as two digestion degrees showed similar trends (compare first two rows in Figure 2.1B).

We hypothesized that the uneven nucleosome coverage could arise from an improper agarose gel extraction or during manual library preparation. Therefore, we omitted the mononucleosome DNA isolation from the agarose gel step and prepared sequencing libraries directly from the whole MNase digested DNA (labeled as “Whole lane”). To identify an ideally digested sample upon MNase titration, we loaded 50% of the MNase digested DNA on an agarose gel and prepared sequencing libraries from the remaining DNA. Libraries were prepared using the NEB Ultra II library prep kit. Only 3 – 4 cycles of PCR amplification were employed to reduce bias in amplification of variable size DNA fragments present in the input sample for library preparation. The kit requires at least 3 cycles of PCR to complete the chemistry required to prepare the libraries. After paired-end sequencing, we bioinformatically selected nucleosome size fragments of lengths between 140 and 160 bp.

Using this methodology, we obtained an even coverage of nucleosomes over the entire gene and across the genome (compare “Mononucleosome” rows with “Whole lane” rows in Figure 2.1B). These nucleosome maps were in striking contrast with the maps generated by isolating mononucleosome bands from an agarose gel. Importantly, the individual nucleosomes and the overall nucleosome maps in the genome browser were highly consistent with a published high-quality dataset (Figure 2.1B) (Ocampo et al., 2016).

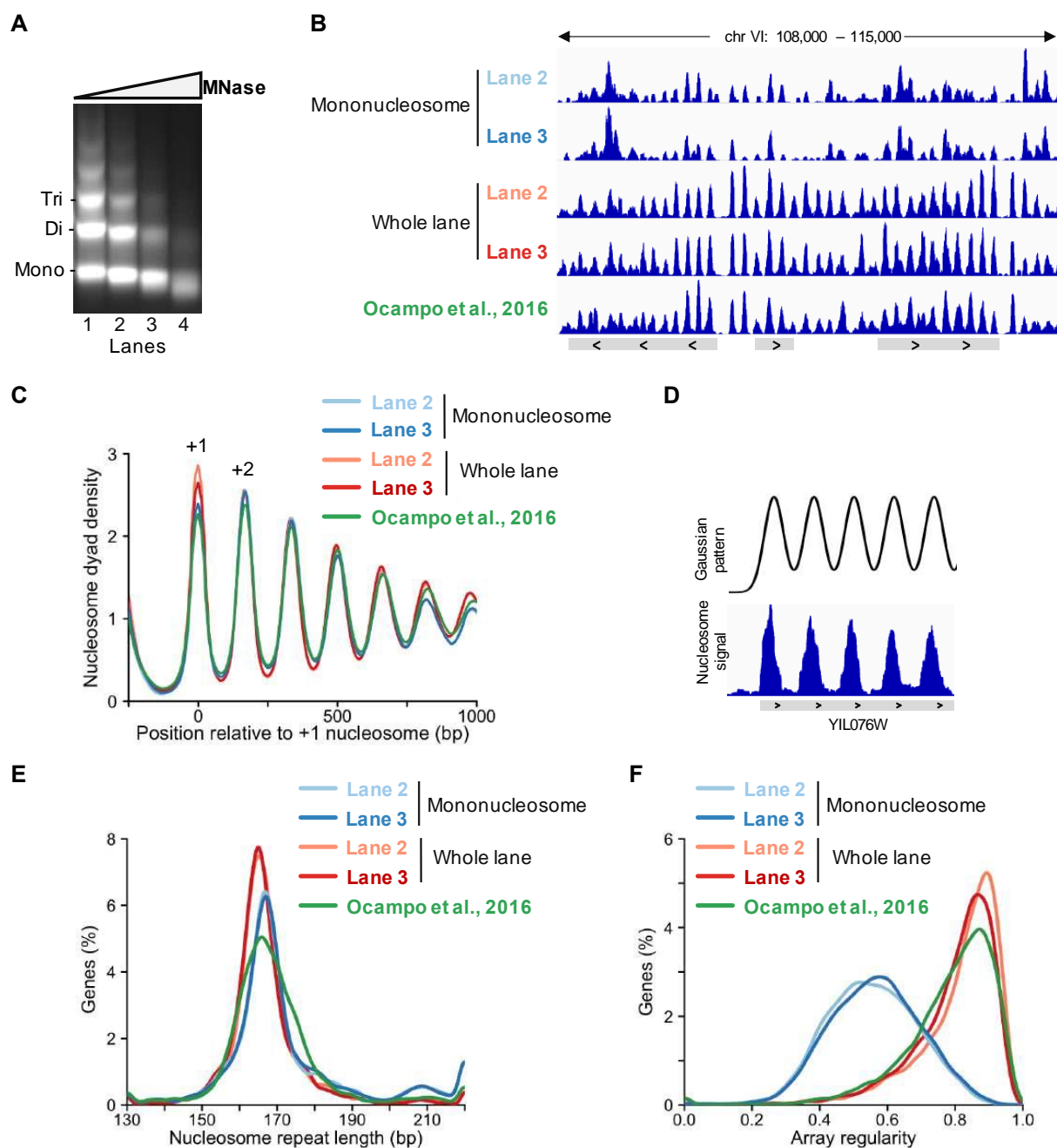


Figure 2.1: An improved MNase-Seq protocol to map nucleosome. (A) A typical agarose gel after MNase digestion of WT yeast nuclei (1 g) with increasing amounts (16 – 128 U/ml) of MNase. Mono-, Di- and Tri- indicate DNA fragments corresponding to mono-nucleosome, di-nucleosome and tri-nucleosome sizes. **(B)** IGV genome browser shot showing nucleosome coverage upon sequencing of either mononucleosome fragments isolated from an agarose gel (“Mononucleosome”) or the whole MNase digested lane (“Whole lane”). Mononucleosome size fragments were then bioinformatically selected from the paired-end reads of the “Whole lane” samples. Lanes 2 and 3 indicate two digestion degrees of MNase digested samples used from (A). WT dataset from (Ocampo et al., 2016) was used as a reference. **(C)** Gene-averaged nucleosome organization of ~5000 genes in samples in (B). **(D)** NRL and array regularity in each gene is calculated by cross-correlating MNase-Seq data with a Gaussian pattern. The best-fitting pattern for the gene YIL076W is shown. **(E)** NRL distributions of samples in (B). For “Mononucleosome” and “Whole lane” samples, peaks are at 165 and 167 bp, respectively. For WT dataset from (Ocampo et al., 2016), peak is at 166 bp. **(F)** Array regularity distributions of samples in (B).

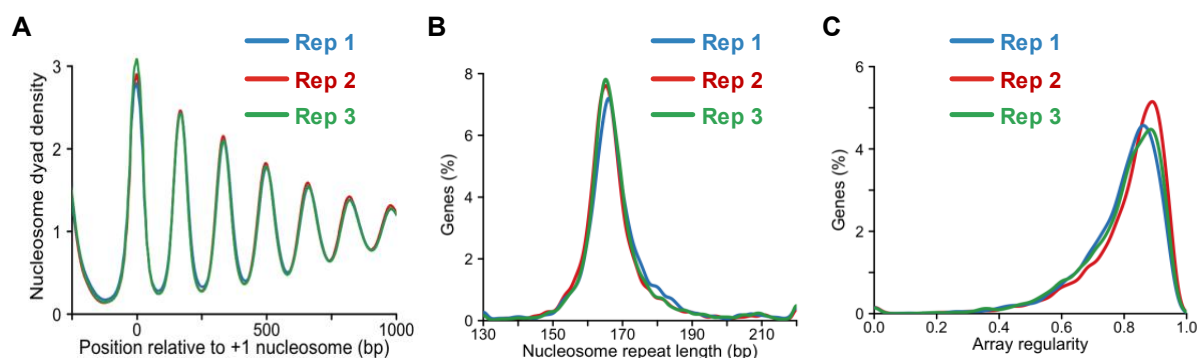


Figure 2.2: The improved MNase-Seq protocol provides highly consistent nucleosome maps. (A) Composite plot showing gene-averaged nucleosome organization of three biological replicates of WT cells prepared using “Whole lane” method. **(B)** NRL distributions of samples in (A). **(C)** Array regularity distributions of samples in (A).

To evaluate nucleosome distribution at the genome-wide level, we prepared composite plots representing average nucleosome signal in ~5000 yeast genes. The lower the peak height in composite plot, the higher the nucleosome fuzziness. We observed minor differences between datasets generated by isolating mononucleosome fragments or from whole lane samples and with the published dataset (Figure 2.1C) (Ocampo et al., 2016). The +1-nucleosome showed maximum difference in peak heights between samples, consistent with its higher susceptibility to MNase (Chereji et al., 2017; Weiner et al., 2010). Other nucleosomes showed similar peak heights. These results suggest that the composite plots are robust to uneven nucleosome distribution observed in each gene.

To decipher the nucleosome organization at each gene, we calculated nucleosome repeat length and array regularity in each gene. To this end, the MNase-Seq signal at each gene is compared to an ideal Gaussian distribution using cross-correlation function. The best match is assigned as NRL (Ocampo et al., 2016) and the correlation coefficient is used as a measure of nucleosome array regularity for each gene (Figure 2.1D) (Shivaswamy et al., 2008). We found similar NRL distributions between the “Mononucleosome” and the “Whole lane” samples and in the published dataset. The peaks differed by 1-2 bp (also see Figure legend 2.1E) and was independent of MNase digestion degree (Figure 2.1E). In contrast, the array regularity distribution differed dramatically between “Mononucleosome” and “Whole lane” samples. The published dataset was similar to the “Whole lane” sample (Figure 2.1F). These results suggest that the array regularity measurement is highly sensitive to quality of nucleosome maps, while the NRL measurement to a lower extent. Lastly, the biological replicates performed months apart with “Whole lane” method were highly consistent in the composite plots, and NRL and array regularity distributions (Figure 2.2A – C).

Below, we will use the “Whole lane” MNase digested DNA instead of the isolated “Mononucleosome” DNA to perform MNase-Seq, unless otherwise stated in the figure legends. We will measure nucleosome organization at each gene using NRL and array regularity determinants to understand the biogenesis of regular nucleosome arrays.

2.1.3 High histone density and nucleosome remodelers cooperate to generate regular nucleosome arrays

Previous experiments from our and Korber labs have shown that the ISWI- and Chd1-family of remodelers maintain a constant NRL regardless of nucleosome density *in vitro*, possibly via a “clamping” mechanism (Lieleg et al., 2015a). This model predicts that nucleosome remodelers generate constant NRL irrespective of nucleosome densities. The competing linker length equilibration model, on the other hand, predicts that the NRL increases with decreasing nucleosome density (Yang et al., 2006). Previous histone depletion experiments in WT cells seemed to retain nucleosome arrays with similar NRL, consistent with the clamping mechanism (Celona et al., 2011; Gossett and Lieb, 2012; van Bakel et al., 2013; Zhang et al., 2011). We hypothesized that the largely similar NRL and the residual array was due to spacing remodelers, which “clamp” nucleosomes at fixed distances between nucleosomes.

To test this hypothesis, we deleted ISWI and Chd1 remodelers (TKO) and depleted histones 3 and 4 to ~50% of wild type level using the Gal1-10 promoter system (Mann and Grunstein, 1992) (Figure 2.3). We then mapped nucleosomes with MNase-Seq combined with paired-end sequencing using two independent yeast colonies and considered DNA fragments of size 140-160 bp. We found that the nucleosome arrays were completely abolished upon histone depletion in the TKO strain (TKO HD). The +1 and +2 nucleosomes were still relatively well-positioned (Figures 2.4A, 2.3C).

The well-positioned +1-nucleosome may not be surprising given many redundant mechanisms that position this nucleosome (Krietenstein et al., 2016; Kubik et al., 2019). We wondered, however, if downstream nucleosomes are positioned by unknown mechanisms or if they truly reflect random (statistical) positioning (Fedor et al., 1988; Kornberg and Stryer, 1988; Mavrich et al., 2008a; Mobius and Gerland, 2010; Zhang et al., 2011). To test this, we performed simulations mimicking *in vivo* histone depletion by 50%. Simulated histone depletion resulted in a remarkably similar nucleosome pattern as observed in the TKO HD sample (Figure 2.4B). This result suggests that nucleosomes assume mostly random organization in the TKO HD sample driven by statistical positioning.

To test whether ISWI and Chd1 nucleosome remodelers override statistical positioning driven nucleosome organization, we performed histone depletion in WT cells. We observed a residual nucleosome array with 172 ± 1 bp NRL in two biological replicates upon histone depletion in WT (HD), compared to 165 bp NRL in WT, consistent with previous results (Figures 2.4C, D) (Celona et al., 2011; Gossett and Lieb, 2012; van Bakel et al., 2013). The minor increase in NRL is in contrast with ~200 NRL predicted at 50% nucleosome density (Beshnova et al., 2014). These observations suggest that the ISWI and Chd1 remodelers can maintain largely similar NRL as in WT cells, implying they possess clamping activity *in vivo*. The clamping activity of ISWI and Chd1 remodelers is rather weak as nucleosome arrays dramatically decreased in HD cells which possess ISWI and Chd1 remodelers when compared to WT cells.

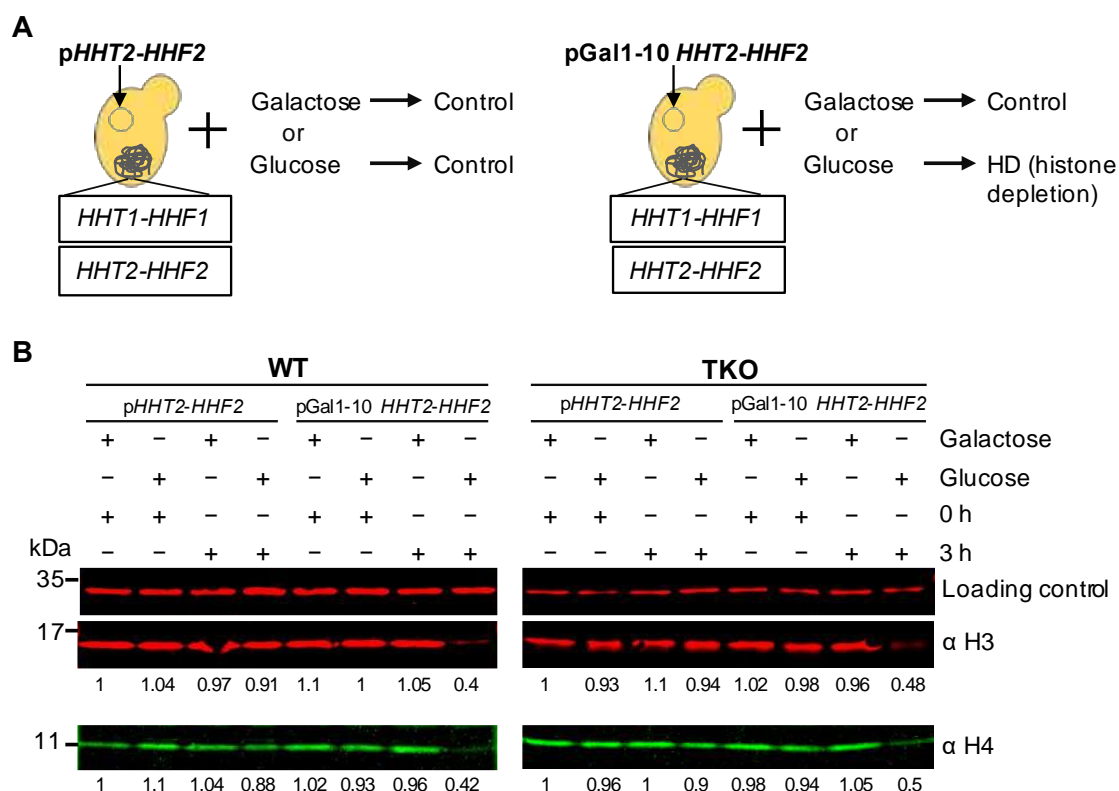


Figure 2.3: Galactose-inducible system to deplete histones in *S. cerevisiae*. (A) Scheme depicting histone depletion experiment. Both genomic copies of H3 and H4 were deleted. A single copy of H3 and H4 was provided on the pRS413 plasmid either under native promoter (left) or galactose-inducible promoter (right). Histones are only depleted in the latter case when cells were grown in glucose-containing media for 3 h. (B) Representative western blots showing controls and histone depletion (last lane in each blot). Loading control is the cross-reacting FLAG band with M2-antibody. (Singh et al., unpublished).

Overall, these results suggest that the ISWI and Chd1 remodelers possess clamping activity *in vivo*, although the clamping activity is rather weak (Lieleg et al., 2015a). When cells have reduced histone density and lack ISWI and Chd1 spacing remodelers, the nucleosome organization is highly similar to what would occur by random chance. Furthermore, high histone density is essential for WT-like nucleosome arrays and NRL. ISWI and Chd1 may help catalyze nucleosome array formation by providing fluidity to nucleosomes (Becker, 2002; Kingston and Narlikar, 1999).

We observed that the +2-nucleosome in the TKO HD sample (Figure 2.4B) seems to be better positioned than in the HD simulation. Also, TKO cells with normal histone levels have residual arrays even though known spacing remodelers are lacking in this strain (Gkikopoulos et al., 2011; Ocampo et al., 2016). We, therefore, hypothesized that more factors exist in the TKO strain which helps generate residual nucleosome arrays. The transcription machinery could be one of those factors.

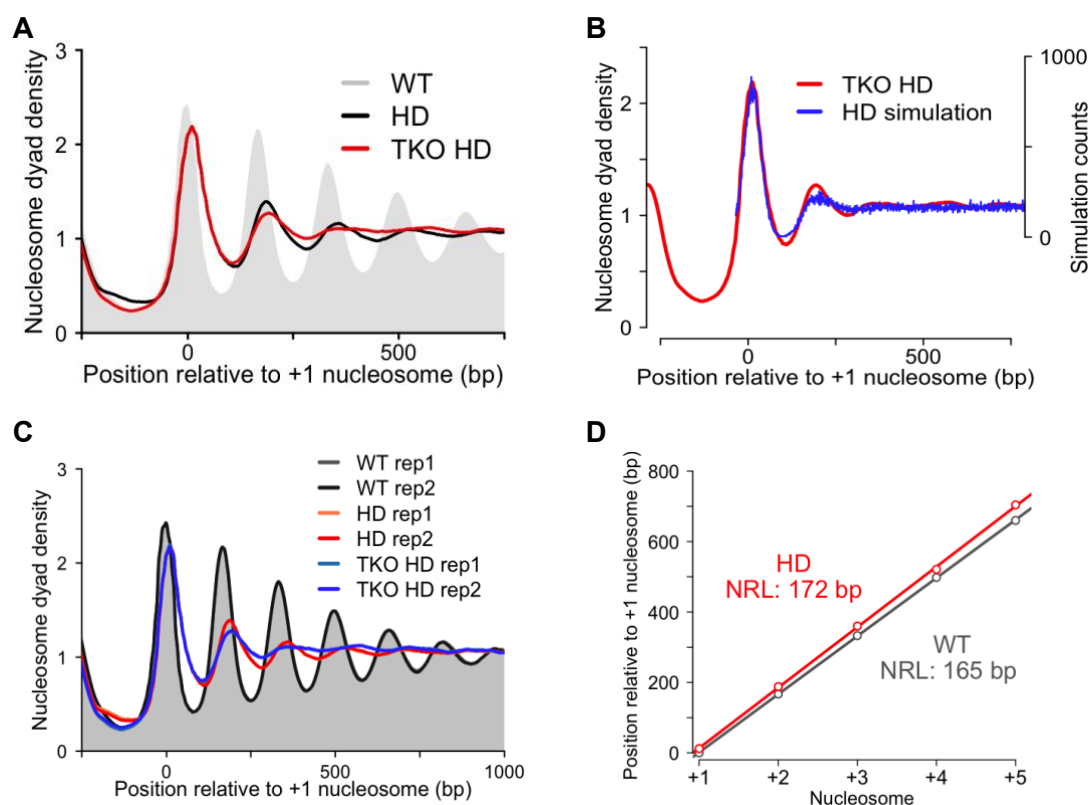


Figure 2.4: ISWI and Chd1 remodelers require high histone density to generate WT-like nucleosome arrays. (A) Composite plot representing nucleosome organization of ~5000 genes in WT, histone depleted (HD) and histone depleted TKO strain (TKO HD). WT is a control sample when cells were grown in glucose-containing media for 0 h. HD and TKO HD cells are depleted for 3 h. The composite plot was aligned to the +1-nucleosome position of WT cells (Chereji et al., 2018). (B) Simulated, nucleosome organization with 50% histone density (HD simulation) downstream of the +1-nucleosome. TKO HD is replotted from (A) to show the overlap of simulation with the TKO HD sample. (C) Individual biological replicates of samples in (A). (D) NRLs determined by slope of the line fitted on positions of +1 to +5 nucleosomes from data in (A). Gene level NRL calculation for HD and TKO HD samples did not provide any discernible peaks. (Singh et al., unpublished).

2.1.4 Transcription destroys the nucleosome array regularity

Pol II has been implicated in establishing nucleosome arrays by clearing the NFR and aligning the +1-nucleosome. ISWI and Chd1 remodelers together with transcription elongation associated factors help generate nucleosome arrays in the gene body (Hughes et al., 2012; Struhl and Segal, 2013; Vasseur et al., 2016). Indeed, deletion of ISWI and Chd1 remodelers (*isw1Δ*, *isw2Δ*, *chd1Δ*; Triple Knock Out, TKO strain) show severely disrupted nucleosome arrays, but relatively well-positioned +1 and +2 nucleosomes (Figure 2.5A, B) (Gkikopoulos et al., 2011; Ocampo et al., 2016).

We hypothesized that the residual nucleosome organization in the TKO strain is due to transcription machinery. If true, a decrease in nucleosome array regularity is expected upon inhibition of transcription in the TKO strain. To test this model, we combined the three remodelers (TKO) deletion with the anchor-away system (Haruki et al., 2008). This method utilizes the flux of ribosomal proteins through the nucleus during ribosome maturation to

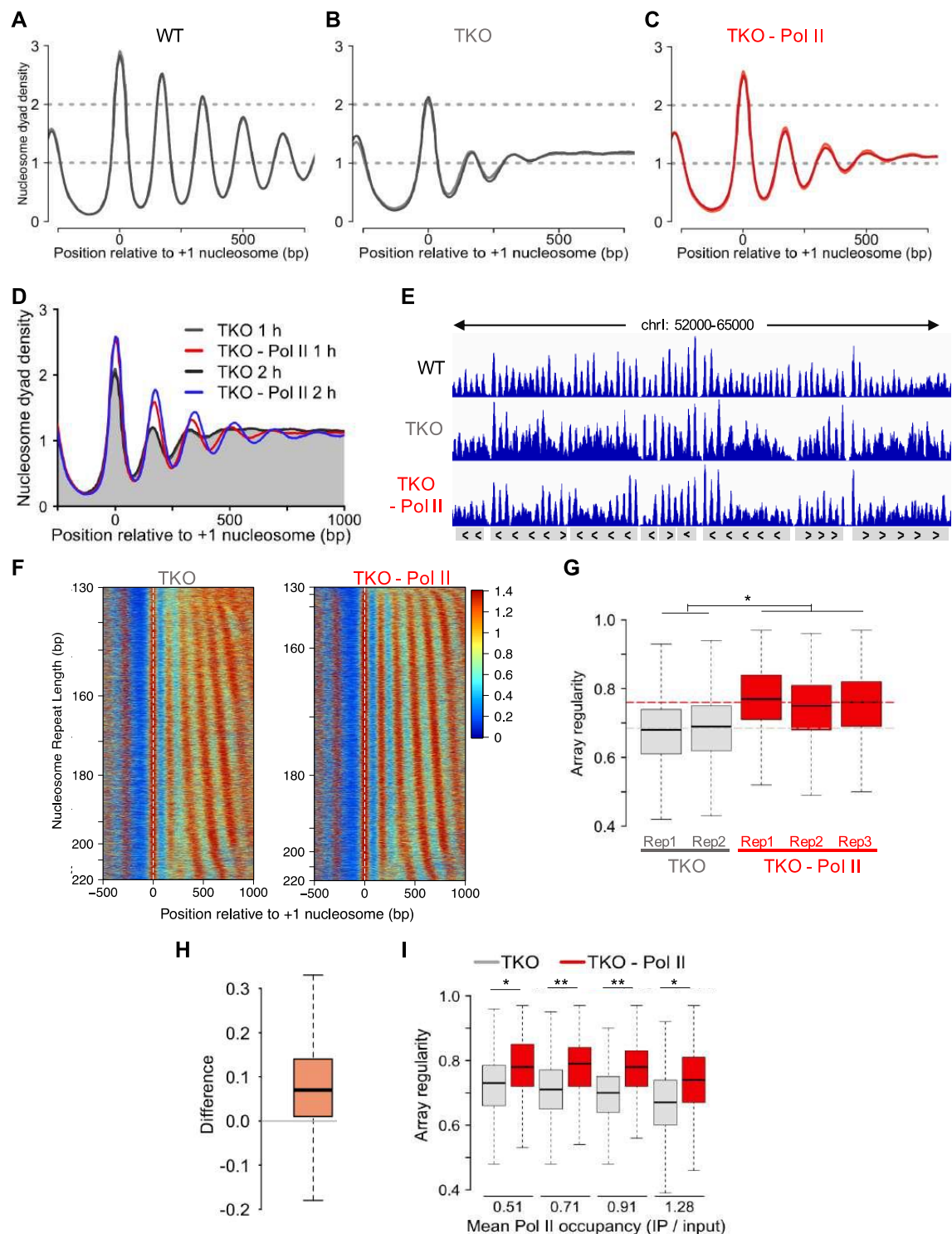


Figure 2.5: Transcription destroys the nucleosome landscape. (A) Composite plots showing the gene-averaged nucleosome organization for a WT control strain in the anchor-away background. Cells were mock treated with vehicle for 1 h. **(B)** Same as (A) but with TKO (*isw1Δ, isw2Δ, chd1Δ*). Shades of grey indicate two biological replicates in (A, B). **(C)** Nucleosome organization upon Pol II depletion in the TKO strain. Pol II was depleted by adding rapamycin for 1 h. Shades of red indicate three replicates from two colonies where Rpb1 is FRB tagged in the TKO background. **(D)** Nucleosome organization after 1 or 2 h of Pol II depletion in the TKO strain. **(E)** IGV genome browser shot of samples in (A-C) showing the rescue of array regularity in individual genes. **(F)** Heatmaps of data in (A-C). Genes are sorted by NRLs observed in the TKO strain. **(G)** Array regularity distribution of ~5000 genes in

control and Pol II depleted TKO strain. Rep1 – 3 are individual biological replicates. The horizontal line indicates the mean regularity of replicates. **(H)** The gene-by-gene difference in array regularity before and after Pol II depletion. The difference is calculated on pooled replicates. **(I)** Rescue of array regularity is independent of transcription strength in genes. Pol II occupancy is Rpb3 ChIP-Seq data for *isw1Δ*, *chd1Δ* strain, taken from (Ocampo et al., 2016). Genes were sorted by array regularity and divided into quartiles. Linear mixed model was fitted on the mean array regularity value of each replicate. * $P < 0.05$, ** $P < 0.01$. (Singh et al., unpublished).

deplete proteins from the nucleus. Using this method, we depleted Pol II for one and two hours as done previously (Kubik et al., 2015). To our surprise, we found that nucleosomes are better positioned, and arrays are dramatically better upon Pol II depletion in the TKO (Figure 2.5A – C). Up to four nucleosomes in the gene body are visible upon 1 h depletion in the composite plots, while only two nucleosomes are visible in the TKO strain. Longer Pol II depletion (2 h) showed mildly better arrays than the 1 h depletion, suggesting maximum rescue of the nucleosome arrays within 1 h depletion (Figure 2.5D). The rescue in individual genes could also be observed in genome browser tracks of individual genes (Figure 2.5E).

To test whether the rescue of nucleosome arrays is genome-wide or limited to a subset of genes, we measured the nucleosome repeat length (NRL) and array regularity in each gene. We found that the rescue of nucleosome arrays upon Pol II depletion occurs genome-wide, as seen in the heatmap with genes sorted by nucleosome repeat length (Figure 2.5F). Average array regularity also increased consistently in three biological replicates upon Pol II depletion (Figure 2.5G). We also measured the difference between array regularity in TKO and Pol II depleted TKO cells in each gene and found that ~77% genes show an increase in array regularity upon Pol II depletion (Figure 2.5H). Moreover, the increase in array regularity was independent of Pol II occupancy in the gene, suggesting that the rescue of nucleosome arrays is not restricted to highly expressed genes (Figure 2.5I).

Taken together, these results suggest that Pol II activity globally disrupts nucleosome arrays in the TKO strain. These results are in conflict with the model that transcription elongation promotes nucleosome array organization (Hughes et al., 2012; Struhl and Segal, 2013; Vasseur et al., 2016).

The results presented above show that Pol II disrupts nucleosome organization in cells lacking known spacing remodelers. Pol II is known to interact with and recruit nucleosome remodelers and thereby help generate nucleosome organization (Lafon et al., 2015; Lee et al., 2017; Park et al., 2014; Poli et al., 2016; Schwabish and Struhl, 2007; Simic et al., 2003; Soutourina et al., 2006). To test whether Pol II is truly disruptive to nucleosome organization or only disruptive in the absence of ISWI and Chd1 remodelers, we depleted Pol II in WT cells. In accord with the results in the TKO strain, we observed a modest increase in the amplitude of the nucleosome array upon Pol II depletion. The effect was visible after the fourth nucleosome inside the gene body (Figure 2.6A). We also re-analyzed previously published results of Pol II depletion in WT cells from two other laboratories and found a similar increase in array regularity (Figure 2.6B – E) (Kubik et al., 2015; Tramantano et al., 2016).

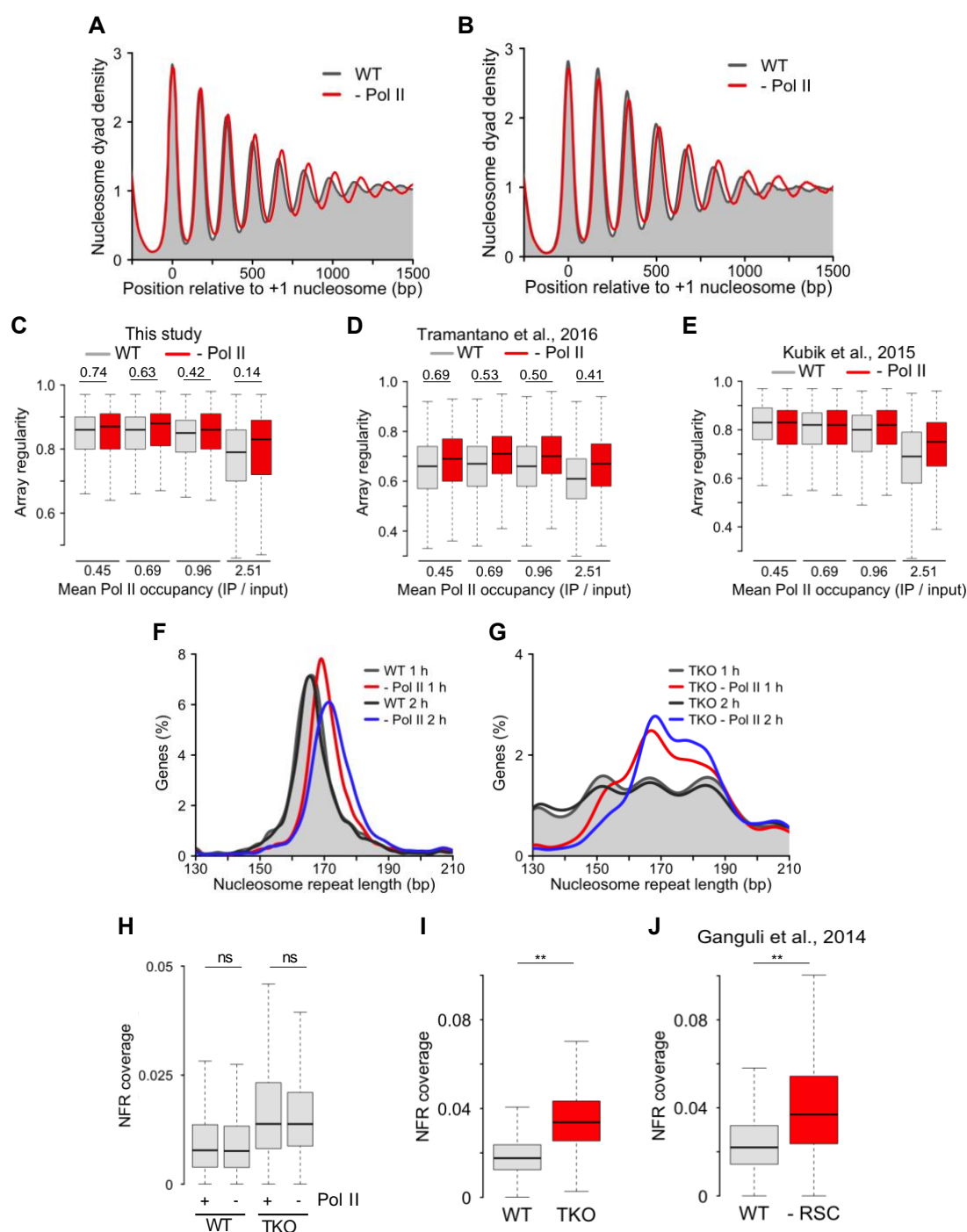


Figure 2.6: Pol II depletion increases NRL and array regularity in WT cells. (A) Composite plots showing the average nucleosome organization in WT and Pol II depleted strain for 1 h. Longer depletion showed similar results (not shown). (B) Same as (A) but for dataset from (Kubik et al., 2015). (C) Increase in array regularity is independent of Pol II occupancy in WT cells. Pol II occupancy is Rpb3 ChIP-Seq data taken from (Ocampo et al., 2016). Genes are sorted by array regularity and divided into quartiles. Values above the bar plot are p-values from a linear mixed model fitted to mean array regularity values of each replicate. (D, E) Same as (C) but for published datasets (Kubik et al., 2015; Tramantano et al., 2016). For (Kubik et al., 2015) study, only high MNase digestion degree sample was used. (F) NRL distribution upon Pol II depletion for 1 and 2 h in WT cells. Peaks maxima are at 165 bp for controls and 169 and 172 bp for 1 and 2 h depletion, respectively. (G) Same as (F) but in TKO background. Peaks are at 167 and 168 bp for 1 and 2 h depletion, respectively. No clear peak was observed in the control TKO samples. (H) Nucleosome coverage in the NFR of ~5000 genes in WT,

TKO and after Pol II depletion. All strains are in the anchor-away background. Coverage is calculated for 50 bp relative to the NFR center of WT cells. **(I)** Same as (H) but for WT and TKO strains. **(J)** Same as (H) but for WT and RSC depleted cells. Data is obtained from (Ganguli et al., 2014). Statistical analyses in (H, I, J) were performed using paired t-test on mean values of at least two biological replicates. Linear mixed model was fitted on the mean array regularity value of each replicate in (C, D). * $P < 0.05$, ** $P < 0.01$, *** $P < 0.001$. (Singh et al., unpublished).

These results suggest that Pol II activity also disrupts nucleosome arrays in WT cells. Overall, both TKO and WT cells show rescue of nucleosome arrays upon Pol II depletion, suggesting that the disruptive activity of Pol II is independent of genotype. TKO cells, however, show higher rescue than in WT cells. This observation suggests that in WT cells, ISWI and Chd1 spacing remodelers counteract the disruptive effect of Pol II.

Pol II depletion is known to increase NRL in WT cells. Previous studies qualitatively demonstrated this using composite plots (Tramantano et al., 2016; Weiner et al., 2010). We quantified this effect by measuring the NRL in each gene. The NRL peaks at 165 bp in WT cells and 172 bp upon Pol II depletion (Figure 2.6F). TKO cells show a broad distribution of NRL with no clear peak in the presence of Pol II. Upon Pol II depletion, a peak emerges at 168 bp (Figure 2.6G). Genes with mostly short NRL attained longer NRL. These results suggest that Pol II, and transcription thereof, decrease NRL genome-wide and is independent of ISWI and Chd1 spacing remodelers.

Pol II, together with the pre-initiation complex, has been proposed to contribute to the NFR generation. This may be aided by nucleosome remodelers recruited by Pol II. We measured nucleosome coverage at the NFR and found no difference upon Pol II depletion in both WT and TKO cells (Figure 2.6H). A previous study measuring depletion of pre-initiation complex (PIC) also found no change (Tramantano et al., 2016). This result suggests that Pol II and PIC have a negligible role in clearing the NFR. In contrast, TKO cells showed higher NFR coverage, suggesting that ISWI and Chd1 remodelers help clear NFR from nucleosomes (Figure 2.6H, I). This effect was comparable to the depletion of RSC remodeler known to clear NFR by evicting or sliding nucleosomes (Figure 2.6J) (Ganguli et al., 2014).

2.1.5 The INO80 remodeler is an *in vivo* nucleosome spacing factor

The increased nucleosome arrays upon Pol II depletion in the TKO strain was intriguing, as the data imply the presence of another spacing factor even though all bona fide spacing remodelers are missing in the strain (Gkikopoulos et al., 2011; Ocampo et al., 2016). The INO80 nucleosome remodeler is an attractive candidate for this activity because it can sense the length of the DNA flanking a mononucleosome and slide nucleosomes to the center on a piece of DNA. INO80 can also space up to three nucleosomes *in vitro* (Krietenstein et al., 2016; Schwarz et al., 2018; Udagama et al., 2011; Willhoft et al., 2017; Zhou et al., 2018). Therefore, we tested if it can space nucleosomes and generate extensive nucleosome arrays *in vivo*.

To test whether INO80 is the missing spacing factor and responsible for the rescue of nucleosome array after Pol II depletion in the TKO, we depleted both Ino80 ATPase and Pol II in the TKO background. Depletion of the Ino80 ATPase would lead to depletion of the whole

INO80 complex as the Ino80 ATPase form a central and essential component for the assembly of the whole INO80 complex (Ayala et al., 2018; Eustermann et al., 2018). Notably, double depletion showed no rescue of arrays and NRL (Figures 2.7A – D, 2.8D). This result strongly suggests that INO80 is the missing factor that is responsible for nucleosome spacing after Pol II depletion in the TKO strain. The spacing activity by INO80 is genome-wide. Most genes attained higher array regularity when INO80 is present in the nucleus which is completely lost upon Ino80 ATPase depletion (Figure 2.7E). This results further suggests that the INO80 remodeler does not require active transcription for its nucleosome spacing activity. The genome-wide spacing activity of the INO80 remodeler is consistent with its binding to most nucleosome positions *in vivo* (Yen et al., 2012).

Having shown that INO80 can generate nucleosome arrays upon Pol II depletion in TKO, we sought to test if this activity can also be detected in cells with active transcription. Therefore, we depleted the INO80 remodeler in the TKO strain. The INO80 depleted TKO cells showed a further decrease in nucleosome array in the composite plot as well as at the gene level in array regularity (Figure 2.8A – C, E). This result suggests that the INO80 remodeler contributes to the residual regularity in the TKO strain with active transcription.

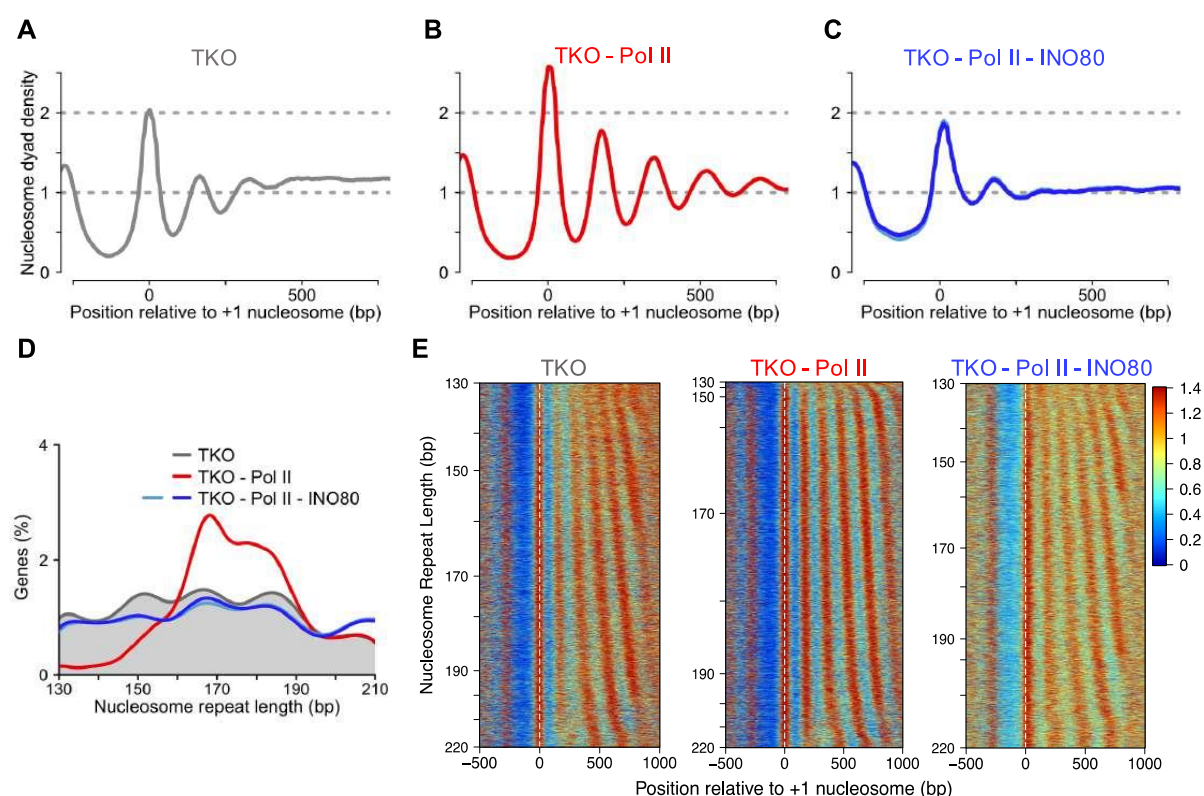


Figure 2.7: INO80 is a nucleosome spacing factor *in vivo*. (A, B) Gene averaged nucleosome organization in the TKO strain where Rbp1 is FRB tagged. Cells were either treated with vehicle or rapamycin for 2 h. (C) Same as (A) but for cells depleted with Pol II and INO80 in the TKO background for 2 h. (D) NRL distribution in strains from (A – C). Shades of blue in (C, D) indicate two biological replicates. (E) Heatmaps showing nucleosome organization in strains from (A – C). Genes were sorted by NRL observed in the TKO strain. All experiments were performed in two biological replicates, represented by shades of a color. (Singh et al., unpublished).

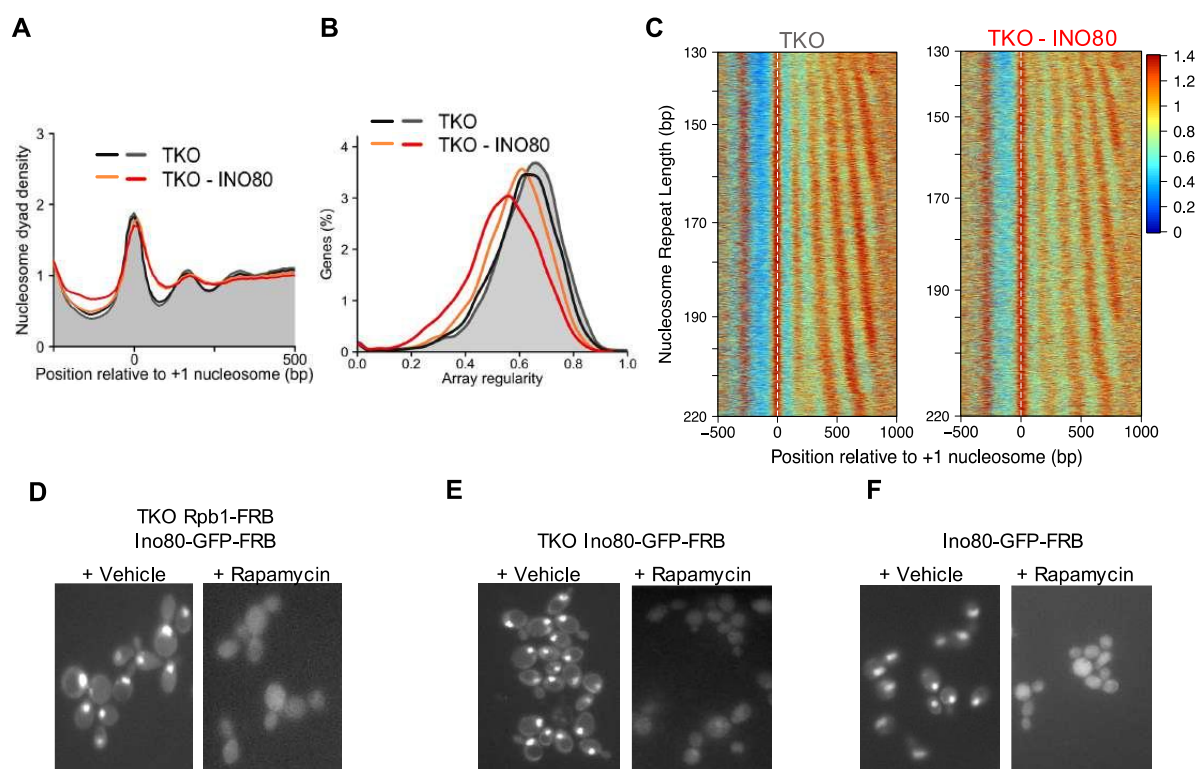


Figure 2.8: INO80 contributes to array regularity in TKO cells. (A) Composite plot showing nucleosome organization upon INO80 depletion in the TKO background. (B) Array regularity distribution in strains from (A). Average of two biological replicates is shown in (A, B). (C) Heatmaps of the MNase-Seq data from (A). Genes were sorted by NRL observed in the TKO strain. (D, E, F) Depletion of the Ino80 ATPase was confirmed by the GFP-tagged Ino80 ATPase. Double depletion of Pol II and Ino80 was complete in 2 h. Single depletion of Ino80 was complete in 1.5 h, consistent with previous results (Tramantano et al., 2016). All experiments were performed in two biological replicates, represented by shades of a color. (Singh et al., unpublished).

We wondered if INO80 also contributes to nucleosome spacing and array regularity in WT cells. To test this, we depleted INO80 in WT cells (Figure 2.8F). Depletion of INO80 for 1.5 hours showed negligible changes in both NRL and array regularity, consistent with previous results (Figure 2.9A, C) (Tramantano et al., 2016). We ruled out that this is due to incomplete depletion of the INO80 remodeler as the GFP-tagged Ino80 ATPase was depleted within 1.5 hours, as judged by a diffused signal in the cytoplasm of cells (Figure 2.8F). The lack of change in NRL and array regularity could arise from high redundancy with ISWI and Chd1 spacing remodelers in WT cells. It is also possible that INO80 has a bigger role in establishing nucleosome organization in the wake of replication. Therefore, we depleted INO80 for 6 h when the cells have divided at least twice and have achieved a new steady state. We observed no decrease in cell viability upon prolonged (6 h) INO80 depletion compared to mock treated cells (not shown).

Consistent with our hypothesis, longer INO80 depletion led to a smaller amplitude of signal in the composite plot, suggesting increased nucleosome fuzziness and lower array regularity (Figure 2.9B). Also, the NRL decreased consistently by 3 bp upon INO80 depletion, suggesting INO80 makes longer NRL *in vivo* (Figure 2.9D). We also reanalyzed a recently published MNase-Seq data for auxin-induced degradation of the Ino80 ATPase and found

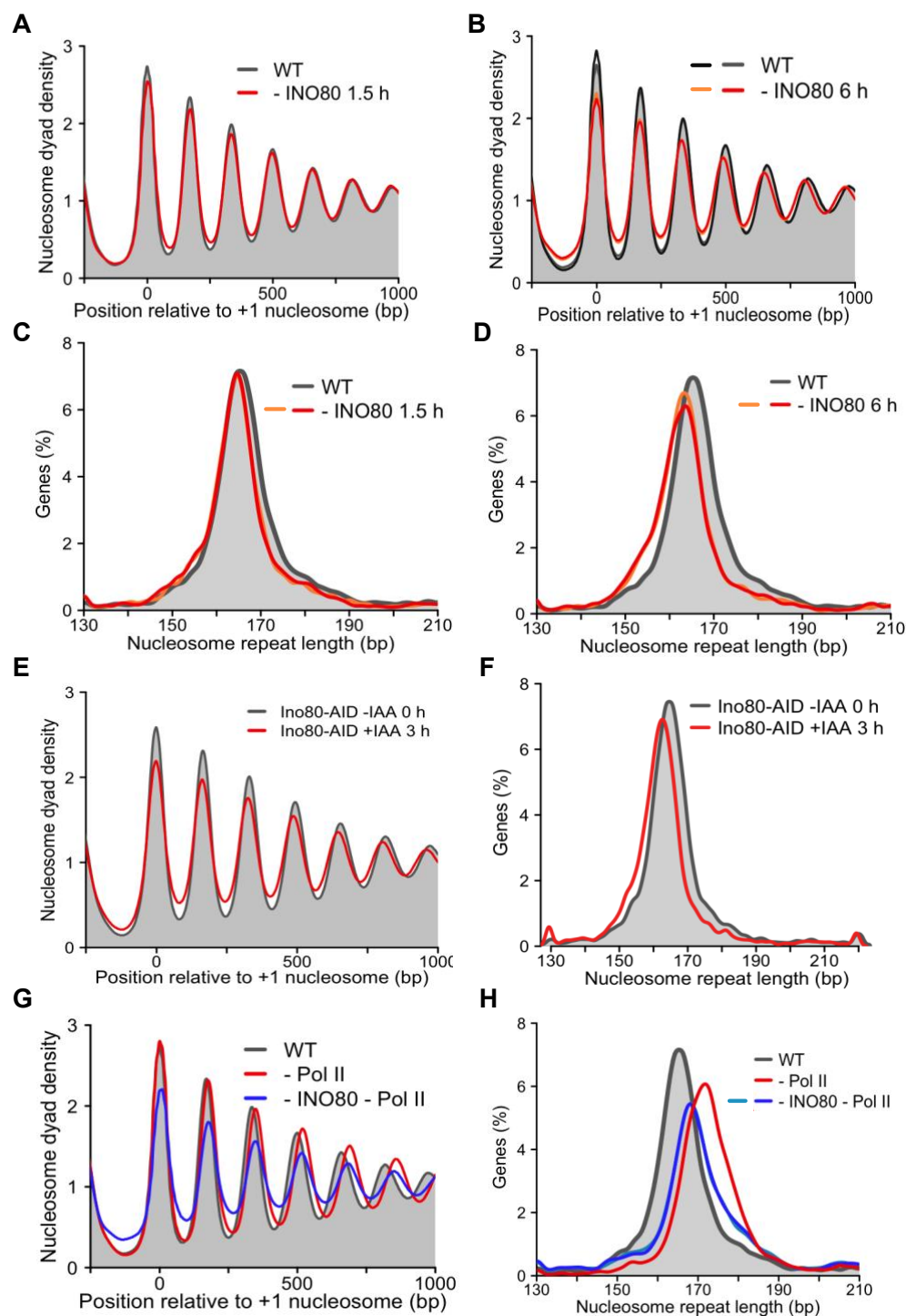


Figure 2.9: INO80 contributes to NRL and array regularity in WT and Pol II depleted cells. (A, B) Gene averaged nucleosome organization in WT and INO80 depleted for 1.5 and 6 h. Longer depletion shows a decrease in array regularity. **(C, D)** NRL distributions of samples in (A, B). Peak maxima are at 165 bp for controls, 164 bp for 1.5 h depletion and 162 bp for 6 h depletion, consistently in two biological replicates. **(E)** Gene averaged nucleosome organization in AID-tagged Ino80 cells treated with Indole-3-acetic acid (IAA) for 3 h. MNase-Seq data is from (Klein-Brill et al., 2019). **(F)** NRL distribution of samples in (E). **(G)** Composite plots showing nucleosome organization upon Pol II or combined Pol II and INO80 depletion for 2h. Combined Pol II and INO80 depletion show lower array regularity than WT and Pol II depleted cells. **(H)** NRL distribution of strains in (G). Peak maxima are at 165 bp for WT, 172 bp for Pol II depletion, and 168 bp for Pol II and INO80 double depletion. All

experiments were performed in two biological replicates, except only Pol II depletion for 2 h in WT background which was performed once. Shades of a color indicate two biological replicates.

similar results (Figure 2.9E, F) (Klein-Brill et al., 2019). Taken together, these results suggest that INO80 contributes to NRL determination and array regularity in WT cells. The decrease in NRL upon INO80 depletion is consistent with the 5' shifted nucleosomes in cells lacking the Ino80 ATPase (van Bakel et al., 2013; Yen et al., 2012).

Because INO80 generates longer NRL in WT cells, we hypothesized that the increased NRL upon Pol II depletion in WT cells (Figure 2.6F) is due to INO80. To test this, we double depleted Pol II and INO80 in WT cells. Consistent with this hypothesis, we found that INO80 is partially responsible for increased NRL upon Pol II depletion in WT cells (Figure 2.9H). The remaining increased NRL is likely from ISWI and Chd1 remodelers which are still present in the cell. Indeed, in cells lacking ISWI and Chd1 remodelers, double depletion of Pol II and INO80 showed no clear NRL peak (Figure 2.7D). We also observed a decrease in array regularity upon combined INO80 and Pol II depletion, compared to WT or only Pol II depletion (Figure 2.9G). This may hint at a role of INO80, besides ISWI and Chd1, towards organizing regular arrays in the wake of transcription (Smolle et al., 2013; Venkatesh and Workman, 2015).

Taken together, our results strongly suggest that INO80 can space nucleosomes and generates regular arrays *in vivo*. INO80 also contributes to NRL and array regularity in WT cells. These results extend the family of spacing remodelers to INO80, in addition to already well-established ISWI and Chd1 remodelers.

2.1.6 Spacing remodelers generate nucleosome arrays at replication origins

Yeast origins have well-positioned nucleosomes flanking the Origin Recognition Complex (ORC) binding sites (Berbenetz et al., 2010; Eaton et al., 2010). How this organization is generated is completely unknown. ISWI, Chd1 and INO80 spacing remodelers could conceivably help in this organization. ISW2 and INO80 remodelers have specifically been shown to help in replication *in vitro* and *in vivo* (Kurat et al., 2017; Vincent et al., 2008). Like promoters, ORC binding sites in *S. cerevisiae* are AT-rich which disfavors nucleosome formation (Berbenetz et al., 2010). The RSC remodeler may thus use these sequence clues to enhance nucleosome depletion at the ORC binding sites. Spacing remodelers were also recently shown to establish different nucleosome organization around replication origins *in vitro* (Azmi et al., 2017).

To test the role of nucleosome remodelers at replication origins *in vivo*, we aligned MNase profiles relative to the ORC binding sites, so called ACS (ARS1 consensus sequence) (Soriano et al., 2014). Single deletion or depletion of ISW1, ISW2, Chd1 and INO80 remodelers showed a negligible change in nucleosome organization (Figure 2.10A – D). This is consistent with the minor effect of individual spacing remodelers at the TSS-aligned nucleosome arrays around promoters, likely due to high redundancy of spacing remodelers (Gkikopoulos et al., 2011; Ocampo et al., 2016). Depletion of the RSC remodeler led to a shift of nucleosomes towards the replication origin, suggesting RSC helps clear NFR and slides nucleosomes away from the replication origin. This activity may be essential for ORC binding.

Moreover, nucleosome arrays became slightly better than WT, suggesting RSC destroys regular arrays near replication origins (Figure 2.10E).

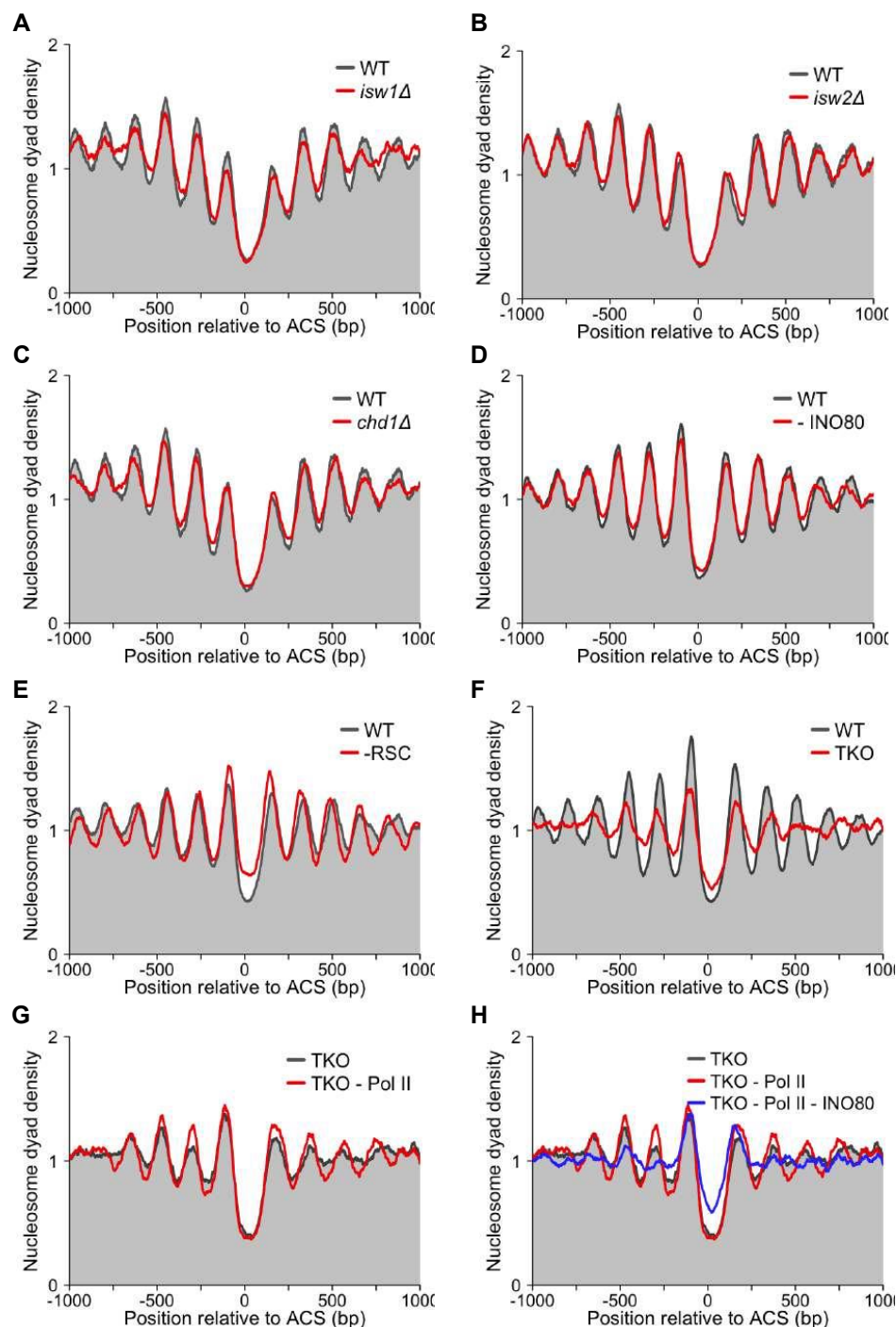


Figure 2.10: Spacing remodelers generate nucleosome arrays at replication origins. (A, B, C, D) Gene averaged nucleosome organization at replication origins in WT and single deletions of *ISW1*, *ISW2* and *CHD1* and depletion of *INO80*. MNase-Seq data are aligned to 316 *ARS1* containing sites (ACS) obtained from (Soriano et al., 2014). MNase-Seq data for *isw1Δ*, *isw2Δ* and *chd1Δ* is from (Ocampo et al., 2016). **(E)** Same as (A) but for RSC depleted cells. Data is from (Ganguli et al., 2014). **(F)** Same as (A) but for TKO cells. **(G)** Same as (A) but for Pol II depleted TKO cells. **(H)** Same as (A) but for Pol II and *INO80* depleted cells in the TKO background.

We next investigated nucleosome organization in the TKO strain which has highly reduced redundancy of the spacing remodelers. We found that the combined deletion of ISWI and Chd1 remodelers dramatically reduces nucleosome arrays and positioning of the +1-nucleosome (Figure 2.10F). This result suggests that ISWI and Chd1 remodelers have a major role in establishing the +1-nucleosome and nucleosome arrays around replication origins.

To isolate the role of INO80 in this process, we exploited the TKO strain with Pol II depletion system, where INO80 activity can be cleanly isolated from other redundant activities. We found that INO80 generates residual arrays and Pol II overrides this organization also at replication origins (Figure 2.10G, H). This result suggests that transcription machinery also affects nucleosome organization at replication origins, likely by disrupting ORC binding and regular arrays (Candelli et al., 2018). Furthermore, we also observed increased nucleosome signal at the ACS (Figure 2.10E, F, H), suggesting that the ISWI, Chd1 and INO80 remodelers also clear ACS from nucleosomes, which may help facilitate ORC loading.

Overall, these analyses suggest that the spacing remodelers, RSC and transcription machinery play an important role in clearing ORC binding sites and establishing nucleosome organization at replication origins. They perform similar roles at replication origins as near gene promoters.

2.1.7 The Arp8, but not the Nhp10, module regulates NRL in the INO80 spacing remodeler

In section 2.1.5, we found that INO80 can space nucleosomes *in vivo*. We asked how does INO80 space nucleosomes? Structural and functional studies on the yeast INO80 have shown that the complex is composed of three major modules: Nhp10, Arp8 and Arp5 module (Figure 2.11A) (Eustermann et al., 2018; Sardiù et al., 2017; Tosi et al., 2013). The Arp8 and Arp5 modules are evolutionarily conserved from yeast to human and plants (Chen et al., 2011; Hogan et al., 2010; Jin et al., 2005; Klymenko et al., 2006; Shen et al., 2000; Wang et al., 2019a), while the Nhp10 module is yeast specific (Hogan et al., 2010; Tosi et al., 2013). The Arp5 module is a central component of the INO80 remodeler, regulates ATP hydrolysis and is essential for nucleosome sliding (Chen et al., 2013b; Eustermann et al., 2018; Shen et al., 2003; Tosi et al., 2013; Watanabe et al., 2015; Yao et al., 2015; Yao et al., 2016). On the other hand, Arp8 and Nhp10 modules modulate nucleosome binding and sliding efficiency of the INO80 complex (Knoll et al., 2018; Shen et al., 2003; Tosi et al., 2013; Watanabe et al., 2015).

Nhp10 module: The Nhp10 module consists of Nhp10, Ies1, Ies3 and Ies5 subunits and assembles over the N-terminus of the Ino80 ATPase subunit (Figure 2.11A) (Shen et al., 2003; Tosi et al., 2013). Deletion of *NHP10* removes all other subunits of the Nhp10 module from the INO80 complex and destabilizes the N-terminus of the Ino80 ATPase *in vitro* (Zhou et al., 2018). Conversely, deletion of the N-terminus (amino acids 2-200) from the Ino80 ATPase removes all subunits of the Nhp10 module from the complex (Papamichos-Chronakis et al., 2006; Zhou et al., 2018). Nhp10 module was recently shown to regulate the switch-like response of the INO80 complex. Yeast INO80 complex requires at least 60 bp linker DNA to

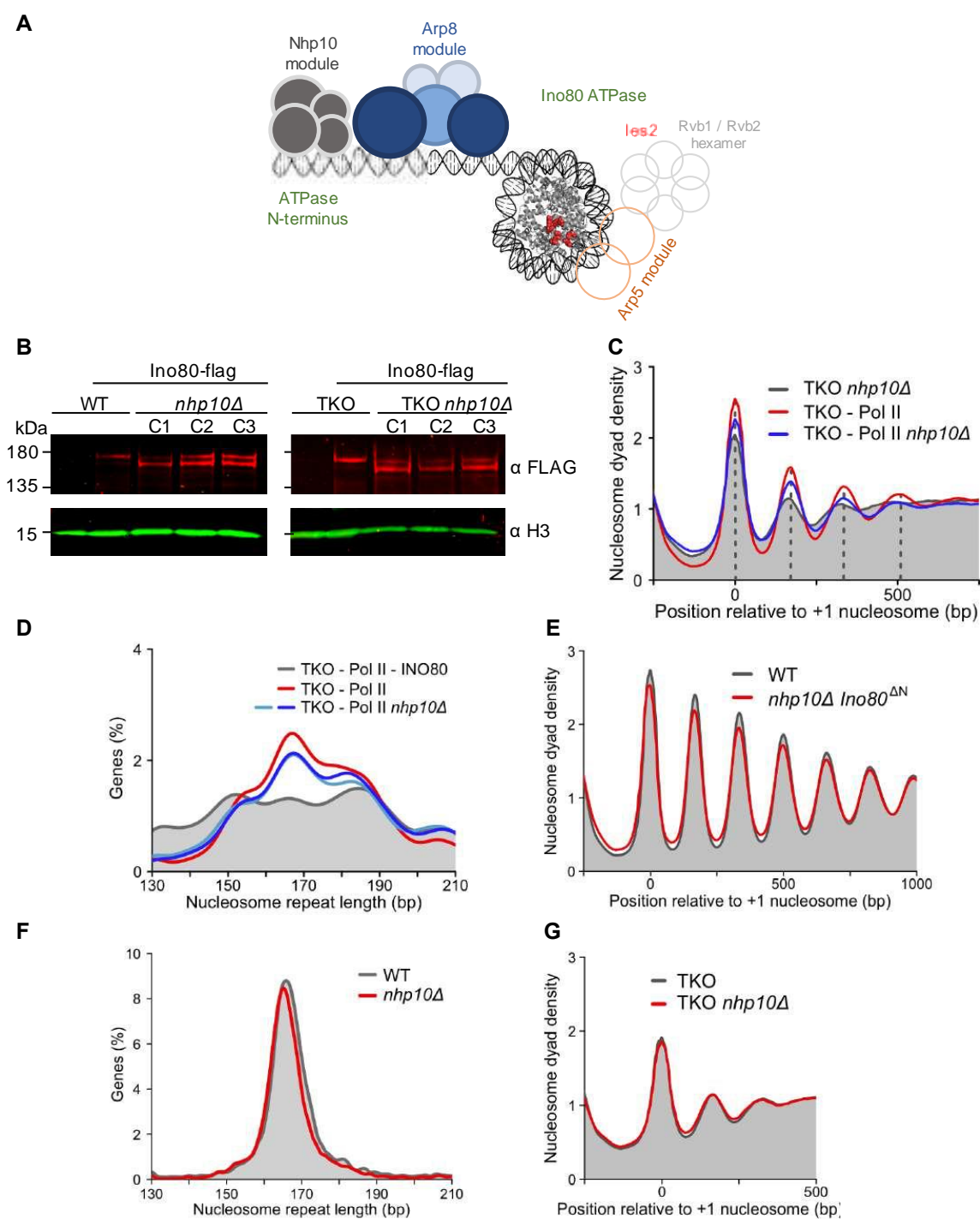


Figure 2.11: The Nhp10 module in the INO80 remodeler has a negligible role in nucleosome organization *in vivo*. (A) Model of the yeast INO80 remodeler bound to a nucleosome. (B) Western blot showing a degradation of the Ino80 ATPase upon *NHP10* deletion in WT and TKO backgrounds. The Ino80 ATPase is C-terminally FLAG-tagged. C1 – 3 indicates three colonies tested. Histone 3 is used as a loading control. (C) Gene averaged nucleosome organization upon *NHP10* deletion in the Pol II depleted TKO strain. Nucleosomes positions does not change with or without Nhp10 (dashed lines). (D) NRL distribution in cells with WT INO80 and INO80 *nhp10Δ* complex in the Pol II depleted TKO background. Cells lacking the INO80 complex served as a negative control. Shades of blue represent two biological replicates. (E) Gene averaged nucleosome organization in WT and *nhp10Δ* cells. (F) NRL distribution in WT and *nhp10Δ* cells. (G) Same as (E) but in the TKO background. All experiments were performed in at least two biological replicates. (Singh et al., unpublished).

efficiently slide end-positioned nucleosomes to the center of DNA. On the other hand, INO80 complex lacking the Nhp10 module can readily slide nucleosomes with only 40 bp (Udugama et al., 2011; Zhou et al., 2018). This suggests that the Nhp10 module is involved in linker length sensing of the INO80 complex and makes it the prime candidate for regulating nucleosome spacing *in vivo*.

We first tested if deletion of *NHP10* destabilizes the N-terminus of the Ino80 ATPase *in vivo*. Indeed, the deletion of *NHP10* degraded the N-terminus of the Ino80-ATPase as evident by a low molecular weight band in western blot (Figure 2.11B). To test the role of Nhp10 module in nucleosome spacing *in vivo*, we exploited the Pol II depleted TKO system, which cleanly shows INO80 activity. Surprisingly, INO80 lacking the Nhp10 module can generate nucleosome arrays with similar NRL as the WT INO80 complex (both peaks at 167 bp), challenging the hypothesis that the Nhp10 module critically regulates nucleosome spacing in the INO80 complex (Figure 2.11C, D). The nucleosome array and positioning of individual nucleosomes were mildly decreased. Deletion of *NHP10* in WT (peaks at 164 bp in *nhp10Δ* vs 165 bp in WT) and TKO strain also showed a negligible effect in both nucleosome positioning and NRL (Figure 2.11E – G). We also reanalyzed published *nhp10Δ* dataset, used for rDNA locus study, and found no change, consistent with our results (not shown) (Cutler et al., 2018).

To further test the role of Nhp10 module, we deleted amino acids 1-300 from the Ino80 ATPase. This specific deletion was previously suggested to inactivate the complete INO80 complex (Papamichos-Chronakis et al., 2006). To test if deletion of amino acids 1-300, including the start codon, abrogates expression of the ATPase subunit, we first FLAG-tagged C-terminus of the Ino80 ATPase and performed western blot. We found that the amino acids 1-300 lacking construct still expresses the truncated construct (Figure 2.12A). The expression of the truncated construct is ~3-fold higher than the WT construct.

We used this construct to test the role of N-terminus in nucleosome spacing *in vivo*. Deletion of the N-terminus of Ino80 showed a negligible change in nucleosome array and NRL genome-wide in WT cells (peaks at 166 bp in mutant vs 165 bp in WT) (Figure 2.12B, C). Similar deletion in TKO also had no effect (Figure 2.12D). These results suggest that the N-terminus of Ino80 ATPase has a negligible role in genome-wide array regularity and NRL determination *in vivo*. This is also in line with negligible role of the Nhp10 module shown above. Lastly, to rule out any compensatory effect of the N-terminus or the Nhp10 module in presence of the other module, we double deleted the N-terminus of Ino80 ATPase and *NHP10* in the same cell. This mutant as well showed no effect on array regularity and NRL (0 bp difference compared to WT) (Figure 2.12E – G).

Overall, these results in three different strain backgrounds conclusively show that the Nhp10 module and the N-terminus of the Ino80 ATPase has no role in nucleosome spacing and array regularity *in vivo*.

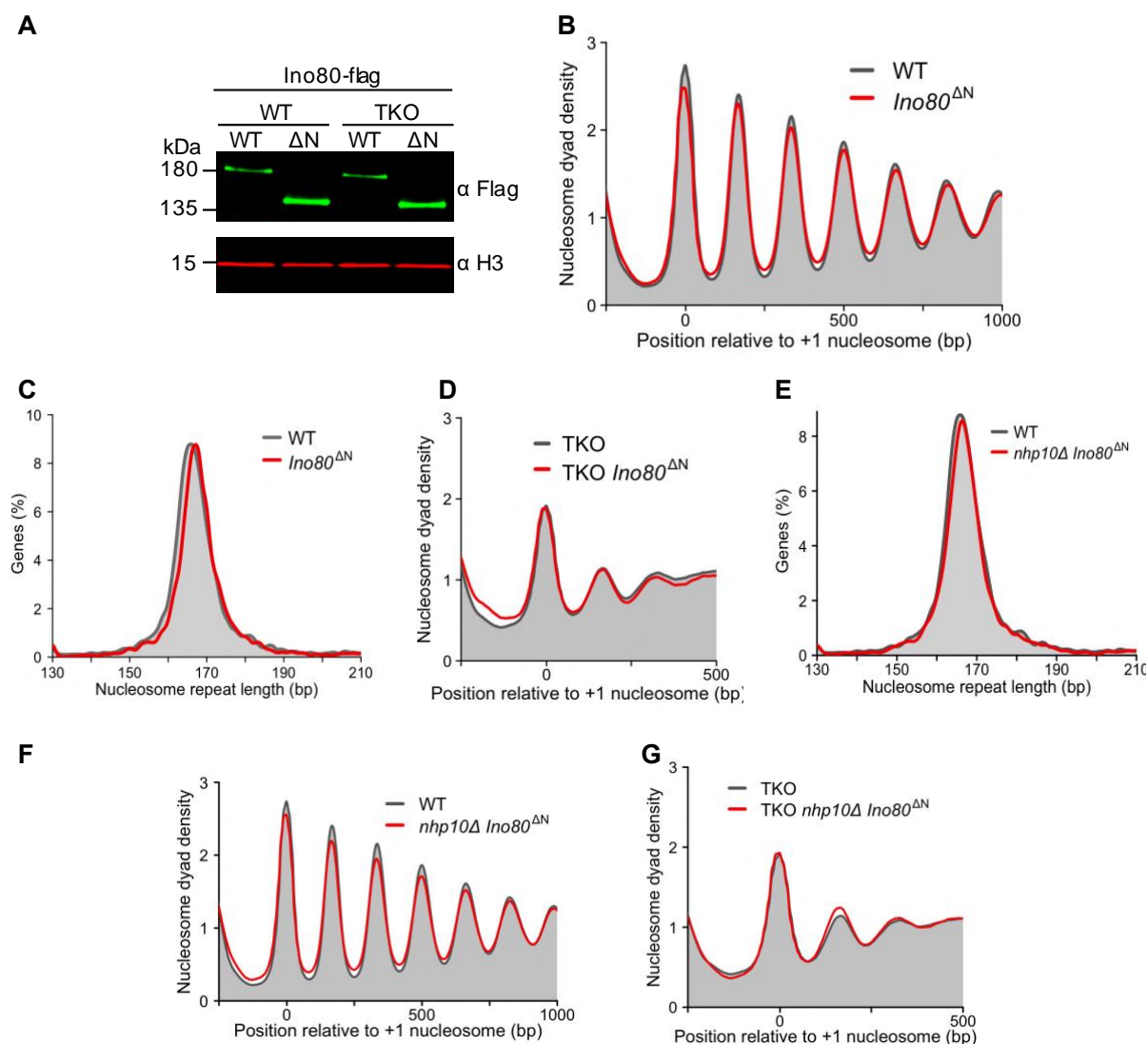


Figure 2.12: The N-terminus of the Ino80 ATPase has a negligible role in nucleosome organization *in vivo*. (A) Western blot showing expression of the Ino80 ATPase upon N-terminus deletion in WT and TKO backgrounds. Ino80 ATPase is C-terminally FLAG-tagged. Histone 3 served as a loading control. (B) Gene averaged nucleosome organization upon deletion of the N-terminus in the Ino80 ATPase. (C) NRL distribution in cells in (B). (D) Same as (B) but in the TKO background. (E) NRL distribution in cells with combined *NHP10* and N-terminus deletion. (F) Composite plot showing nucleosome organization in cells lacking Nhp10 and the Ino80 ATPase N-terminus. (G) Same as (F) but in the TKO background. Average of two biological replicates is shown for MNase-Seq experiments. (Singh et al., unpublished).

Arp8 module: The Arp8 module consists of Arp8, Arp4, Actin, les4 and Taf14 subunits. It assembles over the helicase/SANT-associated (HSA) domain in the Ino80 ATPase subunit. Deletion of the *ARP8* leads to loss of all subunits of the Arp8 module from the INO80 complex (Shen et al., 2003; Tosi et al., 2013; Watanabe et al., 2015). Arp8 module crosslinks to the linker DNA both *in vitro* and *in vivo* (Brahma et al., 2018; Knoll et al., 2018; Yen et al., 2013), suggesting it may be able to sense linker DNA. The INO80 complex lacking the Arp8 subunit can still slide mononucleosomes, but with reduced activity compared to the WT complex (Shen

et al., 2003; Tosi et al., 2013; Watanabe et al., 2015). Therefore, we hypothesized that the Arp8 module regulates the spacing activity of the INO80 complex.

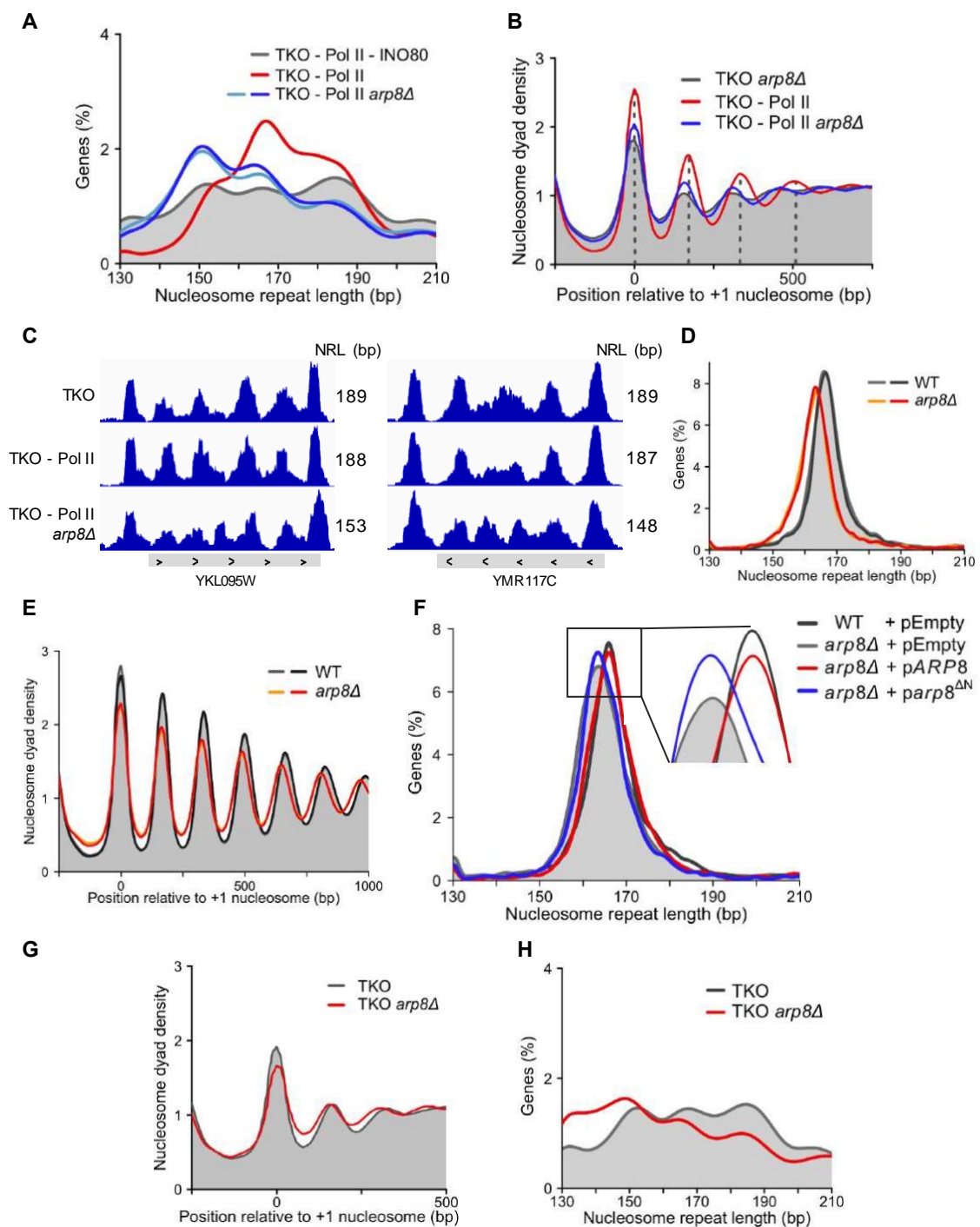


Figure 2.13: The Arp8 module determines NRL in the INO80 complex. (A) NRL distribution in cells with WT INO80 or INO80 *arp8Δ* complex in the Pol II depleted TKO strain. Peak maxima are at 168 bp for WT INO80 and 151 bp for INO80 *arp8Δ* complex. Grey background shows NRL distribution in cells depleted with the INO80 complex. Shades of blue represent two biological replicates. (B) Gene averaged nucleosome organization upon *ARP8* deletion in the Pol II depleted TKO background. *ARP8* deletion leads to a lower NRL (dashed lines). (C) IGV browser shots showing lower NRL upon *ARP8* deletion in individual genes. (D) NRL distribution in WT and cells lacking *ARP8*. Peak maxima are at 166 bp for WT and 163 for *arp8Δ* cells. Shades of orange represent two biological replicates. (E) Gene averaged nucleosome organization in *arp8Δ* cells. Shades of red indicate two biological replicates. (F)

NRL distribution in *arp8Δ* cells expressing WT or the N-terminus (amino acids 2 – 197) lacking Arp8 protein for the pRS413 plasmid. WT and *arp8Δ* cells are transformed with an empty pRS413 plasmid. **(G)** Composite plot showing nucleosome organization upon *ARP8* deletion in the TKO background. **(H)** NRL distribution in cells lacking Arp8 in the TKO background. All experiments were performed using two colonies as biological replicates. Individual replicates are shown as shades of colors. (Singh et al., unpublished).

To test this, we deleted *ARP8* in TKO and depleted Pol II to find the mutant INO80 complex activity. We found that the INO80 complex lacking the Arp8 subunit is severely impaired in nucleosome array formation. Nevertheless, the resulting low levels of nucleosome arrays had 16 bp shorter NRL than the cells with the WT INO80 complex (peaks at 151 bp for mutant vs 167 bp for WT) (Figure 2.13A – C). Importantly, the arrays and the NRL generated by the INO80 *arp8Δ* complex is distinct from cells lacking the complete INO80 complex, ruling out that the INO80 *arp8Δ* complex is catalytically dead (Figures 2.7C, D and 2.13A). These results suggest that the Arp8 module regulates the INO80 nucleosome spacing activity. In the absence of Arp8, the mutant INO80 complex can still slide nucleosomes *in vivo* but with defective linker length sensing. The INO80 *arp8Δ* complex generates shorter NRL than the WT INO80 complex (Figure 2.13A).

To test if the INO80 complex lacking Arp8 generates short linkers also in cells with active transcription, we deleted *ARP8* in WT and TKO cells. Consistent with the results in the Pol II depleted TKO strain, deletion of *ARP8* showed impaired arrays and decrease in NRL in both WT and TKO strains. In WT cells, *ARP8* deletion leads to 3 bp shorter NRL (consistently in two biological replicates) (Figure 2.13D – E). In TKO cells, more genes attained shorter NRL upon *ARP8* deletion (Figure 2.13G, H). These results suggest that the Arp8 module is important for linker length sensing and NRL determination in the INO80 complex.

The Bartholomew lab recently showed that the N-terminus of Arp8 specifically crosslinks to the linker DNA. Deletion of the N-terminus of Arp8 leads to reduced sliding on a mononucleosome template *in vitro* (Brahma et al., 2018). We hypothesized that the N-terminus may regulate Arp8 linker length sensing activity. To test this, we performed complementation experiments in *arp8Δ* in an otherwise WT cell. We expressed either the WT Arp8 or the Arp8 protein lacking amino acids 2-197 under the native promoter on a plasmid. The 3 bp decrease in NRL upon *ARP8* deletion in the WT background could be rescued upon expression of the WT Arp8 protein, suggesting a direct effect of Arp8 and not from secondary effects or mutations. Consistent with our hypothesis, the Arp8 lacking its N-terminus could not complement and remained the same as the Arp8 lacking cells (Figure 2.13F). This result substantiates the importance of the N-terminus of Arp8 for INO80 activity *in vivo* and suggests that the N-terminus of Arp8 regulates INO80 spacing activity *in vivo*. Overall, we conclude that the Arp8 module regulates INO80 spacing and it needs its N-terminus for this activity.

Arp5 module: The Arp5 module consists of Arp5 and Ies6 (Shen et al., 2003; Tosi et al., 2013; Watanabe et al., 2015). These subunits form the central remodeling core of the INO80 remodeler. *ARP5* deletion is lethal in our strain background (W303), like the Ino80 ATPase subunit (Grava et al., 2000). Deletion of *IES6* makes cells severely sick (Figure 2.14C) (Chambers et al., 2012), consistent with its essential role in the INO80 complex. Deletion of

ARP5 subunit in the S288c background leads to loss of *les6* subunit and vice versa (Shen et al., 2003; Yao et al., 2015). *In vitro*, Arp5 and *les6* subunits are required for coupling ATP hydrolysis to nucleosome sliding (Tosi et al., 2013; Willhoft et al., 2016; Yao et al., 2016).

Since *IES6* deletion is not lethal in our strain background, we performed MNase-Seq to map nucleosome position in an otherwise WT cell. The INO80 complex lacking the *les6* subunit cannot slide nucleosomes *in vitro* (Yao et al., 2016). Therefore, it can be a proxy to detect INO80 sliding related functions *in vivo*. We found that *IES6* deletion leads to decreased array regularity and NRL. The NRL decreased by 2 bp genome-wide, largely consistent with 3 bp shorter NRL in the Ino80 depleted cells (Figure 2.14A, B). This result confirms that INO80 remodeler has a role in nucleosome positioning and spacing *in vivo*.

To test the role of *les6* subunit without redundancy of ISWI and Chd1 remodelers, we attempted to delete *IES6* in the TKO background. We could not delete *IES6* via direct transformation in two attempts. Therefore, we tested the viability of cells lacking *les6* in the TKO background via haploid mating and tetrad dissection. We found that *IES6* deletion is synthetic lethal with *ISW2* or *CHD1* deletion, but not with *ISW1* deletion (Figure 2.14C, D). This result suggests that *ISW2*, *Chd1* and INO80 remodelers' function in redundant pathways.

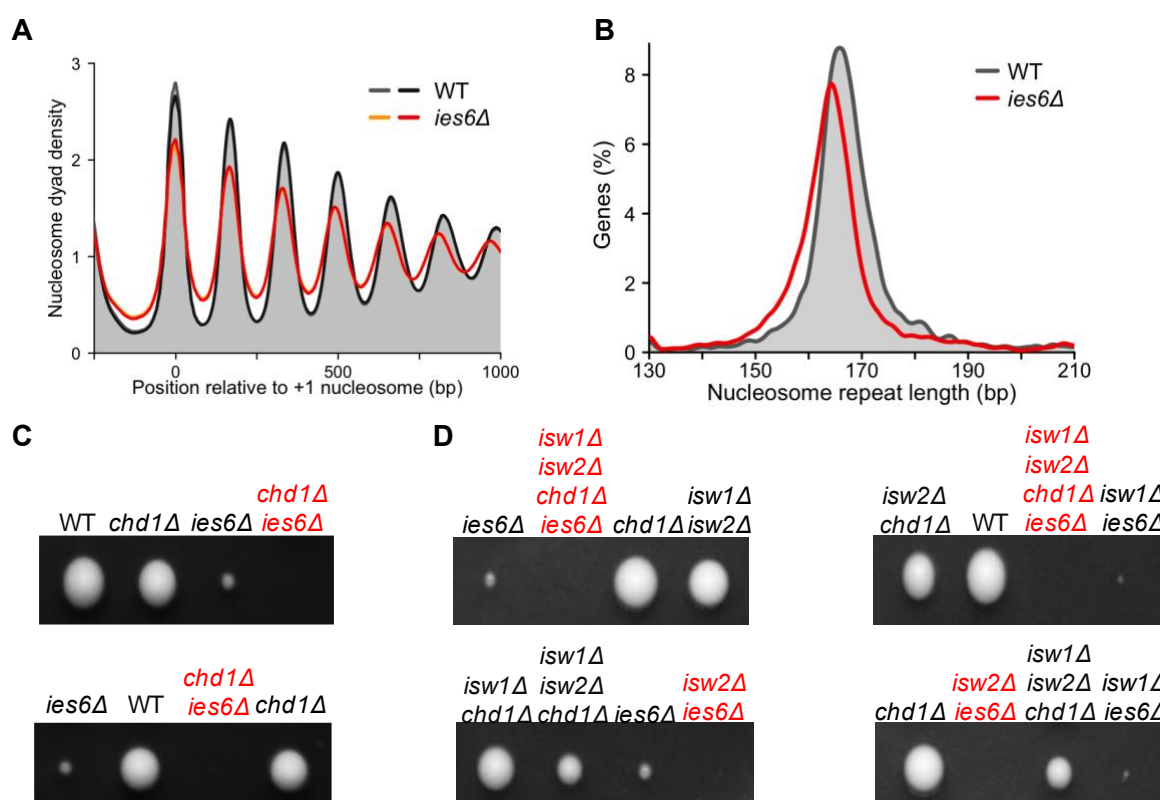


Figure 2.14: The *les6* subunit has an essential role in INO80 dependent nucleosome organization and cell growth. (A) Gene averaged nucleosome organization in *ies6Δ* cells. *IES6* deletion leads to reduced nucleosome array regularity compared to WT. Shades of orange indicate two biological replicates. **(B)** NRL distribution in *ies6Δ* cells. Peak maxima for *ies6Δ* cells is at 164 bp and at 166 bp for WT. **(C)** Tetrad dissection of diploids obtained from mating of *ies6Δ* and *chd1Δ* strains. **(D)** Tetrad dissection of diploids generated by mating TKO with *ies6Δ* cells.

les2 subunit: Lastly, we tested the role of *les2* subunit. *les2* is required for Arp5-*les6* module association in the yeast INO80 complex. *IES2* deletion also abolishes ATPase activity in the INO80 complex (Willhoft et al., 2016; Yao et al., 2015). Recent structural data showed that the *les2* subunit interacts with the H2A-H2B acidic patch on the nucleosome (Eustermann et al., 2018). The Narlikar lab showed that mutations in the nucleosome acidic patch massively reduce INO80 sliding *in vitro* (Gamarra et al., 2018). This reduced activity could arise from regulation of INO80 sliding activity by *les2* via the nucleosome acidic patch.

IES2 could be readily deleted in all our genetic backgrounds despite INO80 being essential in our strain background. It had a negligible effect on cell growth and array regularity in both WT and TKO strains (Figure 2.15A, B, D). Nevertheless, cells lacking *les2* consistently showed 2 bp shorter NRL compared to WT (Figure 2.15C). These results suggest that the INO80 *ies2* Δ complex can slide nucleosomes and generate regular arrays, but with shorter than WT INO80 NRL.

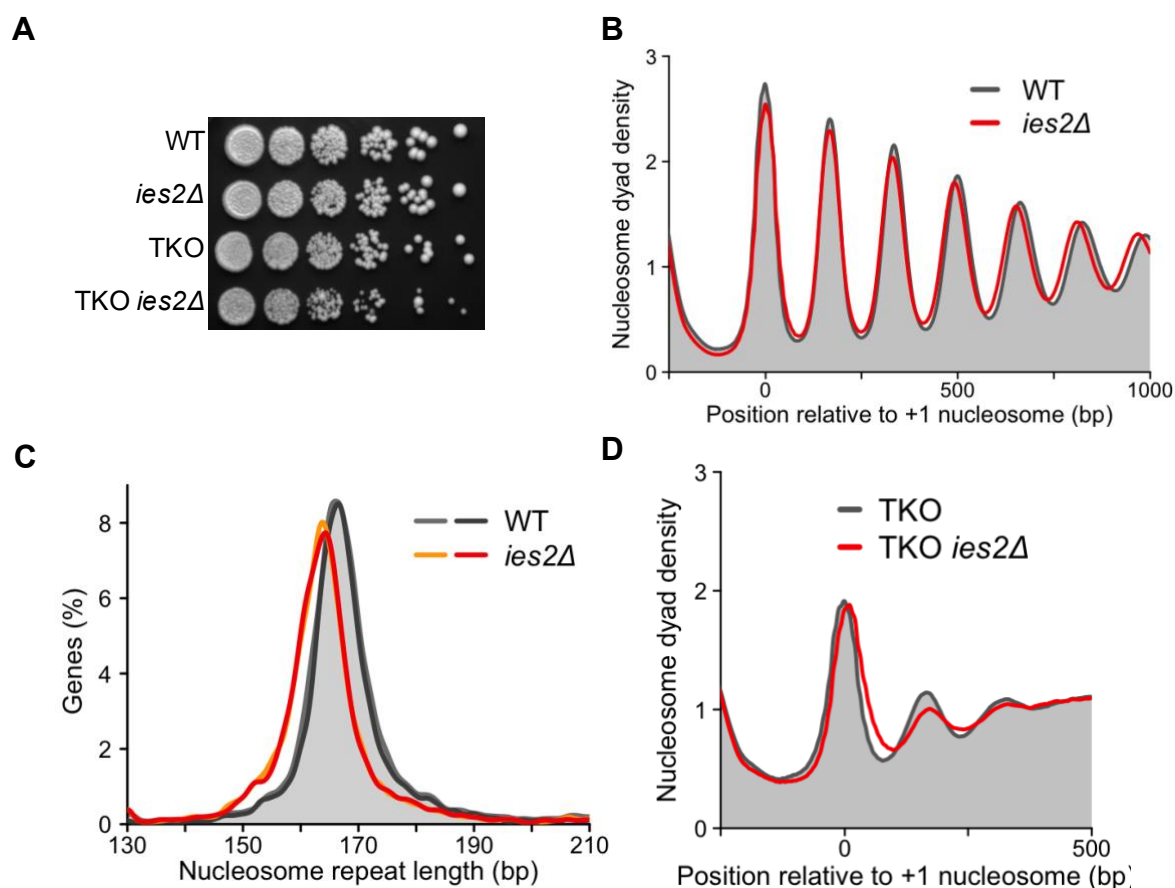


Figure 2.15: The *les2* subunit in the INO80 complex is dispensable for cell growth and array regularity. (A) Growth assay showing a negligible effect of *IES2* deletion in WT and TKO backgrounds. Shown are 10-fold dilutions. (B) Gene averaged nucleosome organization upon *IES2* deletion. *IES2* deletion has no impact on nucleosome arrays. (C) NRL distribution in *ies2* Δ strain with peak maxima at 164 bp. WT peaks are at 166 bp for both replicates. Shades of orange represent two biological replicates. (D) Same as (B) but in the TKO background. All experiments were performed with at least two colonies acting as biological replicates. Either merged or individual replicates are shown as shades of orange.

Overall, the results presented here regarding subunits, domains and modules of the INO80 complex substantially increase our understanding of the INO80 spacing mechanism *in vivo*. Importantly, our results show consistent trends irrespective of the strain background. The effect size indeed varies depending upon the redundancy of spacing remodelers in the strain. Unexpectedly, we found that the Nhp10 module has no role in nucleosome spacing *in vivo* at the genome-wide level. The Arp8 module emerges as an important regulatory subunit for the INO80 spacing function. The Ies2 subunit also has a role in this regard, likely via the nucleosome acidic patch.

We formally cannot rule out that the observed decrease in array regularity and NRL in INO80 mutant cells is due to defects in cell cycle in these cells. It is known that cells lacking the Ino80 ATPase or the Arp8 subunit have a delay in S-phase compared to WT cells (Papamichos-Chronakis and Peterson, 2008; Shimada et al., 2008). On the other hand, cell-cycle dependent nucleosome positioning data does not show any change in NRL in the S-phase compared to G1 and G2/M phases of cell cycle (Deniz et al., 2016). This observation suggests the observed decrease in NRL in the INO80 mutants is not due to cell-cycle defects.

2.1.8 INO80 positions the +1-nucleosome in a H2A.Z-independent manner

The INO80 complex was recently shown to position the +1-nucleosome using *in vitro* reconstitution experiments (Krietenstein et al., 2016). Our Pol II depletion experiment in TKO showed a higher +1-nucleosome peak compared to the TKO control in the composite plots (Figure 2.7A – C). This increase is dependent on the INO80 complex, suggesting INO80 has a role in positioning the +1 nucleosome *in vivo*. INO80 depletion in WT and TKO also increased fuzziness of the +1-nucleosome, corroborating INO80 positions the +1-nucleosome *in vivo* (Figures 2.8A and 2.9B, E, G). To further substantiate this observation, we measured the +1-nucleosome fuzziness at each gene using DANPOS (Chen et al., 2013a). This analysis confirmed that INO80 positions the +1-nucleosome at the genome-wide level (Figure 2.16A, B). Besides INO80, we found that the TKO cells also have an increased +1-nucleosome fuzziness compared to WT, both in composite plot and at each gene level (Figures 2.5A, B and 2.16C). This result suggests that the ISWI and Chd1 remodelers also have a role in the +1-nucleosome positioning genome-wide.

Histone variant H2A.Z is strongly enriched at the +1-nucleosome (Albert et al., 2007; Raisner et al., 2005). Pol II depletion further enriches H2A.Z at the +1-nucleosome (Tramantano et al., 2016). *In vitro* observations from three different laboratories showed that INO80 slides H2A.Z-nucleosomes 2-4 fold faster than the canonical nucleosomes (Brahma et al., 2017; Eustermann et al., 2018; Willhoft et al., 2016). Based on these observations, we hypothesized that INO80 recognizes H2A.Z and, thereby help position the +1-nucleosome. This effect should be best visible upon Pol II depletion in TKO, which cleanly detects INO80 activity.

In contrast to the hypothesis, deletion of *HTZ1* (*S. cerevisiae* H2A.Z) showed no change in the +1-nucleosome position (Figure 2.16D, F). Independent validation of the result by deleting SWR1 remodeler, which is known to deposit H2A.Z, also showed no change (Figure 2.16E, F). Further, *HTZ1* deletion also did not affect the +1-nucleosome near replication origins,

which is also enriched in H2A.Z (Figure 2.16G). We concluded that the INO80 positioning activity at the +1 nucleosome is independent of H2A.Z.

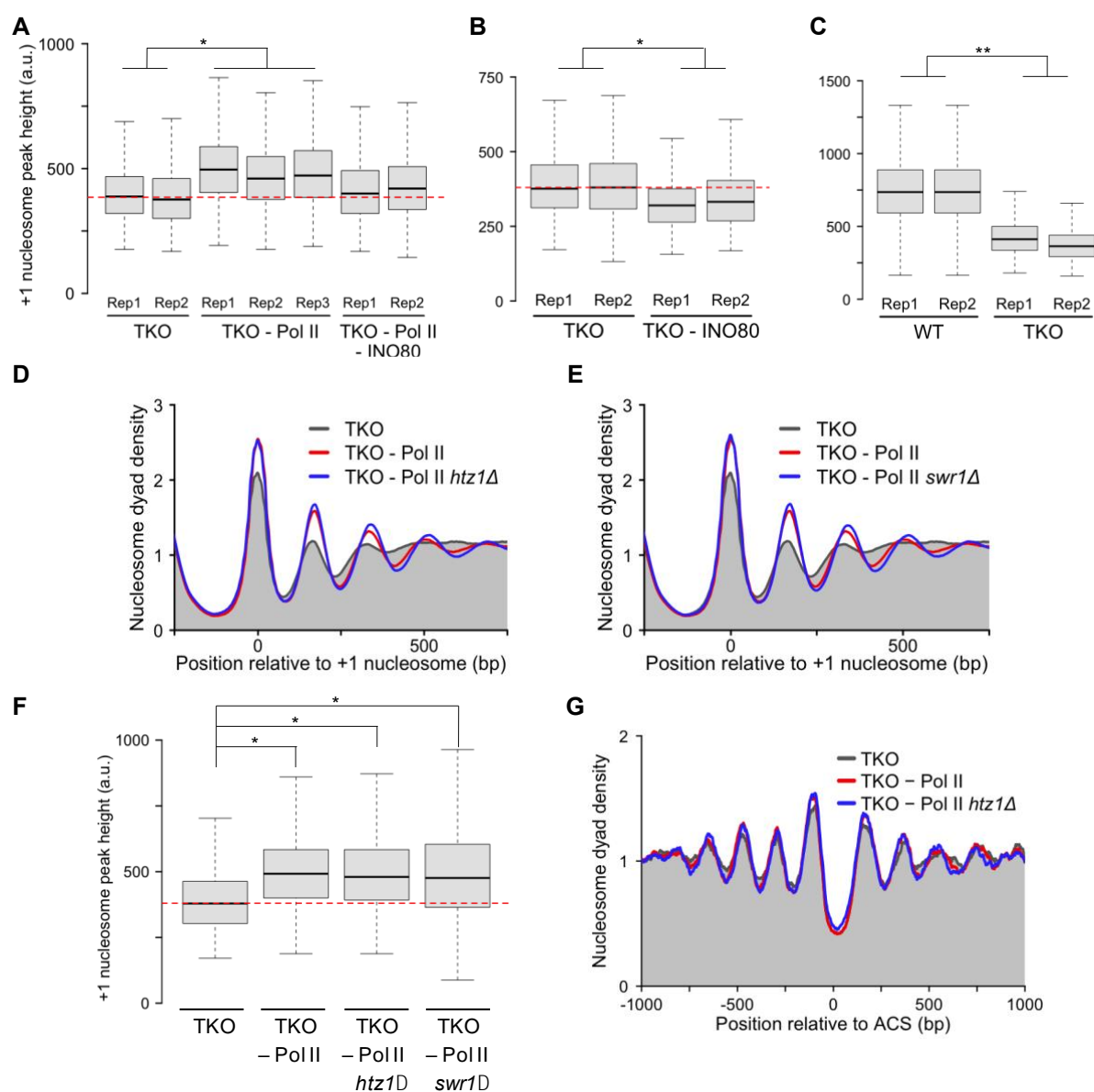


Figure 2.16: INO80 positions the +1-nucleosome independent of the histone variant H2A.Z. (A)

Peak height distribution of the first nucleosome after NFR in ~5000 genes. Pol II depletion in the TKO background leads to better positioned +1 nucleosome. Double depletion of Pol II and INO80 remained similar to TKO. **(B)** INO80 depletion in TKO leads to lower peak height, suggesting increased fuzziness of +1 nucleosome. **(C)** TKO shows increased nucleosome fuzziness compared to WT. This trend is independent of strain background (not shown). **(D)** Gene averaged nucleosome organization upon H2A.Z (Htz1 in yeast) deletion in the Pol II depleted TKO strain. +1 nucleosome fuzziness remained the same with or without H2A.Z upon Pol II depletion. **(E)** Same as (D) but for Swr1 deletion. **(F)** Peak height distribution of the first nucleosome after NFR in ~5000 genes from samples in (D, E). **(G)** Same as (D) but MNase-Seq data is aligned at replication origins. Statistical analyses in (A, B, C, F) were performed using paired t-test on mean values of at least two biological replicates. * $P < 0.05$, ** $P < 0.01$, *** $P < 0.001$. (Singh et al., unpublished).

2.1.9 The DNA sequence contributes to NRL determination

The position of the +1-nucleosome is considered to be partially encoded by the DNA sequence favoring nucleosome formation and stability (Ioshikhes et al., 2006; Satchwell et al., 1986; Travers et al., 2010). To decipher how nucleosome remodelers influence the position of the +1-nucleosome, we calculated peak-to-peak distance between the predicted nucleosome position and the *in vivo* nucleosome position in WT and remodeler mutants. We found that in WT cells, the +1-nucleosome is 17 bp downstream shifted relative to the most preferred position based on the DNA sequence. This is due to the RSC remodeler as depletion of RSC shifts nucleosomes within 1 bp distance of the DNA sequence-preferred position (Figure 2.17A) (Ganguli et al., 2014). Cells lacking ISWI and Chd1 remodelers showed no change in position compared to WT, suggesting ISWI and Chd1 do not contribute to this process at the global level. Curiously, depletion of INO80 in TKO cells shifted nucleosomes by 10 bp into the gene body (Figure 2.17A). This result suggests that the INO80 and RSC remodelers engage in a tug-of-war to position the nucleosome relative to DNA sequence. INO80 slides nucleosomes towards the promoter while RSC slides it away from the promoter region.

The contribution of the DNA sequence towards nucleosome positioning has been controversial. It was proposed initially that the DNA sequence determines nucleosome organization in most parts of the yeast genome (Field et al., 2009; Field et al., 2008; Kaplan et al., 2010; Kaplan et al., 2009; Segal et al., 2006). Later studies showed that nucleosome positions are majorly determined by nucleosome remodelers, and the DNA sequence is less influential (Zhang et al., 2009; Zhang et al., 2011). In this context, we tested if the DNA sequence has a role in nucleosome array formation and specifically in NRL determination.

To this end, we calculated nucleosome positions for the whole yeast genome using a recently published software (Kato et al., 2019). Previous nucleosome affinity calculations were restricted to -931 to -528 bp relative to the start codon of genes (Ioshikhes et al., 2006). Therefore, we re-calculated nucleosome affinity to the DNA sequence of the whole gene and aligned it to the *in vivo* +1-nucleosome position. Next, we sorted the MNase-Seq data of WT cells by NRL in each gene and divided into quartiles (Figure 2.17B). We then compared the MNase-Seq data to the DNA sequence predicted nucleosome organization in each quartile. Intriguingly, all quartiles showed peaks based on the DNA sequence representing individual nucleosomes in the gene body (Figure 2.17B, D). These peaks overlapped remarkably in 3 out of 4 quartiles (Q2 – 4) with the nucleosome positions observed *in vivo* (Figure 2.17D). We observed similar trends for first 3 nucleosomes when we used previously published nucleosome predictions (Figure 2.18A, B) (Ioshikhes et al., 2006). These results suggest that the DNA sequence has a role in determining NRL in most part of the genome.

Based on these results, we hypothesized that in TKO cells nucleosomes should attain more DNA sequence-preferred position than in WT. Therefore, we sorted the MNase-Seq data from TKO and Pol II depleted TKO cells by NRL in each gene, divided into quartiles and overlapped with DNA sequence-preferred nucleosome positions.

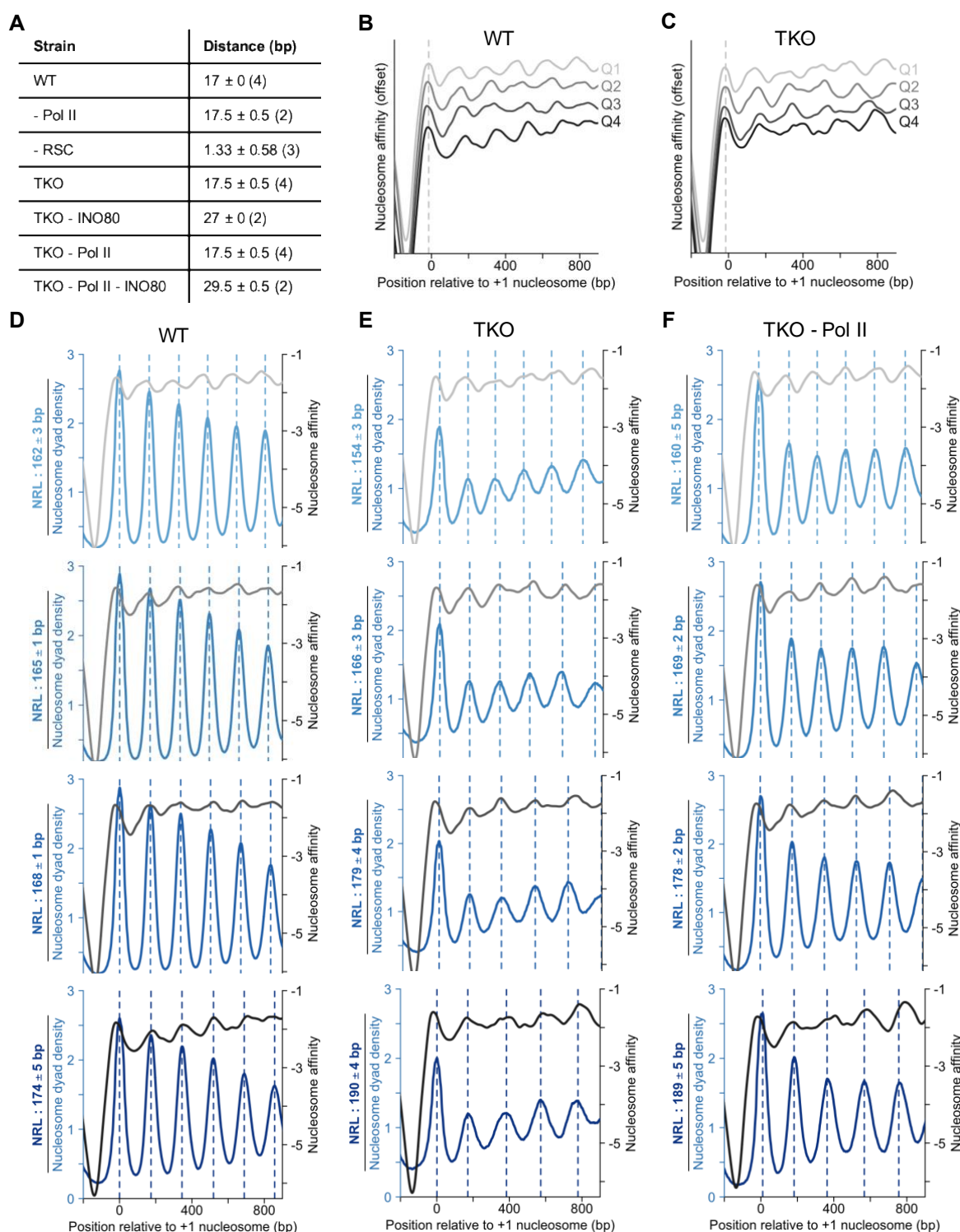


Figure 2.17: The DNA sequence contributes to NRL determination catalyzed by the spacing remodelers. (A) Peak to peak distance between the +1-nucleosome position determined by MNase-Seq and DNA sequence-based nucleosome affinities. Mean and standard deviation is reported. Values in bracket indicate the number of replicates. (B) Gene-averaged DNA sequence-based nucleosome affinities. Genes are sorted by NRL observed in WT cells and divided into quartiles. Data is aligned to the +1-nucleosome position. (C) Same as (B) but for TKO cells. (D) Overlap of MNase-Seq data and nucleosome affinities. Genes are sorted by NRL and divided into quartiles. Mean signal of each quartile is plotted to show the overlap of peaks observed in WT cells and nucleosome affinities. Dashed lines are drawn relative to peaks in the MNase-Seq data. Mean and standard deviation of NRL in each

quartile is reported. **(E)** Same as (D) but genes were sorted for NRL observed in TKO cells. **(F)** Same as (D) but genes were sorted for NRL observed in the Pol II depleted TKO cells. (Singh et al., unpublished).

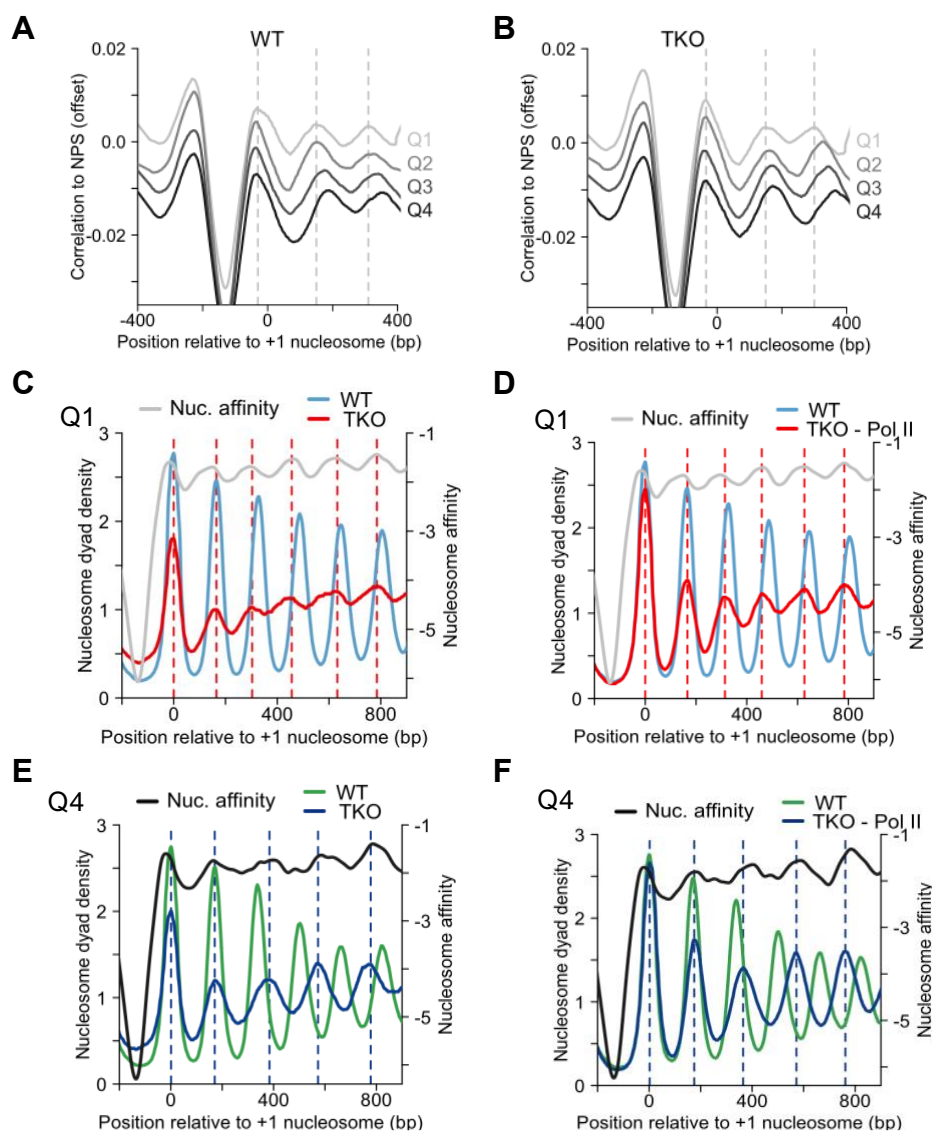


Figure 2.18: Nucleosome removers override DNA sequence influenced NRL. **(A)** Nucleosome positioning sequences (NPS) from the Pugh lab (Ioshikhes et al., 2006) shows similar results as nucleosome affinities calculated in this study. Genes were sorted by NRL observed in WT and divided into quartiles. Mean signal in each quartile is plotted. **(B)** Same as (A) but for genes sorted with NRL observed in TKO cells. **(C)** ISWI and Chd1 remodelers override DNA sequence driven short NRLs. The MNase-Seq data of genes with shortest NRL (Q1) in WT were plotted with MNase-Seq data from TKO and calculated nucleosome affinities. MNase-Seq data in TKO (dotted lines) overlaps better than WT with nucleosome affinities. **(D)** Same as (C) but for the Pol II depleted TKO cells. **(E)** ISWI and Chd1 remodelers also override DNA sequence driven long NRLs. The MNase-Seq data of genes with longest NRL (Q4) in TKO cells were overlapped with the MNase-Seq data in WT and calculated nucleosome affinities. WT cells show much shorter NRL than TKO and nucleosome affinities. **(F)** Same as (E) but genes with longest NRL (Q4) from the Pol II depleted TKO cells. (Singh et al., unpublished).

We found that peaks from the MNase-Seq data and the nucleosome affinities overlapped in all four quartiles, even though NRL observed in TKO are more widely distributed than in WT (Figure 2.17E, F). Even in Q4, genes with an average NRL 200 bp overlapped well. Unexpectedly, the amplitude of nucleosome affinities did not increase in TKO compared to WT (Figure 2.17C, E, F). This result suggests that nucleosomes find DNA sequence preferred positions in cells lacking ISWI and Chd1 remodelers, but the DNA sequence driven nucleosome affinities are mild.

We noticed that Q4 in TKO cells showed unusually long NRL and WT cells lack this (Figure 2.17D – F). We, therefore, hypothesized that spacing remodelers override DNA sequence-preferred NRL in these genes and generate short NRL. To test this, we overlapped the MNase-Seq data for these genes from WT and TKO with nucleosome affinities. Indeed, WT cells show much shorter NRL than observed in TKO and from DNA sequence (Figure 2.18E, F). Similarly, Q1 genes in WT cells show higher overlap with the DNA sequence-preferred NRL in TKO cells than the WT cells (Figures 2.17D and 2.18C, D). Here, DNA sequence influences to establish short NRL which is overridden by remodelers. Overall, we conclude that ISWI and Chd1 remodelers override DNA sequence-influenced NRL in certain genes to establish near WT-like NRL.

Curiously, in cells lacking spacing remodelers, Q4 genes consistently showed a higher nucleosome affinity at the +5-nucleosome (Figure 2.18E, F). This was quite intriguing because the data was aligned to the +1-nucleosome. To rule out that this signal does not emerge from nucleosomes of neighbouring genes, we repeated the analysis with genes longer than 1500 bp. These genes still showed similar +5-nucleosome affinities (not shown). We therefore propose that, in genes with extremely long NRL, the +5-nucleosome may play a role in NRL determination by freezing +1- and +5- nucleosomes.

Overall, the results presented in this section show that DNA sequence positively contributes to nucleosome array formation and NRL determination in most of the genome. ISWI and Chd1 override nucleosome organization in genes with either very short or very long NRLs influenced by the DNA sequence. In the rest of the genome, remodelers help catalyze nucleosome sliding such that nucleosomes find DNA sequence preferred positions and NRLs. Nevertheless, the contribution of the DNA sequence is mild because we did not find increased nucleosome affinities in TKO cells. The DNA sequence is compatible with many nucleosome positions found in cells.

2.1.10 Regular nucleosome arrays protect the genome from genotoxic stress

Regular nucleosome arrays are conserved from yeast to human. All organisms with nucleosomes have evolved at least three families of spacing remodelers which can generate regular nucleosome arrays. Even though this phenomenon is pervasive, the functional importance of evenly spaced nucleosome arrays remains elusive (Lohr et al., 1977; Noll, 1974). We hypothesized that the regular nucleosome arrays contribute to genomic integrity by protecting the genome from external insults. For this purpose, we compared WT cells to TKO cells harboring severely reduced regular arrays. Importantly, the absolute nucleosome

occupancy is not affected in the TKO cells compared to WT (Daan G. F. Verhagen, unpublished results), arguing against the presence of large amounts of naked DNA in TKO cells.

DNA damage: First, we checked the susceptibility of cells with reduced nucleosome arrays to varied extents towards DNA damage. We employed Zeocin, belonging to the bleomycin family, which induces free radicals and thereby generates double-stranded (ds) breaks (Claussen and Long, 1999). We found that the loss of ISWI and Chd1 remodelers in TKO makes cells highly sensitive to Zeocin (Figure 2.19A). We also observe that the growth defect upon Zeocin stress largely negatively correlates with the nucleosome array regularity measured in the mutant strains (Figure 2.19A). The Zeocin stress response of TKO is surprisingly higher than the *arp8Δ* mutant known to be highly sensitive to DNA damage (Papamichos-Chronakis et al., 2011; Seeber et al., 2013). The combined TKO and *ARP8* deleted strain is completely dead under Zeocin conditions, likely due to the combined effect of both deletions (Figure 2.19A). Overall, these results suggest that regular arrays may prevent double-stranded breaks.

The increased susceptibility of TKO could arise from a higher number of double-strand breaks or due to delayed DNA damage response and repair (Lans et al., 2012; Sanchez-Molina et al., 2011). To distinguish between these possibilities, we monitored the immediate response of cells to Zeocin exposure. After only 10 min of Zeocin treatment, TKO cells exhibit higher fragmentation of genomic DNA than WT and *arp8Δ*, consistent with array regularity preventing double-stranded breaks (Figure 2.19B).

To test a different genotoxic stress, we employed Methyl methanesulfonate (MMS). MMS is an alkylating agent and generates genome instability by stalling replication fork (Larson et al., 1985; Lundin et al., 2005). We found that, like Zeocin, remodeler deficient cells are susceptible to MMS. Curiously, *arp8Δ* cells show higher growth response than TKO cells, even though TKO cells have lower array regularity than *arp8Δ* cells (Figure 2.19A). This result suggests that INO80 plays a bigger role in relieving stalled replication forks than the ISWI and Chd1 remodelers combined. Also, the Zeocin-induced response is different from the MMS-induced response, suggesting fundamentally different mechanisms of DNA damage from these two compounds.

To test if naturally occurring double-stranded breaks are also influenced by array regularity, we correlated array regularity at each gene to Spo11- or Top2- induced ds breaks (Gittens et al., 2019). Spo11 catalyzes the formation of ds breaks during meiotic recombination (Keeney et al., 1997). Top2 generates ds breaks to relax topological constraints (Nitiss, 2009). We found that genes with lower array regularity are more prone to ds breaks than genes with higher array regularity in WT cells (Figure 2.19C, D). Overall, these experiments and correlations suggest that regular nucleosome arrays prevent DNA double-strand breaks.

Ectopic recombination: Second, we tested if regular nucleosome arrays prevent ectopic recombination in the genome. To this end, we used an assay monitoring homologous recombination rates at two genomic loci (Hauer et al., 2017). We found that the ectopic transgenes recombined ~two-fold higher in TKO compared to WT (Figure 2.19E). This result

show that ISWI and Chd1 remodelers suppress ectopic recombination in the genome and suggest that regular arrays may prevent insertion of foreign DNA into the genome.

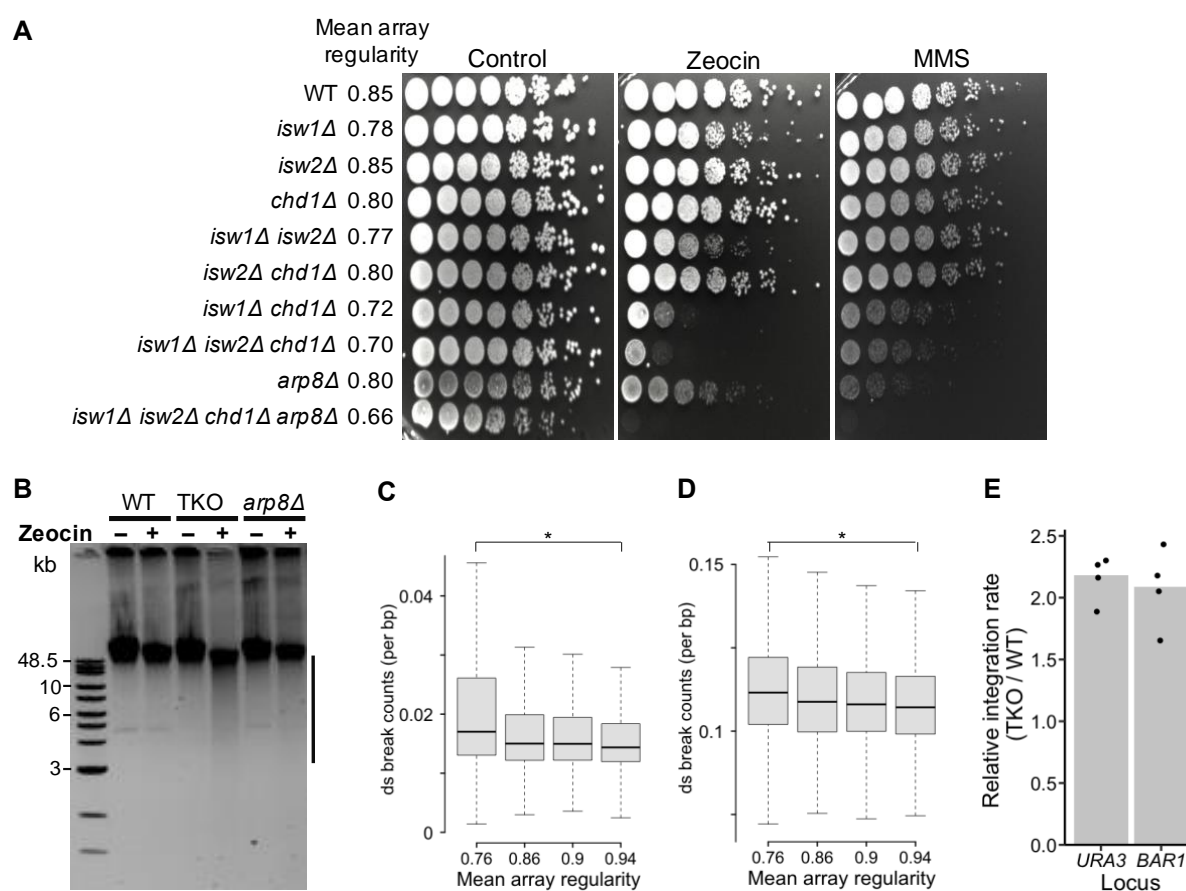


Figure 2.19: Regular nucleosome arrays protect the genome from DNA damage and ectopic recombination. (A) Growth assay of the indicated strains in the presence of Zeocin (100 μ g/ml) or MMS (0.05%). Control is cells grown on full media (YPAD). (B) Genomic DNA fragmentation induced by Zeocin in WT, TKO and *arp8Δ* cells. Cells were incubated with water or Zeocin (1 mg/ml) for 10 min. Spotting assay was repeated twice with consistent results. (C) Spo11-induced ds breaks anticorrelates with nucleosome array regularity. Genes were first sorted by nucleosome array regularity measured in each gene and then divided into quartiles. (D) Same as (C) but for Top2-induced ds breaks. Spo11 and Top2 ds break count data are obtained from (Gittens et al., 2019). (E) TKO cells show two-fold higher ectopic recombination at two loci. Cells were transformed either with the linearized pRS406 plasmid (*URA3* locus) or with the *HIS3* marker amplified from the pRS403 plasmid (*BAR1* locus). Statistical analyses in (C, D) were performed using two-sided t-test on Q1 and Q4 values. For (E), mean values of biological replicates of ATAC-Seq data in Q1 and Q4 were considered. * $P < 0.05$, ** $P < 0.01$, *** $P < 0.001$. (Singh et al., unpublished).

Transposon integration: Third, we hypothesized that the regular nucleosome arrays limit DNA accessibility and protect the genome from transposon integration. As a proxy to transposon integration, we performed ATAC-Seq on WT and TKO strains. ATAC-Seq measures chromatin accessibility by preferentially integrating transposons in the accessible genome (Buenrostro et al., 2013; Schep et al., 2015). We found higher ATAC signal in the gene body and at the transcription termination sites in the TKO strain compared to WT (Figure 2.20A). About 80% of genes attained higher ATAC signal in the TKO. The number of ATAC

integration in the gene body correlated with array regularity in genes of same cells. The lower the array regularity, the higher the ATAC signal (Figure 2.20B).

ATAC-Seq experiments performed above measures chromatin accessibility *ex vivo*. To test if array regularity also prevents transposon integration *in vivo*, we made use of induced, saturated transposon integration data (Michel et al., 2017). Consistent with our hypothesis, we found that *in vivo* transposon integration also anti-correlates with array regularity (Figure 2.20C). Overall, these results suggest that even spacing of nucleosome arrays prevent transposon integration in the gene body, and thus regulates the accessibility of the underlying DNA.

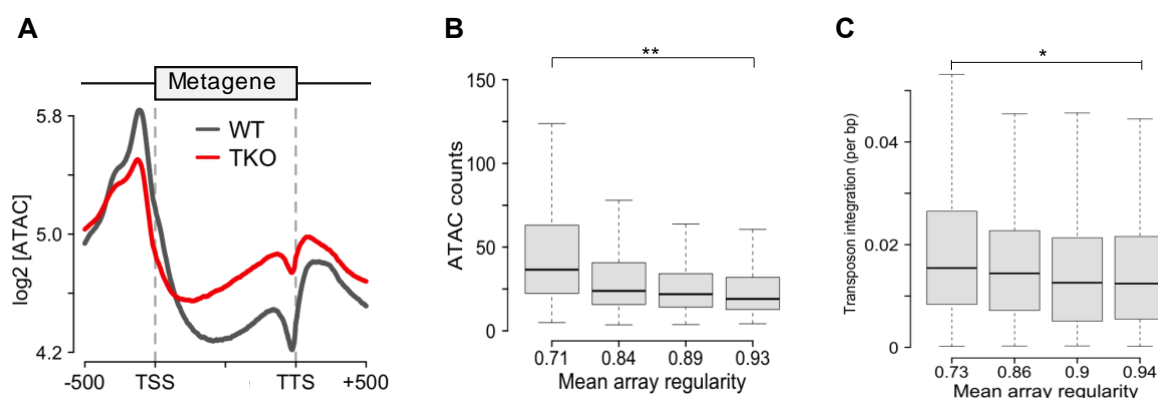


Figure 2.20: Regular nucleosome arrays protect the genome from transposon integration and regulate chromatin accessibility. (A) Metagene plot showing ATAC-Seq signal distribution at TSS, gene body and TTS in WT and TKO cells. The signal in the gene body is scaled to 1000 bp. **(B)** ATAC-Seq insertion counts in gene body anti-correlates with array regularity. Genes were sorted with array regularity and divided into quartiles. **(C)** Ectopically induced transposon integration counts anti-correlates with array regularity. Transposon integration data is obtained from (Michel et al., 2017). Statistical analyses in (B, C) were performed using two-sided t-test on Q1 and Q4 values. For (G), mean values of biological replicates of ATAC-Seq data in Q1 and Q4 were considered. * $P < 0.05$, ** $P < 0.01$, *** $P < 0.001$. (Singh et al., unpublished).

2.1.11 Spacing remodelers and array regularity modulate Pol II progression

Regular nucleosome arrays coat the gene body established by the spacing remodelers. Transcription machinery has to plough through these nucleosome array during transcription (Ehara et al., 2019; Farnung et al., 2018; Kujirai et al., 2018). The functional relevance of the +1-nucleosome in the array is quite well-known (Kubik et al., 2019; Weber et al., 2014). On the other hand, how nucleosome array in the gene body affect transcription is not clear. We hypothesized that the regular arrays and spacing remodelers modulate transcription elongation in the gene body.

To investigate the role of regular arrays and spacing remodelers in transcription elongation, we performed native elongating sequencing (NET-Seq) in WT and TKO cells (one replicate). We calculated 5' to 3' ratio of Pol II occupancy using the NET-Seq signal in genes, as done previously (Topal et al., 2019). The 5' to 3' ratio corresponds to NET-Seq signal densities in

the TSS to TSS+250 bp region divided by the densities upstream of the TSS+250 bp to the TTS region in each gene.

We first calculated the 5' to 3' ratio for WT and TKO NET-Seq datasets. We found that TKO cells have higher 5' to 3' ratio compared to WT cells (Figure 2.21A), suggesting that TKO cells have a higher Pol II distribution near the TSS and lower in the gene body compared to WT cells. This result is consistent with a suggested transcription elongation defect near +1 and +2 nucleosomes in *isw1Δ chd1Δ* cells (Ocampo et al., 2019). Overall, this result suggests that the spacing remodelers or the regular arrays modulate Pol II distribution near the TSS and in the gene body.

To distinguish between the roles of spacing remodelers or regular arrays towards Pol II distribution, we sorted genes in WT according to array regularity in each gene and divided into quartiles. We found that array regularity correlates with the 5' to 3' ratio. The higher the array regularity, the higher the 5' to 3' ratio. (Figure 2.21B). This suggests that genes with more regular arrays have higher Pol II signal in the gene body and lower near the TSS when compared to less regular arrays. To confirm these results, we reanalyzed published WT NET-Seq datasets from three different laboratories and found similar results (Churchman and Weissman, 2011; Mischo et al., 2018; Topal et al., 2019) (Figure 2.21C, D and not shown). We also ruled out that these differences are due to different nucleosome occupancies in the gene body of each quartile as all quartiles showed same mean nucleosome occupancy (0.83) (Oberbeckmann et al., 2019). Lastly, we performed similar analysis by sorting genes with their array regularity in TKO cells and observed similar trends as WT cells (Figure 2.21E). Overall, these results hint towards regular arrays facilitating Pol II elongation in the gene body.

Next, we investigated if regular nucleosome arrays prevent cryptic transcription initiation in the gene body. Recent high-throughput TSS-Seq studies have revealed transcription initiation is pervasive and not restricted to gene promoters (Lu and Lin, 2019). How cells regulate transcription initiation in the gene body remains elusive. Here, we hypothesized that array regularity prevents cryptic transcription initiation from the gene body. To test this, we correlated TSSs arising in the gene body (defined as TSS+100 to TTS-100 bp) with array regularity in each gene. We first sorted genes by array regularity, divided into quartiles and plotted TSSs counts for each quartile. We found that genes with higher array regularity tend to have fewer cryptic TSSs arising from the gene body (Figure 2.21F). This results also holds for cryptic TSSs arising on the sense as well as the antisense strand (Figure 2.21G, H). We ruled out that this is due to differential nucleosome occupancy, as TSS counts do not correlate with nucleosome occupancy (Figure 2.21I). In support of these correlations, TKO cells also show higher cryptic antisense transcription (Smolle et al., 2012). Overall, these results suggest that array regularity prevent cryptic TSSs in the gene body, likely by occluding initiation sites and preventing assembly of the transcription machinery.

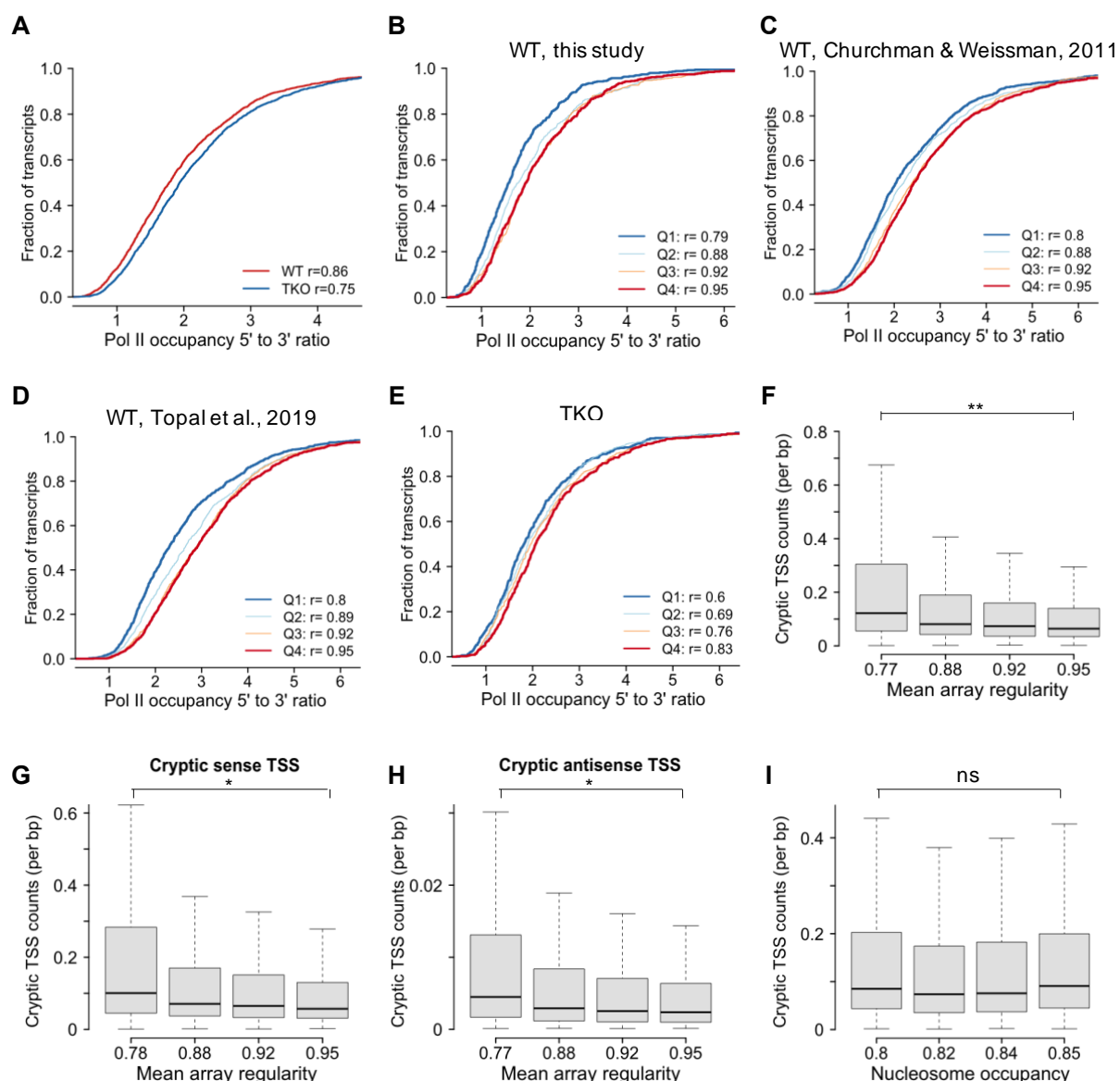


Figure 2.21: Nucleosome arrays modulate transcription elongation and prevent cryptic TSSs.

(A) Cumulative distribution function (CDF) plot of 5' to 3' ratio calculated from NET-Seq signal in WT and TKO cells. r indicates mean array regularity for 3342 genes with transcripts longer than 500 bp and absolute nucleosome occupancy between 0.78 and 0.88 (Oberbeckmann et al., 2019). **(B)** Same as (A) but only for WT dataset where 3342 genes were sorted by array regularity and divided into quartiles. 5' to 3' ratio was calculated for each quartile. **(C)** Same as (B) but for WT dataset from (Churchman and Weissman, 2011) **(D)** Same as (B) but for WT dataset from (Topal et al., 2019). **(E)** Same as (B) but for TKO cells. **(F)** Cryptic TSSs in gene body anti-correlates with array regularity. TSS data is taken from (Lu and Lin, 2019). Genes were sorted by array regularity and divided into quartiles. Genes with absolute nucleosome occupancy >0.78 and <0.88 were used. **(G)** Same as (F) but for cryptic TSS on the coding strand. **(H)** Same as (F) but for cryptic TSS on the non-coding strand. **(I)** Cryptic TSS in the gene body does not correlate with nucleosome occupancy. Nucleosome occupancy data is obtained from (Oberbeckmann et al., 2019). The NET-Seq experiment was performed once. Statistical analyses in (F, G, H, I) were performed using two-sided t-test on mean values of Q1 and Q4 from the TSS data. * $P<0.05$, ** $P<0.01$, *** $P<0.001$. (Singh et al., unpublished).

2.1.12 DISCUSSION (related to this chapter)

The mechanism of nucleosome positioning and spacing has been studied for more than a decade. It has remained an experimental challenge to cleanly dissect the role of an individual factor due to high redundancy of factors involved in it. Here we use a sensitive yeast strain lacking ISWI and Chd1 remodelers to substantially reduce the functional redundancy of nucleosome landscape organizing factors. Using this clean system, we show that transcription overrides nucleosome organization driven by nucleosome remodelers and high nucleosome density. We find that INO80 can space nucleosomes *in vivo*. We further utilize this system to dissect the spacing mechanism by INO80 *in vivo*, an endeavor which is traditionally performed *in vitro*. Importantly, the conclusions derived from this sensitive system are consistent with observations in functionally redundant systems, like WT. Finally, we provide multiple lines of evidence to suggest that nucleosome array help maintain genome integrity by protecting underlying DNA from external stress. Together, our results extend previously proposed models of biogenesis of nucleosome landscape and suggest their function beyond promoter regulation.

Transcription destroys the nucleosome landscape

Transcription has been proposed to play a major role in nucleosome organization. According to this model, PIC assembly during transcription initiation fine-tunes position of the +1-nucleosome and helps clearing the NFR. In the next step, transcription elongation helps establish the nucleosome array. These steps are modulated by cis- and trans-acting factors like DNA sequence and nucleosome remodelers of ISWI and Chd1 families (Hughes et al., 2012; Struhl and Segal, 2013; Vasseur et al., 2016).

Our results in both TKO and WT background are inconsistent with this model (Figures 2.5 and 2.6). We observe no increase in nucleosome signal at the NFR and nucleosome arrays become more regular upon Pol II depletion. These results clearly show that transcription is highly disruptive to nucleosome arrays in the gene body. The disruptive effect is genome-wide and not restricted to highly transcribed genes (Cole et al., 2011; Cole et al., 2014; Cui et al., 2012; Shivaswamy et al., 2008). This activity also appears to be true in higher organisms as shown recently in *Drosophila* with a correlative comparison between expressed and silent genes (Baldi et al., 2018b). Furthermore, a recent study measuring absolute nucleosome occupancy showed that nucleosome occupancy does not correlate with transcription activity, ruling out that decreased array regularity is due to lower nucleosome occupancy (Oberbeckmann et al., 2019).

With these results, we suggest that the net effect of Pol II transcription is disruptive to array regularity. In WT cells, Pol II and nucleosome remodelers compete to establish the TSS-aligned nucleosome arrays. A high redundancy of spacing remodelers leads to well-positioned nucleosomes and regular arrays. At highly transcribed genes, transcription wins over nucleosome remodelers and other factors, thus leading to a highly disrupted nucleosome organization. Upon a decrease in remodeler redundancy in TKO cells, the net disruptive effect of transcription increases which leads to irregular array in TKO cells.

The transcription machinery may mitigate its disruptive effect by interacting with or recruiting remodelers, histone chaperones and histone modifiers. Chd1 and ISW1 remodelers work majorly in the gene body as their single deletions affect the positioning of only genic nucleosomes (Ocampo et al., 2019; Pointner et al., 2012; Tirosh et al., 2010; van Bakel et al., 2013; Zentner et al., 2013). They interact with the elongating Pol II or H3K36me3 and are recruited to the gene body where they slide and space nucleosomes (Alen et al., 2002; Maltby et al., 2012; Morillon et al., 2003; Santos-Rosa et al., 2018; Simic et al., 2003; Smolle et al., 2012). They may also help to assemble nucleosomes in the wake of transcription (Smolle et al., 2012; Vasseur et al., 2016).

The two faceted role of transcription leads to a trade-off between regular and disrupted nucleosome organization. We propose that the trade-off between nucleosome organizing and disruptive factors provide an opportunity for chromatin-based regulation. The imperfectness in the nucleosome array may be useful for antisense and cryptic transcription arising within the gene body, particularly upon cellular stress. The transcription elongation has also been proposed to re-establish chromatin accessibility within the gene body post replication, likely via its disruptive effect (Stewart-Morgan et al., 2019). Pervasive transcription has also been suggested to regulate replication origin licensing and activation (Candelli et al., 2018; Soudet et al., 2018).

Biogenesis of regular nucleosome arrays

Nucleosome organization is disrupted every cell cycle during replication. Transcription also destroys nucleosome arrays. How cells re-establish the nucleosome landscape is highly studied. We here extend the previously proposed three-step models taking into account findings in this chapter (Hughes et al., 2012; Krietenstein et al., 2016).

We propose a four-step model. In the first step, nucleosomes find thermodynamically preferred position based on DNA sequence when they are deposited in the wake of replication and transcription. They accumulate over these positions in both WT and remodeler lacking cells. Despite their preference over thermodynamically preferred positions, they do not seem to enrich in remodeler lacking cells. This suggests that multiple, equally preferred positions exist in the genome and the landscape is mild. This is also consistent with salt gradient dialyzed chromatin which shows no defined nucleosome positions (Zhang et al., 2009; Zhang et al., 2011).

In the second step, NFR is first cleaned by nucleosome remodelers largely by the RSC family. Nucleosome destabilizing sequences enriched at the NFR also play an important role either in its own or in cooperation with GRFs and remodelers (Chereji and Clark, 2018; Lieleg et al., 2015b). Our results show ISWI and Chd1 remodelers also contribute to this process. On the other hand, transcription machinery, including pre-initiation complex, has no direct role in it.

In the third step, the +1-nucleosome position is determined by a tug-of-war between RSC and INO80 remodelers. RSC shifts the +1 nucleosome by ~17 bp away from the NFR. This activity is counteracted by the INO80 remodeler on a genome-wide scale by sliding nucleosomes towards the NFR. The ISW2 remodeler also performs a similar function as INO80, but only at

certain genes. Histone variant H2A.Z although has no role in +1-positioning, in line with previous observations (Hartley and Madhani, 2009).

In the fourth step, high histone density and nucleosome remodelers of ISWI, Chd1 and INO80 families cooperate to establish regular arrays aligned at the TSS. Our results suggest that the NRL observed in WT cells requires both high histone density and spacing remodelers. Remodelers can 'clamp' nucleosomes under reduced histone densities, leading to only 7-8 bp increase upon histone depletion (Lieleg et al., 2015a). The clamping activity is weak because nucleosome organization is severely compromised upon histone depletion in WT cells. Therefore, remodelers alone cannot generate regular nucleosome organization under reduced histone densities. They require high histone densities to generate WT-like NRL in the genome.

The ~165 bp NRL in WT was proposed to be a result of competition between ISWI and Chd1 remodelers (Ocampo et al., 2016). We show that INO80 also contributes to nucleosome spacing. Even in our TKO Pol II depletion system with reduced redundancy, INO80 generated broad NRL peaking at 168 bp. This is inconsistent with ~200 bp linker length generated by INO80 *in vitro* (Krietenstein et al., 2016). This observation suggests that even though INO80 and other spacing remodelers can generate varied linker length *in vitro*, their preferred/ideal NRL is counteracted by high nucleosome density, which leads to smaller than expected NRL for all remodelers, except Chd1 (Stockdale et al., 2006; Torigoe et al., 2013; Udugama et al., 2011). The remodelers may be free to generate their preferred NRL during cellular ageing or DNA damage when histone densities drop in the cell (Groth et al., 2007; Hu et al., 2014).

Mechanism of INO80 spacing activity

Our data suggest that INO80 can space nucleosomes *in vivo*, in addition to ISWI and Chd1 remodelers (Figures 2.7, 2.8 and 2.9). We could observe this activity to different extents in four genetic backgrounds with varying levels of redundancy. Surprisingly, we could clearly detect INO80 activity when cells lacked active transcription. This suggests that INO80 does not require transcription for recruitment or function. Other remodelers, like ISWI and Chd1, may depend more on transcription. We also observed INO80 activity in WT cells upon Pol II depletion. This suggests that INO80 may work in the wake of transcription to generate regular arrays, besides ISWI and Chd1 remodelers.

How does INO80 space nucleosomes *in vivo*? We utilized our TKO Pol II depleted system to directly test two prominent modules involved in linker length sensing. Our results in three genetic backgrounds show that Arp8 is required for generating longer linker length by INO80 complex and Nhp10 has a negligible role in this process (Figures 2.11 and 2.13). INO80 complex lacking Arp8 is defective in linker length sensing and actively generates arrays with ~16 bp shorter NRL. These results are consistent with *in vitro* results that Arp8 can sense linker length. Our complementation experiments with Arp8 lacking N-terminus suggest that N-terminus is required for Arp8 spacing activity. Arp8 and its N-terminus have been shown to interact with and crosslink to linker DNA and the HSA domain in the Ino80 ATPase (Brahma et al., 2018; Knoll et al., 2018; Tosi et al., 2013).

How Arp8 modulates and achieves this NRL in the INO80 complex is unclear. Arp8 module protrudes out of the complex and thus extensively interacts with the linker DNA (Eustermann et al., 2018; Knoll et al., 2018; Watanabe et al., 2015). Arp8 module may also exist in different conformations in the INO80 complex (Zhang et al., 2019). This conformational flexibility may help couple linker length sensing to nucleosome sliding. Human INO80 complex slide nucleosomes by regulating cooperativity between two functional INO80 monomers (Willhoft et al., 2017). Arp8 module may help connect two INO80 complexes via its propensity to dimerize (Saravanan et al., 2012).

The yeast-specific Nhp10 module was shown to regulate the switch-like response to linker DNA from 40 bp to 60 bp (Zhou et al., 2018), suggesting that the Nhp10 module can sense linker DNA length and regulate NRL. In contrast with these predictions, we observe no change in NRL generated by the INO80 complex lacking the Nhp10 module compared to the WT INO80 complex. It remains possible that the Nhp10 module is required under specific conditions, for example under reduced nucleosome density during DNA damage, where Nhp10 has a known role (Morrison et al., 2004; van Attikum et al., 2004).

The H2A-H2B acidic patch on the nucleosome has recently emerged as a new regulatory module for nucleosome remodelers (Dann et al., 2017; Dao et al., 2019; Gamarra et al., 2018; Han et al., 2020; He et al., 2020; Levendosky and Bowman, 2019; Wagner et al., 2020; Ye et al., 2019). The acidic patch regulates INO80 sliding activity by ~200-fold. The Ies2 subunit within the INO80 complex interacts with the acidic patch, suggesting it may regulate INO80 sliding activity via the acidic patch. To our surprise, *IES2* deletion has no effect on cell viability and nucleosome array regularity *in vivo*. Nevertheless, genome NRL is decreased by 2 bp, suggesting Ies2-acidic patch interactions may regulate nucleosome spacing (Figure 2.15).

Overall, our results show that Arp8 is required for nucleosome spacing in the INO80 complex. The Nhp10 module, on the other hand, is not required for this activity. Arp8 is also conserved from yeast to human, suggesting INO80 spacing mechanism is likely similar in higher organisms.

Function of nucleosome arrays

Our results regarding the function of nucleosome arrays suggest that they protect the underlying DNA from double-stranded breaks, transposon integration and ectopic recombination, in addition to its role of genome packaging (Figures 2.19 and 2.20). The regular spacing of nucleosomes may prevent occasional exposure of the underlying DNA, thus protecting the genome from genotoxic stress. We propose that nucleosome remodelers and arrays may have evolved to protect the genome. This could also be an evolutionary driving force as archaea also possess nucleosome-like structures (Brunk and Martin, 2019; Hocher et al., 2019; Mattioli et al., 2017).

Regularly spaced nucleosomes have been suggested to promote 3D chromatin folding. A recent study showed that nucleosome arrays phase separate *in vitro* (Gibson et al., 2019), which could regulate access to underlying DNA to the cellular machinery. It is conceivable that

cells lacking spacing remodelers have disrupted 3D folding of chromatin due to a lack of evenly spaced nucleosome arrays.

Our results suggest that nucleosome arrays modulate Pol II elongation near TSS and in the gene body. While the increase in cryptic transcription upon diminished nucleosome organization have been reported, the underlying mechanism remained unclear. We suggest that regular arrays prevent exposure of DNA where transcription machinery could assemble to initiate transcription. We also found that nucleosome arrays also affect transcription elongation. Evenly spaced nucleosomes appear to facilitate transcription elongation than irregularly spaced nucleosomes. We ruled that this is due to increased nucleosome occupancy as all quartiles show similar nucleosome occupancy but harbor different array regularity.

2.2 Chapter: Functional dissection of the ISW2 nucleosome remodeler

Contributions

Results presented in this chapter are from a study conceived by Prof. Dr. Felix Mueller-Planitz and me. Sarah Schaefer, Arun Kumar Sundaramurthy and Lena Pfaller contributed to initial experiments during their Master internships at the Department of Biology, LMU Munich.

2.2.1 Background

The ISW2 nucleosome remodeler

S. cerevisiae consists of two ISWI-family related nucleosome remodeling complexes: ISW1 and ISW2. The ISW2 complex consists of an Isw2 ATPase and an accessory subunit Itc1. It may also associate with two histone-fold containing proteins, Dls1 and Dpb4 (McConnell et al., 2004; Tsukiyama et al., 1999). The ISW2 complex is considered an ortholog of *Drosophila* and human CHRAC complexes. The Isw2 ATPase is homologous to *Drosophila* and human ISWI ATPase. Itc1, on the other hand, shares limited homology with *Drosophila* and human ACF1 subunit, restricted to DDT and WAC domains (discussed below). Dls1 is a homolog of *Drosophila* CHRAC-16 and human HuCHRAC-15. Dpb4 is homologous to *Drosophila* CHRAC-14 and human HuCHRAC-17 (Corona et al., 2000; Eberharter et al., 2001; Poot et al., 2000).

The Isw2 ATPase consists of a central ATPase domain and a C-terminal Hand, Sant and Slide (HSS) domain. Itc1 consists of an N-terminal WAC domain and a central DDT domain. The N-terminus, including the WAC domain, of *Drosophila* and human ACF1 is important for DNA binding as well as sensing length of the linker DNA, suggesting a role of N-terminus of ACF1 in nucleosome spacing activity of the ISW2 remodeler (Fyodorov and Kadonaga, 2002a; Hwang et al., 2014). Deletion of the N-terminus of ACF1 impairs nucleosome sliding activity of the ACF complex and dramatically reduces cellular growth in yeast. Importantly, Itc1/ACF1 lacking the N-terminus can form a protein complex with the ATPase subunit. The DDT domain, on the other hand, connects *Drosophila* ACF1 to the ISWI ATPase subunit as deletion of the DDT domain abolishes interaction between ISWI and ACF1 (Donovan et al., 2020; Eberharter et al., 2004; Fyodorov and Kadonaga, 2002a; Hwang et al., 2014).

The ISW2 complex binds near the promoter region of certain genes, for example near cell-type specific and early meiotic genes (Gelbart et al., 2005; Goldmark et al., 2000; Yen et al., 2012; Zentner et al., 2013). Sequence-specific transcription factors (TFs), like Ume6, are important for targeting the ISW2 remodeler to specific genes. DNA loops established by these TFs may further increase ISW2 recruitment to regions lacking TF binding sites (Bachman et al., 2005; Goldmark et al., 2000; Yadon and Tsukiyama, 2013).

ISW2 slides the +1-nucleosome towards the NFR because deletion of the Isw2 ATPase shifts the +1-nucleosome away from the NFR. This activity is restricted to ~200 genes, consistent with ISW2 recruitment to specific sites in the genome (Kubik et al., 2019; Whitehouse et al., 2007). ISW2 has a minor contribution towards setting nucleosome spacing *in vivo*. Deletion of the Isw2 ATPase in an otherwise WT cells shows no change in NRL. The spacing activity of

ISW2 is only visible at lowly expressed genes in *isw1Δ chd1Δ* background, likely due to reduced redundancy of the spacing remodelers in these cells. Nevertheless, ISW2 can space nucleosomes *in vitro* and generates longer NRL than ISW1 and Chd1 remodelers (Azmi et al., 2017; Krietenstein et al., 2016; Oberbeckmann et al., 2020; Ocampo et al., 2016; Tsukiyama et al., 1999).

The specific aims of this chapter are:

1. Do cells lacking the N-terminus of Itc1 show a growth defect compared to WT?
2. Does the N-terminus of Itc1 regulate the +1-nucleosome positioning activity of the ISW2 remodeler?
3. Does the N-terminus of Itc1 regulate ISW2 nucleosome spacing function?
4. Is there any role of ISW2 in resolving closely packed dinucleosomes?
5. What is the role of ISW2 remodeler in setting cell-type specific nucleosome architecture?
6. How is ISW2 targeted to promoter region of specific genes?

2.2.2 Deletion of the N-terminus of Itc1 has no effect on cell growth

A recent study from the Zhuang lab showed that cells lacking the N-terminus (amino acids 2-374) of Itc1 protein show a severe growth defect (Hwang et al., 2014). The authors suggested that the N-terminus of Itc1 is important for linker length sensing by the ISW2 complex. On the other hand, a complete deletion of Itc1 or Isw2 subunits show no growth defect (Tsukiyama et al., 1999). To confirm the growth defect of *itc1^{ΔN}* cells, we deleted one copy of the N-terminus of Itc1 (amino acids 2-374) in WT diploid cells and performed sporulation followed by tetrad dissection. If true, *itc1^{ΔN}* haploids obtained from tetrad dissection should show severe growth defect. Contrary to this, we observed no growth defect in *itc1^{ΔN}* cells compared to WT cells, as judged by similar growth of all four haploids arising from a single diploid cell (Figure 2.22A). This result was validated by Lena Pfaller using a mutant diploid strain obtained from an independent transformation event and by performing tetrad dissections on two different days (see Figure 2.22B for a representative plate).

To further confirm these results, we generated *itc1^{ΔN}* strain by replacing Itc1 with ΔN -*itc1* construct via transformation of a linear product in a WT haploid strain. In line with the tetrad dissection results, these cells also showed no growth defect, as judged by serial dilutions (Figure 2.22C). Lastly, we deleted the N-terminus of Itc1 in *isw1Δ chd1Δ* background with reduced redundancy of spacing remodelers and also found no growth defect (Figure 2.22D). Taken together, these results show that the deletion of N-terminus of Itc1 does not lead to a growth defect and are in conflict with the published result (Hwang et al., 2014). It is possible that transformation of the mutant construct in Hwang et al. 2014 study may have led to secondary mutations elsewhere in the genome (see discussion).

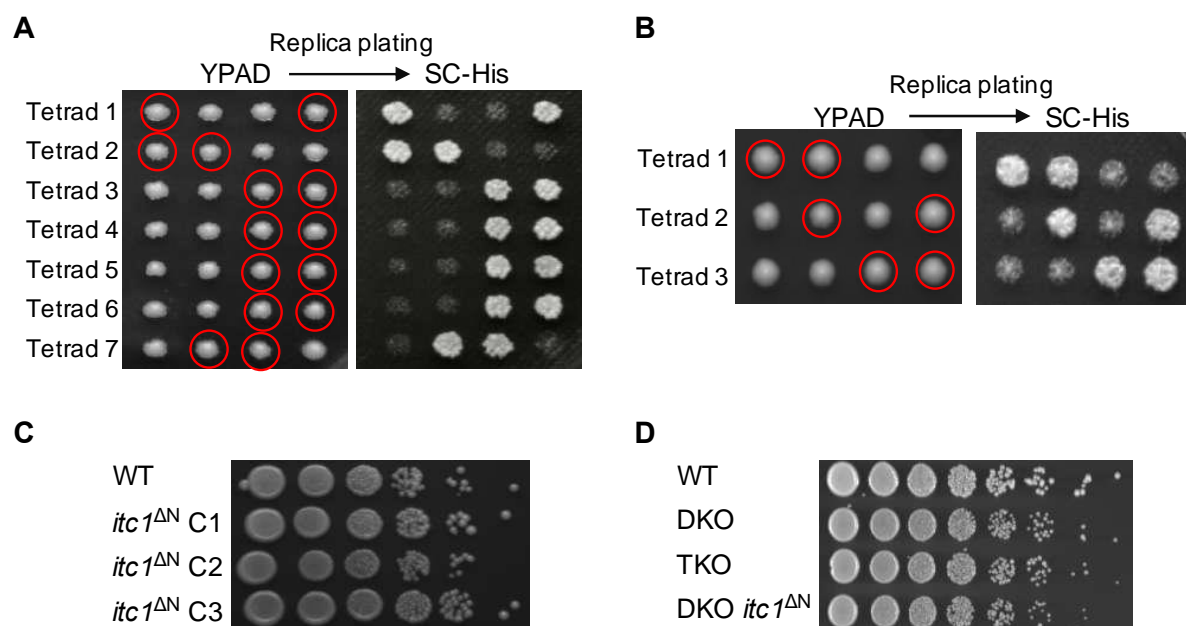


Figure 2.22: Cells lacking the N-terminus of *Itc1* show no growth defect, in conflict with published result. (A) Representative tetrad dissections of a BY4743 diploid strain harboring the *Itc1* construct lacking amino acids 2-374. Diploid strain was generated by transforming a *itc1 Δ2-374-HIS3* construct in the WT BY4743 strain. Diploids were dissected on a non-selective (YPAD) plate and replica plated after 3 days on a selective plate lacking histidine (SC-His). Haploids originating from a diploid cell should segregate 2:2 with 2 colonies harboring *itc1 Δ2-374-HIS3* construct and other two WT *ITC1* locus. Only haploids containing the *itc1 Δ2-374-HIS3* construct can grow on the selective plate. Empty red circles denote the colonies with the *itc1 Δ2-374-HIS3* construct. (B) Same as (A) but for tetrad dissections performed by Lena Pfaller using a colony obtained from transformation of the *itc1 Δ2-374-HIS3* construct in the WT BY4743 diploid strain. (C) Growth assay of WT (BY4741) and cells lacking the N-terminus of *Itc1* in an otherwise BY4741 strain. C1-3 denote three colonies obtained from a transformation event. Shown as 10-fold serial dilutions. (D) Same as (C) but for WT, DKO (*isw1Δ chd1Δ*), TKO (*isw1Δ chd1Δ isw2Δ*) and DKO lacking the N-terminus of *Itc1* strains. Shown are 5-fold dilutions. Plates in (C, D) were incubated for 3 days at 30 °C.

2.2.3 Deletion of the N-terminus of *Itc1* leads to enhanced shmoo formation

Cells lacking *Isw2* or *Itc1* show aberrant shmoo-like morphology in the mating type (mat) alpha background. This is due to the de-repression of mat a-specific genes in *Isw2* lacking mat alpha cells (Ruiz et al., 2003; Sugiyama and Nikawa, 2001; Trachtulcova et al., 2004). The ISW2 complex is recruited to these a-specific genes and slides nucleosomes towards the NFR to repress genes. To test if the ISW2 complex lacking the N-terminus (amino acids 2-374) of *Itc1* can also repress a-specific genes, we examined cell morphology in *itc1^{ΔN}* cells. We found that *itc1^{ΔN}* cells in mat alpha background also show aberrant shmoo-like morphology. A higher number of *itc1^{ΔN}* cells displayed shmoo-like morphology than *isw2Δ* and *itc1Δ* cells (Figure 2.23). These results suggest that the ISW2 complex lacking the N-terminus of *Itc1* is defective in gene repression of mat a-specific genes, as judged by shmoo-like morphology. The higher number of shmoo-like cells may suggest a dominant negative nature of the mutant *Itc1* protein / ISW2 complex or additional defects in cells lacking the N-terminus of *Itc1* compared to *isw2Δ* and *itc1Δ* cells.

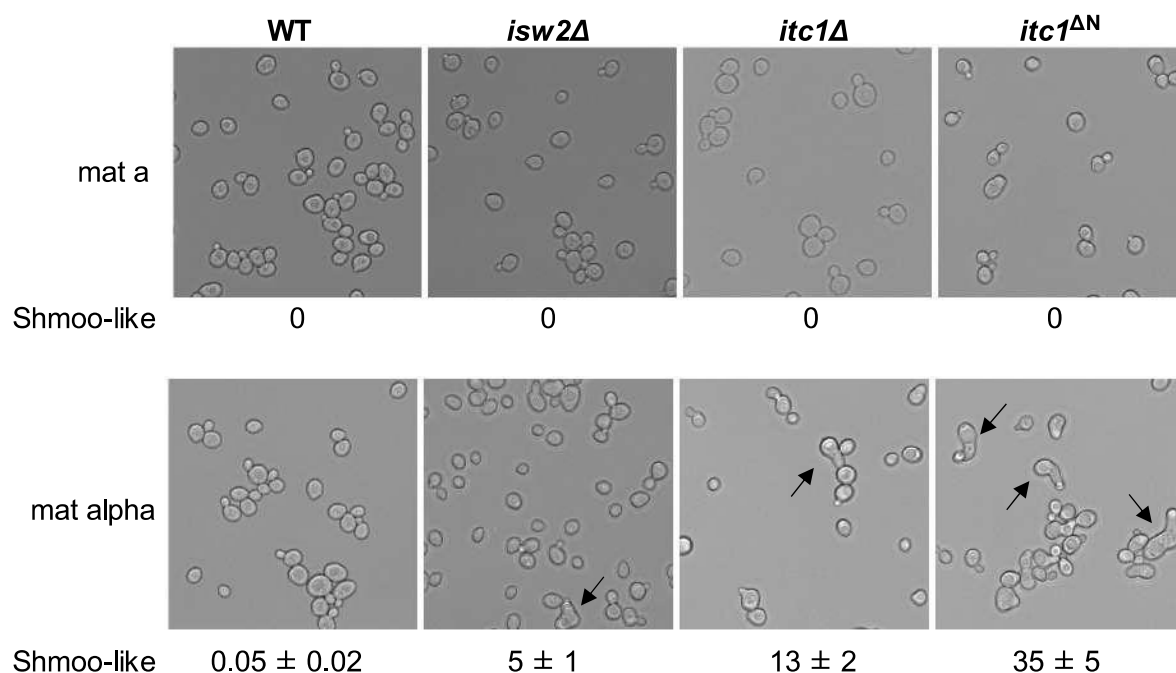


Figure 2.23: Loss of the N-terminus of *Itc1* enhances aberrant shmoo-like morphology compared to *isw2Δ* and *itc1Δ* cells. Representative images of cells lacking *Isw2*, *Itc1* or the N-terminus of *Itc1* in mat a and alpha backgrounds. Mat a cells do not show shmoo-like morphology, consistent with previous results (Ruiz et al., 2003). Arrows indicate cells showing shmoo-like morphology. Numbers indicate mean and standard deviation of cells showing shmoo-like morphology. Three colonies were used for each mutant strain. At least 300 cells were counted for each strain.

2.2.4 *Itc1* lacking its N-terminus shows downstream shift in the +1-nucleosome

ISW2 complex generates repressive chromatin architecture at the promoters (Goldmark et al., 2000; Whitehouse et al., 2007). We wondered if the increased shmoo-like cell morphology in *itc1^{ΔN}* cells is due to defective nucleosome architecture, especially at the +1 nucleosome. To test this, we performed MNase-Seq in cells lacking *Isw2* or *Itc1* or the N-terminus of *Itc1* (two biological replicates of each genotype, all mat a). To test any mating-type specific response in these mutants, we also performed MNase-Seq in WT and mutants mat alpha cells (one replicate).

Genome browser shot of a known responder to ISW2 show a similar downstream shift of nucleosomes in all mutants (Figure 2.24A). This result suggests that the ISW2 complex lacking the N-terminus of *Itc1* is defective in +1-nucleosome sliding. Using DANPOS (Chen et al., 2013a), we identified genes showing a change in the +1-nucleosome position in each sample compared to WT. We identified ~200 genes in cells lacking *Isw2* or *Itc1* which consistently show a shift in the +1-nucleosome by at least 10 bp when compared to WT. Genes which consistently showed a shifted +1-nucleosome in two biological replicates (mat a) were considered. The complete list of genes can be found in Appendix 6.1. GO term analysis suggested genes enriched for meiosis and sporulation, consistent with previous results (Fazio et al., 2001; Gene Ontology, 2015; Goldmark et al., 2000). Besides, genes involved in carbohydrate metabolism and chromosome segregation were also enriched (Figure 2.24B).

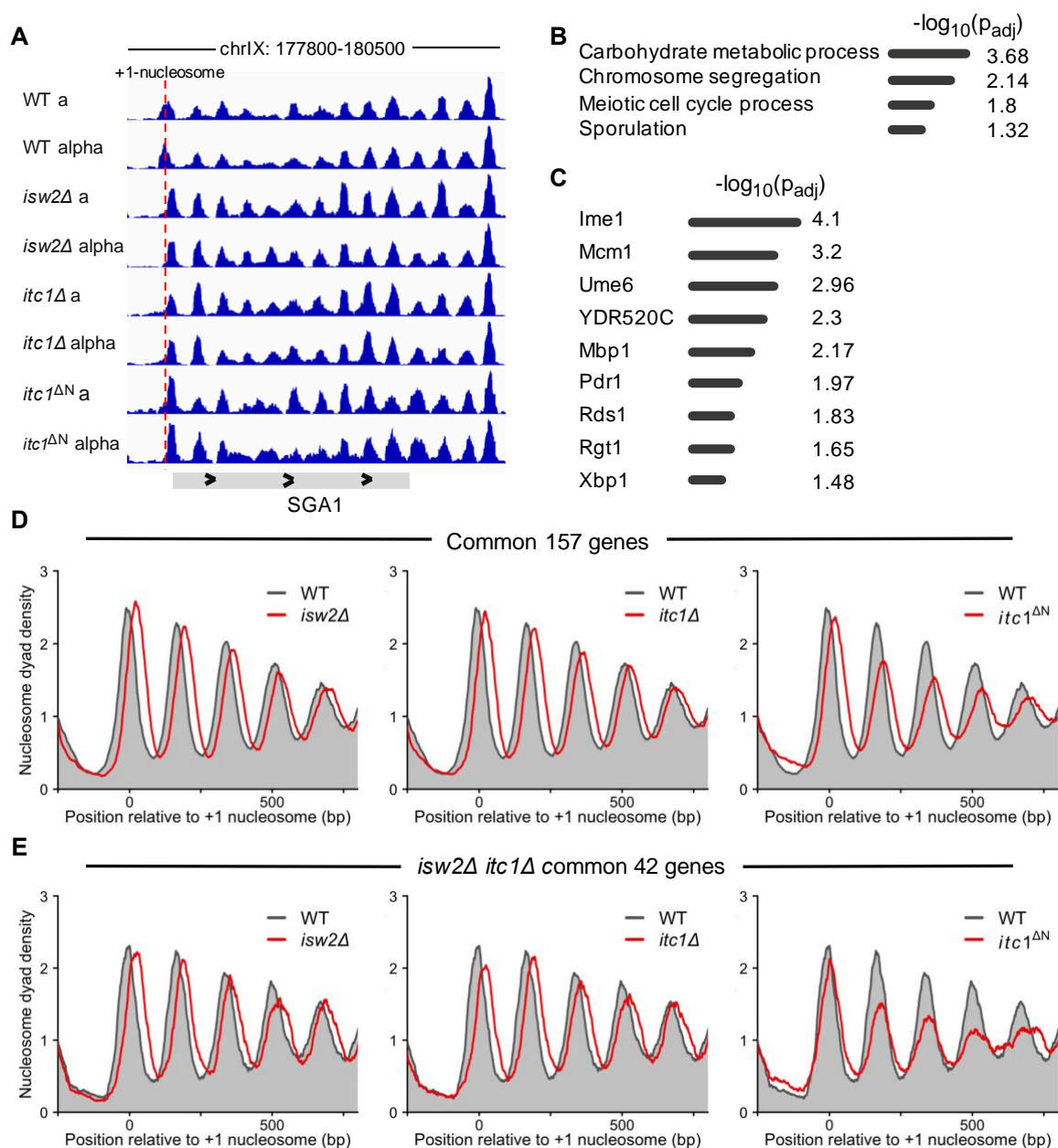


Figure 2.24: ISW2 remodeler lacking the N-terminus of *Itc1* is defective in the +1-nucleosome positioning. (A) IGV browser shot of MNase-Seq in cells lacking *Isw2*, *Itc1* and the N-terminus of *Itc1* in mat a and alpha backgrounds. The +1-nucleosome (red dotted line) in the *SGA1* gene is shifted in all mutants compared to WT. (B) Gene Ontology terms of genes showing a +1-nucleosome shift in *isw2Δ* and *itc1Δ* cells. The horizontal line indicates the strength of $-\log_{10}$ adjusted p-values. (C) Same as (B) but for transcription factor motifs enriched in genes showing the +1-nucleosome shift. (D) Gene-averaged nucleosome organization in common 157 genes showing shift in the +1-nucleosome in cells lacking *ISW2* or *ITC1*. All mutants show similar shift in the +1-nucleosome. (E) Same as (C) but for 42 genes common between *isw2Δ* and *itc1Δ* cells. The +1-nucleosome is shifted to lesser extent in the *itc1Δ^N* cells.

In line with the GO terms, these genes showed binding sites for Rgt1, Xbp1, Mbp1 and Pdr1 transcription factors regulating metabolic pathways (Figure 2.24C) (Raudvere et al., 2019; Yadon et al., 2013). Lastly, these genes showed ~30 bp average shift in the +1 nucleosome.

The whole nucleosome array in the gene body is shifted, instead of only the +1-nucleosome (Figure 2.24D, E and 2.25B, C).

In cells lacking the N-terminus of *Itc1*, we identified 232 genes (Appendix 6.1) with +1-nucleosome shift (Figure 2.25A). Among these genes, 157 genes were also found in *isw2Δ* and *itc1Δ* with similar +1 shifts (Figures 2.25A, B and 2.24 D). We also found 42 genes which showed +1 shift in *isw2Δ* and *itc1Δ* but not in the N-terminus *Itc1* mutant (Figures 2.25A, C and 2.24E). Moreover, 33 genes showed only a shift in the N-terminus *Itc1* mutant, among which 26 displayed downstream and 9 upstream shifts (Appendix 6.1). GO term and transcription factor motif analyses did not show any enrichment in these 33 genes (not shown). Therefore, the functional relevance of these genes and why they respond specifically in the *Itc1* N-terminus lacking cells is unclear.

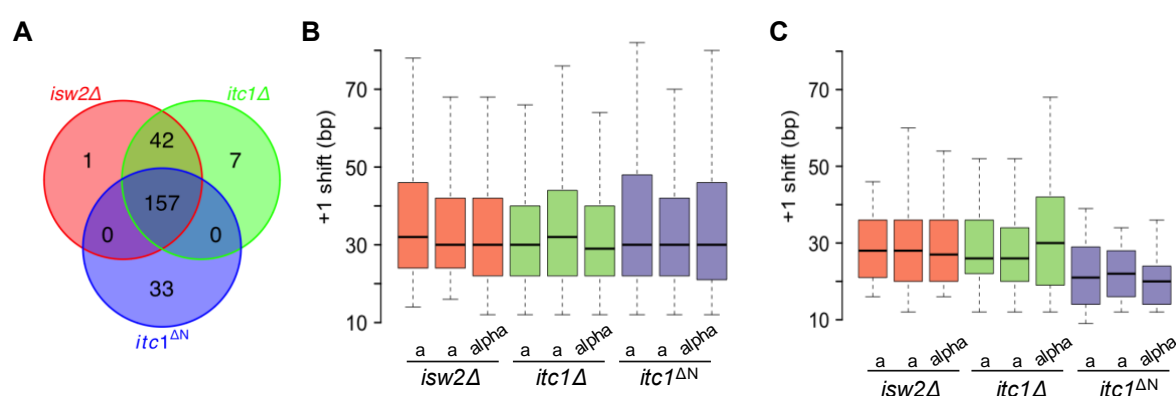


Figure 2.25 ISW2 remodeler lacking the N-terminus of *Itc1* shows similar +1-shift at most genes. (A) Overlap of genes showing the +1-nucleosome shift by at least 10 bp in cells as in (A). (B) Quantification of the +1-nucleosome peak-to-peak distance in mutants compared to WT for common 157 genes in (A). (C) Same as (B) but for 42 genes from (A). For each mutant, two replicates from mat a and one replicate for mat alpha is shown.

2.2.5 Deletion of the N-terminus of *Itc1* leads to global nucleosome re-organization

We observed in genome browser shots that nucleosomes in the gene body tend to become fuzzy upon the *Itc1* N-terminus deletion (Figure 2.24A). Therefore, we plotted composite plot to test the genome-wide nucleosome organization. Consistent with previous results (Gkikopoulos et al., 2011; Ocampo et al., 2016), deletion of *ISW2* or *ITC1* did not show any global change in nucleosome organization. Unexpectedly, deletion of the N-terminus of *Itc1* led to a significant increase in nucleosome fuzziness, as judged by a lower amplitude in the composite plot (Figure 2.26A). To measure change in nucleosome organization at each gene, we calculated nucleosome array regularity and NRL at each gene. The deletion of N-terminus of *Itc1* showed a clear decrease in array regularity while *isw2Δ* and *itc1Δ* did not show any change (Figure 2.26B). Moreover, genes also showed both increased and decreased NRLs compared to WT (Figure 2.26C). The broad distribution of NRL could arise from fuzzy nucleosome architecture in cells lacking the N-terminus of *Itc1* which leads to lower fit quality of nucleosome maps to an ideal Gaussian distribution (Ocampo et al., 2016).

Several possibilities to interpret the results exist, which I will outline in the next two paragraphs. In one possibility, the ISW2 remodeler lacking the N-terminus of Itc1 is defective in linker length sensing. This interpretation would be consistent with *in vitro* results showing that the N-terminus of ACF1 (homologue of Itc1) is important for linker length sensing and spacing activity (Hwang et al., 2014). A second possibility is that the deletion of N-terminus of Itc1 leads to a nonspecific activity of the mutant remodeler. This could arise from defects in folding of the remodeler or from aberrant nucleosome sliding activity.

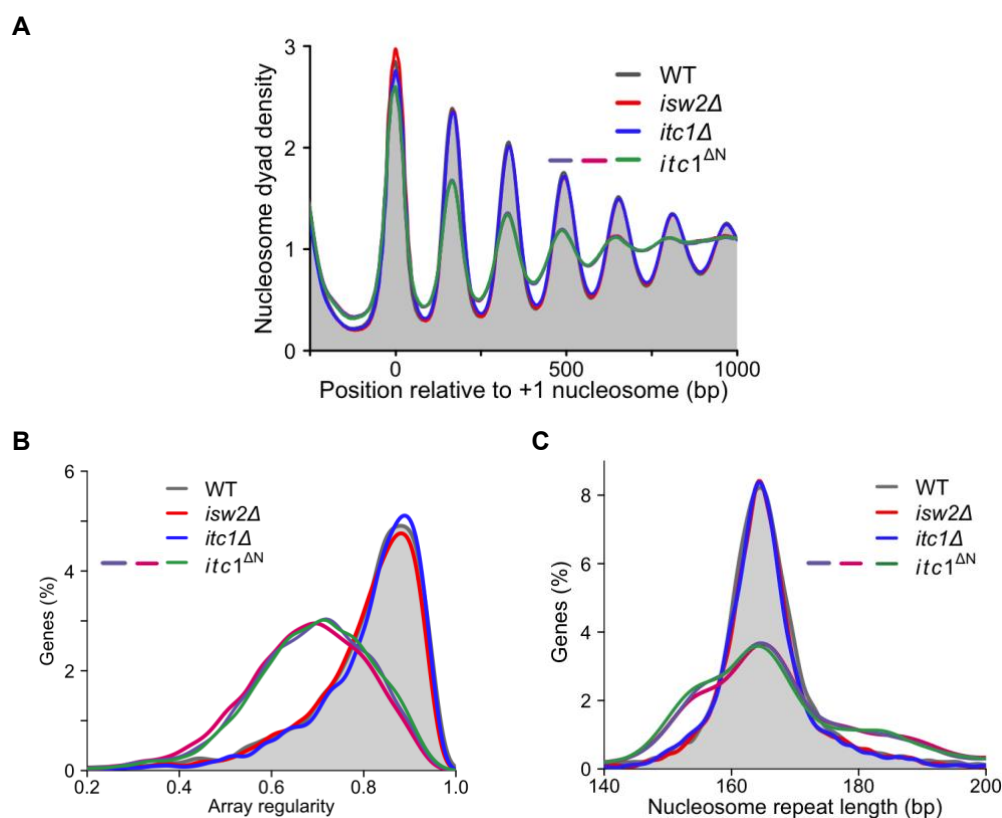


Figure 2.26: ISW2 remodeler lacking the N-terminus of Itc1 is defective in nucleosome spacing.

(A) Gene-averaged nucleosome organization in cells lacking *Isw2*, *Itc1* or the N-terminus of *Itc1*. The N-terminus deletion leads to lower amplitude in the gene body, suggesting less regular nucleosome arrays. **(B)** Array regularity distribution of ~5000 genes in cells from (A). **(C)** NRL distribution of ~5000 genes in cells from (A). MNase-Seq was performed in three biological replicates (two mat a and one mat alpha cells) showing highly consistent results. Replicates are shown only for the *Itc1* N-terminus mutant for clarity. Replicates were highly consistent as exemplified by overlapping plots in (A, B, C).

A third possibility is that the mutant *Itc1* protein itself negatively affects chromatin architecture, for example by nonspecific binding to chromatin. To test the latter possibility, one can delete the *Isw2* ATPase in cells lacking the N-terminus of *Itc1* (double deletion) and perform MNase-Seq. If the mutant remodeler leads to lower array regularity, then cells lacking both *Isw2* ATPase and *Itc1* N-terminus should show near WT-like array regularity because deletion of the *Isw2* ATPase itself has no effect on array regularity. If the lower array regularity is due to rogue activity of the mutant *Itc1* protein, then array regularity would remain similar to the single mutant of *Itc1* N-terminus.

Despite these possibilities, it is important to note here that a recent bioRxiv study showed nucleosome sliding activity with a similar *Itc1* mutant in the ISW2 complex (Donovan et al., 2020). In fact, this study could show higher *in vitro* nucleosome sliding activity by the mutant remodeler compared to the WT ISW2 remodeler. This may hint that the lower array regularity found in our experiments could arise from a hyperactive mutant remodeler compared to WT.

2.2.6 ISW2 resolves dinucleosomes at specific genes

ISW1 and Chd1 remodelers were recently shown to resolve dinucleosomes (Ocampo et al., 2019). To test whether ISW2 also plays a role in this process, we plotted nucleosome occupancy with 250-350 bp dinucleosome fragment lengths. As a positive control, we measured dinucleosome occupancy of *isw1Δ*, *chd1Δ* cells shown to possess increased levels of dinucleosomes near the +1-nucleosome (Ocampo et al., 2019). Cells lacking *Isw2* or *Itc1* did not show any change in dinucleosome occupancy (Figure 2.27A). On the other hand, *isw1Δ*, *chd1Δ* cells showed a clear increase in di-nucleosome occupancy (Figure 2.27C), consistent with previous results (Ocampo et al., 2019).

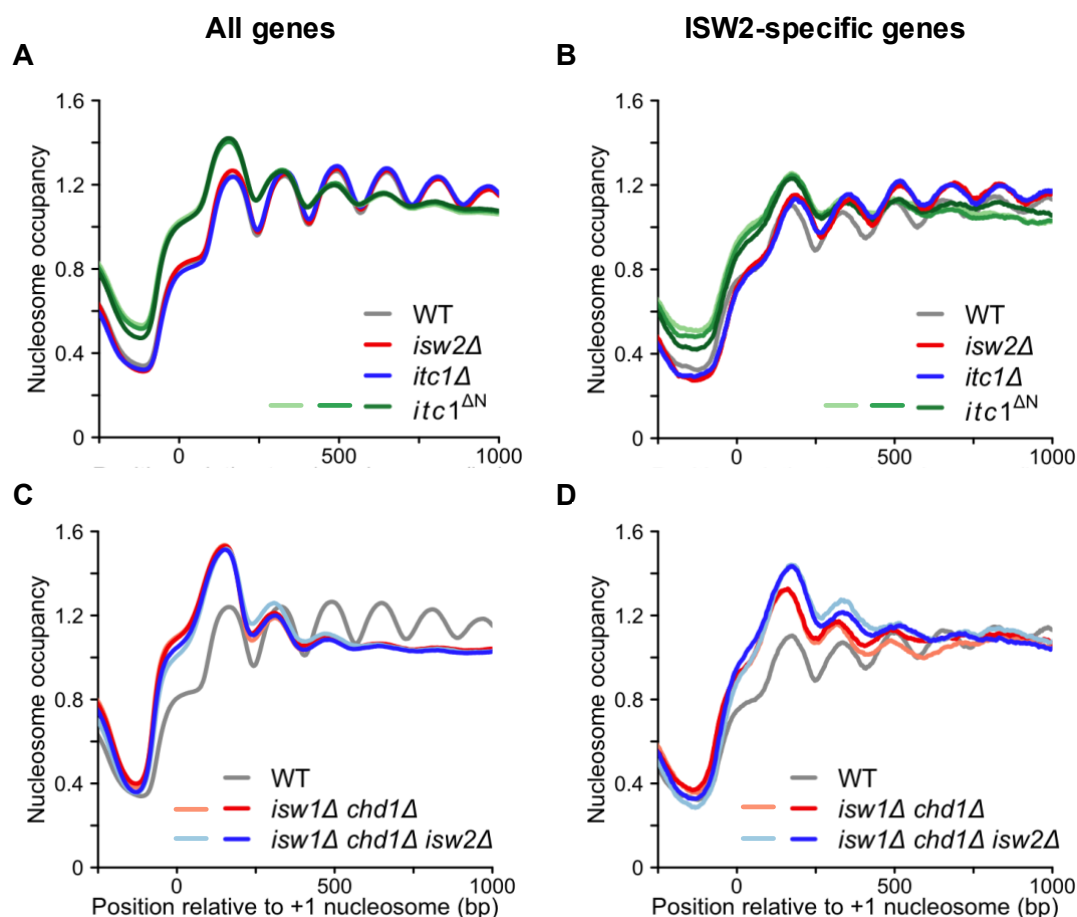


Figure 2.27: The ISW2 remodeler resolves dinucleosomes in the gene body of specific genes. (A) Composite plots showing occupancy of 250-350 bp fragment lengths in cells lacking *Isw2*, *Itc1* and the N-terminus of *Itc1*. (B) Same as (A) but for 200 genes showing +1 shift in *isw2Δ* compared to WT (Figure 2.25A). (C) Same as (A) but for cells with or without *Isw2* in *isw1Δ chd1Δ* background. (D) Same as (C) but for 200 genes showing +1 shift in *isw2Δ* compared to WT (Figure 2.25A). Shades of color represents biological replicates of each strain. When replicates are presented, darkest color represents the mutant strain in alpha background.

Because ISW2 is known to work on specific genes (Fazio et al., 2005; Whitehouse et al., 2007; Yadon et al., 2013), we checked dinucleosome occupancy on these genes. More specifically, we plotted dinucleosome occupancy in the genes showing a shifted +1-nucleosome in *isw2Δ* cells compared to WT, as identified in section 2.2.4. These genes showed a clear increase in dinucleosomes over the gene body in both *isw2Δ* and *itc1Δ* cells (Figure 2.27B). Consistent with these results, deletion of *ISW2* in *isw1Δ*, *chd1Δ* background also showed higher dinucleosome signal only over ISW2-specific genes (Figure 2.27C, D). These results suggest that the ISW2 remodeler helps resolve dinucleosomes in the gene body over specific genes.

Of note, we also found that deletion of the N-terminus in *Itc1* specifically leads to an increase in dinucleosomes over the +1-nucleosome but less so in the gene body (Figure 2.27A). This result suggests that the WAC domain is more important for resolving nucleosomes near the promoter while the WT remodeler performs this function over the whole gene.

2.2.7 ISW2-dependent genome-wide cell-type specific nucleosome architecture

The ISW2 remodeler modulates cell-type specific chromatin architecture. Earlier studies used indirect end-labeling to assess chromatin architecture at individual genes. Here, we used the MNase-Seq data of WT and *isw2Δ* cells in both mat a and alpha to analyze cell-type specific and ISW2-dependent chromatin architecture genome-wide. We measured array regularity as described in section 2.1.2. Importantly, this measure is unaffected by the shifted +1-nucleosome in *isw2Δ* cells because array regularity is measured relative to the +1-nucleosome position found in each dataset and not in comparison to the WT +1-nucleosome position. A list of genes with their array regularity scores in each mutant and WT can be found in Appendix 6.2.

We first identified genes showing cell-type specific array regularity between WT mat a and alpha cells. Consistent with previous results, we found *STE2*, *STE3*, *STE6*, *BAR1* and mating pheromone producing (*MFA1* and *MF(ALPHA)1*) genes (see Figure 2.28A for an example gene *STE2*) (Ercan and Simpson, 2004; Ganter et al., 1993; Morohashi et al., 2006; Ravindra et al., 1999; Shimizu et al., 1991; Teng et al., 2001; Weiss and Simpson, 1997, 1998). In addition to these well-known genes, we found *KAR4* (Figure 2.28B) and *AGA2* (Figure 2.28D) genes showing higher array regularity in mat alpha compared to mat a cells. *SAG1*, on the other hand, showed higher array regularity in mat a compared to alpha cell (Figure 2.28C) (Abraham et al., 2012). *Kar4* is a transcription factor required during meiosis (Kurihara et al., 1996), *Sag1* is an agglutinin required for mating (Doi et al., 1989), and *Aga2* is an adhesion subunit of α -agglutinin (Galgoczy et al., 2004). Besides, we also observed cell-type specific response in *SNL1*, *GYP8*, *CBT1*, *YNL146W* and *TFB3* genes (Appendix 6.2), likely due to their physical proximity with *BAR1*, *STE2*, *STE6*, *MFA2* and *MFA1* genes, respectively.

To identify genes dependent on ISW2 for regular nucleosome arrays, we compared array regularity in *isw2Δ* to WT. Consistent with previous results, *RNR3* was among the strongest responders showing dramatically lower array regularity in *isw2Δ* (Figure 2.28E) (Zhang and Reese, 2004). Also in line with previous results, we found cell-type specific genes (*STE2*,

STE6, *MFA2* and *MFA1*) to be dependent on ISW2. Interestingly, array regularity in *KAR4* and *AGA2* genes (discussed above) was dependent on the ISW2 remodeler while *SAG1* was not (Figure 2.28B – D). This result suggests that *SAG1* is a cell-type specific gene not regulated by ISW2. The ISW2-dependent array regularity in *KAR4* is likely due to neighbouring recombination enhancer which is known to require ISW2 for establishing regular arrays (Figure 2.28B) (Weiss and Simpson, 1997).

Furthermore, we identified several new genes dependent on ISW2 for establishing regular arrays. These genes are involved in processes like sporulation (*RIM4*, *ADY2*) (Deng and Saunders, 2001; Paiva et al., 2004; Soushko and Mitchell, 2000), rDNA transcription (*NOP6*, *RRT6*) (Garcia-Gomez et al., 2011; Hontz et al., 2009), are membrane proteins (*LCB3*, *SCW10*, *PRM8*, *YCR101C*, *RSN1*) or have unknown function (*PAU5*, *PAU20*, *YML131W*, *LEE1*) (see Figure 2.28F for an example gene *YML131W*) (Luo and van Vuuren, 2009; Viswanathan et al., 1994). Overall, these results hint that ISW2 regulates nucleosome array regularity in the gene body of several distinct classes of genes. It is possible that the change in array regularity upon *ISW2* deletion is due to indirect effects, for example via increased transcription of these genes.

To our surprise, we also found a set of genes showing increased nucleosome array regularity in *isw2Δ* compared to WT. These genes (*HIM1*, *DMC1*, *PRM5*, *YAP6*, *POG1*, *STL1*, *YJL218W*, *YFL051C*, *SKS1*) are also involved in sporulation and meiosis or are membrane proteins (see Figure 2.28G for an example gene *YFL051C*). Close inspection of the nucleosome profiles in genome browser revealed that these genes usually show fuzzy +1- to +4-nucleosomes. Upon *ISW2* deletion, nucleosomes shift downstream and establish more regular arrays compared to WT. It is possible that lower array regularity in WT cells is due to opposing remodeler activities in these genes. Upon *ISW2* deletion, other remodelers, like *ISW1* and *Chd1*, may generate more regular array.

Taken together, these results provide a genome-wide cell-type specific nucleosome architecture and array regularity information. Importantly, our results are consistent with single gene studies performed almost two decades ago using indirect end-labeling method. We also identified new genes whose nucleosome architecture is not known to be regulated in a cell-type specific manner. *ISW2* remodeler is known to play a significant role in establishing cell-type specific nucleosome architecture at few genes. Therefore, we used MNase-Seq data in cells lacking *Isw2* in both mat a and alpha backgrounds to test genome-wide response. These experiments revealed several classes of genes not known previously to be regulated at the nucleosome level by the *ISW2* remodeler. Future studies will reveal if the nucleosome architecture generated by *ISW2* affects gene expression of these genes.

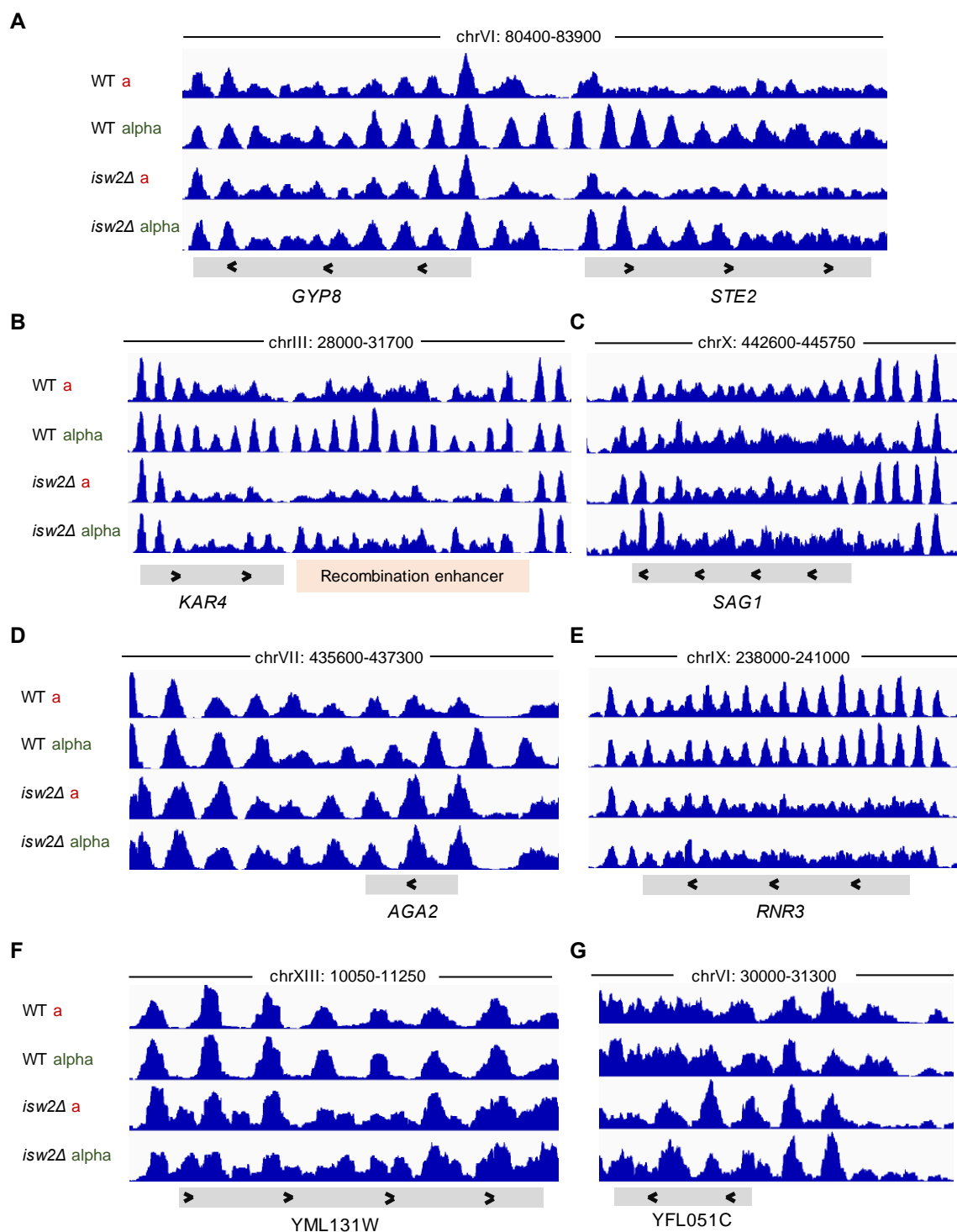


Figure 2.28: The ISW2 remodeler contributes to array regularity in the gene body of specific genes. (A) Genome browser shot showing nucleosome organization in *STE2* and *GYP8* genes in WT and *isw2Δ* cells in mat a and alpha backgrounds. *STE2* is a cell-type specific gene showing ISW2-dependent nucleosome organization while *GYP8* shows less dependence on ISW2 compared to *STE2*. (B) Same as (A) but for the *KAR4* gene and the adjacent recombination enhancer showing ISW2-dependent regular nucleosome arrays in a cell-type specific manner. (C) Same as (A) but for the *SAG1* gene showing ISW2-independent cell-type specific nucleosome arrays. (D) Same as (A) but for cell-type specific *AGA2* gene. (E) Same as (A) but for *RNR3* gene showing dramatically lower array regularity in *isw2Δ*. (F, G) Same as (A) but for the *YML131W* and *YFL051C* genes showing decrease and increase in array regularity, respectively, in *isw2Δ* compared to WT. MNase-Seq experiments were

performed in two biological replicates for mat a and once for mat alpha cells in both WT and *isw2Δ* cells.

2.2.8 Interactome of the ISW2 nucleosome remodeler

How ISW2 complex is recruited to specific genes in the genome is less understood (Yadon et al., 2013). The domain architecture of the Isw2 ATPase in the ISW2 complex is conserved across Isw1 and other nucleosome remodeling ATPases (Clapier et al., 2017). Therefore, we hypothesized that the Itc1 subunit may establish ISW2-specific protein-protein interactions. These interaction partners may have a role in specific recruitment of the ISW2 complex to promoter region. To identify the interaction partners of the ISW2 complex and their dependence on Itc1, we performed Isw2-TAP Protein A immunoprecipitation coupled with mass spectrometry in cells expressing or lacking Itc1 (Cox et al., 2009; Morris et al., 2014; Shevchenko et al., 2006). These experiments were performed in low (150 mM) and high (350 mM) salt conditions. As a negative control, we used untagged WT and *itc1Δ* strains.

With 3-fold enrichment over negative control as a cut-off, we identified 474 and 268 proteins interacting with the WT ISW2 complex in low and high salt conditions, respectively. Deletion of *ITC1* reduced the interacting proteins by ~2-fold (253 and 104 in low and high salt, respectively), suggesting Itc1 mediates many of these interactions either directly or by recruiting the ISW2 complex to specific sites. Convincingly, the accessory subunits Dls1 and Dpb4 were enriched only in the WT ISW2 ATPase dataset (both low and high salt) and were absent from Itc1 lacking samples. The list of proteins identified in each condition can be found in Appendix 6.3.

We found several classes of proteins among which nucleosome remodelers, histones, histone chaperones, RNA metabolism, transcription initiation and elongation factors were enriched (at least by 3-fold) in the ISW2 complex interactome. Gene Ontology enrichment analysis also showed similar terms (Figure 2.29A). Although deletion of Itc1 reduced interaction partners, similar GO terms were enriched as the WT ISW2 complex. (Figure 2.29B). This may hint that the ISW2 complex utilizes both subunits for establishing protein-protein interactions in the cell. Below, I discuss the major interaction partners of the WT ISW2 complex.

Major interaction partners of the ISW2 complex: The nucleosome remodelers of all major families (ISW1, Chd1, RSC, SWI/SNF, INO80, Fun30) and the FACT complex were enriched. All four canonical histones and the histone variant H2A.Z were also found. Only HIR complex (Hir1, Hir2, Hir3, Hpc2) of histone chaperones was enriched, suggesting the ISW2 complex may specifically cooperate with the HIR complex during nucleosome deposition. Surprisingly, we found several proteins involved in RNA processing including several members of the CCR4-NOT complex, mRNA capping (Cet1, Cdc33, Pab1) and decapping (Pat1, Dhh1, Edc3, Dcp2) enzymes, RNA helicases (Hca4, Dbp5, Nam7, Sub2) and RNA polyadenylation (Rrp43, Pap1, Def1, Hrp1, Yra1, Mrn1, Cft1). This result suggests that ISW2 may have a role in regulating mRNA stability and degradation. Furthermore, we found transcription initiation related factors for RNA Pol II and Pol III, such as Abf1, Rap1, Tup1-Cyc8 co-repressor, Pho81, Mot1, Msn2 and Tfc1- 7. These interactions are consistent with ISW2 binding and functional

site near the genic promoter. Lastly, we found nuclear pore proteins and proteins involved in nuclear mRNA export (Los1, Nup192, Nup60, Nup2, Nup188, Dbp5, Tom1, Nsp1, Ssc13, Cex1, Sxm1, Yra1, Crm1, Kap95, Kap104).

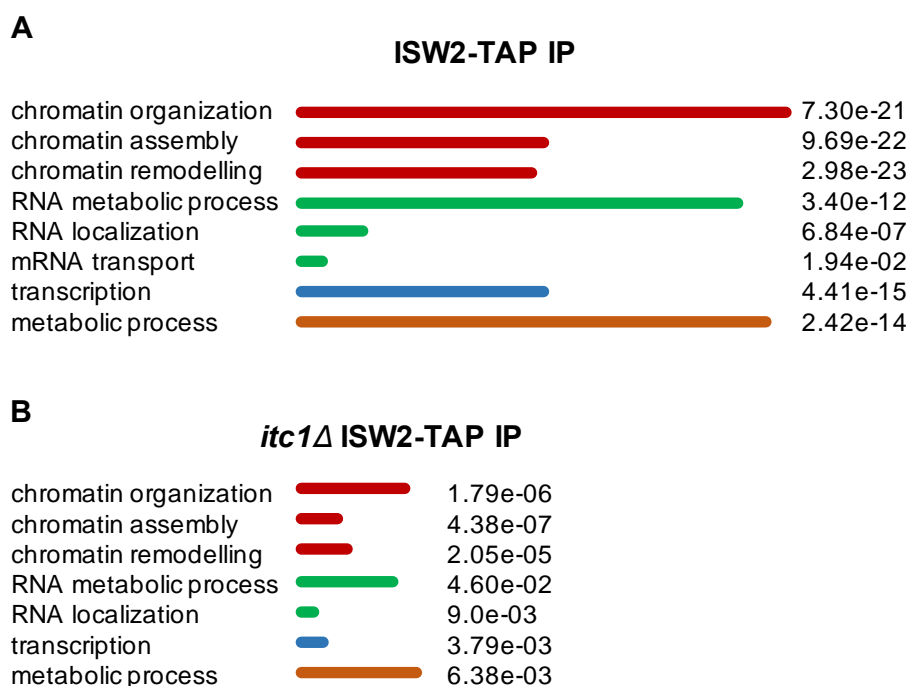


Figure 2.29: Gene Ontology (GO) analysis of the ISW2 interactome. (A) GO terms of proteins enriched at least 3-fold in ISW2-TAP relative to untagged control in low salt (150 mM NaCl) conditions. The length of the colored lines indicates the number of genes enriched in the indicated GO category. Values indicate the p-value associated with each GO term. **(B)** Same as (A) but for cells lacking *Itc1*. Experiment was performed only once.

It is important to note here that the experiment was performed only once. Currently, we cannot distinguish between direct and indirect interaction partners. In future, it is essential to perform biological replicates and further validate interesting interactions, minimally with western blot, before testing the functional relevance of these interactions. Nevertheless, the dataset suggests an involvement of the ISW2 remodeler in functions beyond the well-known nucleosome sliding activity.

2.2.9 ISW2 interacts with RNA *in vivo*

Because our results suggest that the ISW2 complex potentially interacts with several RNA processing factors, we hypothesized that ISW2 itself may interact with RNA *in vivo*, and thereby, help regulate RNA biogenesis. To test if ISW2 binds cellular RNA, we performed *in vivo* UV-crosslink and immunoprecipitated ISW2-TAP to detect any RNA bound to the ISW2 complex. As a negative control, WT untagged strain was tested in parallel. ISW2-TAP immunoprecipitation was performed under high salt (1 M NaCl) conditions to reduce non-specific interactions. To remove contaminating DNA bound to the ISW2 complex, we treated the elution fraction with DNase I. Lastly, we treated a part of the eluted sample with RNase A to test direct binding of RNA to ISW2.

We found that the ISW2 complex interacts with several RNA species in the cell, as deciphered from the molecular weight of RNA molecules in a denaturing PAGE (Figure 2.30, lane 1). The untagged negative control showed reduced RNA amounts with lower molecular weights, suggesting interaction of ISW2 with specific classes of RNA *in vivo* (Figure 2.30, lane 2). RNase A treatment removed virtually all signal in the gel, suggesting presence of RNA in the undigested sample (Figure 2.30, compare lanes 1 and 3) and argues against DNA contamination in the elution fractions. Overall, this result suggests that the ISW2 complex interacts with RNA in the cell. It is possible that the ISW2 remodeler have functions similar to ISW1 (Babour et al., 2016) towards regulating RNA stability or localization (see Discussion related to this chapter).

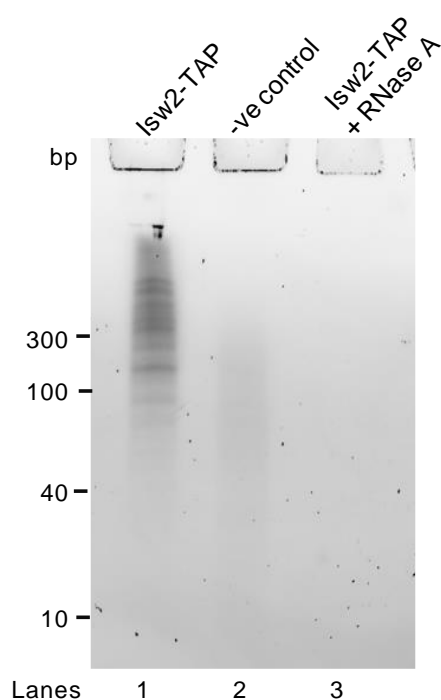


Figure 2.30: ISW2 complex interacts with RNA *in vivo*. Denaturing PAGE of RNA UV-crosslinked to the ISW2 complex *in vivo*. Isw2-TAP lane indicates immunoprecipitated RNA treated with DNase I from TAP-tagged Isw2 cells. Lane “-ve control” indicates immunoprecipitated RNA treated with DNase I from untagged WT cells. Last lane indicates a fraction of sample as in lane 1 but further treated with RNase A. Experiment was performed only once.

2.2.10 DISCUSSION (related to this chapter)

The ISW2 nucleosome remodeler slides and spaces nucleosomes *in vivo* and *in vitro*. *In vivo*, it slides nucleosomes towards the NFR, thus represses transcription of specific classes of genes. Concordant with this, ISW2 depletion leads to increased TBP and Pol II binding at the promoters and in the gene body of these genes, respectively (Kubik et al., 2019). *In vitro*, it helps in chromatin assembly and generates regular nucleosome arrays, suggesting ISW2 can sense linker length between nucleosomes (Baldi et al., 2018a; Fyodorov and Kadonaga, 2002b; Ito et al., 1997; Längst et al., 1999; Lusser et al., 2005; Scacchetti et al., 2018; Tsukiyama et al., 1999).

The linker length sensing activity of the ISW2 complex (or *Drosophila* and human homologue ACF) is quite well understood. It senses the linker DNA length and slides nucleosomes towards the longer linker through an interplay between the Isw2 ATPase and the accessory subunit Itc1 regulated by the H4-tail. When the linker DNA is short, the N-terminus of Itc1 (*Drosophila* ACF1) binds to the H4-tail and competes with the auto-inhibitory motif (AutoN) in the Isw2 ATPase, thereby inhibiting nucleosome sliding. Upon increase in the linker DNA length, the N-terminus of Itc1 preferentially binds linker DNA and releases the H4-tail to activate nucleosome sliding. Deletion of the N-terminus of Itc1 (*Drosophila* ACF1) abolishes linker length sensitivity, suggesting it may regulate nucleosome spacing *in vivo*. This activity was suggested to be important for cellular growth as deletion of the N-terminus of Itc1 led to severe growth defect (Clapier and Cairns, 2012; Eberharter et al., 2001; Fyodorov and Kadonaga, 2002a; Hwang et al., 2014).

Here, we show that cells lacking the N-terminus of Itc1 have no growth defect, contrary to published result (Hwang et al., 2014). We tested the mutant construct in WT and *isw1Δ chd1Δ* backgrounds, consistently showing no growth defect (Figure 2.22). Therefore, we suggest that the growth defect in Hwang et al. study is likely due to nonspecific mutations arising from the transformation event. It is known that transformation of a linear DNA in yeast is prone to high levels of secondary mutations in the genome due to non-specific recombination (Klinner and Schafer, 2004). The severe growth defect was also surprising as complete *ITC1* or *ISW2* deletions have no measurable change in growth compared to WT.

Our results show that cells lacking the N-terminus of Itc1 have higher shmoo formation potential, suggesting that the mutant ISW2 remodeler is defective in nucleosome sliding (Figure 2.23). Indeed, our MNase-Seq results show that deletion of the N-terminus of Itc1 lead to similar shift in the +1-nucleosome as cells lacking Isw2 or Itc1. By measuring shift in the +1-nucleosome, we found that ISW2 slides +1-nucleosomes ~30 bp on average towards the promoter (Figure 2.25). In contrast to the +1 shift, the N-terminus deletion within Itc1 led to a genome-wide decrease in nucleosome array regularity, while *isw2Δ* or *itc1Δ* cells showed no change (Figure 2.26). These results hint that the ISW2 remodeler lacking the N-terminus of Itc1 is defective in linker length sensing and the mutant ISW2 remodeler is not restricted to specific genes like the WT ISW2 remodeler. It is tempting to speculate that the N-terminus of Itc1 limits ISW2 activity to specific genes, for example by inhibiting nucleosome sliding at non-specific regions in the genome or by promoting ISW2 interaction with sequence-specific transcription factors. Nevertheless, it remains possible that the mutant ISW2 remodeler or the Itc1 protein acquires rogue activity in the cell leading to general decrease in nucleosome organization. To test whether the decrease in array regularity is directly due to defective ISW2 remodeler, one should perform a double deletion of *ISW2* and N-terminus of Itc1. This may shed light on direct or indirect nature of the defect observed in cells lacking the N-terminus of Itc1.

We discovered that ISW2 helps resolve dinucleosomes at genes where it slides the +1-nucleosome. This activity is visible over the gene body, in contrast to ISW1 and Chd1 remodelers which resolve dinucleosomes near the +1-nucleosome (Figure 2.27) (Ocampo et

al., 2019). In line with ISW2 activity in the gene body, we observed several genes with decreased array regularity in the gene body compared to WT. Importantly, these genes showed a negligible change in the +1-nucleosome position. These results suggest that ISW2 also slides nucleosomes in the gene body, although it is restricted to specific genes. Our results cannot rule out an indirect effect upon *ISW2* deletion, for example via change in gene expression of these genes.

Lastly, we found several proteins involved in mRNA processing, including capping, decapping, helicases, 3'-A polyadenylation, nuclear export and degradation to potentially interact with the ISW2 remodeler. This result could hint at a previously unknown role of ISW2 in RNA biogenesis. In line with this idea, we found that ISW2 crosslinks to RNA *in vivo*. These results are in line with the role of ISW1 remodeler in regulating transcription termination and export of defective transcripts near the site of transcription (Alen et al., 2002; Babour et al., 2016; Morillon et al., 2003; Ocampo et al., 2019; Santos-Rosa et al., 2018). In future, one can identify the RNA species interacting with ISW2 and even the binding sites of ISW2 in the RNA with nucleotide resolution using techniques like PAR-CLIP and iCLIP (Hafner et al., 2010; Huppertz et al., 2014). This will help understand if ISW2 interacts with any specific class of RNA and biological function of ISW2-RNA interaction *in vivo*.

2.3 Chapter: Mechanistic dissection of the ISW1 nucleosome remodeler

Part of results in this chapter are published (Figure 2.34, panels B-E) at the journal eLife. I performed growth arrays of ISW1 mutants lacking N-terminal regions and tested expression of these constructs (Ludwigsen et al., 2017).

2.3.1 Background

The ISW1 nucleosome remodeler

S. cerevisiae consists of two ISWI-related nucleosome remodeling complexes: ISW1 and ISW2. The *Isw1* ATPase subunit associates with either *loc3* to form ISW1a complex or with *loc2* and *loc4* to form ISW1b complex (Tsukiyama et al., 1995; Tsukiyama et al., 1999; Vary et al., 2003). The ISW1a complex slides nucleosomes to the center to DNA and the ISW1b complex to the end, suggesting ISW1a can space nucleosomes (Stockdale et al., 2006). Indeed, the ISW1a complex can generate nucleosome arrays *in vitro*, while ISW1b cannot (Krietenstein et al., 2016; Vary et al., 2003). The ISW1a complex may act as a “protein ruler” for nucleosome spacing by interacting with two adjacent nucleosomes (Richmond, 2012; Yamada et al., 2011).

Consistent with *in vitro* results, deletion of the *Isw1* ATPase in *S. cerevisiae* shows a decrease in NRL and nucleosome array regularity (Gkikopoulos et al., 2011; Ocampo et al., 2016). ISW1, together with Chd1, also helps to resolve dinucleosomes near the 5' end of genes. This activity may indirectly contribute to nucleosome array regularity and facilitates Pol II elongation in the gene body (Eriksson and Clark, 2020; Ocampo et al., 2019).

The role of the ISW1 remodeler in nucleosome spacing and array regularity is well documented. On the other hand, how ISW1 achieves this function is less understood. Multiple *in vitro* studies have implicated several domains and subunits in the ISW1 complex towards linker length sensing and nucleosome spacing. For example, mutating AutoN or NegC regions in ISWI decreases mononucleosome centering activity (Clapier and Cairns, 2012; Gamarra et al., 2018; Hwang et al., 2014; Leonard and Narlikar, 2015). The C-terminal HSS domain in the ISWI ATPase, together with the accessory subunits, has been suggested to contact the linker DNA which may contribute to ISWI nucleosome spacing activity (Grüne et al., 2003; Yamada et al., 2011). The *Drosophila* ISWI ATPase domain can slide, but not space, nucleosomes *in vitro*, corroborating the role of accessory domains and subunits in ISWI nucleosome spacing (Lieleg et al., 2015a; Mueller-Planitz et al., 2013a; Mueller-Planitz et al., 2013b). In contrast to the *Drosophila* ISWI ATPase subunit, the yeast *Isw1* ATPase cannot slide nucleosomes *in vitro* (Längst et al., 1999; Vary et al., 2003).

To better understand the underlying mechanism of nucleosome spacing by the ISW1 remodeler *in vivo*, we first reintroduced the *Isw1* ATPase in the TKO (*isw1Δ, isw2Δ, chd1Δ*) strain (Tsukiyama et al., 1999). This system provides an opportunity to dissect the role of individual remodelers with reduced redundancy. To investigate the roles of domains and subunits within the ISW1 complex, we ectopically expressed mutants of the *Isw1* ATPase lacking the N- or C- terminus domains (explained below) in the TKO strain. Lastly, we varied

the expression levels of WT and mutant *Isw1* constructs to account for reduced nucleosome binding or affinity of some of the mutant constructs (Blazeck et al., 2012).

The specific aims of this chapter are:

1. What are the roles of the conserved ppHSA, AutoN and AcidicN motifs in the N-terminal region of the ISW1 remodeler?
2. Does AutoN motif regulates ISW1 nucleosome spacing function?
3. Is NegC motif important for nucleosome spacing by the ISW1 remodeler?
4. Can *Isw1* ATPase slide nucleosomes *in vivo* without accessory subunits?
5. Is the yeast *Isw1* ATPase domain, like *Drosophila* ISWI ATPase domain, capable of sliding nucleosomes?

To test the role of individual domains and subunits in ISW1 function *in vivo*, we employed a temperature-sensitive growth assay and MNase-Seq. The TKO strain shows slower growth at a higher temperature (37 °C) than a permissible temperature (30 °C), compared to WT (Figure 2.31C) (Tsukiyama et al., 1999). Nucleosome arrays are also severely compromised in the TKO strain compared to WT cells (Gkikopoulos et al., 2011; Ocampo et al., 2016). Both temperature sensitivity and nucleosome arrays are complemented partially in a DKO (Double Knock Out; *isw2Δ*, *chd1Δ*) strain expressing only ISW1 spacing remodeler when compared to the TKO strain (Figure 2.32A).

Please note that all MNase-Seq experiments in this chapter, except in Figures 2.32 and 2.33, were performed before establishing the optimized protocol described in section 2.1.2. The lower MNase-Seq data quality, due to uneven nucleosome read distribution in genes, hindered a gene-by-gene analysis and showed inconsistent results across biological replicates of the control samples (WT and TKO) (Figure 2.1 and data not shown). Therefore, I present here only the composite plots representing a combined nucleosome organization of ~5000 genes which are more robust to variations in single genes (as shown in Figure 2.1) than the gene-by-gene analyses presented in previous chapters.

2.3.2 A galactose-inducible expression library to study ISW1 remodeling

We used a galactose-inducible promoter library of sixteen plasmids which enables 50-fold dynamic expression of the downstream gene (Blazeck et al., 2012). These plasmids are named here as P1 – P16 (Appendix 6.4), where P stands for the galactose-inducible promoter used. The numbers 1 to 16 denote the sixteen plasmids sorted according to the increasing expression levels of a yECitrine gene under the galactose-inducible promoter (Appendix 6.4) (Blazeck et al., 2012).

To test the expression of the *Isw1* ATPase under the galactose-inducible promoters, we first generated a monoclonal anti-*Isw1* antibody targeted to the ATPase domain (Appendix 6.5). This antibody (clone 3C4) is highly specific to the *Isw1* ATPase and does not cross-react with *Isw2* and other homologous ATPases (Appendix 6.5). Western blot showed an increasing expression of the *Isw1* ATPase from P1 to P16 library (Figure 2.31A). P1 showed lower expression than the *Isw1* levels in the DKO strain (*isw2Δ*, *chd1Δ*). P4 showed the most similar

expression to *Isw1* levels in the DKO strain (Figure 2.31B). We also observed a significant amount of lower molecular weight bands with increasing expression levels of the *Isw1* ATPase. These bands were also present in the DKO strain to a lower extent but absent from the TKO strain lacking *Isw1* (Figure 2.31A). This result suggests that the lower molecular weight bands corresponds to degradation products of the *Isw1* ATPase.

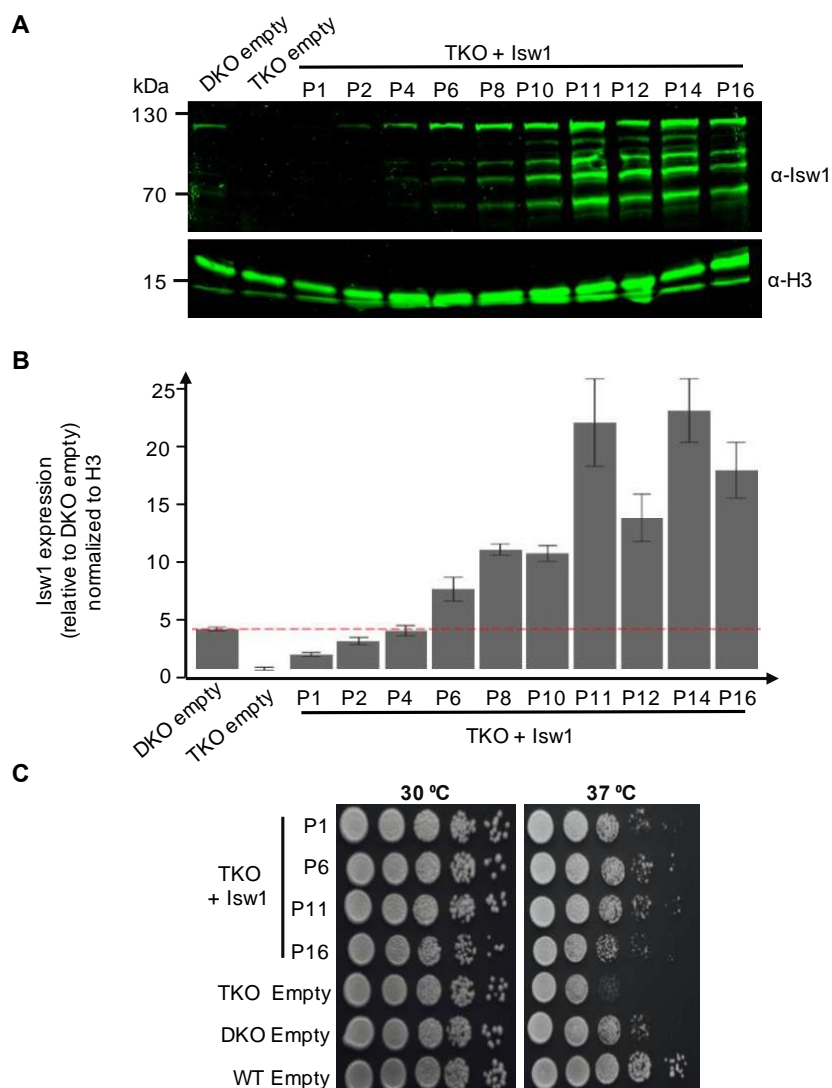


Figure 2.31: An inducible expression library to modulate *Isw1* levels *in vivo*. (A) Representative western blot showing expression of *Isw1* in DKO (*isw2* Δ , *chd1* Δ), TKO (*isw2* Δ , *chd1* Δ , *isw1* Δ) and TKO transformed with a promoter library containing *ISW1* gene. *Isw1* expression was induced overnight with 2% galactose. (B) Bar plots showing expression levels of the *Isw1* ATPase under promoter library relative to the DKO strain expressing *Isw1* ATPase under its native promoter. Top band in the anti-*Isw1* antibody (clone 3C4) blot was selected and normalized to the top band in the anti-histone 3 antibody blot. Error bars indicate minimum and maximum values from two biological replicates (colonies from a single transformation event). (C) Growth assay showing complementation by *Isw1* under indicated expression promoters. Shown are 10-fold dilutions. Images were taken after 3 days. Growth assay was repeated twice with two transformants.

Expression of the *Isw1* ATPase fully complemented the temperature-sensitive phenotype of the TKO strain (Tsukiyama et al., 1999). Even the lowly expressing P1 promoter displayed similar growth as the DKO strain. P16 promoter showed a mild growth defect compared to the

P1 – P11, suggesting higher expression of the *Isw1* ATPase is mildly toxic to cells (Figure 2.31C).

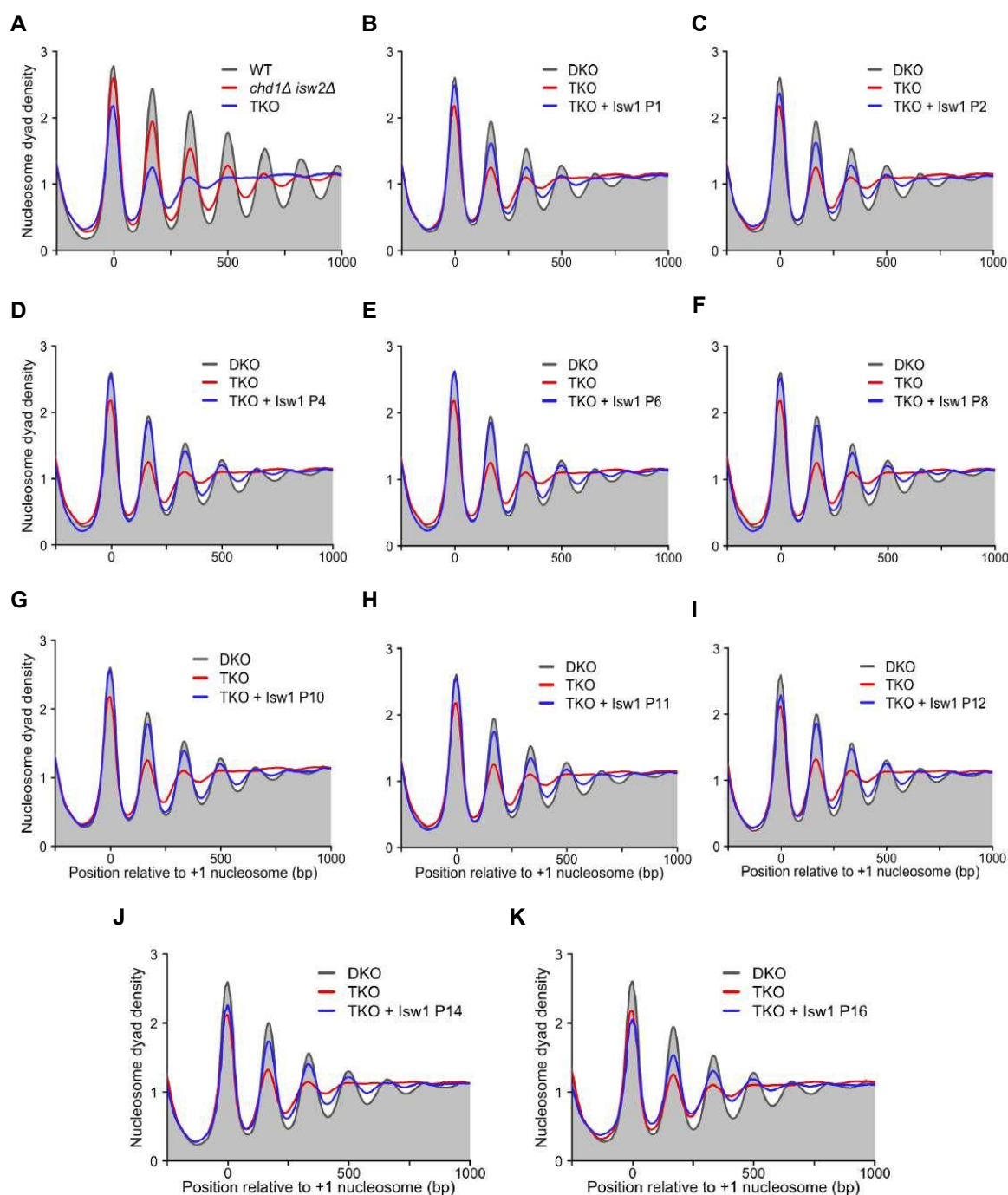


Figure 2.32: Nucleosome array formation by ectopically expressed *Isw1* under a promoter library. (A) Gene-averaged nucleosome organization in WT, DKO (*chd1Δ isw2Δ*) and TKO strains containing an empty plasmid. (B) Same as (A) but with the TKO strain expressing *Isw1* from P1 promoter. (C, D, E, F, G, H, I, J, K) Same as (B) but with *Isw1* expressed from indicated promoters. MNase-Seq was performed with an optimized protocol as described in the Section 2.1.2. MNase-Seq was performed only once for all conditions except for WT, DKO and TKO strains. WT, DKO and TKO strains harbored an empty plasmid where promoter sequence and *yECitrine* gene was deleted from the P1 plasmid. All strains were grown in minimal media with galactose as sole carbon source.

To test the *Isw1* complementation at a molecular level, we performed MNase-Seq in the TKO strains expressing *Isw1* under P1, P2, P4, P6, P8, P10, P11, P12, P14 and P16 plasmids and compared to the DKO strain expressing *Isw1* under native promoter. Composite plots of the mutants were compared to the control strains measured in parallel. We found that *Isw1* under P1 and P2 leads to enhanced nucleosome arrays, but less than the DKO strain (Figure 2.32A – C). Higher expression with P4 – P12 showed similar nucleosome arrays as DKO (Figure 2.32D – I). Lastly, the highest expression with P14 and P16 led to decreased array regularity, consistent with their slower growth (Figure 2.32J, K).

To test complementation due to the *Isw1* ATPase at each gene, we measured nucleosome repeat length and array regularity at each gene. All expression levels, except lowest expression P1, showed similar median NRL, suggesting ISW1 similarly spaces nucleosomes independent of the expression level (Figure 2.32A). Expression of the *Isw1* ATPase also increased array regularity when compared to TKO (Figure 2.32B). The array regularity distributions were largely similar to the DKO strain at most *Isw1* expression levels. Only P1 clearly harbored less regular arrays than other promoters.

Overall, these results show the direct nature of ISW1 remodeler towards establishing nucleosome array *in vivo*. These results are also consistent with the results obtained from cells lacking *ISW1* with decreased array regularity compared to WT (Ocampo et al., 2016). Furthermore, the dynamic range of *Isw1* expression provides an opportunity to dissect the mechanism of ISW1 mediated nucleosome array organization *in vivo*.

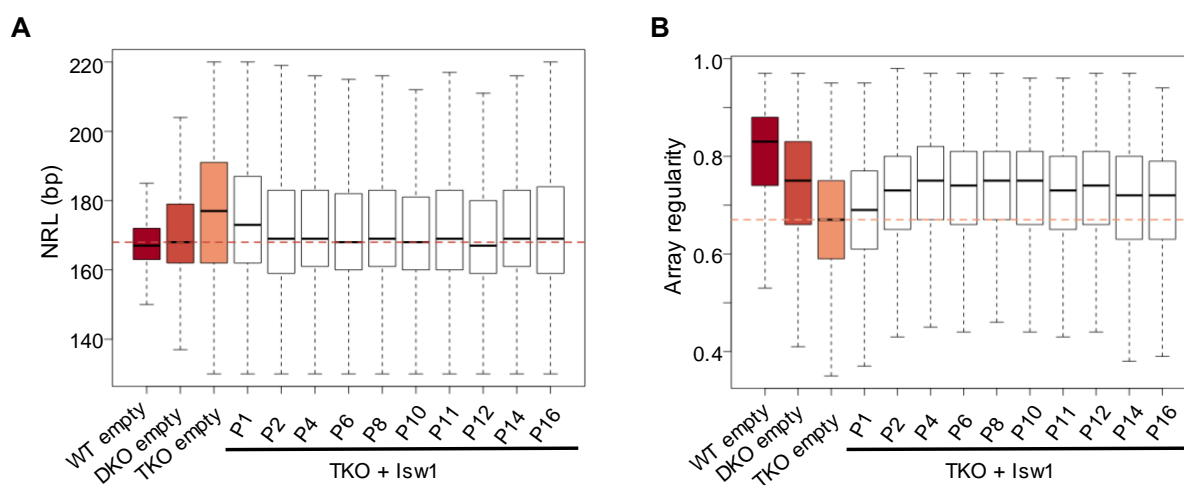


Figure 2.33: Comparison of NRL and array regularity distributions for cells expressing *Isw1* ATPase under a promoter library. (A) Boxplots showing NRL distributions for WT, DKO, TKO and TKO strains expressing the *Isw1* ATPase subunit under the indicated promoters. **(B)** Same as (A) but showing array regularity distributions. MNase-Seq data is from Figure 2.32.

2.3.3 The N-terminus of *Isw1* is essential for ISW1 remodeler function *in vivo*

Having established the role of ISW1 in nucleosome array formation, we tested the role of individual domains within the *Isw1* ATPase in this process. First, we serially deleted previously identified motifs from the N-terminus of *Isw1* and expressed under varying expression levels. The N-terminal region (NTR) of the *Isw1* ATPase contains a conserved post-post-helicase-

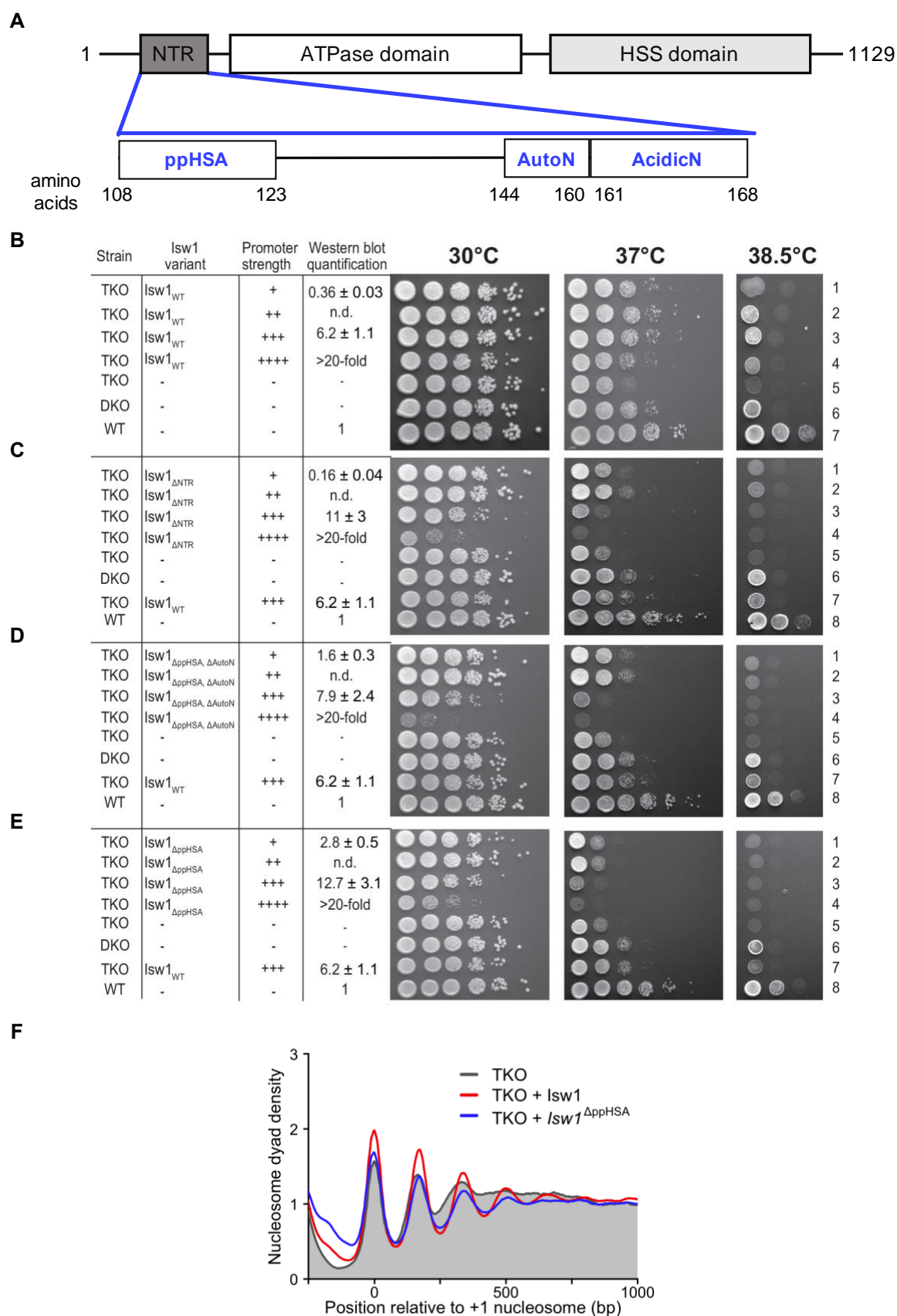


Figure 2.34: The N-terminus of Isw1 is required for the ISW1 remodeler function. (A) Schematic representation of the Isw1 ATPase domain organization. Domains in the N-terminal region (NTR) are highlighted. **(B)** Growth assay showing complementation by WT Isw1 expressed under P1 (+), 6 (++), 11 (+++) and 16 (++++). “-” indicates strains harboring an empty plasmid. DKO strain with

an empty plasmid served as a positive control. **(C)** Same as (B) but for a *Isw1* construct lacking the N-terminal region (NTR, amino acids 2 – 168). **(D, E)** Same as (B) but for *Isw1* constructs lacking the N-terminus up to AutoN (amino acids 2 – 160) or to ppHSA (amino acids 2 – 123) motifs. Western blot quantification indicates expression of WT and mutant TAP-tagged *Isw1* constructs relative to genomically TAP-tagged WT *Isw1*. All WT and mutant *Isw1* constructs were C-terminally TAP-tagged. Values are mean and standard deviation of technical replicates. **(F)** Composite plot showing nucleosome organization by *Isw1* lacking the ppHSA motif under P6 promoter in the TKO strain. Growth assays were performed at least twice with a single colony. MNase-Seq was performed once with an unoptimized protocol by isolating mononucleosome band from an agarose gel, instead of preparing sequencing libraries from the “Whole lane” samples. The panels (B-E) are reproduced from (Ludwigsen et al., 2017). The journal eLife allows free reproduction and distribution of articles and related content subject to appropriate citation (<https://elifesciences.org/terms>).

SANT-associated (ppHSA), N-terminal autoinhibitory (AutoN) and acidic (AcidicN) motifs (Figure 2.34A) (Clapier and Cairns, 2012; Ludwigsen et al., 2017; Mueller-Planitz et al., 2013b; Yan et al., 2016). *Isw1* lacking the N-terminus up to ppHSA (amino acids 2-143) or AutoN (amino acids 2-160) or AcidicN (amino acids 2-168) motifs did not fully complement the temperature-sensitive phenotype, suggesting that the N-terminus region of *Isw1* is important for the remodeler function (Figure 2.34B – E). Nevertheless, the *Isw1* constructs truncated until AutoN or AcidicN grew slightly better than the construct truncated only until ppHSA (compare rows 1 and 2 in Figure 2.34C – E). This observation is in line with the inhibitory role of AutoN and AcidicN (Clapier and Cairns, 2012; Ludwigsen et al., 2017; Yan et al., 2016; Yan et al., 2019). We also observed a growth defect at highest expression levels (P16) at both permissive (30 °C) and non-permissive (37 °C) temperatures. The growth defect could arise from defects in folding of the mutant remodeler.

Consistent with the lack of complementation in growth assays, we found that the *Isw1* truncated until ppHSA motif is defective in nucleosome array formation. Cells expressing the mutant construct showed less prominent arrays in the composite plot compared to the WT *Isw1* construct. In fact, the nucleosome organization was similar to the TKO strain (Figure 2.34F). Overall, these results may suggest that the N-terminus of *Isw1* is required for ISW1 nucleosome sliding *in vivo*.

2.3.4 The AutoN motif is dispensable for ISW1 nucleosome spacing *in vivo*

The N-terminal autoinhibitory (AutoN) motif is known to regulate ISWI activity *in vitro*. Mutation of two arginines to alanines (2RA; amino acids 157 and 159) in the AutoN motif increases DNA-stimulated ATP hydrolysis and nucleosome sliding by the ISWI complex (Clapier and Cairns, 2012; Gamarra et al., 2018; Ludwigsen et al., 2017). Importantly, the 2RA mutation abolishes the linker length sensitivity during nucleosome sliding, suggesting a role of AutoN motif in nucleosome spacing (Hwang et al., 2014). To directly test the role of AutoN in nucleosome spacing and array formation *in vivo*, we expressed the AutoN mutant under varying promoter library (Figure 2.35A). Growth assays showed that the AutoN mutant complements temperature-sensitivity similar to the WT ISW1 complex (Figure 2.35B). Surprisingly, nucleosome mapping experiments suggested that the AutoN mutant does not abolish nucleosome spacing and array regularity function of the ISW1 complex, as judged by

the composite plot. In fact, the AutoN mutant mildly increased nucleosome arrays at two expression levels tested (Figure 2.35C, D). These results are inconsistent with the *in vitro* results suggesting that the AutoN motif regulates nucleosome spacing. On the other hand, the slightly higher signal in the composite plot is consistent with the increased ATPase activity of the AutoN mutant.

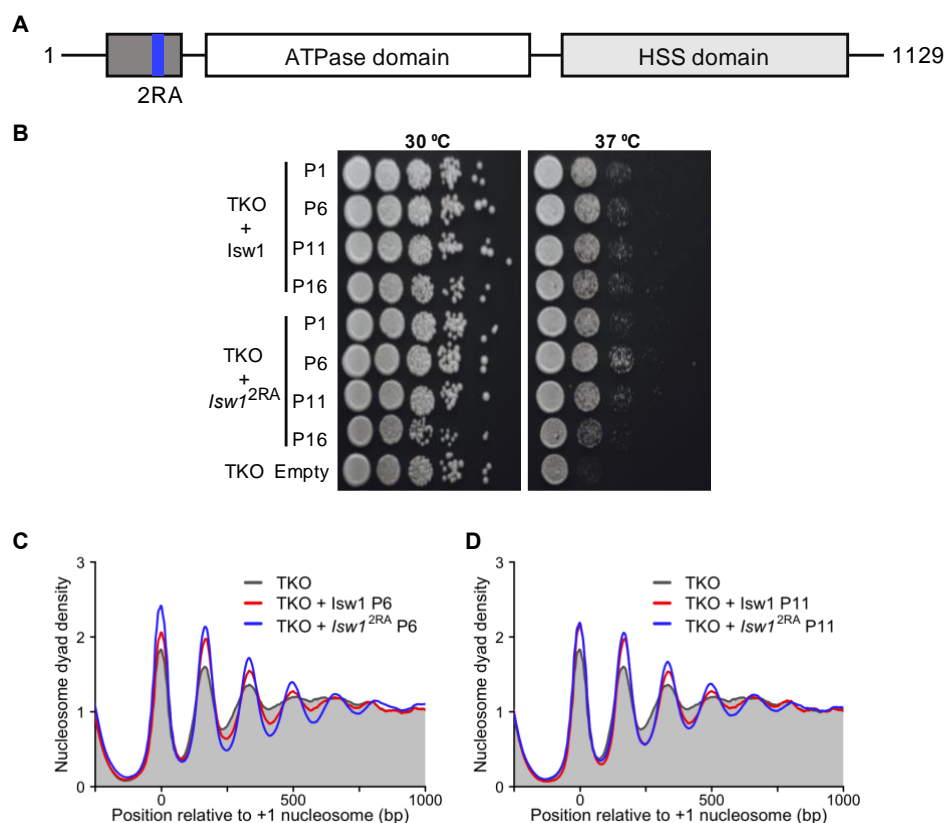


Figure 2.35: The AutoN mutant ISW1 establishes more regular arrays than the WT ISW1 remodeler. (A) Schematic representation of the Isw1 ATPase subunit with the AutoN mutant (2RA, amino acids 157 and 159). **(B)** Growth assay showing similar complementation by the AutoN mutant Isw1 compared to the WT Isw1. The TKO strain transformed with an empty plasmid served as a negative control. **(C, D)** Composite plot showing nucleosome organization by the AutoN mutant Isw1 in the TKO strain with either P6 or P11 expression library. Growth assay was performed at least twice with two colonies obtained from a single transformation event. MNase-Seq was performed once with an unoptimized protocol by isolating mononucleosome band from an agarose gel, instead of preparing sequencing libraries from the “Whole lane” samples.

2.3.5 The NegC motif is important for ISW1 function *in vivo*

The NegC motif follows the lobe 2 of the Isw1 ATPase and negatively regulates ISWI activity *in vitro*. ISWI lacking the NegC motif is defective in coupling ATP hydrolysis to nucleosome sliding. NegC motif also regulates linker length sensing of the ISWI remodeler and deletion of NegC impairs DNA centering activity, suggesting NegC motif regulates nucleosome spacing. Binding of the HSS domain to linker DNA is suggested to relieve NegC mediated autoinhibition in the ISWI remodeler. This observation suggests an interplay of NegC and HSS domain

2.3.6 The *Isw1* ATPase domain may be able to slide nucleosomes *in vivo*

The results presented above suggest the importance of autoinhibitory regions flanking the *Isw1* ATPase domain in nucleosome sliding and spacing. The *Drosophila* ISWI ATPase domain with the autoinhibitory regions can autonomously slide nucleosomes *in vitro* (Mueller-Planitz et al., 2013b). On the other hand, the C-terminus Hand, Sant and Slide (HSS) may have a role in increasing nucleosome affinity, binding or providing directionality to nucleosome sliding as well as spacing nucleosomes (Gangaraju et al., 2009; Grüne et al., 2003; Hota et al., 2013; Kagalwala et al., 2004; McKnight et al., 2011; Mueller-Planitz et al., 2013a; Mueller-Planitz et al., 2013b; Ryan et al., 2011; Zofall et al., 2006).

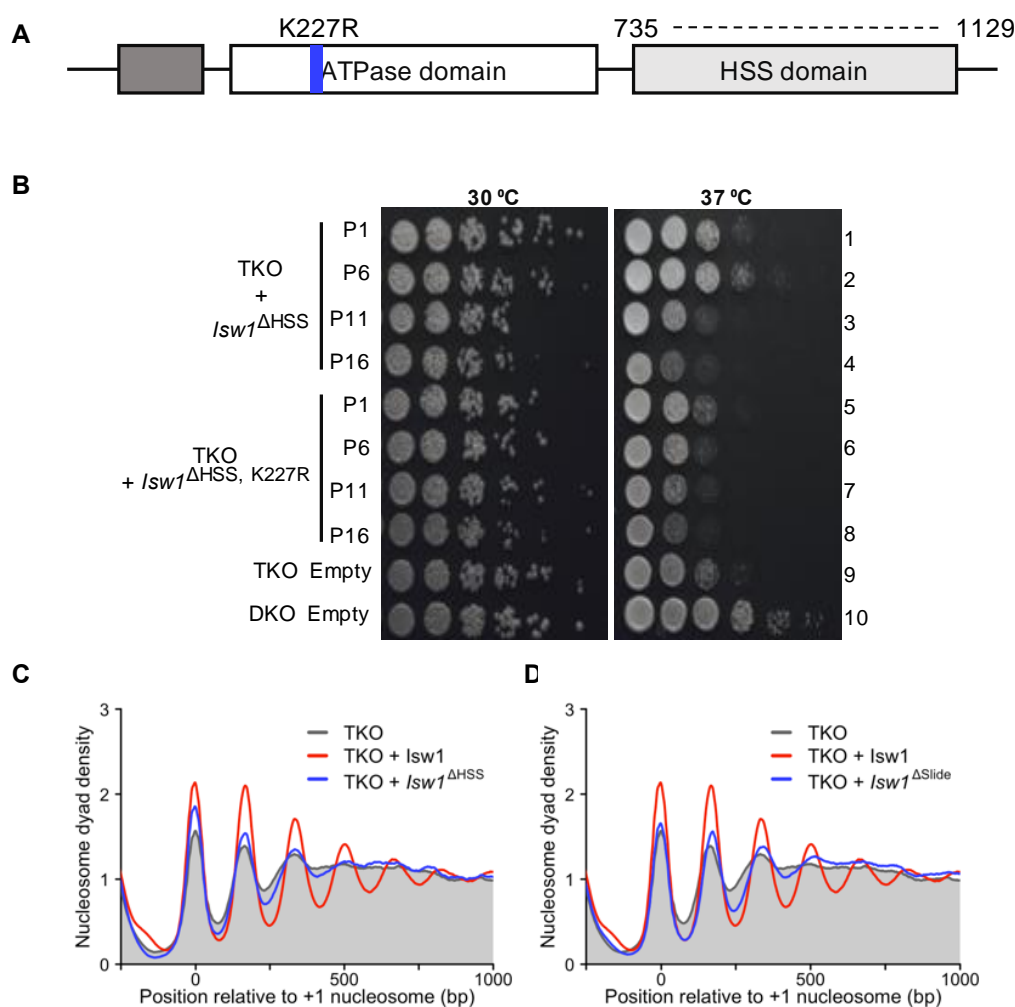


Figure 2.37: The *Isw1* ATPase domain may slide nucleosomes *in vivo*. (A) Schematic representation of the *Isw1* ATPase lacking the HSS domain (amino acids 735 – 1129) and a K227R mutant which abolishes ATP hydrolysis activity in the *Isw1* ATPase. (B) Growth assay showing a mild complementation by the *Isw1* ATPase lacking the HSS domain under the P6 promoter (row 2). ATPase dead *Isw1* mutant did not show any complementation (row 6), suggesting that the mild complementation in row 2 is due to ATP hydrolysis by the *Isw1* ATPase domain. (C) Composite plot showing nucleosome organization established by the *Isw1* ATPase lacking the HSS domain under the P6 promoter in the TKO strain. (D) Same as (C) but with the *Isw1* ATPase lacking the Slide domain (amino acids 952 – 1129). Growth assay was performed at least twice with two colonies obtained from a single transformation event. MNase-Seq was performed only once with an unoptimized protocol by isolating

mononucleosome band from an agarose gel, instead of preparing sequencing libraries from the “Whole lane” samples.

To test whether the Isw1 ATPase lacking the HSS domain (amino acids 1-734) can slide nucleosomes *in vivo*, we deleted the HSS domain in the Isw1 ATPase (Figure 2.37A). To account for the decreased nucleosome binding, we expressed the mutant constructs under varying expression levels.

Intriguingly, Isw1 lacking the HSS domain could mildly complement the temperature-sensitive phenotype at the P6 expression level. This complementation was dependent on ATP hydrolysis of the mutant construct as the ATPase dead mutant did not show similar growth (compare rows 2 and 6 in Figure 2.37B). To directly test nucleosome sliding by Isw1 lacking the HSS domain *in vivo*, we performed MNase-Seq with the P6 promoter. We could observe a mild to negligible increase in nucleosome array pattern compared to the TKO control, but less than the full-length Isw1 ATPase subunit (Figure 2.37C). MNase-Seq in strains expressing Isw1 lacking only the Slide domain (amino acids 1-951) also showed similar results (Figure 2.37D). These results hint that the Isw1 ATPase domain potentially retains residual nucleosome sliding activity *in vivo* but is defective in nucleosome spacing and array formation. These interpretations are also in line with previous *in vitro* results (Lieleg et al., 2015a; Mueller-Planitz et al., 2013b).

It is important to note here that the extreme C-terminus of the Isw1 ATPase harbors a nuclear localization signal (NLS) (Vasicova et al., 2013). The mutant Isw1 constructs lacking the HSS or the Slide domain also lacks this NLS. Therefore, it is likely that these mutants are defective in nuclear localization. Nevertheless, complementation in the growth assay and a mild increase in the composite plots suggest that the mutant Isw1 constructs may partially localize to the nucleus, likely due to overexpression of the mutant protein. Addition of an NLS to the HSS lacking Isw1 construct may further increase its nuclear localization and, thereby, its nucleosome sliding. Furthermore, the nucleosome sliding activity of the Isw1 ATPase domain is independent of the accessory subunits as deletion of the HSS domain abolishes interaction between Isw1 and accessory subunits (Pinskaya et al., 2009).

2.3.7 The Isw1 ATPase subunit may slide nucleosomes without accessory subunits

Results presented above show that the Isw1 ATPase domain may potentially slide nucleosomes *in vivo*. However, the *S. cerevisiae* Isw1 ATPase subunit is shown to lack nucleosome sliding activity *in vitro* (Vary et al., 2003). Therefore, we tested if the Isw1 ATPase subunit can slide nucleosomes on its own without accessory subunits *in vivo*. To test this, we generated septa knock out (SKO) strain lacking accessory subunits *loc2*, *loc3*, *loc4* and *Itc1* together with the Isw1, Isw2 and Chd1 ATPases. This strain did not show any enhanced growth defect compared to the TKO strain (Figure 2.38A). Surprisingly, expression of the Isw1 ATPase in the SKO strain showed clear, but mild, complementation in the temperature-sensitive growth phenotype when compared to the TKO strain (Figure 2.38A). MNase-Seq also showed a mild, but consistent, increase in nucleosome array independent of the Isw1 expression levels (Figure 2.38B).

These results suggest that the Isw1 ATPase subunit may slide nucleosomes *in vivo* without any accessory subunits. This interpretation is in line with an observation that the Isw1 ATPase can act independently from the accessory subunits at the rDNA locus (Mueller and Bryk, 2007). On the other hand, the Isw1 ATPase has been suggested to interact with another protein, called Esc8, which may then form a new functional ISW1 complex capable of sliding nucleosomes *in vivo* (Chen et al., 2016; Cuperus and Shore, 2002).

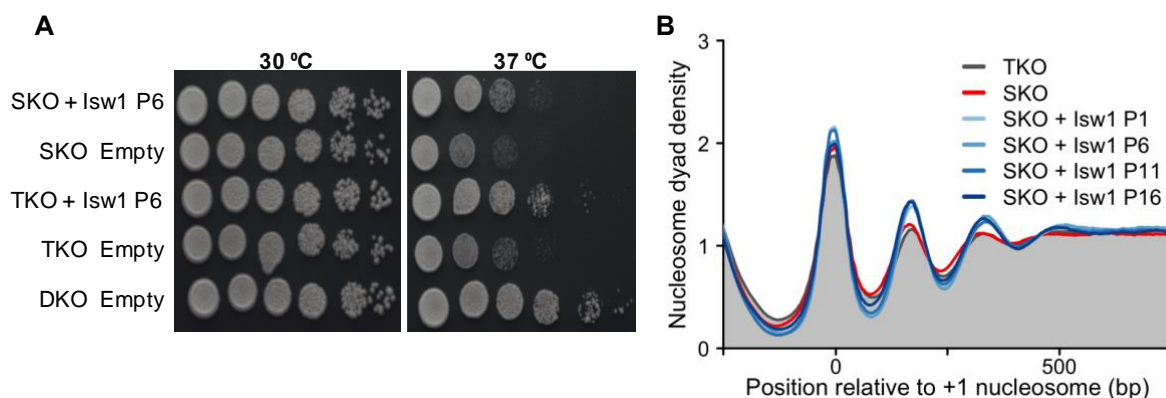


Figure 2.38: The Isw1 ATPase can slide nucleosomes without loc subunits *in vivo*. (A) Growth assay showing complementation by Isw1 expressed in the SKO strain lacking *loc2*, *loc3* and *loc4* subunits. (B) Gene averaged nucleosome organization in the SKO strain with increasing Isw1 levels. Growth assay was performed twice with two colonies obtained from a single transformation event. MNase-Seq was performed only once with an unoptimized protocol by isolating mononucleosome band from an agarose gel, instead of preparing sequencing libraries from the “Whole lane” samples.

2.3.8 DISCUSSION (related to this chapter)

A key unanswered question in the nucleosome spacing field is how nucleosome remodelers sense nucleosome linker length and slide nucleosomes to equalize linker lengths, thus generating regular nucleosome arrays. Recent biochemical studies combined with high-resolution cryo-EM structures of the ISWI and Chd1-type remodelers have begun to provide mechanistic insights into this process (Blosser et al., 2009; Deindl et al., 2013; Farnung et al., 2017; Gamarra et al., 2018; Hauk et al., 2010; Hwang et al., 2014; Leonard and Narlikar, 2015; Levendosky and Bowman, 2019; Nodelman et al., 2017; Qiu et al., 2017; Racki et al., 2009; Sabantsev et al., 2019; Sundaramoorthy et al., 2017; Winger et al., 2018; Yamada et al., 2011; Yan et al., 2016; Yan et al., 2019). Multiple domains and motifs in nucleosome remodelers as well as in the histone octamer have been implicated in the linker length sensing mechanism. Unfortunately, most of these *in vitro* studies utilize mononucleosome centering assay to understand role of each domain and motif. Nucleosome arrays are, in principle, a property of at least three to four successive nucleosomes. Therefore, mononucleosome centering assay may not provide complete insight into the nucleosome spacing mechanism.

To circumvent this problem and understand the mechanism of ISWI mediated nucleosome array formation, we utilized a tunable expression system to modulate Isw1 protein levels in yeast (Blazeck et al., 2012). We employed a TKO strain lacking spacing remodelers of the ISWI- and CHD- families and re-expressed either WT or mutant Isw1 constructs (Tsukiyama

et al., 1999). Overexpression of mutant constructs than WT Isw1 may enhance their binding to nucleosomes *in vivo*. Indeed, we could observe nucleosome sliding by mutant remodelers with severely reduced nucleosome affinity *in vitro* (Figures 2.37 and 2.38). On the other hand, it is possible that upon overexpression of the Isw1 ATPase, not all molecules of the Isw1 ATPase form a functional complex with the Ioc subunits as we do not vary expression of the Ioc subunits in these cells.

We first focused on the N-terminus of the Isw1 ATPase which harbors conserved ppHSA, AutoN and AcidicN motifs. These regions are important for the structural stability of the ISWI remodeler and inhibit the ATPase activity by conferring sensitivity towards the H4-tail (Harrer et al., 2018; Ludwigsen et al., 2017). Consistent with these results, we observed growth defects in cells expressing higher levels of Isw1 lacking different N-terminal regions (Figure 2.34). AutoN motif has been shown to modulate the linker length sensitivity in the ISWI remodeler. Although the precise molecular events in the linker length sensing process are not known, longer linker length is proposed to relieve the H4-tail binding by the ACF1 subunit. The H4-tail then relieves the AutoN inhibition in the ISWI complex. This suggested that AutoN is involved in linker length sensing and NRL determination (Hwang et al., 2014). Unexpectedly, we did not observe any defect in nucleosome spacing and arrays when mutating the AutoN motif. The nucleosome array was mildly better than the WT ISWI complex which could arise from a higher ATPase activity of the AutoN mutant (Figure 2.35) (Clapier and Cairns, 2012; Ludwigsen et al., 2017).

Another inhibitory region, NegC, has been implicated in nucleosome spacing mechanism of the ISWI remodeler (Hwang et al., 2014; Leonard and Narlikar, 2015). Consistent with these results, we found that Isw1 lacking the NegC motif is defective in nucleosome array formation and does not complement in temperature-sensitive growth assay. Curiously, insertion of a Glycine-Glycine-Serine (GGG) linker after the NegC motif severely hampered nucleosome spacing activity of the ISWI complex (Figure 2.36). Importantly, insertion of GGG linker at similar location in *Drosophila* ISWI does not affect nucleosome sliding activity (Ludwigsen et al., 2013). Although our results show the relevance of NegC during linker length sensing process, its molecular mechanism remains unclear. NegC inhibition has been proposed to be relieved by H2A-H2B acidic patch on the nucleosome and the HSS domain in the ISWI remodeler (Clapier and Cairns, 2012; Gamarra et al., 2018). Our results suggest that increasing flexibility by adding GGG linker between NegC and HSS domain hampers nucleosome spacing activity of the ISWI remodeler.

The ISW1a complex generates regular nucleosome arrays *in vitro*. A protein ruler model has been proposed in which ISW1a interacts with the adjacent nucleosomes and set constant spacing between nucleosomes. The HSS domain and the Ioc3 subunit in ISW1a may act as components of the protein ruler (Yamada et al., 2011). Our results are in line with this model as cells lacking the Ioc subunits cannot generate extensive nucleosome arrays (Figure 2.38). Nevertheless, we observed a minor, but consistent, increase in nucleosome positioning upon Isw1 expression in the SKO strain, suggesting that either Isw1 alone can slide nucleosomes *in vivo* or it forms a third remodeling complex together with the Esc8 protein (Chen et al., 2016;

Cuperus and Shore, 2002). Further deletion of Esc8 in the SKO strain may shed light on this hypothesis.

Lastly, our results hint that the Isw1 ATPase without the HSS domain may be functional *in vivo*. To our surprise, it can complement temperature-sensitive growth defect of the TKO strain to some extent. We also observed a minor to negligible increase in nucleosome signal in the composite plots (Figure 2.37). Lower nucleosome map quality of this and other Isw1 mutants precluded finer gene specific analysis. Nevertheless, these results support the *in vitro* results that the ISWI ATPase domain can perform many essential functions during nucleosome sliding (Mueller-Planitz et al., 2013b).

3. GENERAL DISCUSSION AND OUTLOOK

The discussions related to each chapter are presented immediately after results (sections 2.1.12, 2.2.10, 2.3.8). Here I present general discussion about nucleosome positioning, spacing and regular arrays as well as their functional implications. I combine it with future experiments that can be performed to further enhance our understanding of the mechanism and function of regular nucleosome arrays.

In this thesis, we achieved conditions where nucleosome array organization in genes is similar to what is expected at random (Figures 2.4B and 2.8A). The +1-nucleosome is still decently positioned likely due to DNA sequence and other cellular factors still present in our sensitive system. Building on the random nucleosome positioning in the gene body, we propose a modified four-stage model for the biogenesis of regular nucleosome arrays. It is important to note that nucleosome organization in cells is a continuum and do not necessarily need to follow a stepwise model. Therefore, the four stages represent the mechanistic contribution of cellular factors rather than a temporal order (Figure 3.1).

In the first stage, nucleosomes are deposited randomly in the genome (Figure 3.1A). DNA sequence biases the position of nucleosomes in the genome. It also destabilizes nucleosomes near the promoter regions, thus contributing to nucleosome depletion at the NFR. Nucleosome remodelers can also read the DNA sequence and shape to influence the position of nucleosomes. In the second stage, remodelers of the SWI/SNF family together with the GRFs further enhance nucleosome depletion at the NFR (Figure 3.1B). Binding of GRFs may even destabilize nucleosomes at the NFR, leading to fragile nucleosomes. RSC, at a genome-wide level, and SWI/SNF, at stress-responsive genes, slide or even evict nucleosomes.

In the third stage, the +1-nucleosome is positioned by a tug-of-war between RSC and SWI/SNF, on the one hand, and ISW2 and INO80 remodeler, on the other hand (Figure 3.1C). INO80 has also been proposed to read DNA sequence and/or shape to position the +1-nucleosome on its own. ISW1 and Chd1 remodelers further help to enhance positioning of the nucleosome. GRFs also contribute to this process by determining the phasing of nucleosome array.

In the last stage, ISWI, Chd1 and INO80 remodelers cooperate to generate regular nucleosome arrays in the gene body (Figure 3.1D). These spacing remodelers also require high histone density to establish WT-like arrays. They may even “clamp” nucleosomes to determine NRL. RNA Pol II-dependent transcription counteracts the regular arrays generated by the spacing remodelers and destroy the array regularity in the gene body. It is definitely possible that Pol II may interact with or recruit with cellular factors to establish the regular arrays.

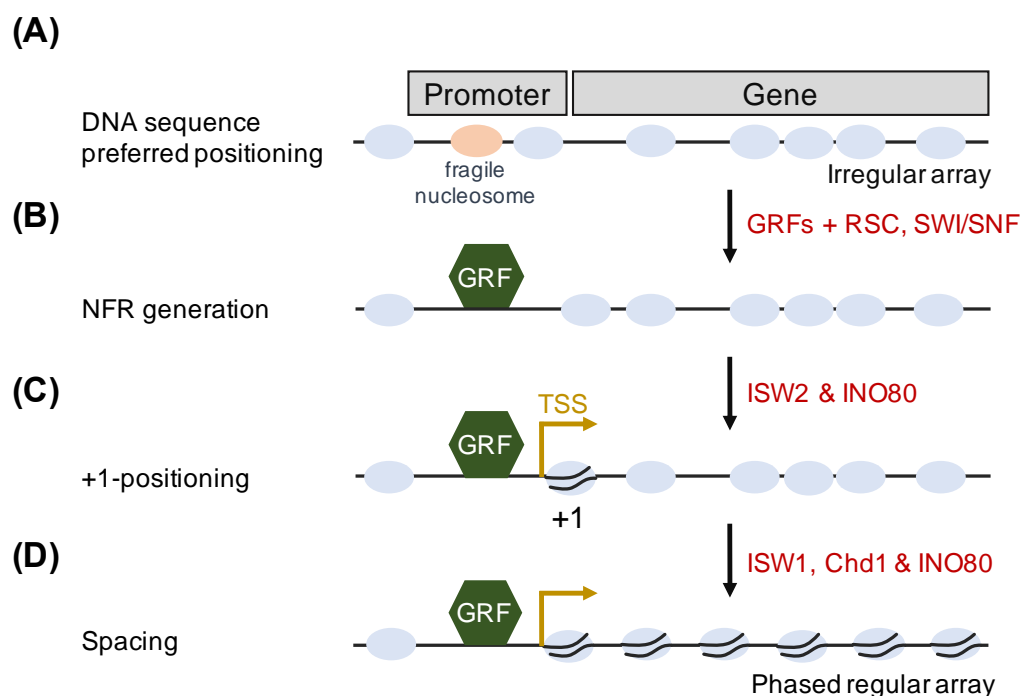


Figure 3.1: A modified four step model for generation of phased regular arrays. (A) Nucleosomes are deposited randomly in the genome. DNA sequence biases stability and positioning of individual nucleosomes Poly(dA:dT) tracts destabilize nucleosomes which leads to fragile nucleosomes in the promoter regions. **(B)** General Regulatory Factors (GRFs) together with RSC and SWI/SNF remodelers enhance nucleosome depletion at the promoter regions by evicting or sliding nucleosomes away from the promoter region. **(C)** ISW2 and INO80 remodelers act opposite of RSC and SWI/SNF remodelers by sliding nucleosomes towards the promoter region. These opposing activities help position the +1-nucleosome and may determine the precise transcription start site (TSS) in the gene. **(D)** The ISW1, Chd1 and INO80 spacing remodelers generate evenly spaced nucleosomes in the gene body which are phased to the TSS in the gene (Singh and Mueller-Planitz, unpublished).

3.1 Interplay of transcription and spacing remodelers towards nucleosome organization

As shown in this thesis, the INO80 remodeler can position and space nucleosomes independent of transcription. This suggests that Pol II dependent recruitment of INO80 cannot be the sole mechanism for recruiting the INO80 remodeler in the gene body. INO80 has even been shown to release Pol II from chromatin upon DNA damage (Lafon et al., 2015). On the other hand, the Chd1 remodeler is considered to depend on transcription elongation for recruitment and organizing nucleosomes in the gene body. Chd1 also physically interacts with Pol II (Lee et al., 2017; Park et al., 2014; Simic et al., 2003). Despite these evidences, whether Chd1 critically depends on Pol II for recruitment and function is not clear. It is possible that Chd1 recognizes disrupted nucleosomes in the wake of transcription to help assemble nucleosomes (Farnung et al., 2020; Jeronimo et al., 2020; Smolle et al., 2012; Smolle et al., 2013).

To test whether Chd1 critically needs transcription to position and space nucleosomes in the gene body, I have generated yeast strains where one can deplete all known spacing remodelers except Chd1, either with or without Pol II (section 4.1.1). Mapping nucleosome

positions in these strains will reveal if Chd1 absolutely requires Pol II to space nucleosomes in the gene body or it can function like INO80 independent of Pol II. Like Chd1, the ISW1b remodeler is also a prime candidate to test for Pol II dependent recruitment and function in the gene body. ISW1b has been shown to prevent histone exchange in the wake of transcription to maintain chromatin integrity. (Smolle et al., 2012). Therefore, I have established yeast strains where one can distinguish the activities of ISW1b, ISW1a and ISW2 with or without Pol II in the nucleus (section 4.1.1). Lastly, these strains will also reveal the relative potential of individual spacing remodelers towards establishing regular array. We now know that INO80 can position up to 5 nucleosomes in the gene body. Whether ISW1a, ISW1b, ISW2 and Chd1 position and space nucleosomes with similar efficiency will be revealed with these strains.

3.2 Spacing mechanism in yeast

The NRL and the regular arrays in the gene bodies of *S. cerevisiae* are suggested to be established by only the ISWI and Chd1 remodelers. It is also proposed that ISW1 depends on Chd1 to space nucleosomes in the gene body (Ocampo et al., 2016). Based on *in vitro* results, it is predicted that Chd1 would generate shorter NRL (~160 bp) and ISW1 longer (~175 bp). Deletion of *ISW1* achieves NRL close to the predicted NRL as Chd1 is now the only major spacing remodeler left in the cell. On the other hand, deletion of *CHD1* decreases average NRL by 1 bp. This result is not in line with the predicted NRL as ISW1 is supposed to generate longer (~175 bp) (Lieleg et al., 2015a; Ocampo et al., 2016; Torigoe et al., 2013; Tsukiyama et al., 1999). Therefore, it remains unclear how spacing remodelers contribute to establish WT-like NRL in yeast. Moreover, whether INO80 also contributes to this process is not known. We have shown that depletion of INO80 as well deleting the Arp8 module decreases the NRL in an otherwise WT context. This suggests that INO80 also contributes to NRL determination in the WT cells.

To decipher the spacing mechanism of yeast, and how spacing remodelers of three families collaborate to generate WT-like NRL, one should perform double mutant cycle of ISW1, ISW2 and Chd1 with the INO80 remodeler. The NRLs in the double mutants measured by MNase-Seq should be compared to the single as well as to the triple mutant combinations. This will reveal contributions and collaborations of the spacing remodelers of three families towards determining NRL in WT cells.

3.3 Mechanistic dissection of ISWI and Chd1 remodelers *in vivo*

In this thesis, we have dissected the spacing mechanism of the INO80 remodeler. We have shown that INO80 critically depends on the Arp8 module to space nucleosomes. We further dissected the role of the N-terminus of Itc1 subunit in the ISW2 remodeler to suggest that it regulates array regularity and NRL in the genome. Our results also show that ISW1 needs its NegC motif to space nucleosomes, while the AutoN motif is dispensable. As we found during this thesis, Pol II overrides the effect of spacing remodelers. Therefore, one should test the described ISW1 and ISW2 mutants in this thesis using the sensitive backgrounds lacking Pol II. This will reveal the effect of individual mutations without redundancy of other spacing remodelers and the overriding effect of Pol II.

Furthermore, one can test the spacing mechanism of the Chd1 remodeler. Chd1 also possess a NegC-like motif after the ATPase domain. The double chromodomains in the N-terminus of Chd1 is suggested to act analogously to the AutoN motif in ISW1 (Hauk et al., 2010; Ludwigsen et al., 2017). Whether these motifs also regulate the NRL generated by Chd1 is not completely clear (Sundaramoorthy et al., 2017). The sensitive systems established in this thesis will be extremely useful to dissect the roles of modules and motifs in the Chd1 remodeler.

3.4 Role of nucleosome spacing in genome 3D-folding

The genome is folded into higher-order chromatin structure in the form of chromatin. How nucleosome spacing and array regularity affects folding of the chromatin fiber *in vivo* is not clear. It is conceivable that that the NRL in arrays affect local folding of the chromatin fiber. Recent technological advancements have suggested that the chromatin fiber is not continuously folded in the cells and rather exist as “clutches” formed of 2-8 nucleosomes (Eltsov et al., 2008; Hsieh et al., 2015; Nishino et al., 2012; Ou et al., 2017; Ricci et al., 2015; Risca et al., 2017). Therefore, it is essential to understand how local folding of the chromatin fiber, at the level of few nucleosomes, affect higher-order folding of chromatin. To test this, one can perform Micro-C (Hsieh et al., 2015) and Hi-C (Lieberman-Aiden et al., 2009) experiments in cells lacking known spacing remodelers, like TKO and TKO cells further depleted with INO80. These experiments may reveal how array regularity in each gene affects local as well as global folding of the chromatin fiber. In line with this hypothesis, a recent study performed Hi-C in cells lacking the ISWI remodeler in mouse ES cells showing that ISWI has an integral role in establishment of chromatin domains, likely via its effect on CTCF binding (Barisic et al., 2019).

3.5 Mechanistic dissection of nucleosome organization in higher organisms

The mechanism of nucleosome array formation and the role of individual remodelers is best understood in *S. cerevisiae*. How the spacing remodelers regulate NRL and array regularity in higher organisms have begun to be understood (Baldi et al., 2018a; Barisic et al., 2019). Specifically, how promoter organization in higher organisms is established is largely unclear. It is possible that, like yeast, GRFs, nucleosome remodelers and even components of the transcription initiation machinery contribute to the nucleosome depletion and positioning of the +1-nucleosome. In higher organisms, the +1-nucleosome plays an important role towards regulating the promoter-proximal pausing of Pol II (Gilchrist et al., 2010; Weber et al., 2014). How the distance between the TSS and the +1-nucleosome is determined and if remodelers determine this distance to regulate productive transcription elongation is an exciting avenue to study.

3.6 Single-molecule and single-cell techniques

Lastly, the nucleosome maps established in this thesis and elsewhere, only provide a snapshot which is averaged over the cell population. How cellular machinery determines nucleosome organization in single cells is not clear. Recent technological advancements have

provided single-cell and single-molecule nucleosome maps (Baldi et al., 2018b; Lai et al., 2018; Shipony et al., 2020; Stergachis et al., 2020; Wang et al., 2019b). In particular, how heterogeneity within chromatin fiber of single cells affect gene expression and higher order chromatin folding remains to be determined. Techniques like scNMT-Seq (Argelaguet et al., 2019; Clark et al., 2018) have begun to measure nucleosome positioning, DNA methylation and gene expression in single cells, paving the way for an exciting future.

4. MATERIALS AND METHODS

4.1 MATERIALS

4.1.1 Yeast and bacterial strains

List of yeast strains used in this study. Source indicates whether the strain is generated in this thesis or procured from published studies. Method defines the methodology used to generate each strain in this thesis.

Strain	General name	Genotype	Source	Method
yFMP001	BY <i>isw1Δ</i>	<i>MATa his3Δ1 leu2Δ0 met15Δ0 ura3Δ0 isw1::kanMX4</i>	Euroscarf	-
yFMP004	BY <i>itc1Δ</i> alpha	<i>MATa his3Δ1 leu2Δ0 met15Δ0 ura3Δ0 itc1::kanMX4</i>	Euroscarf	-
yFMP007	BY <i>isw2Δ</i>	<i>MATa his3Δ1 leu2Δ0 met15Δ0 ura3Δ0 isw2::kanMX4</i>	Euroscarf	-
yFMP009	BY4741	<i>MATa his3Δ1 leu2Δ0 lys2Δ0 ura3Δ0</i>	Euroscarf	-
yFMP010	BY <i>itc1Δ</i> a	<i>MATa his3Δ1 leu2Δ0 met15Δ0 ura3Δ0 itc1::kanMX4</i>	Euroscarf	-
yFMP012	BY4742	<i>MATa his3Δ1 leu2Δ0 lys2Δ0 ura3Δ0</i>	Euroscarf	-
yFMP013	W1588-4c WT	<i>MATa ade2-1 his3-11,15 leu2-3,112 trp1-1 ura3-1 can1-100 RAD5+</i>	(Tsukiyama et al., 1999)	-
yFMP014	YTT227	<i>MATa ade2-1 his3-11,15 leu2-3,112 trp1-1 ura3-1 can1-100 RAD5+ isw1Δ::ADE2 isw2Δ::LEU2 chd1Δ::TRP1</i>	(Tsukiyama et al., 1999)	-
yFMP015	YTT225	<i>MATa ade2-1 his3-11,15 leu2-3,112 trp1-1 ura3-1 can1-100 RAD5+ isw2Δ::LEU2 chd1Δ::TRP1</i>	(Tsukiyama et al., 1999)	-
yFMP016	WZY42	<i>MATa ura3-52 lys2-801 ade2-101 trp1Δ63 his3Δ200 leu2Δ1 hht1-hhf1::LEU, hht2-hhf2::HIS3 Ycp50 HHT2-HHF2</i>	(Zhang et al., 1998)	-
yFMP017	MP28	<i>MATa ura3-1 ade2-1 his3-11,5 trp1Δ leu2-3,112 can1-100 isw1::URA3 chd1::kanMX isw2::TRP1</i>	(Gkikopoulos et al., 2011)	-
yFMP018	BY4743	<i>MATa/MATa his3Δ1/his3Δ1 leu2Δ0/leu2Δ0 lys2Δ0/LYS2 MET15/met15Δ0 ura3Δ0/ura3Δ0</i>	This study	Mating BY4741 and BY4742
yFMP019	YTT227- <i>itc1Δ</i>	<i>MATa ade2-1 his3-11,15 leu2-3,112 trp1-1 ura3-1 can1-100 RAD5+ isw1Δ::ADE2 isw2Δ::LEU2 chd1Δ::TRP1 itc1Δ::HIS5-loxP</i>	This study	Transformation in YTT227
yFMP020	YTT227- <i>itc1Δ</i>	<i>MATa ade2-1 his3-11,15 leu2-3,112 trp1-1 ura3-1 can1-100 RAD5+ isw1Δ::ADE2 isw2Δ::LEU2 chd1Δ::TRP1 itc1Δ</i>	This study	Deleting His-loxP in yFMP019
yFMP021	YTT227- <i>itc1Δ</i> – <i>ioc3Δ</i>	<i>MATa ade2-1 his3-11,15 leu2-3,112 trp1-1 ura3-1 can1-100 RAD5+ isw1Δ::ADE2 isw2Δ::LEU2 chd1Δ::TRP1 itc1Δ::HIS5-loxP ioc3Δ::hphNT1</i>	This study	Transformation in yFMP019
yFMP022	YTT227- <i>itc1Δ</i> – <i>ioc3Δ</i> – <i>ioc4Δ</i>	<i>MATa ade2-1 his3-11,15 leu2-3,112 trp1-1 ura3-1 can1-100 RAD5+ isw1Δ::ADE2 isw2Δ::LEU2 chd1Δ::TRP1 itc1Δ::HIS5-loxP ioc3Δ::hphNT1 ioc4Δ::NAT</i>	This study	Transformation in yFMP021
yFMP023	YTT227- <i>itc1Δ</i> – <i>ioc3Δ</i> – <i>ioc4Δ</i>	<i>MATa ade2-1 his3-11,15 leu2-3,112 trp1-1 ura3-1 can1-100 RAD5+ isw1Δ::ADE2 isw2Δ::LEU2 chd1Δ::TRP1 itc1Δ ioc3Δ::hphNT1 ioc4Δ::NAT</i>	This study	Deleting His-loxP in yFMP022
yFMP024	SKO	<i>MATa ade2-1 his3-11,15 leu2-3,112 trp1-1 ura3-1 can1-100 RAD5+ isw1Δ::ADE2 isw2Δ::LEU2 chd1Δ::TRP1 itc1Δ ioc3Δ::hphNT1 ioc4Δ::cloNAT ioc2Δ::HIS5-loxP</i>	This study	Transformation in yFMP023
yFMP025	YTT186	<i>MATa ade2-1 his3-11,15 leu2-3,112 trp1-1 ura3-1 can1-100 RAD5+ isw1Δ::ADE2</i>	(Tsukiyama et al., 1999)	-
yFMP026	YTT196	<i>MATa ade2-1 his3-11,15 leu2-3,112 trp1-1 ura3-1 can1-100 RAD5+ isw2Δ::LEU2</i>	(Tsukiyama et al., 1999)	-

yFMP027	YTT443	<i>MATa ade2-1 his3-11,15 leu2-3,112 trp1-1 ura3-1 can1-100 RAD5+ isw1::kanMX isw2::HISG</i>	(Tsukiyama et al., 1999)	-
yFMP037	YTT223	<i>MATa ade2-1 his3-11,15 leu2-3,112 trp1-1 ura3-1 can1-100 RAD5+ isw1Δ::ADE2 chd1Δ::TRP1</i>	(Tsukiyama et al., 1999)	-
yFMP039	BY Δ <i>N itc1</i>	<i>MATa his3Δ1 leu2Δ0 met15Δ0 ura3Δ0 itc1Δ::ΔN itc1-His3 colony 1</i>	This study	Transformation in BY4741
yFMP040	BY Δ <i>N itc1</i>	<i>MATa his3Δ1 leu2Δ0 met15Δ0 ura3Δ0 itc1Δ::ΔN itc1-His3 colony 2</i>	This study	Transformation in BY4741
yFMP041	BY Δ <i>N itc1</i>	<i>MATa his3Δ1 leu2Δ0 met15Δ0 ura3Δ0 itc1Δ::ΔN itc1-His3 colony 3</i>	This study	Transformation in BY4741
yFMP043	Diploid Δ <i>N itc1</i>	<i>MATa/MATa his3Δ1/his3Δ1 leu2Δ0/leu2Δ0 lys2Δ0/LYS2 MET15/met15Δ0 ura3Δ0/ura3Δ0 itc1Δ::kanMX4/itc1Δ::ΔN itc1-His3 colony 1</i>	This study	Mating yFMP039 and BY4742
yFMP044	Diploid Δ <i>N itc1</i>	<i>MATa/MATa his3Δ1/his3Δ1 leu2Δ0/leu2Δ0 lys2Δ0/LYS2 MET15/met15Δ0 ura3Δ0/ura3Δ0 itc1Δ::kanMX4/itc1Δ::ΔN itc1-His3 colony 2</i>	This study	Mating yFMP040 and BY4742
yFMP045	Diploid Δ <i>N itc1</i>	<i>MATa/MATa his3Δ1/his3Δ1 leu2Δ0/leu2Δ0 lys2Δ0/LYS2 MET15/met15Δ0 ura3Δ0/ura3Δ0 itc1Δ::kanMX4/itc1Δ::ΔN itc1-His3 colony 3</i>	This study	Mating yFMP041 and BY4742
yFMP047	lsw1-TAP	<i>Mata his3Δ1 leu2Δ0 met15Δ0 ura3Δ0 lsw1-TAP::HIS3MX6</i>	Prof. Dr. Michaela Smolle	-
yFMP048	SEPTA lsw1 P1	<i>MATa ade2-1 his3-11,15 leu2-3,112 trp1-1 ura3-1 can1-100 RAD5+ isw1Δ::ADE2 isw2Δ::LEU2 chd1Δ::TRP1 itc1Δ ioc3Δ::hphNT1 ioc4Δ::cloNAT ioc2Δ::HIS5-loxP P1-ISW1</i>	This study	Transformation in SKO
yFMP049	SEPTA lsw1 P6	<i>MATa ade2-1 his3-11,15 leu2-3,112 trp1-1 ura3-1 can1-100 RAD5+ isw1Δ::ADE2 isw2Δ::LEU2 chd1Δ::TRP1 itc1Δ ioc3Δ::hphNT1 ioc4Δ::cloNAT ioc2Δ::HIS5-loxP P6-ISW1</i>	This study	Transformation in SKO
yFMP050	SEPTA lsw1 P11	<i>MATa ade2-1 his3-11,15 leu2-3,112 trp1-1 ura3-1 can1-100 RAD5+ isw1Δ::ADE2 isw2Δ::LEU2 chd1Δ::TRP1 itc1Δ ioc3Δ::hphNT1 ioc4Δ::cloNAT ioc2Δ::HIS5-loxP P11-ISW1</i>	This study	Transformation in SKO
yFMP051	SEPTA lsw1 P16	<i>MATa ade2-1 his3-11,15 leu2-3,112 trp1-1 ura3-1 can1-100 RAD5+ isw1Δ::ADE2 isw2Δ::LEU2 chd1Δ::TRP1 itc1Δ ioc3Δ::hphNT1 ioc4Δ::cloNAT ioc2Δ::HIS5-loxP P16-ISW1</i>	This study	Transformation in SKO
yFMP084	YTT227 lsw1 P1	<i>MATa ade2-1 his3-11,15 leu2-3,112 trp1-1 ura3-1 can1-100 RAD5+ isw1Δ::ADE2 isw2Δ::LEU2 chd1Δ::TRP1 P1-ISW1</i>	This study	Transformation in YTT227
yFMP085	YTT227 lsw1 P6	<i>MATa ade2-1 his3-11,15 leu2-3,112 trp1-1 ura3-1 can1-100 RAD5+ isw1Δ::ADE2 isw2Δ::LEU2 chd1Δ::TRP1 P6-ISW1</i>	This study	Transformation in YTT227
yFMP086	YTT227 lsw1 P11	<i>MATa ade2-1 his3-11,15 leu2-3,112 trp1-1 ura3-1 can1-100 RAD5+ isw1Δ::ADE2 isw2Δ::LEU2 chd1Δ::TRP1 P11-ISW1</i>	This study	Transformation in YTT227
yFMP087	YTT227 lsw1 P16	<i>MATa ade2-1 his3-11,15 leu2-3,112 trp1-1 ura3-1 can1-100 RAD5+ isw1Δ::ADE2 isw2Δ::LEU2 chd1Δ::TRP1 P16-ISW1</i>	This study	Transformation in YTT227
yFMP088	YTT227 lsw1-2RA P1	<i>MATa ade2-1 his3-11,15 leu2-3,112 trp1-1 ura3-1 can1-100 RAD5+ isw1Δ::ADE2 isw2Δ::LEU2 chd1Δ::TRP1 P1-isw1^{2RA}</i>	This study	Transformation in YTT227
yFMP089	YTT227 lsw1-2RA P6	<i>MATa ade2-1 his3-11,15 leu2-3,112 trp1-1 ura3-1 can1-100 RAD5+ isw1Δ::ADE2 isw2Δ::LEU2 chd1Δ::TRP1 P6-isw1^{2RA}</i>	This study	Transformation in YTT227
yFMP090	YTT227 lsw1-2RA P11	<i>MATa ade2-1 his3-11,15 leu2-3,112 trp1-1 ura3-1 can1-100 RAD5+ isw1Δ::ADE2 isw2Δ::LEU2 chd1Δ::TRP1 P11-isw1^{2RA}</i>	This study	Transformation in YTT227
yFMP091	YTT227 lsw1-2RA P16	<i>MATa ade2-1 his3-11,15 leu2-3,112 trp1-1 ura3-1 can1-100 RAD5+ isw1Δ::ADE2 isw2Δ::LEU2 chd1Δ::TRP1 P16-isw1^{2RA}</i>	This study	Transformation in YTT227
yFMP092	YTT227 lsw1-ppHSA P1	<i>MATa ade2-1 his3-11,15 leu2-3,112 trp1-1 ura3-1 can1-100 RAD5+ isw1Δ::ADE2 isw2Δ::LEU2 chd1Δ::TRP1 P1-isw1^{AppHSA}</i>	This study	Transformation in YTT227
yFMP093	YTT227 lsw1-ppHSA P6	<i>MATa ade2-1 his3-11,15 leu2-3,112 trp1-1 ura3-1 can1-100 RAD5+ isw1Δ::ADE2 isw2Δ::LEU2 chd1Δ::TRP1 P6-isw1^{AppHSA}</i>	This study	Transformation in YTT227
yFMP094	YTT227 lsw1-ppHSA P11	<i>MATa ade2-1 his3-11,15 leu2-3,112 trp1-1 ura3-1 can1-100 RAD5+ isw1Δ::ADE2 isw2Δ::LEU2 chd1Δ::TRP1 P11-isw1^{AppHSA}</i>	This study	Transformation in YTT227

yFMP095	YTT227 lsw1- ppHSA P16	<i>MATa ade2-1 his3-11,15 leu2-3,112 trp1-1 ura3-1 can1-100 RAD5+ isw1Δ::ADE2 isw2Δ::LEU2 chd1Δ::TRP1 P16-isw1^{AppHSA}</i>	This study	Transformation in YTT227
yFMP096	YTT227 lsw1- autoN P1	<i>MATa ade2-1 his3-11,15 leu2-3,112 trp1-1 ura3-1 can1-100 RAD5+ isw1Δ::ADE2 isw2Δ::LEU2 chd1Δ::TRP1 P1-isw1^{AppHSA, ΔAutoN}</i>	This study	Transformation in YTT227
yFMP097	YTT227 lsw1- autoN P6	<i>MATa ade2-1 his3-11,15 leu2-3,112 trp1-1 ura3-1 can1-100 RAD5+ isw1Δ::ADE2 isw2Δ::LEU2 chd1Δ::TRP1 P6-isw1^{AppHSA, ΔAutoN}</i>	This study	Transformation in YTT227
yFMP098	YTT227 lsw1- autoN P11	<i>MATa ade2-1 his3-11,15 leu2-3,112 trp1-1 ura3-1 can1-100 RAD5+ isw1Δ::ADE2 isw2Δ::LEU2 chd1Δ::TRP1 P11-isw1^{AppHSA, ΔAutoN}</i>	This study	Transformation in YTT227
yFMP099	YTT227 lsw1- autoN P16	<i>MATa ade2-1 his3-11,15 leu2-3,112 trp1-1 ura3-1 can1-100 RAD5+ isw1Δ::ADE2 isw2Δ::LEU2 chd1Δ::TRP1 P16-isw1^{AppHSA, ΔAutoN}</i>	This study	Transformation in YTT227
yFMP100	YTT227 lsw1-NTR P1	<i>MATa ade2-1 his3-11,15 leu2-3,112 trp1-1 ura3-1 can1-100 RAD5+ isw1Δ::ADE2 isw2Δ::LEU2 chd1Δ::TRP1 P1-isw1^{ΔNTR}</i>	This study	Transformation in YTT227
yFMP101	YTT227 lsw1-NTR P6	<i>MATa ade2-1 his3-11,15 leu2-3,112 trp1-1 ura3-1 can1-100 RAD5+ isw1Δ::ADE2 isw2Δ::LEU2 chd1Δ::TRP1 P6-isw1^{ΔNTR}</i>	This study	Transformation in YTT227
yFMP102	YTT227 lsw1-NTR P11	<i>MATa ade2-1 his3-11,15 leu2-3,112 trp1-1 ura3-1 can1-100 RAD5+ isw1Δ::ADE2 isw2Δ::LEU2 chd1Δ::TRP1 P11-isw1^{ΔNTR}</i>	This study	Transformation in YTT227
yFMP103	YTT227 lsw1-NTR P16	<i>MATa ade2-1 his3-11,15 leu2-3,112 trp1-1 ura3-1 can1-100 RAD5+ isw1Δ::ADE2 isw2Δ::LEU2 chd1Δ::TRP1 P16-isw1^{ΔNTR}</i>	This study	Transformation in YTT227
yFMP104	YTT227 lsw1-TAP P1	<i>MATa ade2-1 his3-11,15 leu2-3,112 trp1-1 ura3-1 can1-100 RAD5+ isw1Δ::ADE2 isw2Δ::LEU2 chd1Δ::TRP1 P1-ISW1-TAP</i>	This study	Transformation in YTT227
yFMP105	YTT227 lsw1-TAP P6	<i>MATa ade2-1 his3-11,15 leu2-3,112 trp1-1 ura3-1 can1-100 RAD5+ isw1Δ::ADE2 isw2Δ::LEU2 chd1Δ::TRP1 P6-ISW1-TAP</i>	This study	Transformation in YTT227
yFMP106	YTT227 lsw1-TAP P11	<i>MATa ade2-1 his3-11,15 leu2-3,112 trp1-1 ura3-1 can1-100 RAD5+ isw1Δ::ADE2 isw2Δ::LEU2 chd1Δ::TRP1 P11-ISW1-TAP</i>	This study	Transformation in YTT227
yFMP107	YTT227 lsw1-TAP P16	<i>MATa ade2-1 his3-11,15 leu2-3,112 trp1-1 ura3-1 can1-100 RAD5+ isw1Δ::ADE2 isw2Δ::LEU2 chd1Δ::TRP1 P16-ISW1-TAP</i>	This study	Transformation in YTT227
yFMP108	YTT227 lsw1- ppHSA- TAP P1	<i>MATa ade2-1 his3-11,15 leu2-3,112 trp1-1 ura3-1 can1-100 RAD5+ isw1Δ::ADE2 isw2Δ::LEU2 chd1Δ::TRP1 P1-isw1^{AppHSA}-TAP</i>	This study	Transformation in YTT227
yFMP109	YTT227 lsw1- ppHSA- TAP P6	<i>MATa ade2-1 his3-11,15 leu2-3,112 trp1-1 ura3-1 can1-100 RAD5+ isw1Δ::ADE2 isw2Δ::LEU2 chd1Δ::TRP1 P1-ISW1-TAP P6-isw1^{AppHSA}-TAP</i>	This study	Transformation in YTT227
yFMP110	YTT227 lsw1- ppHSA- TAP P11	<i>MATa ade2-1 his3-11,15 leu2-3,112 trp1-1 ura3-1 can1-100 RAD5+ isw1Δ::ADE2 isw2Δ::LEU2 chd1Δ::TRP1 P11-isw1^{AppHSA}-TAP</i>	This study	Transformation in YTT227
yFMP111	YTT227 lsw1- ppHSA- TAP P16	<i>MATa ade2-1 his3-11,15 leu2-3,112 trp1-1 ura3-1 can1-100 RAD5+ isw1Δ::ADE2 isw2Δ::LEU2 chd1Δ::TRP1 P16-isw1^{AppHSA}-TAP</i>	This study	Transformation in YTT227
yFMP112	YTT227 lsw1- autoN- TAP P1	<i>MATa ade2-1 his3-11,15 leu2-3,112 trp1-1 ura3-1 can1-100 RAD5+ isw1Δ::ADE2 isw2Δ::LEU2 chd1Δ::TRP1 P1-isw1^{AppHSA, ΔAutoN}-TAP</i>	This study	Transformation in YTT227
yFMP113	YTT227 lsw1- autoN- TAP P6	<i>MATa ade2-1 his3-11,15 leu2-3,112 trp1-1 ura3-1 can1-100 RAD5+ isw1Δ::ADE2 isw2Δ::LEU2 chd1Δ::TRP1 P6-isw1^{AppHSA, ΔAutoN}-TAP</i>	This study	Transformation in YTT227
yFMP114	YTT227 lsw1- autoN- TAP P11	<i>MATa ade2-1 his3-11,15 leu2-3,112 trp1-1 ura3-1 can1-100 RAD5+ isw1Δ::ADE2 isw2Δ::LEU2 chd1Δ::TRP1 P11-isw1^{AppHSA, ΔAutoN}-TAP</i>	This study	Transformation in YTT227
yFMP115	YTT227 lsw1- autoN- TAP P16	<i>MATa ade2-1 his3-11,15 leu2-3,112 trp1-1 ura3-1 can1-100 RAD5+ isw1Δ::ADE2 isw2Δ::LEU2 chd1Δ::TRP1 P16-isw1^{AppHSA, ΔAutoN}-TAP</i>	This study	Transformation in YTT227

yFMP116	YTT227 Isw1-NTR-TAP P1	<i>MATa ade2-1 his3-11,15 leu2-3,112 trp1-1 ura3-1 can1-100 RAD5+ isw1Δ::ADE2 isw2Δ::LEU2 chd1Δ::TRP1 P1-isw1^{ANTR}-TAP</i>	This study	Transformation in YTT227
yFMP117	YTT227 Isw1-NTR-TAP P6	<i>MATa ade2-1 his3-11,15 leu2-3,112 trp1-1 ura3-1 can1-100 RAD5+ isw1Δ::ADE2 isw2Δ::LEU2 chd1Δ::TRP1 P6-isw1^{ANTR}-TAP</i>	This study	Transformation in YTT227
yFMP118	YTT227 Isw1-NTR-TAP P11	<i>MATa ade2-1 his3-11,15 leu2-3,112 trp1-1 ura3-1 can1-100 RAD5+ isw1Δ::ADE2 isw2Δ::LEU2 chd1Δ::TRP1 P11-isw1^{ANTR}-TAP</i>	This study	Transformation in YTT227
yFMP119	YTT227 Isw1-NTR-TAP P16	<i>MATa ade2-1 his3-11,15 leu2-3,112 trp1-1 ura3-1 can1-100 RAD5+ isw1Δ::ADE2 isw2Δ::LEU2 chd1Δ::TRP1 P16-isw1^{ANTR}-TAP</i>	This study	Transformation in YTT227
yFMP168	Isw2-TAP-LEU2	<i>MATa his3Δ1 leu2Δ0 met15Δ0 ura3Δ0 ISW2-TAP:LEU2</i>	This study	Replacing His3 in yFMP706 with LEU2
yFMP179	YSC001	<i>MATa his3Δ1 leu2Δ0 met15Δ0 ura3Δ0 rpb3::NATMX</i>	(Churchman and Weissman, 2011)	-
yFMP200	Isw2-TAP ΔN- <i>itc1</i> -FLAG	<i>MATa his3Δ1 leu2Δ0 met15Δ0 ura3Δ0 isw2::Isw2:TAP:LEU2 itc1::itc1Δ2-374:FLAG:HIS3</i>	This study	Transformation in yFMP168
yFMP224	DY5734	<i>MATa trp1-1 ura3-1 his3-11,15 leu2-3,112 ade2-1 can1-100 hht1-hhf1Δ::LEU2 hht2-hhf2Δ::kanMX3 YCp50-HHT2-HHF2</i>	(Wittschieben et al., 2000)	-
yFMP225	RMY102a	<i>MATa ade2-101 his3-Δ200 lys2-801 trp1Δ901 ura3-52 hht1-hhf1Δ::LEU2 hht2-hhf2Δ::HIS3 pRM102 p(GAL10)-HHT2 p(GAL1)-HHF2</i>	(Mann and Grunstein, 1992)	-
yFMP231	TKO ΔN-Ino80	<i>MATa ade2-1 his3-11,15 leu2-3,112 trp1-1 ura3-1 can1-100 RAD5+ isw1Δ::ADE2 isw2Δ::LEU2 chd1Δ::TRP1 ino80 1-900::HIS3 colony 1</i>	This study	Transformation in YTT227
yFMP232	TKO ΔN-Ino80	<i>MATa ade2-1 his3-11,15 leu2-3,112 trp1-1 ura3-1 can1-100 RAD5+ isw1Δ::ADE2 isw2Δ::LEU2 chd1Δ::TRP1 ino80 1-900::HIS3 colony 2</i>	This study	Transformation in YTT227
yFMP254	TKO Ino80-FLAG	<i>MATa ade2-1 his3-11,15 leu2-3,112 trp1-1 ura3-1 can1-100 RAD5+ isw1Δ::ADE2 isw2Δ::LEU2 chd1Δ::TRP1 INO80-3xFLAG:NATMX</i>	This study	Transformation in YTT227
yFMP255	TKO ΔN-Ino80-FLAG	<i>MATa ade2-1 his3-11,15 leu2-3,112 trp1-1 ura3-1 can1-100 RAD5+ isw1Δ::ADE2 isw2Δ::LEU2 chd1Δ::TRP1 ino80 1-900::HIS3 3xFLAG::NATMX</i>	This study	Transformation in yFMP231
yFMP257	Ino80-FLAG	<i>MATa ade2-1 his3-11,15 leu2-3,112 trp1-1 ura3-1 can1-100 RAD5+ INO80-3xFLAG:NATMX</i>	This study	Transformation in W1588-4C
yFMP258	HHY168	<i>MATa ade2-1 trp1-1 can1-100 leu2-3,112 his3-11,15 ura3 tor1-1 fpr1Δ::NAT RPL13A-2xFKBP12::TRP1 rad5-G535R</i>	Euroscarf	-
yFMP259	HHY170	<i>MATa ade2-1 trp1-1 can1-100 leu2-3,112 his3-11,15 ura3 tor1-1 fpr1Δ::NAT RPL13A-2xFKBP12::TRP1 rad5-G535R RPO21-FRB::kanMX6</i>	Euroscarf	-
yFMP262	HHY170 x TKO	<i>MATa/MATa leu2-3,112/ leu2-3,112 trp1-1/ trp1-1 can1-100/ can1-100 ura3-1/ ura3-1 ade2-1/ ade2-1 his3-11,15/ his3-11,15 [phi+] ISW1/isw1::ADE2 ISW2/isw2::LEU2 CHD1/chd1::TRP1 TOR1/tor1-1 FPR1/fpr1::NAT RPL13A/RPL13A-2xFKBP12::TRP1 RPO21/RPO21-FRB::kanMX6 RAD5/rad5-G535R</i>	-	Mating HHY170 and YTT227
yFMP263	HHY170 x TKO	<i>MATa/MATa leu2-3,112/ leu2-3,112 trp1-1/ trp1-1 can1-100/ can1-100 ura3-1/ ura3-1 ade2-1/ ade2-1 his3-11,15/ his3-11,15 [phi+] ISW1/isw1::ADE2 ISW2/isw2::LEU2 CHD1/chd1::TRP1 TOR1/tor1-1 FPR1/fpr1::NAT RPL13A/RPL13A-2xFKBP12::TRP1 RPO21/RPO21-FRB::kanMX6 RAD5/rad5-G535R</i>	-	Mating HHY170 and YTT227
yFMP264	HHY168 TKO C1	<i>MATa ade2-1 trp1-1 can1-100 leu2-3,112 his3-11,15 ura3 tor1-1 fpr1Δ::NAT RPL13A-2xFKBP12::TRP1 isw1Δ::ADE2 isw2Δ::LEU2 chd1Δ::TRP1 rad5-G535R colony 1</i>	This study	Mating YTT227 and HHY170; tetrad dissection
yFMP265	HHY168 TKO C2	<i>MATa ade2-1 trp1-1 can1-100 leu2-3,112 his3-11,15 ura3 tor1-1 fpr1Δ::NAT RPL13A-2xFKBP12::TRP1 isw1Δ::ADE2 isw2Δ::LEU2 chd1Δ::TRP1 rad5-G535R colony 2</i>	This study	Mating YTT227 and HHY170; tetrad dissection
yFMP266	HHY170 TKO C1	<i>MATa ade2-1 trp1-1 can1-100 leu2-3,112 his3-11,15 ura3 tor1-1 fpr1Δ::NAT RPL13A-2xFKBP12::TRP1 RPO21-FRB::kanMX6 isw1Δ::ADE2 isw2Δ::LEU2 chd1Δ::TRP1 RAD5+ colony 1</i>	This study	Mating YTT227 and HHY170; tetrad dissection
yFMP267	HHY170 TKO C2	<i>MATa ade2-1 trp1-1 can1-100 leu2-3,112 his3-11,15 ura3 tor1-1 fpr1Δ::NAT RPL13A-2xFKBP12::TRP1</i>	This study	Mating YTT227 and HHY170; tetrad dissection

		<i>RPO21-FRB::kanMX6 isw1Δ::ADE2 isw2Δ::LEU2 chd1Δ::TRP1 rad5-G535R</i> colony 2		
yFMP268	HHY170 TKO C3	<i>MATa ade2-1 trp1-1 can1-100 leu2-3,112 his3-11,15 ura3 tor1-1 fpr1Δ::NAT RPL13A-2xFKBP12::TRP1 RPO21-FRB::kanMX6 isw1Δ::ADE2 isw2Δ::LEU2 chd1Δ::TRP1 RAD5+</i> colony 3	This study	Mating YTT227 and HHY170; tetrad dissection
yFMP289	DY5734 x TKO	<i>MATa/MATa leu2-3,112/ leu2-3,112 trp1-1/ trp1-1 can1-100/ can1-100 ura3-1/ ura3-1 ade2-1/ ade2-1 his3-11,15/ his3-11,15 HHT1-HHF1/hht1-hhf1Δ::LEU2 HHT2-HHF2/hht2-hhf2Δ::kanMX3 ISW1/isw1::ADE2 ISW2/isw2::LEU2 CHD1/chd1::TRP1 YCp50: HHT2-HHF2::URA3</i>	This study	Mating DY5734 and YTT227
yFMP290	DY5734 x TKO	<i>MATa/MATa leu2-3,112/ leu2-3,112 trp1-1/ trp1-1 can1-100/ can1-100 ura3-1/ ura3-1 ade2-1/ ade2-1 his3-11,15/ his3-11,15 HHT1-HHF1/hht1-hhf1Δ::LEU2 HHT2-HHF2/hht2-hhf2Δ::kanMX3 ISW1/isw1::ADE2 ISW2/isw2::LEU2 CHD1/chd1::TRP1 YCp50: HHT2-HHF2::URA3</i>	This study	Mating DY5734 and YTT227
yFMP291	DY5734 Ycp50 TKO C1	<i>MATa trp1-1 ura3-1 his3-11,15 leu2-3,112 ade2-1 can1-100 hht1-hhf1Δ::LEU2 hht2-hhf2Δ::kanMX3 isw1::ADE2 isw2::LEU2 chd1::TRP1 YCp50-HHT2-HHF2</i> colony 1	This study	Mating YTT227 and DY5734; tetrad dissection
yFMP293	DY5734 Ycp50 TKO C3	<i>MATa trp1-1 ura3-1 his3-11,15 leu2-3,112 ade2-1 can1-100 hht1-hhf1Δ::LEU2 hht2-hhf2Δ::kanMX3 isw1::ADE2 isw2::LEU2 chd1::TRP1 YCp50-HHT2-HHF2</i> colony 3	This study	Mating YTT227 and DY5734; tetrad dissection
yFMP294	<i>isw1 x chd1</i>	<i>MATa/MATa his3Δ1/his3Δ1 leu2Δ0/leu2Δ0 LYS2/lys2Δ0 met15Δ0/MET15 ura3Δ0/ura3Δ0 ISW1/isw1::kanMX chd1::HYG/CHD1</i>	This study	Mating yFMP296 and yMP001
yFMP295	<i>isw1 x chd1</i>	<i>MATa/MATa his3Δ1/his3Δ1 leu2Δ0/leu2Δ0 LYS2/lys2Δ0 met15Δ0/MET15 ura3Δ0/ura3Δ0 ISW1/isw1::kanMX chd1::HYG/CHD1</i>	This study	Mating yFMP296 and yMP001
yFMP298	Diploid Isw2-TAP x ΔN- <i>itc1</i> - His3	<i>MATa/MATa his3Δ1/his3Δ1 leu2Δ0/leu2Δ0 LYS2/lys2Δ0 met15Δ0/MET15 ura3Δ0/ura3Δ0 ISW2/isw2-TAP:LEU2 ITC1/<i>itc1</i>ΔN2-374:HIS3</i>	This study	Mating yFMP200 and yFMP009
yFMP299	Diploid Isw2-TAP x ΔN- <i>itc1</i> - His3	<i>MATa/MATa his3Δ1/his3Δ1 leu2Δ0/leu2Δ0 LYS2/lys2Δ0 met15Δ0/MET15 ura3Δ0/ura3Δ0 ISW2/isw2-TAP:LEU2 ITC1/<i>itc1</i>ΔN2-374:HIS3</i>	This study	Mating
yFMP296	<i>chd1 alpha</i>	<i>MATa his3Δ1 leu2Δ0 lys2Δ0 ura3Δ0 chd1::HYG</i>	This study	Transformation in BY4742
yFMP318	INO80- GFP-FRB C1	<i>MATa ade2-1 trp1-1 can1-100 leu2-3,112 his3-11,15 ura3 tor1-1 fpr1Δ::NAT RPL13A-2xFKBP12::TRP1 rad5-G535R INO80-GFP-FRB::hphMX6</i> colony 1	This study	Transformation in HHY168
yFMP319	INO80- GFP-FRB C2	<i>MATa ade2-1 trp1-1 can1-100 leu2-3,112 his3-11,15 ura3 tor1-1 fpr1Δ::NAT RPL13A-2xFKBP12::TRP1 rad5-G535R INO80-GFP-FRB::hphMX6</i> colony 2	This study	Transformation in HHY168
yFMP320	PoIII-FRB INO80- GFP-FRB C1	<i>MATa ade2-1 trp1-1 can1-100 leu2-3,112 his3-11,15 ura3 tor1-1 fpr1Δ::NAT RPL13A-2xFKBP12::TRP1 rad5-G535R RPO21-FRB::kanMX6 INO80-GFP-FRB::hphMX6</i> colony 1	This study	Transformation in HHY170
yFMP321	PoIII-FRB INO80- GFP-FRB C2	<i>MATa ade2-1 trp1-1 can1-100 leu2-3,112 his3-11,15 ura3 tor1-1 fpr1Δ::NAT RPL13A-2xFKBP12::TRP1 rad5-G535R RPO21-FRB::kanMX6 INO80-GFP-FRB::hphMX6</i> colony 2	This study	Transformation in HHY170
yFMP324	W303 RAD5+	<i>MATa ade2-1 his3-11,15 leu2-3,112 trp1-1 ura3-1 can1-100 RAD5+</i>	Thomas and Rothstein, 1989	Obtained from Boris Pfander
yFMP325	W303 RAD5+	<i>MATa ade2-1 his3-11,15 leu2-3,112 trp1-1 ura3-1 can1-100 RAD5+</i>	Thomas and Rothstein, 1989	Obtained from Boris Pfander
yFMP328	W303 RAD5+	<i>MATa ade2-1/ ade2-1 his3-11/ his3-11,15 leu2-3/ leu2-3,112 trp1-1/ trp1-1 ura3-1/ ura3-1 can1-100/ can1-100 RAD5+/ RAD5+</i> colony 1	This study	Mating yFMP324 and 325
yFMP329	W303 RAD5+	<i>MATa ade2-1/ ade2-1 his3-11/ his3-11,15 leu2-3/ leu2-3,112 trp1-1/ trp1-1 ura3-1/ ura3-1 can1-100/ can1-100 RAD5+/ RAD5+</i> colony 2	This study	Mating yFMP324 and 325
yFMP333	TKO INO80- GFP-FRB C1	<i>MATa ade2-1 trp1-1 can1-100 leu2-3,112 his3-11,15 ura3 tor1-1 fpr1Δ::NAT RPL13A-2xFKBP12::TRP1 isw1Δ::ADE2 isw2Δ::LEU2 chd1Δ::TRP1 rad5-G535R INO80-GFP-FRB::hphMX6</i>	This study	Transformation in yFMP264

yFMP335	TKO INO80- GFP-FRB C2	<i>MATa ade2-1 trp1-1 can1-100 leu2-3,112 his3-11,15 ura3 tor1-1 fpr1Δ::NAT RPL13A-2xFKBP12::TRP1 isw1Δ::ADE2 isw2Δ::LEU2 chd1Δ::TRP1 rad5-G535R INO80-GFP-FRB::hphMX6</i>	This study	Transformation in yFMP265
yFMP337	PoIII-FRB TKO INO80- GFP-FRB C1	<i>MATa ade2-1 trp1-1 can1-100 leu2-3,112 his3-11,15 ura3 tor1-1 fpr1Δ::NAT RPL13A-2xFKBP12::TRP1 RPO21-FRB::kanMX6 isw1Δ::ADE2 isw2Δ::LEU2 chd1Δ::TRP1 RAD5+ INO80-GFP-FRB::hphMX6</i>	This study	Transformation in yFMP266
yFMP339	PoIII-FRB TKO INO80- GFP-FRB C2	<i>MATa ade2-1 trp1-1 can1-100 leu2-3,112 his3-11,15 ura3 tor1-1 fpr1Δ::NAT RPL13A-2xFKBP12::TRP1 RPO21-FRB::kanMX6 isw1Δ::ADE2 isw2Δ::LEU2 chd1Δ::TRP1 rad5-G535R INO80-GFP-FRB::hphMX6</i>	This study	Transformation in yFMP267
yFMP341	W303 alpha x YTT227	<i>MATa/MATa his3Δ1/his3Δ1 leu2Δ0/leu2Δ0 lys2Δ0/LYS2 MET15/met15Δ0 ura3Δ0/ura3Δ0 ISW1/isw1Δ::ADE2 ISW2/isw2Δ::LEU2 CHD1/chd1Δ::TRP1 colony 1</i>	This study	Mating YTT227 to yFMP325
yFMP342	W303 alpha x YTT227	<i>MATa/MATa his3Δ1/his3Δ1 leu2Δ0/leu2Δ0 lys2Δ0/LYS2 MET15/met15Δ0 ura3Δ0/ura3Δ0 ISW1/isw1Δ::ADE2 ISW2/isw2Δ::LEU2 CHD1/chd1Δ::TRP1 colony 2</i>	This study	Mating YTT227 to yFMP325
yFMP344	RC757 (test for a- factor)	<i>MATa sst2-1 rme his6 met1 can1 cyh2</i>	(Chan and Otte, 1982)	Obtained from Sigurd Braun lab
yFMP345	RC844 (test for alpha- factor)	<i>MATa sst1-2 rme his6 met1 leu1 trp5 can1 cyh2</i>	Chan and Otte, 1982)	Obtained from Sigurd Braun lab
yFMP356	DY5734 TKO pFMP519 C1	<i>MATa trp1-1 ura3-1 his3-11,15 leu2-3,112 ade2-1 can1-100 hht1-hhf1Δ::LEU2 hht2-hhf2Δ::kanMX3 isw1::ADE2 isw2::LEU2 chd1::TRP1 pRS413 p(GAL10)-HHT2 p(GAL1)-HHF2</i>	This study	FOA-based plasmid switch with pRS413 p(GAL10)-HHT2 p(GAL1)-HHF2 (pFMP519) in yFMP291
yFMP357	DY5734 TKO pFMP519 C2	<i>MATa trp1-1 ura3-1 his3-11,15 leu2-3,112 ade2-1 can1-100 hht1-hhf1Δ::LEU2 hht2-hhf2Δ::kanMX3 isw1::ADE2 isw2::LEU2 chd1::TRP1 pRS413 p(GAL10)-HHT2 p(GAL1)-HHF2</i>	This study	FOA-based plasmid switch with pRS413 p(GAL10)-HHT2 p(GAL1)-HHF2 (pFMP519) in yFMP293
yFMP358	DY5734 pFMP519 C1	<i>MATa trp1-1 ura3-1 his3-11,15 leu2-3,112 ade2-1 can1-100 hht1-hhf1Δ::LEU2 hht2-hhf2Δ::kanMX3 pRS413 p(GAL10)-HHT2 p(GAL1)-HHF2 colony 1</i>	This study	FOA-based plasmid switch with pRS413 p(GAL10)-HHT2 p(GAL1)-HHF2 (pFMP519) in DY5734
yFMP359	DY5734 pFMP519 C2	<i>MATa trp1-1 ura3-1 his3-11,15 leu2-3,112 ade2-1 can1-100 hht1-hhf1Δ::LEU2 hht2-hhf2Δ::kanMX3 pRS413 p(GAL10)-HHT2 p(GAL1)-HHF2 colony 2</i>	This study	FOA-based plasmid switch with pRS413 p(GAL10)-HHT2 p(GAL1)-HHF2 (pFMP519) in DY5734
yFMP360	BY <i>isw1Δ chd1Δ a</i>	<i>MATa his3Δ1 leu2Δ0 met15Δ0 ura3Δ0 isw1::kanMX chd1::HYG</i>	This study	Mating and tetrad dissection of yFMP294
yFMP361	BY <i>isw1Δ chd1Δ a</i>	<i>MATa his3Δ1 leu2Δ0 met15Δ0 ura3Δ0 isw1::kanMX chd1::HYG</i>	This study	Mating and tetrad dissection of yFMP294
yFMP362	BY <i>isw1Δ chd1Δ alpha</i>	<i>MATa his3Δ1 leu2Δ0 met15Δ0 ura3Δ0 isw1::kanMX chd1::HYG</i>	This study	Mating and tetrad dissection of yFMP294
yFMP363	BY <i>isw1Δ chd1Δ alpha</i>	<i>MATa his3Δ1 leu2Δ0 met15Δ0 ura3Δ0 isw1::kanMX chd1::HYG</i>	This study	Mating and tetrad dissection of yFMP294
yFMP364	ΔN- <i>itc1 a</i>	<i>MATa his3Δ1 leu2Δ0 met15Δ0 ura3Δ0 itc1::Δ2-374-itc1-FLAG-HIS3</i>	This study	Mating yFMP200 and BY4742, tetrad dissection
yFMP365	ΔN- <i>itc1 a</i>	<i>MATa his3Δ1 leu2Δ0 met15Δ0 ura3Δ0 itc1::Δ2-374-itc1-FLAG-HIS3</i>	This study	Mating yFMP200 and BY4742, tetrad dissection
yFMP366	ΔN- <i>itc1 alpha</i>	<i>MATa his3Δ1 leu2Δ0 met15Δ0 ura3Δ0 itc1::Δ2-374-itc1-FLAG-HIS3</i>	This study	Mating yFMP200 and BY4742, tetrad dissection
yFMP367	ΔN- <i>itc1 alpha</i>	<i>MATa his3Δ1 leu2Δ0 met15Δ0 ura3Δ0 itc1::Δ2-374-itc1-FLAG-HIS3</i>	This study	Mating yFMP200 and BY4742, tetrad dissection

yFMP368	ΔN-Ino80 C1	<i>MATa ade2-1 his3-11,15 leu2-3,112 trp1-1 ura3-1 can1-100 RAD5+ ino80 1-900::HIS3</i> colony 1	This study	Transformation in W1588-4C
yFMP369	ΔN-Ino80 C2	<i>MATa ade2-1 his3-11,15 leu2-3,112 trp1-1 ura3-1 can1-100 RAD5+ ino80 1-900::HIS3</i> colony 2	This study	Transformation in W1588-4C
yFMP370	ΔN-Ino80-FLAG	<i>MATa ade2-1 his3-11,15 leu2-3,112 trp1-1 ura3-1 can1-100 RAD5+ ino80 1-900::HIS3 3xFLAG::NATMX</i>	This study	Transformation in yFMP368
yFMP371	Diploid <i>isw1 chd1</i> ΔN- <i>itc1</i>	<i>MATa/MATα his3Δ1/his3Δ1 leu2Δ0/leu2Δ0 LYS2/lys2Δ0 met15Δ0/MET15 ura3Δ0/ura3Δ0 ISW1/isw1::kanMX CHD1/chd1::HYG itc1ΔN2-374:HIS3/ITC1</i>	This study	Mating yFMP362 and yFMP364
yFMP372	Diploid <i>isw1 chd1</i> ΔN- <i>itc1</i>	<i>MATa/MATα his3Δ1/his3Δ1 leu2Δ0/leu2Δ0 LYS2/lys2Δ0 met15Δ0/MET15 ura3Δ0/ura3Δ0 ISW1/isw1::kanMX CHD1/chd1::HYG itc1ΔN2-374:HIS3/ITC1</i>	This study	Mating yFMP362 and yFMP364
yFMP373	Diploid <i>isw1 chd1 isw2</i>	<i>MATa/MATα his3Δ1/his3Δ1 leu2Δ0/leu2Δ0 LYS2/lys2Δ0 met15Δ0/MET15 ura3Δ0/ura3Δ0 ISW1/isw1::kanMX CHD1/chd1::HYG isw2::kanMX/ISW2</i>	This study	Mating yFMP362 and yFMP010
yFMP374	Diploid <i>isw1 chd1 isw2</i>	<i>MATa/MATα his3Δ1/his3Δ1 leu2Δ0/leu2Δ0 LYS2/lys2Δ0 met15Δ0/MET15 ura3Δ0/ura3Δ0 ISW1/isw1::kanMX CHD1/chd1::HYG isw2::kanMX/ISW2</i>	This study	Mating yFMP362 and yFMP010
yFMP377	BY TKO C1	<i>MATa his3Δ1 leu2Δ0 lys2Δ0 ura3Δ0 isw1::kanMX isw2::kanMX chd1::HYG</i>	This study	Mating and tetrad dissection yFMP373
yFMP378	BY TKO C2	<i>MATa his3Δ1 leu2Δ0 lys2Δ0 ura3Δ0 isw1::kanMX isw2::kanMX chd1::HYG</i>	This study	Mating and tetrad dissection yFMP373
yFMP381	BY <i>ISW2</i> alpha	<i>MATa his3Δ1 leu2Δ0 met15Δ0 ura3Δ0 YOR304W::kanMX4</i>	This study	Mating and tetrad dissection
yFMP400	DKO ΔN- <i>itc1</i>	<i>Mat his3Δ1 leu2Δ0 met15Δ0 ura3Δ0 YBR245c::kanMX4 YER164::hphNT1 YGL133W::ΔN:Itc1:FLAG:His3</i> colony 1	This study	Mating and tetrad dissection yFMP428
yFMP401	DKO ΔN- <i>itc1</i>	<i>Mat his3Δ1 leu2Δ0 met15Δ0 ura3Δ0 YBR245c::kanMX4 YER164::hphNT1 YGL133W::ΔN:Itc1:FLAG:His3</i> colony 2	This study	Mating and tetrad dissection yFMP428
yFMP424	TKO (same as YTT227)	<i>MATa ade2-1 his3-11,15 leu2-3,112 trp1-1 ura3-1 can1-100 RAD5+ isw1Δ:ADE2 isw2Δ::LEU2 chd1Δ::TRP1</i>	This study	Mating and tetrad dissection of yFMP341, 342
yFMP425	TKO	<i>MATa ade2-1 his3-11,15 leu2-3,112 trp1-1 ura3-1 can1-100 RAD5+ isw1Δ:ADE2 isw2Δ::LEU2 chd1Δ::TRP1</i>	This study	Mating and tetrad dissection of yFMP341, 342
yFMP426	TKO	<i>MATa ade2-1 his3-11,15 leu2-3,112 trp1-1 ura3-1 can1-100 RAD5+ isw1Δ:ADE2 isw2Δ::LEU2 chd1Δ::TRP1</i>	This study	Mating and tetrad dissection of yFMP341, 342
yFMP427	TKO (same as YTT227)	<i>MATa ade2-1 his3-11,15 leu2-3,112 trp1-1 ura3-1 can1-100 RAD5+ isw1Δ:ADE2 isw2Δ::LEU2 chd1Δ::TRP1</i>	This study	Mating and tetrad dissection of yFMP341, 342
yFMP428	Diploid <i>isw1 chd1</i> ΔN- <i>itc1</i>	<i>MATa/MATα his3Δ1/his3Δ1 leu2Δ0/leu2Δ0 LYS2/lys2Δ0 met15Δ0/MET15 ura3Δ0/ura3Δ0 ISW1/isw1::kanMX CHD1/chd1::HYG itc1ΔN2-374:FLAG:HIS3/ITC1</i>	This study	Mating yFMP362 and yFMP364
yFMP458	<i>arp8Δ</i> pRS416	<i>MATa ade2-1 his3-11,15 leu2-3,112 trp1-1 ura3-1 can1-100 RAD5+ arp8Δ::NATMX6 pRS416</i> colony 1	This study	Transformation in yFMP476
yFMP459	<i>arp8Δ</i> pRS416	<i>MATa ade2-1 his3-11,15 leu2-3,112 trp1-1 ura3-1 can1-100 RAD5+ arp8Δ::NATMX6 pRS416</i> colony 2	This study	Transformation in yFMP477
yFMP460	<i>arp8Δ</i> pRS416-ARP8	<i>MATa ade2-1 his3-11,15 leu2-3,112 trp1-1 ura3-1 can1-100 RAD5+ arp8Δ::NATMX6 pRS416 Arp8</i> colony 1	This study	Transformation in yFMP476
yFMP461	<i>arp8Δ</i> pRS416-ARP8	<i>MATa ade2-1 his3-11,15 leu2-3,112 trp1-1 ura3-1 can1-100 RAD5+ arp8Δ::NATMX6 pRS416 Arp8</i> colony 2	This study	Transformation in yFMP477
yFMP462	<i>arp8Δ</i> pRS416- <i>arp8</i> ^{ΔN}	<i>MATa ade2-1 his3-11,15 leu2-3,112 trp1-1 ura3-1 can1-100 RAD5+ arp8Δ::NATMX6 pRS416 Arp8 Δ2-197</i> colony 1	This study	Transformation in yFMP476
yFMP463	<i>arp8Δ</i> pRS416- <i>arp8</i> ^{ΔN}	<i>MATa ade2-1 his3-11,15 leu2-3,112 trp1-1 ura3-1 can1-100 RAD5+ arp8Δ::NATMX6 pRS416 Arp8 Δ2-197</i> colony 2	This study	Transformation in yFMP477
yFMP468	TKO x <i>IES6</i> Diploid 1	<i>MATa/MATα his3Δ1/his3Δ1 leu2Δ0/leu2Δ0 lys2Δ0/LYS2 MET15/met15Δ0 ura3Δ0/ura3Δ0 ISW1/isw1Δ::ADE2 ISW2/isw2Δ::LEU2 CHD1/chd1Δ::TRP1 IES6/ies6Δ::NATMX6</i> colony 1	This study	Mating YTT227 and yFMP628
yFMP469	TKO x <i>IES6</i> Diploid 2	<i>MATa/MATα his3Δ1/his3Δ1 leu2Δ0/leu2Δ0 lys2Δ0/LYS2 MET15/met15Δ0 ura3Δ0/ura3Δ0</i>	This study	Mating YTT227 and yFMP628

		<i>ISW1/isw1Δ::ADE2 ISW2/isw2Δ::LEU2 CHD1/chd1Δ::TRP1 IES6/ies6Δ::NATMX6 colony 2</i>		
yFMP470	TKO x <i>IES6</i> Diploid 3	<i>MATa/MATa his3Δ1/his3Δ1 leu2Δ0/leu2Δ0 lys2Δ0/LYS2 MET15/met15Δ0 ura3Δ0/ura3Δ0 ISW1/isw1Δ::ADE2 ISW2/isw2Δ::LEU2 CHD1/chd1Δ::TRP1 IES6/ies6Δ::NATMX6 colony 3</i>	This study	Mating YTT227 and yFMP628
yFMP476	<i>arp8Δ</i>	<i>MATa ade2-1 his3-11,15 leu2-3,112 trp1-1 ura3-1 can1-100 RAD5+ arp8Δ::NATMX6 colony 1</i>	This study	Transformation in W1588-4C
yFMP477	<i>arp8Δ</i>	<i>MATa ade2-1 his3-11,15 leu2-3,112 trp1-1 ura3-1 can1-100 RAD5+ arp8Δ::NATMX6 colony 2</i>	This study	Transformation in W1588-4C
yFMP480	TKO <i>arp8Δ</i>	<i>MATa ade2-1 his3-11,15 leu2-3,112 trp1-1 ura3-1 can1-100 RAD5+ isw1Δ::ADE2 isw2Δ::LEU2 chd1Δ::TRP1 arp8Δ::NATMX6 colony 1</i>	This study	Transformation in YTT227
yFMP481	TKO <i>arp8Δ</i>	<i>MATa ade2-1 his3-11,15 leu2-3,112 trp1-1 ura3-1 can1-100 RAD5+ isw1Δ::ADE2 isw2Δ::LEU2 chd1Δ::TRP1 arp8Δ::NATMX6 colony 2</i>	This study	Transformation in YTT227
yFMP483	<i>nhp10Δ</i>	<i>MATa ade2-1 his3-11,15 leu2-3,112 trp1-1 ura3-1 can1-100 RAD5+ nhp10Δ::NATMX6 colony 1</i>	This study	Transformation in W1588-4C
yFMP484	<i>nhp10Δ</i>	<i>MATa ade2-1 his3-11,15 leu2-3,112 trp1-1 ura3-1 can1-100 RAD5+ nhp10Δ::NATMX6 colony 2</i>	This study	Transformation in W1588-4C
yFMP486	TKO <i>nhp10Δ</i>	<i>MATa ade2-1 his3-11,15 leu2-3,112 trp1-1 ura3-1 can1-100 RAD5+ isw1Δ::ADE2 isw2Δ::LEU2 chd1Δ::TRP1 nhp10Δ::NATMX6 colony 1</i>	This study	Transformation in YTT227
yFMP487	TKO <i>nhp10Δ</i>	<i>MATa ade2-1 his3-11,15 leu2-3,112 trp1-1 ura3-1 can1-100 RAD5+ isw1Δ::ADE2 isw2Δ::LEU2 chd1Δ::TRP1 nhp10Δ::NATMX6 colony 2</i>	This study	Transformation in YTT227
yFMP489	<i>nhp10Δ ΔN-ino80</i>	<i>MATa ade2-1 his3-11,15 leu2-3,112 trp1-1 ura3-1 can1-100 RAD5+ nhp10Δ::NATMX6 ino80 1-900::HIS3</i>	This study	Transformation in yFMP368
yFMP490	<i>nhp10Δ ino80^{AN}</i>	<i>MATa ade2-1 his3-11,15 leu2-3,112 trp1-1 ura3-1 can1-100 RAD5+ nhp10Δ::NATMX6 ino80 1-900::HIS3</i>	This study	Transformation in yFMP369
yFMP492	TKO <i>nhp10Δ ino80^{AN}</i>	<i>MATa ade2-1 his3-11,15 leu2-3,112 trp1-1 ura3-1 can1-100 RAD5+ isw1Δ::ADE2 isw2Δ::LEU2 chd1Δ::TRP1 nhp10Δ::NATMX6 ino80 1-900::HIS3</i>	This study	Transformation in yFMP231
yFMP493	TKO <i>nhp10Δ ino80^{AN}</i>	<i>MATa ade2-1 his3-11,15 leu2-3,112 trp1-1 ura3-1 can1-100 RAD5+ isw1Δ::ADE2 isw2Δ::LEU2 chd1Δ::TRP1 nhp10Δ::NATMX6 ino80 1-900::HIS3</i>	This study	Transformation in yFMP232
yFMP505	yFMP264 <i>swr1Δ C1</i>	<i>MATa ade2-1 trp1-1 can1-100 leu2-3,112 his3-11,15 ura3 tor1-1 fpr1Δ::NAT RPL13A-2xFKBP12::TRP1 isw1Δ::ADE2 isw2Δ::LEU2 chd1Δ::TRP1 rad5-G535R swr1Δ::HphNT1 colony 1</i>	This study	Transformation in yFMP264
yFMP508	yFMP265 <i>swr1Δ C2</i>	<i>MATa ade2-1 trp1-1 can1-100 leu2-3,112 his3-11,15 ura3 tor1-1 fpr1Δ::NAT RPL13A-2xFKBP12::TRP1 isw1Δ::ADE2 isw2Δ::LEU2 chd1Δ::TRP1 rad5-G535R swr1Δ::HphNT1 colony 1</i>	This study	Transformation in yFMP265
yFMP510	yFMP266 <i>swr1Δ C1</i>	<i>MATa ade2-1 trp1-1 can1-100 leu2-3,112 his3-11,15 ura3 tor1-1 fpr1Δ::NAT RPL13A-2xFKBP12::TRP1 RPO21-FRB::kanMX6 isw1Δ::ADE2 isw2Δ::LEU2 chd1Δ::TRP1 rad5-G535R swr1Δ::HphNT1 colony 1</i>	This study	Transformation in yFMP266
yFMP512	yFMP267 <i>swr1Δ C2</i>	<i>MATa ade2-1 trp1-1 can1-100 leu2-3,112 his3-11,15 ura3 tor1-1 fpr1Δ::NAT RPL13A-2xFKBP12::TRP1 RPO21-FRB::kanMX6 isw1Δ::ADE2 isw2Δ::LEU2 chd1Δ::TRP1 rad5-G535R swr1Δ::HphNT1 colony 2</i>	This study	Transformation in yFMP267
yFMP515	yFMP264 <i>htz1Δ C1</i>	<i>MATa ade2-1 trp1-1 can1-100 leu2-3,112 his3-11,15 ura3 tor1-1 fpr1Δ::NAT RPL13A-2xFKBP12::TRP1 isw1Δ::ADE2 isw2Δ::LEU2 chd1Δ::TRP1 rad5-G535R htz1Δ::HphNT1 colony 1</i>	This study	Transformation in yFMP264
yFMP516	yFMP265 <i>htz1Δ C2</i>	<i>MATa ade2-1 trp1-1 can1-100 leu2-3,112 his3-11,15 ura3 tor1-1 fpr1Δ::NAT RPL13A-2xFKBP12::TRP1 isw1Δ::ADE2 isw2Δ::LEU2 chd1Δ::TRP1 rad5-G535R htz1Δ::HphNT1 colony 1</i>	This study	Transformation in yFMP265
yFMP520	yFMP266 <i>htz1Δ C1</i>	<i>MATa ade2-1 trp1-1 can1-100 leu2-3,112 his3-11,15 ura3 tor1-1 fpr1Δ::NAT RPL13A-2xFKBP12::TRP1 RPO21-FRB::kanMX6 isw1Δ::ADE2 isw2Δ::LEU2 chd1Δ::TRP1 rad5-G535R htz1Δ::HphNT1 colony 1</i>	This study	Transformation in yFMP266
yFMP522	yFMP267 <i>htz1Δ C1</i>	<i>MATa ade2-1 trp1-1 can1-100 leu2-3,112 his3-11,15 ura3 tor1-1 fpr1Δ::NAT RPL13A-2xFKBP12::TRP1 RPO21-FRB::kanMX6 isw1Δ::ADE2 isw2Δ::LEU2 chd1Δ::TRP1 rad5-G535R htz1Δ::HphNT1 colony 2</i>	This study	Transformation in yFMP267
yFMP525	yFMP264 <i>nhp10Δ C1</i>	<i>MATa ade2-1 trp1-1 can1-100 leu2-3,112 his3-11,15 ura3 tor1-1 fpr1Δ::NAT RPL13A-2xFKBP12::TRP1 isw1Δ::ADE2 isw2Δ::LEU2 chd1Δ::TRP1 rad5-G535R nhp10Δ::HphNT1 colony 1</i>	This study	Transformation in yFMP264

yFMP528	yFMP265 <i>nhp10Δ</i> C2	<i>MATa ade2-1 trp1-1 can1-100 leu2-3,112 his3-11,15 ura3 tor1-1 fpr1Δ::NAT RPL13A-2xFKBP12::TRP1 isw1Δ::ADE2 isw2Δ::LEU2 chd1Δ::TRP1 rad5-G535R nhp10Δ::HphNT1</i> colony 2	This study	Transformation in yFMP265
yFMP530	yFMP266 <i>nhp10Δ</i> C1	<i>MATa ade2-1 trp1-1 can1-100 leu2-3,112 his3-11,15 ura3 tor1-1 fpr1Δ::NAT RPL13A-2xFKBP12::TRP1 RPO21-FRB::kanMX6 isw1Δ::ADE2 isw2Δ::LEU2 chd1Δ::TRP1 rad5-G535R nhp10Δ::HphNT1</i> colony 1	This study	Transformation in yFMP266
yFMP533	yFMP267 <i>nhp10Δ</i> C2	<i>MATa ade2-1 trp1-1 can1-100 leu2-3,112 his3-11,15 ura3 tor1-1 fpr1Δ::NAT RPL13A-2xFKBP12::TRP1 RPO21-FRB::kanMX6 isw1Δ::ADE2 isw2Δ::LEU2 chd1Δ::TRP1 rad5-G535R nhp10Δ::HphNT1</i> colony 2	This study	Transformation in yFMP267
yFMP534	yFMP264 <i>arp8Δ</i> C1	<i>MATa ade2-1 trp1-1 can1-100 leu2-3,112 his3-11,15 ura3 tor1-1 fpr1Δ::NAT RPL13A-2xFKBP12::TRP1 isw1Δ::ADE2 isw2Δ::LEU2 chd1Δ::TRP1 rad5-G535R arp8Δ::HphNT1</i> colony 1	This study	Transformation in yFMP264
yFMP535	yFMP264 <i>arp8Δ</i> C2	<i>MATa ade2-1 trp1-1 can1-100 leu2-3,112 his3-11,15 ura3 tor1-1 fpr1Δ::NAT RPL13A-2xFKBP12::TRP1 isw1Δ::ADE2 isw2Δ::LEU2 chd1Δ::TRP1 rad5-G535R arp8Δ::HphNT1</i> colony 2	This study	Transformation in yFMP265
yFMP537	yFMP266 <i>arp8Δ</i> C1	<i>MATa ade2-1 trp1-1 can1-100 leu2-3,112 his3-11,15 ura3 tor1-1 fpr1Δ::NAT RPL13A-2xFKBP12::TRP1 RPO21-FRB::kanMX6 isw1Δ::ADE2 isw2Δ::LEU2 chd1Δ::TRP1 rad5-G535R arp8Δ::HphNT1</i> colony 1	This study	Transformation in yFMP266
yFMP539	yFMP267 <i>arp8Δ</i> C1	<i>MATa ade2-1 trp1-1 can1-100 leu2-3,112 his3-11,15 ura3 tor1-1 fpr1Δ::NAT RPL13A-2xFKBP12::TRP1 RPO21-FRB::kanMX6 isw1Δ::ADE2 isw2Δ::LEU2 chd1Δ::TRP1 rad5-G535R arp8Δ::HphNT1</i> colony 2	This study	Transformation in yFMP267
yFMP543	lsw1 left upon Rapamycin treatment	<i>ade2-1 trp1-1 can1-100 leu2-3,112 his3-11,15 ura3 tor1-1 fpr1Δ::NAT RPL13A-2xFKBP12::TRP1 RPO21-FRB::kanMX6 isw2Δ::LEU2 chd1Δ::TRP1 INO80-GFP-FRB::hphMX6</i> colony 1-1	This study	Mating and tetrad dissection, INO80-GFP-FRB transformation
yFMP544	lsw1 left upon Rapamycin treatment	<i>ade2-1 trp1-1 can1-100 leu2-3,112 his3-11,15 ura3 tor1-1 fpr1Δ::NAT RPL13A-2xFKBP12::TRP1 RPO21-FRB::kanMX6 isw2Δ::LEU2 chd1Δ::TRP1 INO80-GFP-FRB::hphMX6</i> colony 1-2	This study	Mating and tetrad dissection, INO80-GFP-FRB transformation
yFMP546	lsw1 left upon Rapamycin treatment	<i>ade2-1 trp1-1 can1-100 leu2-3,112 his3-11,15 ura3 tor1-1 fpr1Δ::NAT RPL13A-2xFKBP12::TRP1 RPO21-FRB::kanMX6 isw2Δ::LEU2 chd1Δ::TRP1 INO80-GFP-FRB::hphMX6</i> colony 2-1	This study	Mating and tetrad dissection, INO80-GFP-FRB transformation
yFMP547	lsw1 left upon Rapamycin treatment	<i>ade2-1 trp1-1 can1-100 leu2-3,112 his3-11,15 ura3 tor1-1 fpr1Δ::NAT RPL13A-2xFKBP12::TRP1 RPO21-FRB::kanMX6 isw2Δ::LEU2 chd1Δ::TRP1 INO80-GFP-FRB::hphMX6</i> colony 2-2	This study	Mating and tetrad dissection, INO80-GFP-FRB transformation
yFMP550	lsw1 + Pol II left upon Rapamycin treatment	<i>ade2-1 trp1-1 can1-100 leu2-3,112 his3-11,15 ura3 tor1-1 fpr1Δ::NAT RPL13A-2xFKBP12::TRP1 isw2Δ::LEU2 chd1Δ::TRP1 INO80-GFP-FRB::hphMX6</i> colony 1-1	This study	Mating and tetrad dissection, INO80-GFP-FRB transformation
yFMP551	lsw1 + Pol II left upon Rapamycin treatment	<i>ade2-1 trp1-1 can1-100 leu2-3,112 his3-11,15 ura3 tor1-1 fpr1Δ::NAT RPL13A-2xFKBP12::TRP1 isw2Δ::LEU2 chd1Δ::TRP1 INO80-GFP-FRB::hphMX6</i> colony 1-2	This study	Mating and tetrad dissection, INO80-GFP-FRB transformation
yFMP554	lsw1 + Pol II left upon Rapamycin treatment	<i>ade2-1 trp1-1 can1-100 leu2-3,112 his3-11,15 ura3 tor1-1 fpr1Δ::NAT RPL13A-2xFKBP12::TRP1 isw2Δ::LEU2 chd1Δ::TRP1 INO80-GFP-FRB::hphMX6</i> colony 2-1	This study	Mating and tetrad dissection, INO80-GFP-FRB transformation
yFMP555	lsw1 + Pol II left upon Rapamycin treatment	<i>ade2-1 trp1-1 can1-100 leu2-3,112 his3-11,15 ura3 tor1-1 fpr1Δ::NAT RPL13A-2xFKBP12::TRP1 isw2Δ::LEU2 chd1Δ::TRP1 INO80-GFP-FRB::hphMX6</i> colony 2-2	This study	Mating and tetrad dissection, INO80-GFP-FRB transformation
yFMP558	lsw2 left upon Rapamycin treatment	<i>ade2-1 trp1-1 can1-100 leu2-3,112 his3-11,15 ura3 tor1-1 fpr1Δ::NAT RPL13A-2xFKBP12::TRP1 RPO21-FRB::kanMX6 isw1Δ::ADE2 chd1Δ::TRP1 INO80-GFP-FRB::hphMX6</i> colony 1-1	This study	Mating and tetrad dissection, INO80-GFP-FRB transformation
yFMP559	lsw2 left upon Rapamycin treatment	<i>ade2-1 trp1-1 can1-100 leu2-3,112 his3-11,15 ura3 tor1-1 fpr1Δ::NAT RPL13A-2xFKBP12::TRP1 RPO21-FRB::kanMX6 isw1Δ::ADE2 chd1Δ::TRP1 INO80-GFP-FRB::hphMX6</i> colony 1-2	This study	Mating and tetrad dissection, INO80-GFP-FRB transformation
yFMP564	lsw2 left upon Rapamycin treatment	<i>ade2-1 trp1-1 can1-100 leu2-3,112 his3-11,15 ura3 tor1-1 fpr1Δ::NAT RPL13A-2xFKBP12::TRP1 RPO21-FRB::kanMX6 isw1Δ::ADE2 chd1Δ::TRP1 INO80-GFP-FRB::hphMX6</i> colony 2-1	This study	Mating and tetrad dissection, INO80-GFP-FRB transformation

yFMP565	Isw2 left upon Rapamycin treatment	<i>ade2-1 trp1-1 can1-100 leu2-3,112 his3-11,15 ura3 tor1-1 fpr1Δ::NAT RPL13A-2xFKBP12::TRP1 RPO21-FRB::kanMX6 isw1Δ::ADE2 chd1Δ::TRP1 INO80-GFP-FRB::hphMX6 colony 2-2</i>	This study	Mating and tetrad dissection, INO80-GFP-FRB transformation
yFMP568	Isw2 + Pol II left upon Rapamycin treatment	<i>ade2-1 trp1-1 can1-100 leu2-3,112 his3-11,15 ura3 tor1-1 fpr1Δ::NAT RPL13A-2xFKBP12::TRP1 isw1Δ::ADE2 chd1Δ::TRP1 INO80-GFP-FRB::hphMX6 colony 1-1</i>	This study	Mating and tetrad dissection, INO80-GFP-FRB transformation
yFMP569	Isw2 + Pol II left upon Rapamycin treatment	<i>ade2-1 trp1-1 can1-100 leu2-3,112 his3-11,15 ura3 tor1-1 fpr1Δ::NAT RPL13A-2xFKBP12::TRP1 isw1Δ::ADE2 chd1Δ::TRP1 INO80-GFP-FRB::hphMX6 colony 1-2</i>	This study	Mating and tetrad dissection, INO80-GFP-FRB transformation
yFMP570	Isw2 + Pol II left upon Rapamycin treatment	<i>ade2-1 trp1-1 can1-100 leu2-3,112 his3-11,15 ura3 tor1-1 fpr1Δ::NAT RPL13A-2xFKBP12::TRP1 isw1Δ::ADE2 chd1Δ::TRP1 INO80-GFP-FRB::hphMX6 colony 1-3</i>	This study	Mating and tetrad dissection, INO80-GFP-FRB transformation
yFMP572	Chd1 left upon Rapamycin treatment	<i>ade2-1 trp1-1 can1-100 leu2-3,112 his3-11,15 ura3 tor1-1 fpr1Δ::NAT RPL13A-2xFKBP12::TRP1 RPO21-FRB::kanMX6 isw1Δ::ADE2 isw2Δ::LEU2 INO80-GFP-FRB::hphMX6 colony 1-1</i>	This study	Mating and tetrad dissection, INO80-GFP-FRB transformation
yFMP573	Chd1 left upon Rapamycin treatment	<i>ade2-1 trp1-1 can1-100 leu2-3,112 his3-11,15 ura3 tor1-1 fpr1Δ::NAT RPL13A-2xFKBP12::TRP1 RPO21-FRB::kanMX6 isw1Δ::ADE2 isw2Δ::LEU2 INO80-GFP-FRB::hphMX6 colony 1-2</i>	This study	Mating and tetrad dissection, INO80-GFP-FRB transformation
yFMP577	Chd1 left upon Rapamycin treatment	<i>ade2-1 trp1-1 can1-100 leu2-3,112 his3-11,15 ura3 tor1-1 fpr1Δ::NAT RPL13A-2xFKBP12::TRP1 RPO21-FRB::kanMX6 isw1Δ::ADE2 isw2Δ::LEU2 INO80-GFP-FRB::hphMX6 colony 2-1</i>	This study	Mating and tetrad dissection, INO80-GFP-FRB transformation
yFMP578	Chd1 left upon Rapamycin treatment	<i>ade2-1 trp1-1 can1-100 leu2-3,112 his3-11,15 ura3 tor1-1 fpr1Δ::NAT RPL13A-2xFKBP12::TRP1 RPO21-FRB::kanMX6 isw1Δ::ADE2 isw2Δ::LEU2 INO80-GFP-FRB::hphMX6 colony 2-2</i>	This study	Mating and tetrad dissection, INO80-GFP-FRB transformation
yFMP582	Chd1 + Pol II left upon Rapamycin treatment	<i>ade2-1 trp1-1 can1-100 leu2-3,112 his3-11,15 ura3 tor1-1 fpr1Δ::NAT RPL13A-2xFKBP12::TRP1 isw1Δ::ADE2 isw2Δ::LEU2 INO80-GFP-FRB::hphMX6 colony 1-1</i>	This study	Mating and tetrad dissection, INO80-GFP-FRB transformation
yFMP583	Chd1 + Pol II left upon Rapamycin treatment	<i>ade2-1 trp1-1 can1-100 leu2-3,112 his3-11,15 ura3 tor1-1 fpr1Δ::NAT RPL13A-2xFKBP12::TRP1 isw1Δ::ADE2 isw2Δ::LEU2 INO80-GFP-FRB::hphMX6 colony 1-2</i>	This study	Mating and tetrad dissection
yFMP584	Chd1 + Pol II left upon Rapamycin treatment	<i>ade2-1 trp1-1 can1-100 leu2-3,112 his3-11,15 ura3 tor1-1 fpr1Δ::NAT RPL13A-2xFKBP12::TRP1 isw1Δ::ADE2 isw2Δ::LEU2 INO80-GFP-FRB::hphMX6 colony 1-3</i>	This study	Mating and tetrad dissection, INO80-GFP-FRB transformation
yFMP585	Chd1 + Pol II left upon Rapamycin treatment	<i>ade2-1 trp1-1 can1-100 leu2-3,112 his3-11,15 ura3 tor1-1 fpr1Δ::NAT RPL13A-2xFKBP12::TRP1 isw1Δ::ADE2 isw2Δ::LEU2 INO80-GFP-FRB::hphMX6 colony 1-4</i>	This study	Mating and tetrad dissection, INO80-GFP-FRB transformation
yFMP589	ISW1 + INO80 left upon Rapamycin treatment	<i>ade2-1 trp1-1 can1-100 leu2-3,112 his3-11,15 ura3 tor1-1 fpr1Δ::NAT RPL13A-2xFKBP12::TRP1 RPO21-FRB::kanMX6 isw2Δ::LEU2 chd1Δ::TRP1 colony 1</i>	This study	Mating and tetrad dissection
yFMP590	ISW1 + INO80 left upon Rapamycin treatment	<i>ade2-1 trp1-1 can1-100 leu2-3,112 his3-11,15 ura3 tor1-1 fpr1Δ::NAT RPL13A-2xFKBP12::TRP1 RPO21-FRB::kanMX6 isw2Δ::LEU2 chd1Δ::TRP1 colony 2</i>	This study	Mating and tetrad dissection
yFMP591	ISW1 + INO80 left upon Rapamycin treatment	<i>ade2-1 trp1-1 can1-100 leu2-3,112 his3-11,15 ura3 tor1-1 fpr1Δ::NAT RPL13A-2xFKBP12::TRP1 RPO21-FRB::kanMX6 isw2Δ::LEU2 chd1Δ::TRP1 colony 3</i>	This study	Mating and tetrad dissection
yFMP593	ISW1 + INO80 + Pol II left upon	<i>ade2-1 trp1-1 can1-100 leu2-3,112 his3-11,15 ura3 tor1-1 fpr1Δ::NAT RPL13A-2xFKBP12::TRP1 isw2Δ::LEU2 chd1Δ::TRP1 colony 1</i>	This study	Mating and tetrad dissection

	Rapamycin treatment			
yFMP594	ISW1 + INO80 + Pol II left upon Rapamycin treatment	<i>ade2-1 trp1-1 can1-100 leu2-3,112 his3-11,15 ura3 tor1-1 fpr1Δ::NAT RPL13A-2xFKBP12::TRP1 isw2Δ::LEU2 chd1Δ::TRP1</i> colony 2	This study	Mating and tetrad dissection
yFMP595	ISW1 + INO80 + Pol II left upon Rapamycin treatment	<i>ade2-1 trp1-1 can1-100 leu2-3,112 his3-11,15 ura3 tor1-1 fpr1Δ::NAT RPL13A-2xFKBP12::TRP1 isw2Δ::LEU2 chd1Δ::TRP1</i> colony 3	This study	Mating and tetrad dissection
yFMP598	ISW2 + INO80 left upon Rapamycin treatment	<i>ade2-1 trp1-1 can1-100 leu2-3,112 his3-11,15 ura3 tor1-1 fpr1Δ::NAT RPL13A-2xFKBP12::TRP1 RPO21-FRB::kanMX6 isw1Δ::ADE2 chd1Δ::TRP1</i> colony 1	This study	Mating and tetrad dissection
yFMP599	ISW2 + INO80 left upon Rapamycin treatment	<i>ade2-1 trp1-1 can1-100 leu2-3,112 his3-11,15 ura3 tor1-1 fpr1Δ::NAT RPL13A-2xFKBP12::TRP1 RPO21-FRB::kanMX6 isw1Δ::ADE2 chd1Δ::TRP1</i> colony 2	This study	Mating and tetrad dissection
yFMP600	ISW2 + INO80 left upon Rapamycin treatment	<i>ade2-1 trp1-1 can1-100 leu2-3,112 his3-11,15 ura3 tor1-1 fpr1Δ::NAT RPL13A-2xFKBP12::TRP1 RPO21-FRB::kanMX6 isw1Δ::ADE2 chd1Δ::TRP1</i> colony 3	This study	Mating and tetrad dissection
yFMP601	ISW2 + INO80 left upon Rapamycin treatment	<i>ade2-1 trp1-1 can1-100 leu2-3,112 his3-11,15 ura3 tor1-1 fpr1Δ::NAT RPL13A-2xFKBP12::TRP1 RPO21-FRB::kanMX6 isw1Δ::ADE2 chd1Δ::TRP1</i> colony 4	This study	Mating and tetrad dissection
yFMP602	ISW2 + INO80 + Pol II left upon Rapamycin treatment	<i>ade2-1 trp1-1 can1-100 leu2-3,112 his3-11,15 ura3 tor1-1 fpr1Δ::NAT RPL13A-2xFKBP12::TRP1 isw1Δ::ADE2 chd1Δ::TRP1</i>	This study	Mating and tetrad dissection
yFMP603	Chd1 + INO80 left upon Rapamycin treatment	<i>ade2-1 trp1-1 can1-100 leu2-3,112 his3-11,15 ura3 tor1-1 fpr1Δ::NAT RPL13A-2xFKBP12::TRP1 RPO21-FRB::kanMX6 isw1Δ::ADE2 isw2Δ::LEU2</i> colony 1	This study	Mating and tetrad dissection
yFMP604	Chd1 + INO80 left upon Rapamycin treatment	<i>ade2-1 trp1-1 can1-100 leu2-3,112 his3-11,15 ura3 tor1-1 fpr1Δ::NAT RPL13A-2xFKBP12::TRP1 RPO21-FRB::kanMX6 isw1Δ::ADE2 isw2Δ::LEU2</i> colony 2	This study	Mating and tetrad dissection
yFMP605	Chd1 + INO80 left upon Rapamycin treatment	<i>ade2-1 trp1-1 can1-100 leu2-3,112 his3-11,15 ura3 tor1-1 fpr1Δ::NAT RPL13A-2xFKBP12::TRP1 RPO21-FRB::kanMX6 isw1Δ::ADE2 isw2Δ::LEU2</i> colony 3	This study	Mating and tetrad dissection
yFMP606	Chd1 + INO80 left upon Rapamycin treatment	<i>ade2-1 trp1-1 can1-100 leu2-3,112 his3-11,15 ura3 tor1-1 fpr1Δ::NAT RPL13A-2xFKBP12::TRP1 RPO21-FRB::kanMX6 isw1Δ::ADE2 isw2Δ::LEU2</i> colony 4	This study	Mating and tetrad dissection
yFMP607	Chd1 + INO80 + Pol II left	<i>ade2-1 trp1-1 can1-100 leu2-3,112 his3-11,15 ura3 tor1-1 fpr1Δ::NAT RPL13A-2xFKBP12::TRP1 isw1Δ::ADE2 isw2Δ::LEU2</i>	This study	Mating and tetrad dissection

	upon Rapamycin treatment			
yFMP608	<i>arp8Δ</i> alpha	<i>MATa ade2-1 his3-11,15 leu2-3,112 trp1-1 ura3-1 can1-100 RAD5+ arp8Δ::NATMX6</i> colony 1	This study	Mating yFMP476 and yFMP325, tetrad dissection
yFMP609	<i>arp8Δ</i> alpha	<i>MATa ade2-1 his3-11,15 leu2-3,112 trp1-1 ura3-1 can1-100 RAD5+ arp8Δ::NATMX6</i> colony 2	This study	Mating yFMP477 and yFMP325, tetrad dissection
yFMP611	<i>arp8Δ</i> a	<i>MATa ade2-1 his3-11,15 leu2-3,112 trp1-1 ura3-1 can1-100 RAD5+ arp8Δ::NATMX6</i> colony 1	This study	Mating yFMP476 and yFMP325, tetrad dissection
yFMP612	<i>arp8Δ</i> a	<i>MATa ade2-1 his3-11,15 leu2-3,112 trp1-1 ura3-1 can1-100 RAD5+ arp8Δ::NATMX6</i> colony 2	This study	Mating yFMP477 and yFMP325, tetrad dissection
yFMP614	<i>nhp10Δ</i> Ino80-FLAG C1	<i>MATa ade2-1 his3-11,15 leu2-3,112 trp1-1 ura3-1 can1-100 RAD5+ nhp10Δ::HphNT1 INO80-3xFLAG::NATMX</i> colony 1	This study	Transformation in yFMP257
yFMP615	<i>nhp10Δ</i> Ino80-FLAG C2	<i>MATa ade2-1 his3-11,15 leu2-3,112 trp1-1 ura3-1 can1-100 RAD5+ nhp10Δ::HphNT1 INO80-3xFLAG::NATMX</i> colony 2	This study	Transformation in yFMP257
yFMP616	<i>nhp10Δ</i> Ino80-FLAG C3	<i>MATa ade2-1 his3-11,15 leu2-3,112 trp1-1 ura3-1 can1-100 RAD5+ nhp10Δ::HphNT1 INO80-3xFLAG::NATMX</i> colony 3	This study	Transformation in yFMP257
yFMP617	TKO <i>nhp10Δ</i> Ino80-FLAG C1	<i>MATa ade2-1 his3-11,15 leu2-3,112 trp1-1 ura3-1 can1-100 RAD5+ isw1Δ::ADE2 isw2Δ::LEU2 chd1Δ::TRP1 nhp10Δ::HphNT1 INO80-3xFLAG::NATMX</i> colony 1	This study	Transformation in yFMP254
yFMP618	TKO <i>nhp10Δ</i> Ino80-FLAG C2	<i>MATa ade2-1 his3-11,15 leu2-3,112 trp1-1 ura3-1 can1-100 RAD5+ isw1Δ::ADE2 isw2Δ::LEU2 chd1Δ::TRP1 nhp10Δ::HphNT1 INO80-3xFLAG::NATMX</i> colony 2	This study	Transformation in yFMP254
yFMP619	TKO <i>nhp10Δ</i> Ino80-FLAG C3	<i>MATa ade2-1 his3-11,15 leu2-3,112 trp1-1 ura3-1 can1-100 RAD5+ isw1Δ::ADE2 isw2Δ::LEU2 chd1Δ::TRP1 nhp10Δ::HphNT1 INO80-3xFLAG::NATMX</i> colony 3	This study	Transformation in yFMP254
yFMP626	JPY17	<i>MATa ade2-1 his3-11,15 leu2-3,112 trp1-1 ura3-1 can1-100 RAD5+ chd1Δ::TRP1</i>	(Tsukiyama et al., 1999)	-
yFMP627	<i>ies6Δ</i> C1	<i>MATa ade2-1 his3-11,15 leu2-3,112 trp1-1 ura3-1 can1-100 RAD5+ ies6Δ::NATMX6</i>	This study	Transformation in yFMP324
yFMP628	<i>ies6Δ</i> C2	<i>MATa ade2-1 his3-11,15 leu2-3,112 trp1-1 ura3-1 can1-100 RAD5+ ies6Δ::NATMX6</i>	This study	Transformation in yFMP325
yFMP629	<i>ies2Δ</i> C1	<i>MATa ade2-1 his3-11,15 leu2-3,112 trp1-1 ura3-1 can1-100 RAD5+ ies2Δ::NATMX6</i> colony 1	This study	Transformation in W1588-4c
yFMP630	<i>ies2Δ</i> C2	<i>MATa ade2-1 his3-11,15 leu2-3,112 trp1-1 ura3-1 can1-100 RAD5+ ies2Δ::NATMX6</i> colony 2	This study	Transformation in W1588-4c
yFMP632	TKO <i>ies2Δ</i> C1	<i>MATa ade2-1 his3-11,15 leu2-3,112 trp1-1 ura3-1 can1-100 RAD5+ isw1Δ::ADE2 isw2Δ::LEU2 chd1Δ::TRP1 ies2Δ::NATMX6</i> colony 1	This study	Transformation in YTT227
yFMP633	TKO <i>ies2Δ</i> C2	<i>MATa ade2-1 his3-11,15 leu2-3,112 trp1-1 ura3-1 can1-100 RAD5+ isw1Δ::ADE2 isw2Δ::LEU2 chd1Δ::TRP1 ies2Δ::NATMX6</i> colony 2	This study	Transformation in YTT227
yFMP706	<i>isw2-TAP-His3</i>	<i>Mata his3Δ1 leu2Δ0 met15Δ0 ura3Δ0 isw2::isw2-TAP::HIS3MX6</i>	Dr. Frank Pugh	-

Bacterial strain used in this thesis is *E. coli* NEB 5-alpha (Cat# C2987).

4.1.2 Oligonucleotide sequences

List of oligonucleotides used in this study. Purification strategy indicates whether the oligonucleotide was only desalted or additionally purified using HPLC or PAGE. All oligonucleotides were synthesized from Sigma. F and R stand for forward and reverse primers.

Name	5'-3' sequence	Purpose	Purification
------	----------------	---------	--------------

oFMP437	CAAGGATATACCATTCTATCTAGAAAAATGGCCTATAT GTTAGCTATTG	Clone <i>ISW1</i> in Alper P1-P14 plasmids F	Desalt
oFMP438	CGAGGTGCGACGGTATCGATTTAATGAGTGGTTTCGTT TTCC	Clone <i>ISW1</i> in Alper P1-P14 plasmids R	Desalt
oFMP439	CAATTCTTGCAATGAAAAGG	<i>ISW1</i> sequencing 1	Desalt
oFMP440	TCATTGCGCCTAAGTCTACC	<i>ISW1</i> sequencing 2	Desalt
oFMP441	ATTTATTCGATGGTGCTGAG	<i>ISW1</i> sequencing 3	Desalt
oFMP442	TGGTTCAGGAGAAAAAGGAG	<i>ISW1</i> sequencing 4	Desalt
oFMP443	AGTTCGCGCATATGCTAAGG	<i>ISW1</i> sequencing 5	Desalt
oFMP444	AAGCGAGTCACCTTCAGAAG	<i>ISW2</i> fl sequencing 1	Desalt
oFMP445	GACTCCAACGTC AATGTCC	<i>ISW2</i> fl sequencing 2	Desalt
oFMP446	AGACTGAAGGAAAAGGGATC	<i>ISW2</i> fl sequencing 3	Desalt
oFMP447	TCAGAAAAGCAAGCAAATCC	<i>ISW2</i> fl sequencing 4	Desalt
oFMP448	CAAGTACGGACTTCGTGCTG	<i>ISW2</i> fl sequencing 5	Desalt
oFMP449	CAAGGATATACCATTCTATCTAGAAAAATGACGACCCA GCAAGAGGAGC	Clone <i>ISW2</i> in Alper P1-P14 plasmids F	Desalt
oFMP450	GACTCGAGGTGCGACGGTATCGATTCATGCTTCTTGAT CAATTTTGG	Clone <i>ISW2</i> in Alper P1-P14 plasmids R	Desalt
oFMP456	GGATAATACCGATCAGAAAAATCC	Check <i>ITC1</i> locus F	
oFMP462	GGAGAAAAAACCCCGGATTCTAGAAAAATGGCCTATA TGTTAGCTATTG	Clone <i>ISW1</i> in Alper P15-P16 plasmids F	Desalt
oFMP463	GGAGAAAAAACCCCGGATTCTAGAAAAATGACGACCC AGCAAGAGGAGC	Clone <i>ISW2</i> in Alper P15-P16 plasmids F	Desalt
oFMP464	CACGTGCCCATGCAAAAACAGAAAAGGAGGAAGATGC TG	Mutate 2RA <i>ISW2</i> F	Desalt
oFMP465	GTTTTTGCATGGGCACGTGATGACGAACTGACGGTG	Mutate 2RA <i>ISW2</i> R	Desalt
oFMP466	GATGTTGCTAGAGCAAAGACTGAACACGAAGAAGATG	Mutate 2RA <i>ISW1</i> F	Desalt
oFMP467	GTCTTTGCTCTAGCAACATCTTGGTGTTCCTTTG	Mutate 2RA <i>ISW1</i> R	Desalt
oFMP468	CATCTACCTAGTCAGCTGGTACGCCGGAAC	Stop NegC G 690 TAG <i>ISW1</i> F	Desalt
oFMP469	CAGCTGACTAGGTAGATGTACCACTTTTGAATACATCG	Stop NegC G 690 TAG <i>ISW1</i> R	Desalt
oFMP470	CAAGTAAATAGACTGTTGATGCTGATATCGATG	Stop NegC V 676 TAG <i>ISW2</i> F	Desalt
oFMP471	ATCAACAGTCTATTTACTTGCTTTCTTTTCAAACA	Stop NegC V 676 TAG <i>ISW2</i> R	Desalt
oFMP472	ATGATTTGTAGAAATTCACCAAGATTCGGC	Stop after NegC Q 735 TAG <i>ISW1</i> F	Desalt
oFMP473	GTTGAATTTCTACAAATCATCAAGACCTAAAGTTTCA	Stop after NegC Q 735 TAG <i>ISW1</i> R	Desalt
oFMP474	CGACTTATAGAAGTTCAATGGGATCGAGAAC	Stop after NegC Q 709 TAG <i>ISW2</i> F	Desalt
oFMP475	CATTGAACCTTCTATAAGTCGTCAAGTCCTAACTTTGG	Stop after NegC Q 709 TAG <i>ISW2</i> R	Desalt
oFMP476	CTTGGTGAATAGAAAAATGAAAACTGAAATTCAGG	Stop slide K 955 TAG <i>ISW2</i> F	Desalt
oFMP477	CATTTTCTATTACCAAGTTCTACATTATGTAATACT TC	Stop slide K 955 TAG <i>ISW2</i> R	Desalt
oFMP478	ATGAAGAATAGAAGATCAAGCGTGTCAAATG	Stop slide E 952 TAG <i>ISW1</i> F	Desalt
oFMP479	CTTGATCTTCTATTCTTCAATTATTTTCAGATA TTTC	Stop slide E 952 TAG <i>ISW1</i> R	Desalt
oFMP480	CAAGGATATACCATTCTATCTAGAAAAATGAAAGCAAA TGCCAAAGGCAAAG	Clone <i>ISW1</i> lacking N- terminus before AutoN F Alper P1-P14	HPLC
oFMP481	GGAGAAAAAACCCCGGATTCTAGAAAAATGAAAGCAA ATGGCAAAGGCAAAG	Clone <i>ISW1</i> lacking N- terminus before AutoN F Alper P15-P16	HPLC
oFMP482	CAAGGATATACCATTCTATCTAGAAAAATGAACTTTC CAAATCACACAGC	Clone <i>ISW2</i> lacking N- terminus before AutoN F Alper P1-P14	HPLC
oFMP483	GGAGAAAAAACCCCGGATTCTAGAAAAATGAACTTT CCAAATCACACAGC	Clone <i>ISW2</i> lacking N- terminus before AutoN F Alper P15-P16	HPLC
oFMP484	CAAGGATATACCATTCTATCTAGAAAAATGACTGAACA CGAAGAAGATGC	Clone <i>ISW1</i> lacking N- terminus incl. AutoN F Alper P1-P14	HPLC
oFMP485	GGAGAAAAAACCCCGGATTCTAGAAAAATGACTGAAC ACGAAGAAGATGC	Clone <i>ISW1</i> lacking N- terminus incl. AutoN F Alper P15-P16	HPLC
oFMP486	CAAGGATATACCATTCTATCTAGAAAAATGACAGAAAA GGAGGAAGATGCTG	Clone <i>ISW2</i> lacking N- terminus incl. AutoN F Alper P1-P14	HPLC

oFMP487	GGAGAAAAACCCCGGATTCTAGAAAAATGACAGAAA AGGAGGAAGATGCTG	Clone <i>ISW2</i> lacking N-terminus incl. AutoN F Alper P15-P16	HPLC
oFMP488	GAAAAAACAATAGGAGGAAGTAAAGAAAGCCGTAA TAAACAAGATTGACTGAGAGTGCACC	Delete <i>ITC1</i> F	HPLC
oFMP489	GAATACTACAATTTACCATCAGTTACAAAGGAAGTTTT TTATATAATCTGTGCGGTATTTACACAC	Delete <i>ITC1</i> R	HPLC
oFMP490	CAAGGATATACCATTCTATCTAGAAAA ATG ATGGTGTTATATAAAAAGGAAACCTATATTAC	Clone <i>ITC1</i> in Alper P1-P14	HPLC
oFMP491	CTCGAGGTCGACGGTATCGAT TTAATTTGGGGCAGGTGTTAC	Clone <i>ITC1</i> in Alper P1-P14	HPLC
oFMP492	CAAGGATATACCATTCTATCTAGAAAA ATG GAGCCTCAGGCTGTAACAATAAC	Clone <i>ITC1</i> lacking N-terminus (2-374) in Alper P1-P14	HPLC
oFMP502	GTTTGATATCGATATTTT CAGAAGCTG	Check <i>ITC1</i> locus R	Desalt
oFMP513	GAAACCTATATTACTTCTGATC	<i>ITC1</i> sequencing 1	Desalt
oFMP514	CACTTTCACTAAGCACTTAATC	<i>ITC1</i> sequencing 2	Desalt
oFMP515	GTCTCTCATTTTAGCCTTG	<i>ITC1</i> sequencing 3	Desalt
oFMP516	GAACCTACCGCAATGTTAACTG	<i>ITC1</i> sequencing 4	Desalt
oFMP517	CTACAAAGATTAAGCCGTTG	<i>ITC1</i> sequencing 5	Desalt
oFMP518	CACCAAAAATGAAGAAAAGTTG	<i>ITC1</i> sequencing 6	Desalt
oFMP520	ATCGATACCGTCGACCTC	<i>ISW1</i> PCR TAP tag R in Alper plasmids	Desalt
oFMP527	GAAAGGAAGTGCCATTTTTCC	Check <i>IOC3</i> locus F	Desalt
oFMP528	GGAAGGATACAAAACAGAAGAATG	Check <i>IOC3</i> locus R	Desalt
oFMP563	GTTTAGGTAGAACCCTGCAAACTATTTCAATTTCTG	Mutate <i>ISW1</i> K227R F	Desalt
oFMP564	GCAGGGTTCTACCTAAACCCATTTTCATCAGC	Mutate <i>ISW1</i> K227R R	Desalt
oFMP565	ATGAGTGGTTTTCGTTTTCC	<i>ISW1</i> PCR TAP tag F in Alper plasmids	Desalt
oFMP566	CGGAAAACGAAACCACTCATGGTGGTTCTGGTGGTTC TTTAGAAGTTTTGTTTCAAGTCCAGGTGGTTCT	PCR TAP tag and clone F in Alper plasmids	HPLC
oFMP567	GGTCGACGGTATCGATTCAGGTTGACTTCCCCGC	PCR TAP tag and clone R in Alper plasmids	Desalt
oFMP571	GAGCCTCAGGCTGTAACA	<i>ITC1</i> sequencing 2.1	Desalt
oFMP572	TTCTCATTGAAGTTTTACTGC	<i>ITC1</i> sequencing 3.1	Desalt
oFMP573	CATGGAATATGTGGTCAA	<i>ITC1</i> sequencing 4.1	Desalt
oFMP574	GTTCCGGATCTTATAATTACG	<i>ITC1</i> sequencing 5.1	Desalt
oFMP575	TCCATAATAAATTCGCAGAG	<i>ITC1</i> sequencing 6.1	Desalt
oFMP591	GTTTAGGTGCTACCCTGCAAACTATTTCAATTTCTG	<i>ISW1</i> K227A F	Desalt
oFMP592	GCAGGGTAGCACCTAAACCCATTTTCATCAGC	<i>ISW1</i> K227A R	Desalt
oFMP593	CATTGATCAAGCTCACAGAATCAAGAATGAAGAG	<i>ISW1</i> E325Q F	Desalt
oFMP594	CTGTGAGCttgATCAATGATAATACTCCCAGTTAATCT TC	<i>ISW1</i> E325Q R	Desalt
oFMP595	CATTGATCAAGCTCACAGAATCAAGAATGAAGAG	<i>ISW1</i> E325A F	Desalt
oFMP596	CTGTGAGCttgATCAATGATAATACTCCCAGTTAATCT TC	<i>ISW1</i> E325A R	Desalt
oFMP626	GTTTTGTTTTCACTGCATTTAGTAC	Check <i>ISW1</i> locus +100 F	Desalt
oFMP627	CAATTATCCGGAACAATAAATAATAC	Check <i>ISW1</i> locus -100 R	Desalt
oFMP628	CTTATATCAATGGTAGCTGCTTC	Check <i>ISW1</i> locus +500 F	Desalt
oFMP629	GCAGTATAAAGAATTGGAAGAAC	Check <i>ISW1</i> locus -500 R	Desalt
oFMP630	AAGAAAATAACAATAGGAGGAAGTAAAGAAAGCCGTT AATAAACA CAGCTGAAGCTTCGTACGC	Delete <i>ITC1</i> with His-loxP F	HPLC
oFMP631	GAATACTACAATTTACCATCAGTTACAAAGGAAGTTTT TTATATA GCATAGGCCACTAGTGGATCTG	Delete <i>ITC1</i> with His-loxP R	HPLC
oFMP640	CACTTACCAAGTACTTCAAGCAAAGTTTGCAATCCCCT ATTGTTT AGATCTGTTTAGCTTGCCTCG	Delete <i>IOC3</i> F	HPLC
oFMP641	CTGTAAGGAGTTTCAAACTTTCACGTTTCGTTGAAAGC TAGTTGT TAAAGCCTTCGAGCGTC	Delete <i>IOC3</i> R	HPLC
oFMP644	GACTGTGAATTTGTGTCAACG	Check <i>IOC2</i> locus F	Desalt
oFMP645	CGTTCTCACCATCCCCTT	Check <i>IOC2</i> locus R	Desalt
oFMP650	GAAATTGTTAACTACATTTTT CAGAACGGCGTGTCATT CTCCGATA CAGATCTGTTTAGCTTGCCTC	Delete <i>IOC4</i> F	HPLC
oFMP651	CCTCTATTGTTCAAAGCAGAGTACATCAACTGCAATA GCAACAGG AGCTCGTTAACTGGATGG	Delete <i>IOC4</i> R	HPLC
oFMP654	GAGAAACCACACATAACTTGTATAC	Check <i>IOC4</i> locus F	Desalt
oFMP657	GATTCTATATCCTTGAGGAGAAC	Check <i>IOC4</i> locus R	Desalt
oFMP658	AGTCACATCAAGATCGTTTATGG	Check mating locus 1	Desalt
oFMP659	GCACGGAATATGGGACTACTCG	Check mating locus 2	Desalt
oFMP660	ACTCCACTTCAAGTAAAGATTTG	Check mating locus 3	Desalt
oFMP665	GATATATATTTACTATATACTTTTGCTGTGTATTTCTAT ATGAGG CAGCTGAAGCTTCGTACGC	Delete <i>IOC2</i> with His-loxP F	HPLC
oFMP666	CACTGGCTAATCATATATAGATACAAAGCCGTTGAATCA CGGATCG GCATAGGCCACTAGTGGATCTG	Delete <i>IOC2</i> with His-loxP R	HPLC

oFMP667	TACATCGGCGGCACCATG	Delete <i>ISW1</i> NegC F	Desalt
oFMP668	CAAAGGGATATTATAAGTCCGCTACTG	Delete <i>ISW1</i> NegC R	Desalt
oFMP669	GGTGCCGCCGATGATTCAAAGTGGTACATCTACC	GS linker <i>ISW1</i> F	Desalt
oFMP670	GACTTATAATATCCCTTTGTATTTTCTTCTTGAATCTTGAC	GS linker <i>ISW1</i> R	Desalt
oFMP671	CATGGTATTTTGGCCTACTCG	Check <i>ISW2</i> locus +300 F	Desalt
oFMP672	GCAGGCTTTAGTTTTTCAGCA	Check <i>ISW2</i> locus -300 R	Desalt
oFMP673	TCCGGACATCTAAGTCAAGTTG	Check <i>CHD1</i> locus +300 F	Desalt
oFMP674	GAACTGGAGCGAAAGAGAAC	Check <i>CHD1</i> locus -300 R	Desalt
oFMP681	CAAATCATCAAGACCTAAAGTTTC	Amplify <i>ISW1</i> after NegC F	Desalt
oFMP682	CAAAAATTCAACCAAGATTC	Amplify <i>ISW1</i> after NegC R	Desalt
oFMP683	TTAGGTCTTGATGATTTGGGTTCTGGAAGTGGCAGTG	Amplify GS linker & clone F	Desalt
oFMP684	AATCTTGGTTGAATTTTGGAGGCTGAACCGGACCC	Amplify GS linker & clone R	Desalt
oFMP689	GAATACAGGAAGTCCCTCGA	<i>ISW1</i> sequencing 6	Desalt
oFMP690	GTCTCATCTACTGACAAAGGCA	Check <i>HHT2-HHF2</i> locus F	Desalt
oFMP691	GGATATAGACACTCCACAATACAGC	Check <i>HHT2-HHF2</i> locus R	Desalt
oFMP692	GTCTGTGTAGAAGACCACACA	Check <i>HHT1-HHF</i> locus F	Desalt
oFMP693	CTACTCCAAGGCTGCCTC	Check <i>HHT1-HHF1</i> locus R	Desalt
oFMP698	caatccctgcTTCTTCAATTATTTTCAGATATTTTC	<i>ISW1</i> delSlide + NLS F	Desalt
oFMP699	gaatgaagaaGCAGGGATTGTATTGGATGAC	<i>ISW1</i> delSlide + NLS F	Desalt
oFMP712	CAAGGATATACCATTCTATCTAGAAAAATGTTATTGAAAGAAGAAGACTCGGATG	Clone <i>ISW1</i> lacking N-terminus incl. AcidicN F Alper P1-P14	HPLC
oFMP713	GGAGAAAAACCCCGGATTCTAGAAAAATGTTATTGAAAGAAGAAGACTCGGATG	Clone <i>ISW1</i> lacking N-terminus incl. AcidicN F Alper P15-P16	HPLC
oFMP925	GAACATACGACACGATATACCT	Check <i>RPB3</i> locus +300 F	Desalt
oFMP926	GTAGACGAACTAAGTCCAGGA	Check <i>RPB3</i> locus -300 F	Desalt
oFMP931	GGCGGCCACTTCTAAATAAGCGAATTTCTTATGATTTATGATTTGCAGATTGACTGAGAGTGCA	Replace His3 with Leu2 in <i>Isw2-TAP-His3</i> strain F	HPLC
oFMP932	TCGATGAATTCGAGCTCGTTAAACTGGATGGCGGCGT TAGTATC TCCTGATGCGGTATTTTCTC	Replace His3 with Leu2 in <i>Isw2-TAP-His3</i> strain R	HPLC
oFMP954	AGACAGCGAGTTCATAGATAGTTTGGTGGATGAAGAA GAAGAGGACGTTTCCGGTATGACCGTG	Delete <i>INO80</i> amino acids 1-300 F	HPLC
oFMP955	ATTAGCAAAGCAAGGCTTAAGACATATAGAAGAGCATT TATAGACTTCCGTGATGCGGTATTTTCTCC	Delete <i>INO80</i> amino acids 1-300 R	HPLC
oFMP958	CAATTGGTGAACCTCCTCTTC	Check <i>INO80</i> 1-300 deletion F	Desalt
oFMP959	GAGCGTATAGTGTACGTGTTC	Check <i>INO80</i> 1-300 deletion R	Desalt
oFMP965	GCCTATGAACGTGAGTATCTG	Check <i>INO80</i> 1-300 deletion R2	Desalt
oFMP967	CAAGCAGAAGACGGCATAACGA	NET-Seq oLSC006	Desalt
oFMP996	CAAGCAGAAGACGGCATAACGA	NET-Seq oNT1231	Desalt
oFMP1005	AATGATACGGCGACCACCGAGATCTACA CGATCGGAAGAGCACACGTCTGAACTCC AGTCACTGACCATCCGACGATCATTGAT GG	NET-Seq barcode 4	HPLC
oFMP1006	AATGATACGGCGACCACCGAGATCTACA CGATCGGAAGAGCACACGTCTGAACTCC AGTCAACACAGTGTCCGACGATCATTGAT GG	NET-Seq barcode 5	HPLC
oFMP1007	AATGATACGGCGACCACCGAGATCTACA CGATCGGAAGAGCACACGTCTGAACTCC AGTCAACGCAATTCCGACGATCATTGAT GG	NET-Seq barcode 6	HPLC
oFMP1008	AATGATACGGCGACCACCGAGATCTACA CGATCGGAAGAGCACACGTCTGAACTCC AGTCAACAGATCTCCGACGATCATTGAT GG	NET-Seq barcode 7	HPLC
oFMP1009	⁵ PHOS/ATCTCGTATGCCGTCTTCTGCTTG/ISP18/CACT CA/IS P18/TCCGACGATCATTGATGGTGCCTACAG 3	NET-Seq oLSC007	PAGE
oFMP1010	/5RAPP/(N1:25252525)(N1)(N1)(N1)(N1)(N1) CTGTAGGCCACCATCAAT/3DDC/	NET-Seq DNA linker with molecular barcode	PAGE
oFMP1018	GATACCTAGACCACCTGCTCTTG	<i>INO80</i> sequencing 1	Desalt
oFMP1019	CCTCGAGTAGCTCTTGAGTAATGG	<i>INO80</i> sequencing 2	Desalt
oFMP1020	AGACATCAATTTCAATCTTGTCG	<i>INO80</i> sequencing 3	Desalt
oFMP1021	TGGTTCTCGGCTAGATGAGC	<i>INO80</i> sequencing 4	Desalt
oFMP1022	GATCTCTTTCTTACGCTCATT	<i>INO80</i> sequencing 5	Desalt
oFMP1023	TGATCATGCTCATATCACGGTAC	<i>INO80</i> sequencing 7	Desalt
oFMP1036	ACTGCTCTTTGCATTTTCCAAGTTATTGCATTACAAGA ATATATGCGGATCCCCGGTTAATTAAG	Delete <i>SWR1</i> F	HPLC
oFMP1037	TTTGGACAACCTAAGGCAGCGGTGAAGAGTAGAACCTG GTCCTTCAGAAATTCGAGCTCGTTTAAACTGG	Delete <i>SWR1</i> R	HPLC
oFMP1038	GATGCAGTAGTGAACATATTGCTCG	Check <i>SWR1</i> locus F	Desalt
oFMP1039	CTTTGGAAAAACCAACCTTGATCG	Check <i>SWR1</i> locus R	Desalt
oFMP1092	TGGATGAGAAGCAGCCAGGATATAGGTAATAGTAACA CATAAGAAGATCCCCGGTTAATTAAGG	Delete <i>NHP10</i> F	HPLC

oFMP1093	TACGATATCTTCAAAGAAAATAGAAAAAATGGAATTT TTAATTTGAATTCGAGCTCGTTTAAACTGG	Delete <i>NHP10</i> R	HPLC
oFMP1096	TACTAGTCAATAGTACATAAATACAGGGATACAATCGC ACCTAACGATCCCCGGGTTAATTAAGG	Delete <i>ARP8</i> F	HPLC
oFMP1097	AGACCTTTCAGAAAAAAGATAACAAAAAATTCCATAT GCATATCGAATTCGAGCTCGTTTAAACTGG	Delete <i>ARP8</i> R	HPLC
oFMP1098	GCAGTTACGGTGATAGTCG	Check <i>NHP10</i> locus F	Desalt
oFMP1099	ACCTTGGGAATAGAAGAAAGGTC	Check <i>NHP10</i> locus R	Desalt
oFMP1102	CAGTGTGCTGTGAACAACCTC	Check <i>ARP8</i> locus F	Desalt
oFMP1103	GCACCTTTCGATAAACTTCCTG	Check <i>ARP8</i> locus R	Desalt
oFMP1106	CTTGTTGGTTTAAAGTCGTAACAAAAGAAAACCTTACAA TCAGATC GATCCCCGGGTTAATTAAGG	Delete <i>ISW2</i> F	HPLC
oFMP1107	AAATTATATCTCTCACGTCACCTTATTTAATGCACAATA CATGAT GAATTCGAGCTCGTTTAAACTGG	Delete <i>ISW2</i> R	HPLC
oFMP1110	GAAGGTTAAATTGTCATCATCATCAGCGTGAGAAAGT CGAAACA GATCCCCGGGTTAATTAAGG	Delete <i>IES6</i> F	HPLC
oFMP1111	GAAAGTTGTCTACAAGCTAAAATACATACATACATAT ACAATGC GAATTCGAGCTCGTTTAAACTGG	Delete <i>IES6</i> R	HPLC
oFMP1112	CGATGACGACGACTACCT	Check <i>IES6</i> locus F	Desalt
oFMP1113	CAAAGTGGAGACGATGCTG	Check <i>IES6</i> locus R	Desalt
oFMP1114	GATCACACGCCAATTTATTAAC	Check <i>ISW1</i> locus F2	Desalt
oFMP1115	CCAAGCTACAATTTCCAACG	Check <i>ISW2</i> locus F2	Desalt
oFMP1116	GGTAAGCTTCTATGTTGATCG	Check <i>CHD1</i> locus F2	Desalt
oFMP1117	CGCTTAGATGATGCCGTC	Check <i>INO80</i> locus F2	Desalt
oFMP1118	ACCCAATTCAAAGCAGAACCTTTTCTAATTTAATTCTCA CTTATA GATCCCCGGGTTAATTAAGG	Delete <i>CHD1</i> F	HPLC
oFMP1119	TATGGGGGGAAGGAACAATGGAAAATGTGGTGAAGAA AAATTGTT GAATTCGAGCTCGTTTAAACTGG	Delete <i>CHD1</i> R	HPLC
oFMP1122	CATGCGTATTCTGAGCCATC	Check <i>INO80</i> locus R	Desalt
oFMP1125	GCAGCAGGACCATGTAAACG	Check <i>rad5-535</i> F	Desalt
oFMP1126	AAACTCGTTACTCCACTGCG	Check <i>rad5-535</i> R	Desalt
oFMP1171	GATAAAACGCCTAACTAGCAAATAACTGGCGATTAGC AGACTACA GATCCCCGGGTTAATTAAGG	Delete <i>IES2</i> F	HPLC
oFMP1172	ATAAAACAAACGATATACATCAAATACTTAAATTGCGT CCTCTAC GAATTCGAGCTCGTTTAAACTGG	Delete <i>IES2</i> R	HPLC
oFMP1173	GAGAGAAGAAAAGGAGGAAAGTATAACG	Check <i>IES2</i> locus F	Desalt
oFMP1176	GTCTTACCACAGTTGATCTCTC	Check <i>tor1-1</i> F	Desalt
oFMP1177	GAGATCATGAGTAGCCAGAAGC	Check <i>tor1-1</i> R	Desalt
oFMP1178	CTTATGCCAGAACTATCGGTATC	Check <i>RPL13A</i> locus +300 F	Desalt
oFMP1179	CTATATATAATGCCAGTTGTGC	Check <i>RPL13A</i> locus -300 R	Desalt
oFMP1180	CAACGTCGCCTTCCTAC	Check <i>RPO21</i> locus +300 F	Desalt
oFMP1181	GTAAGCGGTAGTTCCACTC	Check <i>RPO21</i> locus -300 R	Desalt
oFMP1182	CCTGAATAACAAGGAAGCC	Check <i>FPR1</i> locus +300 F	Desalt
oFMP1183	GGTAATACTAGCAATGAAACCTC	Check <i>FPR1</i> locus -300 R	Desalt
oFMP1184	CAAGCCCTTGATGGCATT	Check <i>IES2</i> locus R	Desalt
oFMP1185	TATCGATAAGCTTGATATCGAATTTAATAGAGGCAAA CATAGAACG	Clone <i>HHT2-HHF2</i> Gal1-10 F	HPLC
oFMP1186	CGGCCGCTCTAGAAGTAGTGGATCCAATTCTCCTACT TAGCCAGTG	Clone <i>HHT2-HHF2</i> Gal1-10 R	HPLC
oFMP1191	TATCGATAAGCTTGATATCGAATTTAATAGAGGCAAA CAGTTG	Clone <i>ARP8</i> in pRS416 F	Desalt
oFMP1192	CGGCCGCTCTAGAAGTAGTGGATCCCATGGACAATCT TCCTGC	Clone <i>ARP8</i> in pRS416 R	Desalt
oFMP1193	ACCTAACATG ATCAACCAAAAAAATACTACTCATCAG	Delete amino acids 2-197 from <i>ARP8</i> F	Desalt
oFMP1194	TTTGGTTGAT CATGTTAGGTGCGATTGTATCC	Delete amino acids 2-197 from <i>ARP8</i> R	Desalt
oFMP1197	TGAAAAAGGTATTCATATTGTGTTATTTAC	<i>INO80</i> C-terminus FLAG tag F	Desalt
oFMP1198	TGCCAATGCACTTGCC	<i>INO80</i> C-terminus FLAG tag R	Desalt
oFMP1221	AATTCAATTTTCGCACTATAGCCGCACGTAAAAATAACT TAACATATGGCTTAACTATGCGGCAT	Delete <i>Htz1</i> F	HPLC
oFMP1221	AATTCAATTTTCGCACTATAGCCGCACGTAAAAATAACT TAACATA TGGCTTAACTATGCGGCAT	Delete <i>HTZ1</i> F	HPLC
oFMP1222	GGAGCAGGGAGAATTACGGGAAATGGGAAAGAAAAA CTATTCTTCCTTACGCATCTGTGC	Delete <i>Htz1</i> R	HPLC
oFMP1222	GGAGCAGGGAGAATTACGGGAAATGGGAAAGAAAAA CTATTCTTC CTCCTTACGCATCTGTGC	Delete <i>HTZ1</i> R	HPLC
oFMP1223	CGTAACTTACTACTCGTAGAACTGG	Check <i>HTZ1</i> locus F	Desalt
oFMP1223	CGTAACTTACTACTCGTAGAACTGG	Check <i>HTZ1</i> locus F	Desalt
oFMP1224	TGCGTACATAACGGCTACTG	Check <i>HTZ1</i> locus R	Desalt
oFMP1224	TGCGTACATAACGGCTACTG	Check <i>HTZ1</i> locus R	Desalt
oFMP1229	CACAAGCGGTAGTAAGCAC	Check <i>HTZ1</i> locus F2	Desalt

oFMP1229	CACAAGCGGTAGTAAGCAC	Check <i>HTZ1</i> locus F2	Desalt
----------	---------------------	----------------------------	--------

4.1.3 Plasmids

List of plasmids used or generated in this thesis.

Name	Original Name	Reference	Source
pFMP281	pRS315	(Sikorski and Hieter, 1989)	PD Dr. Philipp Korber
pFMP282	pRS415	(Sikorski and Hieter, 1989)	PD Dr. Philipp Korber
pFMP283	pRS425	(Sikorski and Hieter, 1989)	PD Dr. Philipp Korber
pFMP284	Gal4pBS2 - Pleum	(Blazeck et al., 2012)	Prof. Dr. Hal Alper
pFMP285	Gal4pBS1 - Pleum	(Blazeck et al., 2012)	Prof. Dr. Hal Alper
pFMP286	Gal4pBS12 - Pleum	(Blazeck et al., 2012)	Prof. Dr. Hal Alper
pFMP287	Gal4pBS24 - Pleum	(Blazeck et al., 2012)	Prof. Dr. Hal Alper
pFMP288	UASgal - CU2 - Pcyc	(Blazeck et al., 2012)	Prof. Dr. Hal Alper
pFMP289	Gal4pBS4 - Pleum	(Blazeck et al., 2012)	Prof. Dr. Hal Alper
pFMP290	Gal4pBS3 - Pleum	(Blazeck et al., 2012)	Prof. Dr. Hal Alper
pFMP291	UASgal - CU1 - Pcyc	(Blazeck et al., 2012)	Prof. Dr. Hal Alper
pFMP292	Gal4pBS13 - Pleum	(Blazeck et al., 2012)	Prof. Dr. Hal Alper
pFMP293	UASgal - Pcyc	(Blazeck et al., 2012)	Prof. Dr. Hal Alper
pFMP294	UASgal - A9 - Pcyc	(Blazeck et al., 2012)	Prof. Dr. Hal Alper
pFMP295	Gal4pBS34 - Pleum	(Blazeck et al., 2012)	Prof. Dr. Hal Alper
pFMP296	Gal4pBS134 - Pleum	(Blazeck et al., 2012)	Prof. Dr. Hal Alper
pFMP297	UASgal - Pleum	(Blazeck et al., 2012)	Prof. Dr. Hal Alper
pFMP298	Pgal	(Blazeck et al., 2012)	Prof. Dr. Hal Alper
pFMP299	UASgal - Pgal	(Blazeck et al., 2012)	Prof. Dr. Hal Alper
pFMP509	YCP50 H3-H4	(Wittschieben et al., 2000)	Prof. Dr. Alain Verreault
pFMP510 / 567	BP83	-	Dr. Boris Pfander / Dr. Christoph Kurat
pFMP511	pRM102	(Mann and Grunstein, 1992)	PD Dr. Philipp Korber
pFMP519	pRS413 <i>HHT2-HHF2</i> Gal1-10	This study	-
pFMP525	pFA6a-KanMX6	Euroscarf	Dr. Sigurd Braun
pFMP549	pRS416-Arp8	This study	-
pFMP550	pRS416 delN Arp8	This study	-
pFMP551	pRS403	(Sikorski and Hieter, 1989)	PD Dr. Philipp Korber
pFMP552	pRS404	(Sikorski and Hieter, 1989)	PD Dr. Philipp Korber
pFMP553	pRS405	(Sikorski and Hieter, 1989)	PD Dr. Philipp Korber
pFMP554	pRS426	(Sikorski and Hieter, 1989)	PD Dr. Philipp Korber
pFMP555	BYP7569 pMK200	(Kubota et al., 2013)	NRBP Japan
pFMP556	BYP7434 pMK198	(Kubota et al., 2013)	NRBP Japan
pFMP557	BYP7433 pMK154	(Kubota et al., 2013)	NRBP Japan
pFMP558	BYP7430 pMK151	(Kubota et al., 2013)	NRBP Japan
pFMP559	pUG27	(Gueldener et al., 2002)	NRBP Japan
pFMP560	pUG72	(Gueldener et al., 2002)	NRBP Japan
pFMP561	pSH47	(Gueldener et al., 2002)	NRBP Japan
pFMP562	pSH62	(Gueldener et al., 2002)	NRBP Japan
pFMP563	pUG73	(Gueldener et al., 2002)	NRBP Japan
pFMP572	ISW1 - P1	This study	-
pFMP573	ISW1 - P2	This study	-
pFMP574	ISW1 - P3	This study	-
pFMP575	ISW1 - P4	This study	-
pFMP576	ISW1 - P5	This study	-
pFMP577	ISW1 - P6	This study	-
pFMP578	ISW1 - P7	This study	-
pFMP579	ISW1 - P8	This study	-
pFMP580	ISW1 - P9	This study	-
pFMP581	ISW1 - P10	This study	-
pFMP582	ISW1 - P11	This study	-

pFMP583	ISW1 - P12	This study	-
pFMP584	ISW1 - P13	This study	-
pFMP585	ISW1 - P14	This study	-
pFMP586	ISW1 - P15	This study	-
pFMP587	ISW1 - P16	This study	-
pFMP588	ISW1-TAP - P1	This study	-
pFMP589	ISW1-TAP - P6	This study	-
pFMP590	ISW1-TAP - P11	This study	-
pFMP591	ISW1-TAP - P16	This study	-
pFMP592	ISW1-delNTR - P1	This study	-
pFMP593	ISW1-delNTR - P6	This study	-
pFMP594	ISW1-delNTR - P11	This study	-
pFMP595	ISW1-delNTR - P16	This study	-
pFMP596	ISW1-delNTR-TAP - P1	This study	-
pFMP597	ISW1-delNTR-TAP - P6	This study	-
pFMP598	ISW1-delNTR-TAP - P11	This study	-
pFMP599	ISW1-delNTR-TAP - P16	This study	-
pFMP600	ISW1-delppHSA - P1	This study	-
pFMP601	ISW1-delppHSA - P6	This study	-
pFMP602	ISW1-delppHSA - P11	This study	-
pFMP603	ISW1-delppHSA - P16	This study	-
pFMP604	ISW1-delppHSA-TAP - P1	This study	-
pFMP605	ISW1-delppHSA-TAP - P6	This study	-
pFMP606	ISW1-delppHSA-TAP - P11	This study	-
pFMP607	ISW1-delppHSA-TAP - P16	This study	-
pFMP608	ISW1-delppHSA,delAutoN - P1	This study	-
pFMP609	ISW1-delppHSA,delAutoN - P6	This study	-
pFMP610	ISW1-delppHSA,delAutoN - P11	This study	-
pFMP611	ISW1-delppHSA,delAutoN - P16	This study	-
pFMP612	ISW1-delppHSA,delAutoN-TAP - P1	This study	-
pFMP613	ISW1-delppHSA,delAutoN-TAP - P6	This study	-
pFMP614	ISW1-delppHSA,delAutoN-TAP - P11	This study	-
pFMP615	ISW1-delppHSA,delAutoN-TAP - P16	This study	-
pFMP616	ISW1-delSlide - P1	This study	-
pFMP618	ISW1-delSlide - P6	This study	-
pFMP619	ISW1-delSlide - P11	This study	-
pFMP621	ISW1-delSlide - P16	This study	-
pFMP626	ISW1-K227R-delSlide - P1	This study	-
pFMP627	ISW1-K227R-delSlide - P6	This study	-
pFMP628	ISW1-K227R-delSlide - P11	This study	-
pFMP629	ISW1-K227R-delSlide - P16	This study	-
pFMP638	ISW1-delHSS - P1	This study	-
pFMP639	ISW1-delHSS - P6	This study	-
pFMP640	ISW1-delHSS - P11	This study	-
pFMP641	ISW1-delHSS - P16	This study	-
pFMP642	ISW1-2RA P1	This study	-
pFMP643	ISW1-2RA P6	This study	-
pFMP644	ISW1-2RA P11	This study	-
pFMP645	ISW1-2RA P16	This study	-
pFMP646	ISW1-K227R P1	This study	-
pFMP647	ISW1-K227R P6	This study	-
pFMP648	ISW1-K227R P11	This study	-
pFMP649	ISW1-K227R P16	This study	-
pFMP678	ISW1-K227R-delHSS P11	This study	-
pFMP679	ISW1-K227R-delHSS P16	This study	-

pFMP692	ISW1 delNegC::GGs linker P11	This study	-
pFMP696	ISW1 NegC+GGs linker P11	This study	-
pFMP701	GGs linker plasmid	This study	-
pFMP742	Alper empty plasmid	This study	-

4.1.4 Enzymes and kits

Description	Manufacturer (Catalog number)
Agilent DNA 1000 Kit	Agilent Technologies (5067-1504)
Agilent DNA High Sensitivity Kit	Agilent Technologies (5067-4626)
BamHI	NEB (R0136L)
Benzonase	Millipore (1016540001)
Calmodulin Sepharose 4B	Sigma (17-0529-01)
Circligase ssDNA Ligase	Illumina (CL4111K)
DpnI	R0176S
EcoRI	NEB (R0101L)
Fast SYBR Green Master Mix	Life technologies (4385612)
IgG Sepharose 6 Fast Flow	Sigma (17-0969-01)
Illumina Tagment DNA Enzyme and Buffer Small Kit	Illumina (20034197)
Klenow Fragment (3'→5' exo-)	NEB (M0212L)
Micrococcal Nuclease (MNase)	Sigma (N5386-500UN)
MinElute PCR Purification Kit	Qiagen (28004)
miRNeasy Mini Kit	Qiagen (217004)
NEBNext High-Fidelity 2X PCR Master Mix	NEB (M0541S)
NEBNext Ultra II DNA Library Prep Kit for Illumina	NEB (E7645L)
NucleoBond Xtra Midi	Macherey-Nagel (740410.50)
NucleoSpin Gel and PCR Cleanup	Macherey-Nagel (740609.250)
NucleoSpin Plasmid EasyPure	Macherey-Nagel (740727.250)
One Taq DNA Polymerase	NEB (M0482S)
Phusion High-Fidelity DNA Polymerase	NEB (M0530S)
Proteinase K	Bioline (BIO-37039)
Qubit Assay Tubes	Thermo Fisher Scientific (Q32856)
Qubit dsDNA HS Assay Kit	Thermo Fisher Scientific (Q32854)
RNase A	Sigma (R4875)
RQ1 RNase-Free DNase	Promega (M6101)
SmaI	NEB (R0141S)
SUPERase In RNase Inhibitor	Life technologies (AM2694)
T4 DNA Ligase	NEB (M0202L)
T4 DNA Polymerase	NEB (M0203L)
T4 Polynucleotide Kinase	NEB (M0201L)
T4 RNA ligase 2 (truncated, K227Q)	NEB (M0351S)
T5 exonuclease	NEB (M0363S)
Taq DNA Polymerase	NEB (M0273S)
Taq Ligase	NEB (M0208S)
XbaI	NEB (R0145S)
XmaI	NEB (R0180S)
Zymolyase-100T	Gerbu Biotechnik (07665)

4.1.5 Antibodies

Description	Dilution used	Type	Manufacturer (Catalog number)
α FLAG (mouse IgG M2)	1:15000	monoclonal	Sigma (F3165)
α H3 (Rabbit IgG)	1:20000	polyclonal	Abcam (ab1791)
α H4 (Rabbit IgG)	1:5000	polyclonal	Abcam (ab10158)

α Mouse (Goat IgG)	1:20000	IRDye 680	Li-Cor (926-68070)
α Mouse (Goat IgG)	1:20000	IRDye 800	Li-Cor (926-32210)
α Rabbit (Goat IgG)	1:20000	IRDye 800	Li-Cor (926-32211)
Anti-TAP (Rabbit IgG)	1:10000	polyclonal	Thermo-Fischer Scientific (CAB1001)
Anti-mini-AID-tag mAb (Mouse IgG2a)	1:5000	Monoclonal	MBL Biozol (M214-3)

4.1.6 Sources of chemicals and consumables

Description	Manufacturer (Catalog number)
1 kb DNA Ladder	NEB (N3232S)
1-Naphthaleneacetic acid	Sigma (35745)
10 bp DNA Ladder	Life technologies (10821015)
100 bp DNA Ladder	NEB (N3231S)
3-Indoleacetic acid	Sigma (45533)
3XFLAG peptide	Sigma (F4799)
5-Fluoroorotic Acid Monohydrate (5-FOA)	Biozol (F59500)
50 bp DNA Ladder	NEB (N3236S)
Agarose Universal	Bio&SELL (BS20.46.500)
Agencourt AMPure XP beads	Beckmann Coulter (A63882)
Alpha factor	Hölzel Diagnostika (RP01002)
Ampicillin	Roth (K029.2)
Anti-Flag M2 Affinity Gel	Sigma (A2220)
Aprotinin	Genaxxon (M6361.0100)
Arginine	BD Biosciences, 214010
Bacto Agar	BD Biosciences (211820)
Bacto Peptone	Life technologies (211820)
Bromophenol Blue	Sigma (B0126-25G)
BSA	Sigma (A9418)
Calcium Chloride	Sigma (C3306)
Calmodulin-Sepharose 4B	Sigma (GE17-0529-01)
Chloroform	VWR Chemicals (22711.324)
ClonNAT (Nourseothricin)	Werner BioAgents GmbH (5.000.200)
Complete Protease Inhibitor Cocktail tablet	Sigma (11836145001)
Costar Spin-X centrifuge tube filters	Sigma (CLS8162-96EA)
Coverslips	Roth (0657.2)
Cryobox	Kisker Biotech (R034-7)
DAPI	Sigma (DUO82040)
DEPC-Treated Water	Thermo Fisher (AM9906)
Dewar	Roth (0442.1)
Diethyl pyrocarbonate	Sigma (D5758)
Difco Yeast Nitrogen Base	BD Biosciences (291920)
DMSO	Sigma (D2438)
dNTPs	NEB (N0447S)
Drop out powder components (Ade, Ala, Asn, Asp, PABA, Cys, Glu, Gln, Gly, Ile, Myo-Inositol, Leu, Lys, Met, Phe, Pro, Ser, Thr, Trp, Tyr, Ura, Val)	Sigma (A8626, A7627, A9256, A5040, C1276, G1251, G3126, G8790, I2752, I5125, L8000, L5626, M9625, P2126, P0380, S4500, T8625, T0254, T3754, U0750, V0500)
DTT (Dithiothreitol)	Life technologies (R0861)
ECL Western Blotting detection reagents	Sigma (GERPN2235)
EDTA	Pan Reac Appli Chem (131669.1210)
EGTA	Roth (3054.3)
EtOH 100% - high quality	Sigma (32205-2.5L-M)
EtOH 96% - low quality	CLN GmbH (N-1196.9025)
Ficoll PM400	Sigma (F4375)
Filterin Flask, Ultra-Ware	Fisher Scientific (11619758)
Formaldehyde	Sigma (47608)
Freeze 'N-Squeeze DNA Gel Extraction	Biorad (7326166)

Funnel/Support Assy 90 mm	Fisher Scientific (13451979)
G418	Sigma (G8168)
Galactose	Sigma (G0625)
Glass beads	Roth (N030.1)
Glass slides	Roth (H879.1)
Glucose	VWR (1.08342.1000)
Glycerol	VWR (1.04092.2500)
Glycoblue	Thermo Fisher Scientific (AM9515)
Glycogen	Sigma (10901393001)
Haemocytometer	Fischer Scientific (11314052)
HEPES	VWR Chemicals (1.10110.1000)
Histidine	VWR (1.04351.0100)
Hydroxyurea	Sigma (H8627)
Hygromycin B	Thermo Fisher Scientific (10687010)
IGEPAL	Sigma (I8896)
Isoamyl alcohol	Roth (T870.1)
Isopropanol (2-Propanol)	Sigma (34863-2.5L-M)
K ₂ HPO ₄ *3H ₂ O	VWR (1.05099.1000)
KCl	Sigma (P9541)
KH ₂ PO ₄	VWR (1.04873.1000)
Leupeptin	Genaxxon (M6100.0100)
LiCl	VWR (25009.236)
Low-melt agarose	Biozym (850070)
Magnesium Chloride	VWR (25108.295)
Magnetic Rack	GE Healthcare (28948964)
Mahlbecher für MM 400, 50 ml	Retsch GmbH (01.462.0216)
Mahlkugel 25 mm	Retsch GmbH (05.368.0105)
MaXtract High Density	Qiagen (129073)
Methyl methanesulfonate	Sigma (129925)
Methylenblau	Roth (A514.1)
Milk Powder (Bio Magermilchpulver)	ReformKontor (3030)
NAD	NEB (B9007S)
Nitrocellulose membrane	Kisker (D10600018)
Nonstick RNase-free Microfuge Tubes 0,5ml	Life technologies (AM12350)
Nonstick RNase-free Microfuge Tubes, 1,5ml	Life technologies (AM12450)
Nuclease free water (DEPC treated)	Life technologies (AM9906)
Orange G	Sigma (O-1625)
PEG (Polyethylene glycol) 3350	Sigma (P-3640)
PEG 8000	Promega (V3011)
Pepstatin	Genaxxon (M6359.0100)
Phenol:Chloroform:Isoamyl alcohol (25:24:1)	Roth (A156.1)
PMSF (Phenylmethanesulfonylfluoride)	Sigma (P7626)
Poly-L-lysine	Sigma (P8920)
Potassium acetate	VWR (1.04820.1000)
Protease Inhibitor Cocktail	Sigma (P8215)
qPCR foil	Sarstedt (95.1994)
Rapamycin	Hölzel Diagnostika (R-5000)
RNase away	ThermoFisher Scientific (10328011)
Röhre 13ml, 95x16,8mm, PP	Sarstedt (55.518)
Schraubhilfe für Mahlbecher MM400	Retsch GmbH (22.486.0005)
SDS-PAGE gel, NuPAGE Bis-Tris Protein Gel, 10%, 12%, and 8-16%	Serva (0043266.01, 0043280.01, 0043263.01)
Sodium chloride	Serva (30183.01)
Sodium deoxycholate	Sigma (D6750)
Sodium dodecyl sulfate (SDS)	Serva Electrophoresis (20765.03)
Sodium hydroxide	Neolab (LC-4994.2)
Sodium perchlorate	Sigma (381225)
Sorbitol	Serva Electrophoresis (35230.02)
Sybr Gold	Life technologies (S11494)

TCA (Trichloroacetic acid)	Sigma (T0699)
Triple Color Protein Standard II	Serva (39257.01)
Triple Color Protein Standard III	Serva (39258.01)
Tris ultrapure	Diagonal (A1086.1000)
Triton X-100	Sigma (T8787)
Tween-20	Sigma (P9416)
Ultra Pure Salmon Sperm DNA Solution	Life technologies (15632011)
Urea	Life technologies (15505027)
Whatman blotting paper	VWR (588-3148)
Yeast Extract	BD Biosciences (212750)
Zirconia/Silica Beads 0.5mm diameter	Biospec (11079105z)
β -Mercaptoethanol	Sigma (M6250)
Nitrocellulose filter	Roth (A014.1)

4.1.7 Buffers and solutions

Description	Components
5X Gibson assembly buffer	450 mM Tris-HCl pH7.5, 25% PEG 8000, 50 mM MgCl ₂ , 50 mM DTT, 1 mM dNTPs, 5 mM NAD
1X TE buffer	10 mM Tris-HCl, 1 mM EDTA, pH 7.5 or 8.0
5X TBE buffer	VWR (J885-4L)
10X MNase digestion buffer	150 mM Tris-HCl pH 7.5, 500 mM NaCl, 14 mM CaCl ₂ , 2 mM EGTA, 2 mM EDTA, 50 mM β -mercaptoethanol
1X MNase dilution buffer	10 mM Tris-HCl pH 7.4, 0.1 mg/ml BSA
EX 50 buffer	10 mM HEPES pH 7.6, 50 mM NaCl, 1.5 mM MgCl ₂ , 0.5 mM EDTA, 10% (v/v) glycerol, 1 mM DTT, 0.2 mM PMSF
Preincubation solution	0.7 M β -mercaptoethanol, 28 mM EDTA pH 8.0
Ficoll buffer	18% Ficoll, 20 mM KH ₂ PO ₄ pH 6.8, 1 mM MgCl ₂ , 0.25 mM EGTA, 0.25 mM EDTA
Proteinase K buffer	50% glycerol, 50 mM Tris-HCl pH 8.0, 50 mM CaCl ₂
Genomic DNA resuspension buffer	0.9 M sorbitol, 50 mM Na-Pi pH 7.5, 140 mM β -mercaptoethanol
Zymolyase solution (for tetrad dissection)	0.1 M KPO ₄ /1.2 M sorbitol, 0.5 μ g/ μ l zymolyase 100T
PEG solution	149 mM PEG 3350, 0.1 M LiOAc, 10 mM Tris-HCl, 1 mM EDTA
Single-stranded carrier DNA	10 mg/ml salmon sperm DNA, 10 mM Tris-HCl pH 8.0, 1 mM EDTA
1X LiOAc buffer	0.1 M LiOAc, 10 mM Tris-HCl pH 8.0, 1 mM EDTA
Protein lysis buffer	1.86 M NaOH, 7.5% (v/v) β -mercaptoethanol
HU buffer	8 M urea, 5% (w/v) SDS, 200 mM Tris pH 6.8, 1 mM EDTA, Bromophenol blue, 1.5% (v/v) DTT added freshly
1X SDS running buffer	2.5 mM Tris, 19.2 mM glycine, 0.01% SDS, pH 8.3
Staining solution	7.5% (v/v) acetic acid, 5% (v/v) EtOH
Coomassie Brilliant Blue	0.25% (w/v) Coomassie Brilliant Blue G-250, 100% EtOH
Western Blot Transfer buffer	48 mM Tris-HCl, 39 mM glycine, 10% SDS, 20% MeOH
1X PBS	137 mM NaCl, 2.7 mM KCl, 10 mM Na ₂ HPO ₄ , 1.8 mM KH ₂ PO ₄ , in dH ₂ O, pH 7.4
1X PBST	1X PBS, 0.1% Tween20
1.33X Gibson Reagent Mix	1.33X 5X Gibson Assembly Buffer, 0.005 U/ μ l TS exonuclease, 0.033 U/ μ l Phusion polymerase, 5.33 U/ μ l Taq Ligase
ATAC buffer	1.4 M sorbitol, 40 mM HEPES-KOH pH 7.5, 0.5 mM MgCl ₂
10X NET-Seq lysis buffer	200 mM HEPES pH 7.4, 1100 mM KOAc, 5% TritonX-100, 1% Tween-20
TAP extraction buffer	40 mM Hepes-KOH pH 7.5, 10 % Glycerol, 150 mM or 350 mM NaCl, 0.1% Tween-20
TEV cleavage buffer	10 mM Tris pH 8.0, 150 mM NaCl, 0.1% NP-40, 0.5 mM EDTA, 10% Glycerol

4.1.8 Yeast media

Description	Components
-------------	------------

YPAD (full media)	1 g/l KH ₂ PO ₄ , 10 g/l Yeast Extract, 20 g/l peptone, 20 g/l glucose or galactose, 100 mg/l adenine
YNB (synthetic media)	6.7 g/l Yeast Nitrogen Base, 1.6 g/l amino acid dropout-mix (-His, -Leu, -Ura, -Trp), 20 g/l glucose or galactose, pH 5.4. Optional supplement with 84 mg/l His / Trp / Ura, 168 mg/l Leu
Pre-SPO media	YPAD except 4% glucose (instead of 2% glucose)
Minimal SPO media	1% Potassium acetate in dH ₂ O, strain specific supplement with essential amino acids according to genotype (25% of Cold Spring Harbor recommendation for synthetic complete media)

4.2 METHODS

4.2.1 Yeast strain generation

4.2.1.1 Gene deletion or tagging via direct transformation

Yeast strains generated in this thesis are derived from the W303 or S288c background. The appropriate background for each strain is mentioned next to the strain. To delete a gene by replacing with a selection marker, HPLC-purified oligonucleotides with 45 bp homology before the start codon and after the stop codon of the gene were designed. Selection marker was PCR amplified using the pRS- or pFA6a- based plasmids using the OneTaq DNA Polymerase from NEB. T_m for each oligonucleotide was determined using the online tool T_m Calculator (<https://tmcaculator.neb.com>). PCR amplified DNA was purified from agarose gels using the Macherey-Nagel NucleoSpin Gel and PCR Clean-up kit (Cat# 740609.250) and following the protocol and recommendations as stated in the kit. For gene tagging, desalted oligonucleotides were used. Constructs containing the tag and selection marker were amplified from the C-terminus of the gene and gel purified as above. All oligonucleotides used in this thesis were ordered from Sigma and purification was decided based on the length of the primers. Mostly, oligonucleotides shorter than 30 bases were salt purified and longer than 40 bp were HPLC purified.

All constructs were transformed according to the transformation protocol in (Dunham et al., 2015). To validate deletions and mutations in genes, the modified loci were confirmed by PCR either using genomic DNA or by colony PCR. Primers were designed to bind approximately 300 bp flanking the loci tested. When required, primers binding the internal region of the loci and selection marker were used.

When mentioned, the status of the *RAD5* gene was confirmed using oligonucleotides oFMP1125 and oFMP1126 to amplify the *RAD5* locus and sequencing the PCR amplified fragment (Elserafy and El-Khamisy, 2018).

4.2.1.2 Yeast tetrad dissection and synthetic lethality test

Specific strains were generated via mating, sporulation and tetrad dissection methodology. First, haploid strains of a and α background containing desired mutations or deletions were mated on a non-selective YPAD plate for 4 hours or overnight. Cells were plated again on a non-selective YPAD plate such that single colonies appear. After 24-30 hours, bigger colonies

were picked and checked under microscope for bigger and elongated shape. As a negative control, individual haploid strains were checked in parallel for smaller, roundish shape. Multiple diploids were picked and grown in a non-selective YPAD media with 4% glucose until saturation at 23 °C. Cells were washed with sterile water for 3 times and dissolved to OD 0.2-0.3 in minimal sporulation media. Diploids were allowed to sporulate for 4-5 days at 23 °C followed by 1-2 days at 30 °C. Spores were dissected on a Singer MSM 400 dissection microscope on YPAD plates. Tetrads were grown at 30 °C for 2-3 days. Tetrads were replica-plated on plates containing appropriate selection markers. For markers which are redundant in strains mated, non-parental ditype cells were selected initially and further confirmed by PCR of desired loci. When testing for synthetic lethality, tetrads were incubated for 5-7 days at 30 °C and scored based on growth on YPAD and appropriate selection plates.

4.2.2 Cloning via Gibson assembly

To clone a desired gene in a yeast vector, DNA was amplified using Phusion DNA Polymerase (New England Biolabs, Cat# M0530S) from WT yeast genomic DNA. Yeast plasmids were linearized using restriction enzyme digestion. All DNA fragments were purified from agarose gel using Macherey-Nagel NucleoSpin Gel and PCR Clean-up kit. Gibson assembly was performed using a master mix prepared in-house (section 4.1.7) and transformation into NEB 5-alpha competent *Escherichia coli* (Cat# C2987). Correct clones were validated by restriction digestion and sanger sequencing using M13 universal primers as well as using primers binding within the gene when required. To generate point mutants or delete a defined region in a gene, inverse PCR was performed on a plasmid containing the WT gene. DNA fragments were circularized using Gibson assembly master mix (Gibson, 2011).

4.2.3 MNase-Seq

4.2.3.1 Yeast nuclei preparation

“Yeast nuclei were prepared largely as described in (Almer and Horz, 1986).” (Singh et al., unpublished). Cells were generally grown overnight to OD 600 0.8-1.0 (Thermo Scientific GENESYS 20 spectrophotometer) in 500 ml to 1L YPAD complete media. Yeast cells were collected by centrifugation in the Heraeus Cryofuge 6000i at 3000 x g for 8 min at 4 °C. The pellet was washed once with cold water, weighed (wet weight) and resuspended in 2 times of preincubation solution (0.7 M β-mercaptoethanol, 28 mM EDTA pH 8.0). Cells were shaken for 25-30 min at 30 °C, then washed with 40 ml cold 1 M sorbitol and finally resuspended in buffer containing 5 volumes of 1 M sorbitol, 5 mM β-mercaptoethanol. To digest the cell wall (spheroplasting), freshly dissolved Zymolyase (Gerbu Biotechnik, Cat# 07665-Zymolyase®-100T) in water was added to the cell pellet. 1 mg Zymolyase was added per g of cell weight and incubated at 30 °C for 20-30 min. Cell wall was digested until the absorbance at 600 nm was decreased to 80-90% of the starting OD when the digestion was considered to be complete. OD was measured after 1:100 dilution in water. Digestion of the cell wall was also checked under the light microscope for presence of 80-90% ghosts. Spheroplasts were harvested (4 °C, 2500 x g, 5 min TX-1000 rotor ThermoFisher Scientific), washed with 40 ml

cold 1 M sorbitol and resuspended with inoculation loops or glass pipettes in a Ficoll buffer (18% Ficoll, 20 mM KH_2PO_4 pH 6.8, 1 mM MgCl_2 , 0.25 mM EGTA, 0.25 mM EDTA). 7 ml of the Ficoll buffer was added per g weight of cells. “Lastly, nuclei were aliquoted to desired wet weight (mostly 1 g) and centrifuged at 12000 x g (Beckman Coulter JA 20.1 rotor) for 30 min at 4 °C. Nuclei was stored at -80 °C until next step (see below).” (Singh et al., unpublished).

4.2.3.2 MNase digestion

For Micrococcal Nuclease digestion of the nuclei derived from the step above, nuclei obtained from 1 g wet weight cells were kept on ice for 10 min. Nuclei was washed with “8 ml MNase digestion buffer (15 mM Tris-Cl pH 7.5, 50 mM NaCl, 1.4 mM CaCl_2 , 0.2 mM EGTA pH 8.0, 0.2 mM EDTA pH 8.0, 5 mM β -mercaptoethanol)” (Singh et al., unpublished). Pellet was dissolved in 1 ml of the MNase digestion buffer using a 1000 μl Micropipette and divided equally into 5 equal aliquots. MNase (Sigma Cat# N5386) dissolved in MNase buffer “(10 mM HEPES-KOH pH 7.6, 50 mM NaCl, 1.5 mM MgCl_2 , 0.5 mM EDTA, 10% Glycerol, 1 mM DTT, 0.2 mM PMSF)” (Singh et al., unpublished) was added in increasing amounts (between 4-256 U / ml), mixed by quick vortexing twice. Nuclei was incubated for 20 min, 37 °C, 400 rpm. To stop MNase digestion, “35 μl quenching solution (10 mM EDTA, 1% SDS, 50 mM Tris-Cl pH 8.5)” (Singh et al., unpublished) was added. Proteinase K (50 μl of 10 mg/ml) was added and incubated at 37 °C, 30 min, 600 rpm. Then, 5 M NaClO_4 (70 μl) was added and nucleic acids were extracted with Phenol: Chloroform: Isoamyl alcohol mix (25:24:1), and with Chloroform: Isoamyl alcohol mix (24:1). Nucleic acids were precipitated using 1 ml of 100% ethanol. “DNA pellet was washed with 70% ice-cold ethanol and dissolved in 250 μl TE buffer. RNA was digested away by incubating with 10 μg RNase A at 37 °C for 60 min. DNA was precipitated with 0.2 M NaCl and 0.7 volumes of 2-propanol. Pellets were washed with 70% ethanol and dissolved in 50 μl TE buffer. To test the MNase digestion degree, 25 μl of DNA was mixed with 3 μl of a loading dye (0.5% Orange G, 50% glycerol). DNA was separated on a 15 cm long low-melt agarose gel (1.7%; Biozym LE GeneticPure agarose, Cat# 850070)” (Singh et al., unpublished). DNA was resolved for 4 h at 2 V/cm. For high-throughput sequencing, samples showing 70% mono-, 20% di-, 10% tri-nucleosome bands were selected out of the 5 MNase digestions of each sample.

4.2.3.3 DNA isolation and MNase-Seq library preparation

Sequencing libraries were prepared directly from “Whole lane” samples, and not from mononucleosome sized fragments, unless otherwise stated. AMPure size selection was employed to remove DNA fragments longer than 500 bp. Briefly, 300 ng DNA from the step above (quantified using Qubit) was diluted in 50 μl 0.1X TE buffer. 32 μl of AMPure XP beads (Beckman Coulter, Cat# A63882) were added, mixed and incubated for 5 min at room temperature. The supernatant was transferred to a new 1.5 ml eppendorf tube containing 104 μl of AMPure XP beads. The beads from the 32 μl step were discarded and not used further. The new solution (with 104 μl AMPure XP beads) was mixed and incubated for 5 min at room temperature. These beads (104 μl AMPure XP beads) were separated by incubating the eppendorf tube on a magnetic stand. After 5 min, “beads were washed twice with 500 μl of

80% ethanol (freshly prepared). DNA was eluted in 30 μ l 0.1X TE buffer. Eluted DNA was quantified using the Qubit dsDNA High Sensitivity kit (Thermo Fisher Cat# Q32854) (Singh et al., unpublished). High-throughput sequencing libraries were prepared using NEBNext Ultra II DNA Library Prep kit for Illumina (Cat# E7645L), according to the manufacturer's protocol with 50 ng input DNA. Only 3 or 4 cycles were performed during the PCR amplification step to avoid any potential bias which may arise from the PCR amplification of different fragment sizes in the input sample of the library preparation. Final libraries were visualized using the Bioanalyzer DNA 1000 kit (Cat# 5067-1504) showing usually fragment distribution between 270 and 280 base pairs. The libraries were sequenced at the "Laboratory for Functional Genome Analysis (LAFUGA), Gene Center, LMU on Illumina HiSeq for 50 cycles in the paired-end mode" (Singh et al., unpublished). Usually, 10 million reads per library were obtained.

4.2.4 ATAC-Seq

A detailed ATAC-Seq protocol (Schep et al., 2015) was graciously provided by Dr. William J. Greenleaf, Stanford University and used further with minor changes. Cells were grown overnight in YPAD media. "Next day, cells were reinoculated to OD 0.05 and grown till OD 0.2-0.4." (Singh et al., unpublished). Cell number was determined using a hemocytometer. 2.5 million cells were harvested (20 $^{\circ}$ C, 1 min, 3000 x g, FA-45-18-11 Eppendorf rotor). Pellets were washed with "sorbitol buffer (1.4 M sorbitol, 40 mM HEPES-KOH pH 7.5, 0.5 mM MgCl₂, 10 mM DTT)" (Singh et al., unpublished) and resuspended in 200 μ l of sorbitol buffer. Cell wall was digested using 200 μ g Zymolyase and incubating for 5 min, 30 $^{\circ}$ C, 400 rpm. Cell was digested spheroplasts were collected (1 min, 20 $^{\circ}$ C, 2000 x g, FA-45-18-11 rotor Eppendorf) and washed once with sorbitol buffer without DTT. Spheroplasts were incubated in 25 μ l tagmentation mix (12.5 μ l 2X TD buffer, 11.25 μ l water, 1.25 μ l Transposase (Illumina, Cat# 20034197)) for 15 min, 37 $^{\circ}$ C, 400 rpm. (Singh et al., unpublished) Transposition reaction was stopped, and DNA was purified using the MinElute PCR purification kit (Cat# 28004) and eluted in 11 μ l elution buffer. DNA was PCR amplified in 50 μ l volume (10 μ l tagmented DNA, 10 μ l water, 2.5 μ l index i5 and i7 primers (pre-made, generously provided by Prof. Dr. Gunnar Schotta), 25 μ l NEBNext High-Fidelity 2X PCR Master Mix (New England BioLabs, Cat# M0541S)) for 5 cycles. To calculate the number of cycles required before introduction of known biases in the library (Buenrostro et al., 2013), qPCR was performed on the pre-amplified PCR samples in 20 μ l volume with Fast SYBR Green Master Mix (Life technologies, Cat# 4385612). Total of 8-9 PCR cycles were performed usually. DNA was purified using the Qiagen MinElute PCR purification kit and AMPure size selected "as performed in library preparation for MNase-Seq) aiming for final fragments size less than 600 bp." (Singh et al., unpublished). The libraries were visualized on Bioanalyzer using the High Sensitivity DNA kit (Cat# 5067-4626) and sequenced on the Illumina HiSeq with 50 bp, paired-end method (Singh et al., unpublished).

4.2.5 NET-Seq

A detailed NET-Seq protocol was provided by Stirling Churchman, largely similar to (Churchman and Weissman, 2011, 2012). In first step, cells grown to log-phase were

collected. Yeast cells expressing Rpb3-3x-FLAG were grown to OD 0.8 in 1L YPAD media and quickly filtered using 90 mm, UltraWare microfiltration assembly (Thermo Fisher Cat# K953825-0090). Cells were quickly scrapped off the nitrocellulose filter (0.45 μm , 90 mm diameter; Roth Cat# A014.1) using pre-chilled spatula and transferred into 50 ml falcon immersed into liquid nitrogen. Special care was taken that cells remain immersed in liquid nitrogen bath until all liquid nitrogen evaporated from the tube. Cells were stored at $-80\text{ }^{\circ}\text{C}$ until use. In second step, frozen cells were lysed using mixer mill in liquid nitrogen condition. Cells were lysed in 50 ml stainless steel chambers (Retsch, Cat# 01.462.0216) with 25 mm balls (Retsch, Cat# 05.368.0105) for 3 min at 15 Hz in Mixer Mill MM400 (Retsch, Cat# 20.745.0001). This cycle was repeated 6 times. Metal chamber was immersed between every cycle in liquid nitrogen. Powder was transferred into 50 ml falcon immersed in liquid nitrogen and stored $-80\text{ }^{\circ}\text{C}$ until use.

In third step, IP was performed on Rbp3-FLAG and RNA associated with Pol II was purified. Powder was dissolved in ice-cold lysis buffer and DNA was digested using 660 U DNase I (Promega, Cat# M6101) along with RNase inhibitor SUPERas.In (Thermo Fisher Cat# AM2694) for 20 min. FLAG IP was performed by incubating with FLAG beads (Sigma, Cat# A2220) for 2.5 hours at $4\text{ }^{\circ}\text{C}$, then washing with 10 ml lysis buffer for 4 times at $4\text{ }^{\circ}\text{C}$. Elution was performed twice using 0.2 mg/ml 3. FLAG peptide (Sigma, Cat# F4799) dissolved in lysis buffer for 30 min on ice. Pol II associated RNA was purified using Qiagen miRNeasy mini kit (Cat# 217004). RNA was eluted twice using 30 μl nuclease-free water (Life Technologies, Cat# AM9906), ethanol precipitated and dissolved in 11 μl 10 mM Tris-Cl, pH 7.0. RNA was flash frozen and stored at $-80\text{ }^{\circ}\text{C}$.

In the fourth step, sequencing libraries were prepared from RNA Pol II associated RNA such that 3' end of nascent RNA is preserved and sequenced to identify the last nucleotide incorporated by RNA Pol II. Isolated RNA (1.5 μg) was denatured at $-80\text{ }^{\circ}\text{C}$ for 2 min and ligated to DNA linker using T4 RNA ligase 2 (truncated, K227Q) (NEB Cat# M0351S) for 3 hours at $25\text{ }^{\circ}\text{C}$. RNA was fragmented by adding 20 μl 2X alkaline fragmentation buffer and incubating at $95\text{ }^{\circ}\text{C}$. Fragmented RNA was precipitated using Isopropanol and dissolved in 10 μl of 10 mM Tris-Cl, pH 7.0. Fragmented RNA was size separated along with 10 bp ladder on a RNase-free 15% TBE-urea polyacrylamide gel (Thermo Fisher Cat# EC6885BOX) at 200 V for 65 min. Gel was stained using SYBR gold. Smear corresponding to 50 – 100 nucleotides was gel isolated using Costar Spin-X column (Sigma Cat# CLS8162-24EA). Size-selected RNA was precipitated using Isopropanol, resuspended in 10 μl of 10 mM Tris-Cl, pH 7.0 and stored at $-80\text{ }^{\circ}\text{C}$. RNA was reverse transcribed using oFMP1009 and 164 U Superscript III (Thermo Fisher Cat# 18080093) in 15 μl reaction mix. RNA was degraded by adding 1.8 μl 1 M NaOH and incubating at $98\text{ }^{\circ}\text{C}$ for 20 min. cDNA was size-selected on a 10% TBE-urea polyacrylamide gel (Thermo Fisher Cat# EC6875BOX) at 200 V for 65 min. cDNA smear corresponding to 80 -130 nucleotides were gel extracted and isolated as above. Next, cDNA was circularized using 100 U CircLigase (Epicentre Cat# CL4111K) for 60 min at $60\text{ }^{\circ}\text{C}$. Finally, to identify correct number of PCR cycles for library amplification, small-scale PCR reaction was set using 5 μl circularized cDNA. PCR was performed for 6, 8, 10 and 12 cycles. PCR products were separated on 8% TBE gel (Thermo Fisher Cat# EC6215BOX) for 40 min at 180

V. Correct number of cycles were identified based on smear with no high-molecular weight products. Large scale PCR was performed with identified 8 cycles and products were separated on as above. DNA was extracted using Spin-X column, ethanol precipitated and dissolved in 7 μ l of 10 mM Tris-Cl, pH 8.0. Ideal libraries were checked using high sensitivity Bioanalyzer chip. A good library trace showed 150 – 200 bp size distribution. 50 bp single-end sequencing was performed using oFMP967 primer to obtain at least 50 million reads.

4.2.6 Immunoprecipitation-Mass Spectrometry

Yeast strains containing Isw2-TAP tag were grown to OD 0.8-1.0 in 6L culture volume. An untagged strain was used as a negative control for each genotype (WT and *itc1 Δ*). Cells were harvested by centrifugation (5000 rpm, 10 min, 4°C, 8 min, JLA8.1 rotor) and resuspended in 20 ml TAP extraction buffer (40 mM HEPES-KOH pH 7.5, 10 % Glycerol, 150 mM or 350 mM NaCl, 0.1% Tween-20, 1 μ g/ml Pepstatin A, 2 μ g/ml Leupeptin, 1 mM PMSF) and 100 μ l of Sigma Yeast Protease Inhibitors (Cat# P8250). Cells were homogenized using Biospec bead beater with 30 sec on / 90 sec off cycle for 35 min in ice suspension. Supernatant was transferred in 50 ml centrifuge tubes and incubated with 500 μ g Heparin and 125 U Benzoylarginine hydroxide (Merck Millipore, Cat# 1016540001) at room temperature for 15 min. Suspension was centrifuged 14000 x g, 20 min, 4°C to remove cell debris. Supernatant was transferred into a new 50 ml tube and protein concentration was adjusted to 10 mg/ml with TAP Extraction Buffer. Supernatant was incubated with pre-washed 600 μ l IgG sepharose beads on a rotating wheel for 4 hours at 4°C. IgG beads were collected by centrifugation (1000 rpm, 10 min, 4°C) and transferred to a new 15 ml tube. Beads were washed thrice for 10 min at 4°C with 10 ml TAP extraction buffer. Finally, beads were resuspended in 1 ml of TEV cleavage buffer (10 mM Tris pH 8.0, 150 mM NaCl, 0.1% NP-40, 0.5 mM EDTA, 10% Glycerol, 1 mM PMSF, 2 μ g/ml Leupeptin, 1 μ g/ml Pepstatin A, 1 mM DTT). TEV protease (5 μ l, 5.5 mg/ml, in-house prepared) was added to the beads and incubated for 16 hours at 4°C on a rotating wheel. Supernatant was collected by centrifugation (1000 rpm, 10 min, 4°C), TCA precipitated and dissolved in 20 μ l 1X SDS loading buffer. Protein sample was loaded into a 4-20% SDS gel and resolved until loading buffer was 1 cm into the gel. Gel pieces were cut from the SDS gel and processed for in-gel tryptic digestion (Shevchenko et al., 2006) using a standard protocol from Zentrallabor für Proteinanalytik (ZfP), LMU Munich. Trypsin digested peptides were further processed by Ignasi Forné with the TripleTOF® 6600 Quadrupole Time-Of-Flight (QTOF) mass analyzer and maxQuant (Cox et al., 2009). iBAQ values were used to determine enrichment (at least 3-fold) for each IP against the untagged control sample processed in parallel. Only one replicate was performed using this protocol. The initial replicate was done using the on-bead trypsin digestion protocol which led to higher background in all samples.

4.2.7 General methods

4.2.7.1 Polymerase Chain Reaction

DNA was amplified using NEB Phusion DNA Polymerase (Cat# M0530L) with High-Fidelity buffer or NEB OneTaq DNA Polymerase (Cat# M0509L) with Quick-Load buffer in 25 μ l

reaction volume in the Eppendorf Mastercycler nexus GX2. Primers were designed such that annealing temperatures were between 60 – 65 °C for Phusion Polymerase and between 52 – 58 °C for OneTaq Polymerase, calculated using the online NEB T_m calculator tool. The PCR reaction mix was as follows:

Water	to 25 µl
5X HF buffer	5 µl
10 mM dNTPs	0.5 µl
10 µM Forward Primer	1.25 µl
10 µM Reverse Primer	1.25 µl
Template DNA	variable (1 – 3 µl)
Phusion Polymerase	0.3 µl

The PCR was performed using following parameters:

Initial denaturation	98°C	30 sec	1 cycle
Denaturation	98°C	10 sec	30 – 35 cycles
Annealing	60-65°C	30 sec	
Extension	72°C	30 sec / kb	
Final extension	72°C	5 min	1 cycle
Hold	10°C	∞	

When required, template DNA was digested by adding 2 µl DpnI and incubating at 37 °C for 2 hours.

4.2.7.2 Restriction digestion

Plasmids were restriction digested with appropriate enzymes in 20 µl reaction volume for 3 – 4 hours at 37 °C. When available, high fidelity version of enzymes were used in the NEV CutSmart buffer. Appropriate temperatures, buffers and input DNA amounts were used for each enzyme as described by the manufacturer (NEB). Digested products were mixed with 6X NEB loading dye and separated on an agarose gel.

4.2.7.3 Yeast genomic DNA isolation and colony PCR

“To isolate genomic DNA, yeast cultures were grown to near saturation overnight. Cells from 5 ml culture volume were harvested, dissolved in resuspension buffer (0.9 M Sorbitol, 50 mM Sodium phosphate pH 7.5, 140 mM β-Mercaptoethanol)” (Singh et al., unpublished) and lysed by Zymolyase (0.5 mg/ml) and subsequently by Proteinase K (2 mg/ml) digestion for 30 min each at 37 °C. Genomic DNA was isolated using Phenol: Chloroform: Isoamyl alcohol mix (25:24:1) and Chloroform:Isoamyl alcohol mix (24:1). DNA was precipitated using 100% ethanol and dissolved in 1X TE buffer. RNA was removed by incubating with RNase A for 1 hour. DNA was precipitated using Isopropanol. DNA pellet was dissolved in 1X TE buffer and diluted to 400 ng/µl final concentration.

Colony PCR was occasionally used when the desired amplicon length is <1500 bp. A small amount of cells were resuspended in 100 µl Zymolyase solution (0.1 M potassium phosphate,

1.2 M sorbitol, 0.5 µg/µl Zymolyase 100T), incubated at 37 °C for 10 min, followed by 95 °C for 5 min. Solution was centrifuged at 15000 rpm and 1 µl supernatant was directly used for PCR.

4.2.7.4 Plasmid isolation from *E. coli* and *S. cerevisiae*

For mini-prep and midi-prep of *E. coli* transformed plasmids, 7 ml and 200 ml LB media with appropriate antibiotic was inoculated with a single colony, respectively, and grown for 16-24 hours. Plasmids were extracted using MN NucleoSpin Plasmid extraction (Cat# 740499.250) or NucleoBond Xtra Midi (Cat# 740410.50) kit following the manufacturer's protocol for high-copy plasmids. Most midi-preps for stock preparation were prepared by a technician, Silvia Härtel, in the lab.

To extract single-copy plasmids from *S. cerevisiae*, yeast cells were grown till saturation and cell wall was digested with 50 µl Zymolyase (20 mg/ml) for 30 min at 30 °C. Buffer A1 from MN NucleoSpin Plasmid extraction kit was added, and the manufacturer's protocol was followed to isolate plasmids. Eluted DNA was transformed in *E. coli* to obtain high amounts of plasmid DNA.

4.2.7.5 *E. coli* transformation

Escherichia coli (NEB 5-alpha) chemically competent cells were prepared by a technician, Andrea Schmid, in the department. Cells were thawed on ice for 10 min, 10 – 100 ng plasmid DNA was added and incubated on ice for 10 min. Cells were heat-shocked for 1 min at 42 °C, followed by incubation on ice for 10 min. Cells were revived by adding 700 µl LB media and incubating at 37 °C for 30 min with vigorous shaking. Cells were plated on LB plates with appropriate antibiotic selection.

4.2.7.6 *S. cerevisiae* transformation

Yeast cells were transformed using high efficiency transformation protocol in (Dunham et al., 2015). Briefly, log-phase cells were washed with 5 ml 1X LiOAc buffer (0.1 M LiOAc, 10 mM Tris-Cl pH 8.0, 1 mM EDTA) and dissolved in 300 µl 1X LiOAc buffer. 100 µl of these cells were mixed with 1 – 2 µg of plasmid DNA or 10 µg of PCR product for genomic deletion / integration. 100 µg boiled salmon-sperm DNA and 280 µl PEG solution (50% PEG 3350, 1X TE, 0.1 M LiOAc) were added and mixed with vortexing for 1 min. Cells were incubated for 20 – 45 min at RT. Then, 43 µl 100% DMSO was added and heat shocked for 15 min at 42 °C. Cells were incubated on ice for 10 min and washed with sterile dH₂O. Cells were resuspended in 100 µl sterile dH₂O and plated on appropriate selection plates. When transforming DNA containing antibiotic markers, cells were recovered in YPAD media for 4 hours before plating on antibiotic plates.

4.2.7.7 Electrophoretic separation of DNA using agarose gel

DNA products were separated usually using 0.8 – 1 % (w/v) agarose in 1X TBE buffer and 0.1 µg/ml Ethidium bromide. PCR product was loaded into wells with 6X NEB loading dye diluted

to 1X in the sample. The gel was electrophoresed at 5 – 10 V/cm until desired separation was achieved. DNA was visualized using Peqlab Vilber Gel Documentation imaging system.

4.2.7.8 SDS-PAGE

Sodium dodecyl sulfate polyacrylamide gel electrophoresis (SDS-PAGE) was used to separate protein samples by mass. Protein samples, like whole cell extracts, were denatured and reduced using 5X Bromophenol blue dye and heated at 95 °C for 5 min. Mixture was vortexed twice during the heating. Samples were loaded onto a 10% or 8 – 16% gradient gel (SERVAGel Precast Vertical Gels) with 10 wells. A prestained VWR Protein-Marker IV (10 – 170 kDa, Cat# 27-2110) or V (10 – 170 kDa, Cat# 27-2210) was used to indicate standard molecular weights. Gels were run in 1X SDS-PAGE buffer at 100 V until desired separation.

4.2.7.9 Western blot

Cells were grown overnight in 5 ml YPAD media. Next day, cells were re-inoculated in 10 ml YPAD to OD 600 0.1 and grown till OD 0.8. “Cells were collected (2500 x g, 3 min, 4 °C, TX-1000 rotor ThermoFisher Scientific), washed with 10 ml of ice-cold water and resuspended in 400 µl extraction buffer (40 mM HEPES-KOH pH 7.5, 10% Glycerol, 350 mM NaCl, 0.1% Tween-20, 1 µg/ml Pepstatin A, 2 µg/ml Leupeptin, 2 µg/ml Aprotinin, 1 mM PMSF). Dissolved cells were transferred to a 1.5 ml eppendorf tube, equal volume of 0.5 mm glass beads (Roth, Cat# N030.1)” (Singh et al., unpublished) added and bead-beaten on a vortex (maximum speed) for 30 sec on / 30 sec off cycle for total of 10 cycles. During the 30 sec off step, eppendorf tubes were incubated in ice. “Cells were centrifuged (10000 x g, 10 min, 4 °C, FA-45-18-11 Eppendorf rotor) and supernatant was collected in a new 1.5 ml eppendorf tube.” (Singh et al., unpublished) Supernatant was flash frozen and stored at -80 °C until use. Occasionally, cells extracts were prepared using the NaOH / TCA precipitation protocol (Knop et al., 1999). Whole cell extracts (100-200 µg) were loaded on a 10% SDS gel (SERVAGel TG PRiME; Cat# 43264.01) and transferred to a nitrocellulose membrane (Amersham Protran 0,45um NC-Nitrocellulose; Cat# D10600018). Membranes were blocked for 30-60 min with 5% skimmed milk (+ 0.1% Tween-20, when required for Licor quantification) and incubated overnight with a primary antibody dissolved in 5% skimmed milk (Heirler Bio Magermilchpulver, ReformKontor, Cat# 3030) and PBS with 0.1% Tween-20. Nitrocellulose membranes were washed three times with 1X PBS and incubated with the desired secondary antibody dissolved in 5% skimmed milk + PBS with 0.1% Tween-20. The Odyssey IR imaging system (ODY-0853) or the ECL detection system (VWR, Cat# RPN2235) were used for visualization.

4.2.7.10 Growth assay

Cells were grown overnight in YPAD media. Next day, OD 600 (Thermo Scientific GENESYS 20 spectrophotometer) “was measured in technical replicates by 1:10 dilution in sterile water. Cells were diluted to OD 1.0 in 200 µl sterile water and 5- or 10- fold serial dilutions were generated” (Singh et al., unpublished). 5 – 10 µl of the serially diluted cells were spotted on

appropriate plates with 2% agar. Plates were incubated at desired temperatures for 2 – 4 days and images were taken using the Peqlab Vilber Gel Documentation imaging system.

4.2.7.11 DNA damage assay

Cells were grown overnight in YPAD media to log phase. Cells were diluted to OD 600 (Thermo Scientific GENESYS 20 spectrophotometer) 0.2 in 5 ml YPAD media. Zeocin (Life technologies, Cat# R25001) was added to final concentration of 1 mg/ml. “Cells were incubated at 30°C for 10 min. Cells were quickly harvested (2500 x g, 2 min, 4°C, TX-1000 rotor ThermoFisher Scientific) and washed with 5 ml ice-cold water. Cell pellets were dissolved in 200 µl cold DNA extraction buffer (0.9 M Sorbitol, 50 mM Na-Pi pH 7.5, 140 mM β-Mercaptoethanol). Cell wall was digested using Zymolyase (0.5 mg/ml final concentration) for 15 min at 30°C and Proteinase K digestion (2 mg/ml, 30 min) for 30 min at 30°C. Phenol: Chloroform: Isoamyl alcohol (25:24:1) extraction was performed once, followed by ethanol (100 %) precipitation. Pellet was dissolved in 100 µl TE buffer. 5 µg RNase A was added and incubated for 30 min at 30°C. DNA was quantified with Nanodrop and Qubit. 20 µg of DNA was loaded on a 0.7% (w/v) low-melt agarose gel in 1X TBE buffer. DNA was separated at 2 V/cm for 4 h at room temperature.” (Singh et al., unpublished) DNA was stained using ethidium bromide (0.5 µg/ml) in 1X TBE for 15 min and quickly washed with sterile water twice. Images were taken using the Peqlab Vilber Gel Documentation imaging system. To avoid DNA fragmentation from pipetting, samples were mixed only three times with a 200 µl micropipette.

4.2.7.12 Ectopic recombination assay

The ectopic recombination rates for the WT and TKO strains were determined as described in (Hauer et al., 2017). Briefly, equal number of log phase cells (10^7) were transformed (Dunham et al., 2015). To test recombination at the *ura3-1* locus, pRS406 plasmid was digested with *StuI* (Cat# R0187S NEB). For at the *BAR1* locus, the *HIS3* marker was PCR amplified from the pRS403 plasmid using oligonucleotides oFMP1235 and oFMP1236. DNA fragments were purified using the MN NucleoSpin Gel and PCR Clean-up kit. To transform DNA fragments, 1 µg of *StuI* digested pRS406 plasmid or 10 µg of *bar1-his3* PCR product were used. 100 ng of undigested pRS406 or pRS403 plasmids were used as a negative control. 100 ng of pRS416 or pRS413 plasmids were used as a positive control. All DNA fragments, including positive and negative controls, were transformed in parallel. Transformed cells were selected on a SC-Ura or a SC-His plate. Colonies were counted after 3-4 days. To calculate the relative integration rates, numbers of colonies observed using the *StuI* digested pRS406 or *HIS3* PCR products were normalized by number of colonies observed for their respective positive controls (pRS416 or pRS413). Normalized counts obtained for replicates were divided by the normalized count observed in the WT cells tested in parallel. For mutant strains, two independent colonies were tested. For the WT strain, α and α strains were tested. All cells were tested twice, therefore providing four replicates per strain. *Arp8* deleted strain was used a positive control and similar results were obtained as shown before (Hauer et al., 2017).

4.2.7.13 Yeast growth conditions

All yeast strains were maintained in the YPAD media, except for strains containing plasmids with auxotrophic markers. “The plasmid containing strains were maintained in SC + 2% glucose media with an appropriate selection. The histones depletion strains were grown in SC media with 2% galactose lacking either Uracil or Histidine.” (Singh et al., unpublished)

To deplete RNA Pol II or INO80 from the nucleus, cells were grown overnight in the YPAD media to OD 0.2-0.3. Rapamycin or vehicle, as a control, were added to the culture. Rapamycin (Hözel Diagnostika, Cat# R-5000-100mg) was dissolved (not sterile filtered) in vehicle (90% ethanol, 10% Tween-20) to 1 mg/ml (stock stored at -20°C indefinitely). Rapamycin was added at a final concentration of 1 µg/ml (Kubik et al., 2015; Tramantano et al., 2016). INO80 depletion was confirmed by tracking Ino80-GFP fluorescence via live cell microscopy and depletion time (90 min) was found similar to a previous observation (Tramantano et al., 2016). RNA Pol II depletion was confirmed by growth assay on a YPAD plate containing 1 µg/ml rapamycin. “Combined depletion of RNA Pol II and INO80 was confirmed by Ino80-GFP fluorescence as well as growth assay on a YPAD plate containing 1 µg/ml rapamycin.” (Singh et al., unpublished).

For the histone depletion (HD) experiments, cells were first grown overnight to OD 600 1.0 in SC media with 2% galactose. Cells were collected (3000 x g, 20 °C, 6 min, JLA 8.1000 rotor Beckman Coulter). Pellets were washed with pre-warmed SC media and dissolved in SC media with 2% glucose such that the OD is 0.5. Cells were incubated at 30 °C for 3 h with gently shaking.

4.2.7.14 Antibody generation against Isw1 and Isw2 proteins

Three peptides from Isw1 and four from Isw2 protein (Appendix 6.5) were synthesized in conjugation with either ovalbumin or biotin. Peptides were immunized in 2 rats and 2 mice. Antibodies were produced by Andrew Flatley and Dr. Regina Feederle at the MAB monoclonal antibody core facility, Helmholtz Zentrum München. Antibodies were tested in western blot for reactivity against Isw1 and Isw2. Because, Isw1 and Isw2 proteins are highly similar, cross reactivity of the antibodies was tested in parallel using whole cell extracts from cells lacking either Isw1 or Isw2. List of useful antibodies recognizing Isw1 can be found in Appendix 6.5. No specific antibody was found against Isw2 against the antigens stated in Appendix 6.5.

4.2.7.15 Yeast GFP live-cell microscopy

Cells with C-terminally GFP-tagged protein constructs were used for microscopy. Cells were grown till OD 0.8 in 10 ml YPAD media. Cells were collected by centrifugation (300 x g, 5 min, 4°C), washed twice with 1X PBS and dissolved in 1X PBS. 2 µl cells were directly applied on a glass slide and visualized immediately under Zeiss Axiovert 200M microscope with 63X magnification.

4.2.7.16 *In vivo* UV-crosslink and TAP-immunoprecipitation

To test interaction of ISW2 with RNA, BY4741 and ISW2-TAP strain were grown in 1L YPAD to OD 0.8. Cells were washed with 50 ml ice-cold PBS and dissolved in 5 ml 1X PBS. Cell suspension was UV crosslinked (365 nm, 10 sec on / 20 sec off, 1 min total UV exposure, 1.2 J/cm²) in a 10 cm petridish at 4°C in the Vilber Bio-Link 365 machine. Cells were washed with 1X PBS and dissolved in 5 ml TN-150 buffer (50 mM Tris-HCl pH 7.8, 150 mM NaCl, 0.1% NP-40, 5 mM beta-mercaptoethanol) with protease inhibitors. Cells were lysed by adding three volume of Zirconia/Silica beads (0.5 mm; BioSpec Cat# 11079105z) and vortexing for 5 min (1 min on / 1 min off cycle) on ice. Supernatant was collected by centrifugation (12000 x g, 5 min, 4°C) and incubated with 300 µl of IgG Sepharose beads (Sigma Cat# 17-0969-01) pre-washed with lysis buffer for 2 hours at 4°C on a rotating wheel. To reduce RNA degradation, 12.5 µl Suprase.In (Thermo Fischer Cat# AM2694) was added in the supernatant. Beads were collected by centrifugation (300 x g, 5 min, 4°C) and washed thrice with TN-1000 buffer (50 mM Tris-HCl pH 7.8, 1000 mM NaCl, 0.1% NP-40, 5 mM β-mercaptoethanol) and thrice with TN-150 buffer for 5 min each. To elute ISW2, beads were incubated with TEV protease (30 µg, home-made) for 2 h at room temperature. RNA was extracted using Qiagen RNAeasy kit (Cat# 74104) with DNase I digestion. To visualize eluted RNA, samples were denatured in Novex TBE-Urea sample prep buffer (Life technologies, Cat# LC6876) at 80°C for 2 min and resolved in 15% TBE-Urea gel (Life technologies, Cat# EC6885BOX). Gels were stained using 1X Sybr-gold (Life technologies, Cat# S11494) in TBE buffer for 15 min and visualized using Peqlab Vilber Gel Documentation imaging system.

4.2.8 Bioinformatic methods

4.2.8.1 Demultiplexing, mapping and coverage vectors

The basic sequence mapping and data analysis scripts were initially established by Tamas Schauer and Tobias Straub at Bioinformatics facility, Biomedical Center, LMU Munich. I used these scripts, modified and tested to generate initial plots. All other analyses scripts for statistics and plot generation were tested and established in this thesis with input from Tamas Schauer.

“The fastq files from the Illumina HiSeq were demultiplexed using the Je demultiplex suite (v1.0.6) (Girardot et al., 2016) with demultiplex-illu in paired-end mode and NEBNext index barcodes. Sequences were then mapped to the *S. cerevisiae* sacCer3 R64-1-1 genome version using the Bowtie2 tool (v2.2.9)” (Singh et al., unpublished) (Langmead and Salzberg, 2012). Default setting was used except the -X 500, --no-discordant, --no-mixed options. The bam files were generated using the samtools tool (v1.3.1) (Li et al., 2009) with minimum mapping quality 2. The mitochondrial (chrM) and the ribosomal DNA reads (coordinates chrXII 451000:469000) were removed. The nucleosome dyad coverage and the bigWig files were generated in R using packages rtracklayer v1.42.2 (Lawrence et al., 2009), GenomicRanges v1.34.0 and GenomicAlignments v1.18.1 (Lawrence et al., 2013) packages. Nucleosome dyad centers were determined by taking the center of 140-160 bp fragments. For bigWig files, dyad centers were usually extended by 50 bp and visualized in Integrative Genomics Viewer

v2.4.18 (Robinson et al., 2011). An equal number of reads (10 million) were taken for each sample and coverage was normalized to reads per million.

4.2.8.2 Composite plot and heatmap generation

Genome coordinates, annotations and the +1-nucleosome coordinate were downloaded from the H3Q85C chemical mapping dataset (Chereji et al., 2018). Matrices aligned to the +1 nucleosome were generated using the `coverageWindowsCenteredStranded` function in the `tsTools` (v0.1.2) (<https://github.com/musikutiv/tsTools>). The composite plots were plotted using the aligned matrices. First, a mean signal for each base pair is calculated for all genes. Then the signal at each base pair was normalized to the mean signal of the desired window. The aligned matrices were also used for generating heatmaps using the `image` function in R v3.5.3 (<https://www.R-project.org/>). Heatmaps were sorted as described in each plot.

4.2.8.3 Nucleosome repeat length and array regularity calculations

Nucleosome repeat length for each gene was calculated using a MATLAB routine was graciously provided by Dr. Răzvan Chereji and Dr. David Clark, NIH. Here, the signal obtained from MNase-Seq was cross-correlated to a simulated Gaussian pattern (Ocampo et al., 2016). Dr. Tobias Straub and Dr. Tamas Schauer further adapted it in R (<https://github.com/musikutiv/tsTools>). I manually validated the predictions generated from the scripts for 50 genes.

The MNase-Seq signal from a -200 to +800 bp window relative to the +1 nucleosome in each gene was used. MNase-Seq data was using a 75 bp smoothing window. Cross-correlation between the smoothed MNase-Seq signal and a Gaussian pattern with increasing repeat lengths (between 130 and 220 bp) was calculated using the `Ccf` function (Brockwell and Davis, 2013). “The repeat length with highest correlation was taken as the NRL for each gene. The cross-correlation score was used as the array regularity score. Higher correlation coefficient indicated higher array regularity. Manual inspection of nucleosome pattern reconciled well with the predicted nucleosome regularity score for about 50 genes tested manually.” (Singh et al., unpublished)

4.2.8.4 ATAC-Seq analysis

Paired-end ATAC-Seq reads were mapped to the `sacCer3 R64-1-1` genome version same as MNase-Seq. Fragment lengths between 0 and 500 bp were selected from the bam files and an equal number of reads (3 million) for each sample was taken. Matrices aligned to the TSS and TTS (taken from (Chereji et al., 2018)) were generated from the coverage vector. Signal in the gene body were re-scaled to 1000 bp. For composite plots, ATAC counts in each gene were normalized by the gene length. Average ATAC counts in the gene body was calculated by using reads mapping to TSS +100 bp and TTS -100 bp. Genes with transcript shorter than 300 bp were discarded.

“For array regularity to ATAC correlation, genes with extreme nucleosome occupancy (<0.78 and >0.88) (Oberbeckmann et al., 2019) were filtered.” (Singh et al., unpublished). Genes

were then sorted by array regularity and divided into quartiles. ATAC-seq data is from (Schep et al., 2015).

4.2.8.5 NET-Seq analysis

NET-Seq reads mapping

50 bp single-end reads were mapped to Saccar3 genome vR64-1-1 by Brendan Smalec (Harvard Medical School, Stirling Churchman lab). Briefly, adaptor sequence was trimmed from individual reads using Cutadapt v1.12 (Martin, 2011) and unique molecular barcodes were removed using PRINSEQ v0.20.2 (Schmieder and Edwards, 2011). PCR duplicates were removed first using unique molecular barcodes. Reads were mapped using TopHat2 v2.0.10 (Kim et al., 2013) and reverse transcriptase misprimed reads in first 6 bp were removed. Bedgraph files were generated using samtools v0.1.19 (Li et al., 2009). Reads were normalized as follows: First, reads mapping to both strands were summed. This number was divided by 1 million and then used to divide each read in the genome. Custom scripts were used when required.

NET-Seq 5' to 3' ratio analysis

Pol II 5' traveling ratio was calculated similar to (Topal et al., 2019). Genes with transcripts longer than 500 bp and nucleosome occupancy between 0.78 and 0.88 were considered for this analysis (Oberbeckmann et al., 2019). Overlapping genes were also discarded. Genes with more than 15 reads were further selected. 5' to 3' ratio was calculated by dividing the read density in TSS to TSS+250 bp region to read density in TSS+250 bp to TTS region. Read density was calculated by dividing number of reads mapping in TSS to TSS+250 bp region by 250 and in TSS+250 bp to TTS region by transcript length-250. Ecdf function in R was used to generate the cumulative distribution plots. Analyses were repeated with NET-Seq datasets from three laboratories (Churchman and Weissman, 2011; Mischo et al., 2018; Topal et al., 2019) showing similar results.

4.2.8.6 ChIP-Seq analysis

“Rpb3 (RNA Pol II subunit) ChIP-Seq datasets for WT and the *isw1Δ*, *chd1Δ* double knockout strain were obtained from (Ocampo et al., 2016).” (Singh et al., unpublished). Paired-end reads were mapped using Bowtie2 considering fragments between 50 and 300 bp. Bam files were then employed to measure the RNA Pol II occupancy (IP / input) for each gene using the bamR package (<https://github.com/rchereji/bamR>) with default options.

4.2.8.7 DANPOS +1-nucleosome fuzziness analysis

“Bam files for MNase-Seq data with fragment lengths between 140 and 160 bp were used as input for DANPOS v2.2.2.” (Singh et al., unpublished). Nucleosomes positions were called in each dataset using the dpos command and parameters -jw 5, -q 200, -m 1 (Chen et al., 2013a). The +1 nucleosome (first nucleosome called after the nucleosome-free region

(downloaded from (Chereji et al., 2018)) was calculated using custom scripts and the summit value or the fuzziness score for each gene was taken.

4.2.8.8 Statistical positioning simulation

The simulations were performed by Prof. Dr. Felix Mueller-Planitz. Simulations were performed in MATLAB considering 50000 fragments between 2000 and 2500 bp. First, the +1 nucleosome was positioned with a sigma of 25 bp. Next, nucleosomes were placed at random positions, considering that a given position was not already occupied by another nucleosome. This process was continued until nucleosome occupancy was ~51%. Then, 20% of randomly picked nucleosomes, except the +1 nucleosome, were dissociated from the DNA. Dissociated nucleosome was placed on the DNA again as described above. This cycle was repeated for 8 times when the nucleosome landscapes converged which suggests equilibrium conditions. Each nucleosome was considered as a hard sphere with a footprint of 146 bp. Individual replicates of three simulations were remarkably similar and replicate 1 was used further.

4.2.8.9 Nucleosome affinity prediction using nuCpos

“The Histone Binding Affinity (HBA) function in nuCpos package v1.6.0 (Kato et al., 2019) was used to calculate nucleosome affinities.” (Singh et al., unpublished). The HBA function provides a nucleosome affinity score for the tested DNA sequence. To calculate affinity score for all genomic positions, *S. cerevisiae* genome was divided into 147 bp sized sequences with 1 bp sliding window. “HBA values were then calculated for each 147 bp sequence and aligned to the +1 nucleosome coordinate for each gene obtained from (Chereji et al., 2018). Signals were further smoothed using a smooth.spline function (spar = 0.4) in R. Smoothing of signals using two other packages (rollmean function (Zoo package, version 1.8-5; <https://cran.r-project.org/web/packages/zoo/index.html>) or sgolayfilt function (signal package, version 0.7-6; <http://r-forge.r-project.org/projects/signal/>)) provided similar results.” (Singh et al., unpublished). Only genes with array regularity larger than 0.5, NRL between 150 and 200 bp and longer than 1000 bp were used. Quartiles represent a mean signal of 688, 786 and 502 genes in TKO - Pol II, WT and TKO samples respectively.

4.2.8.10 Published nucleosome positioning sequences score

“Previously measured nucleosome positioning sequences (NPS) score for coordinates -931 to +528 relative to ATG start codon of each gene (Ioshikhes et al., 2006) was provided by Dr. B. Franklin Pugh. The NPS score was re-aligned to the +1 nucleosome (Chereji et al., 2018). Only genes with array regularity >0.5 and NRL between 150 and 200 bp were used for this analysis. The NPS score was smoothed using rollmean function (step size 51).” (Singh et al., unpublished).

4.2.8.11 Published datasets analysis

“RNA Pol II anchor-away, RSC depletion, INO80 depletion and *nhp10Δ* MNase-Seq datasets in the WT background were taken from (Cutler et al., 2018; Ganguli et al., 2014; Klein-Brill et

al., 2019; Kubik et al., 2015; Tramantano et al., 2016). All datasets were processed similar to the datasets generated during this thesis.” (Singh et al., unpublished).

4.2.8.12 Correlations of nucleosome array regularity to published datasets

For array regularity to cryptic TSS correlations, transcription Start Sites data for cells grown in YPD media was downloaded from the YeastTSS database for *S. cerevisiae* (Lu and Lin, 2019; McMillan et al., 2019). “Genes longer than 500 bp and nucleosome occupancy between 0.78 and 0.88 were selected.” (Singh et al., unpublished). Reads found between TSS +100 bp and TTS -100 bp were defined as cryptic TSSs. These reads were summed for each gene and normalized by the DNA length between TSS +100 bp and TTS -100 bp. “Genes were then sorted by array regularity or nucleosome occupancy, as required.” (Singh et al., unpublished). For cryptic sense and antisense TSS to array regularity correlations, only reads mapping to coding or non-coding strands were considered, respectively.

For Spo11- and topoisomerase 2-generated double-stranded breaks (Gittens et al., 2019) to array regularity correlations, DNA breaks were counted between TSS +100 and TTS -100 bp and normalized by the length considered. Genes longer than 500 bp and nucleosome occupancy between 0.78 and 0.88 were considered.

Transposase insertion data was obtained from reference (Michel et al., 2017). Data for non-essential genes were used because transpositions in the essential genes provides no reads. Genes longer than 500 bp and nucleosome occupancy between 0.78 and 0.88 were considered.

4.2.8.13 Dinucleosome occupancy analysis using bamR

Bam files containing reads from 0-500 bp were used to plot mono- and di- nucleosome occupancy using the bamR package (<https://github.com/rchereji/bamR>) with default options. For dinucleosome occupancy, fragments with 250-350 bp were used. For mononucleosome occupancy, 140-160 bp were used. All plots were aligned to +1 nucleosome (Chereji et al., 2018).

5. BIBLIOGRAPHY

- Abraham, A.L., Nagarajan, M., Veyrieras, J.B., Bottin, H., Steinmetz, L.M., and Yvert, G. (2012). Genetic modifiers of chromatin acetylation antagonize the reprogramming of epi-polymorphisms. *PLoS Genet* 8, e1002958.
- Albert, I., Mavrich, T.N., Tomsho, L.P., Qi, J., Zanton, S.J., Schuster, S.C., and Pugh, B.F. (2007). Translational and rotational settings of H2A.Z nucleosomes across the *Saccharomyces cerevisiae* genome. *Nature* 446, 572-576.
- Alen, C., Kent, N.A., Jones, H.S., O'Sullivan, J., Aranda, A., and Proudfoot, N.J. (2002). A role for chromatin remodeling in transcriptional termination by RNA polymerase II. *Mol Cell* 10, 1441-1452.
- Almer, A., and Horz, W. (1986). Nuclease hypersensitive regions with adjacent positioned nucleosomes mark the gene boundaries of the PHO5/PHO3 locus in yeast. *EMBO J* 5, 2681-2687.
- Altaf, M., Auger, A., Monnet-Saksouk, J., Brodeur, J., Piquet, S., Cramet, M., Bouchard, N., Lacoste, N., Utley, R.T., Gaudreau, L., *et al.* (2010). NuA4-dependent acetylation of nucleosomal histones H4 and H2A directly stimulates incorporation of H2A.Z by the SWR1 complex. *J Biol Chem* 285, 15966-15977.
- Argelaguet, R., Clark, S.J., Mohammed, H., Stapel, L.C., Krueger, C., Kapourani, C.A., Imaz-Rosshandler, I., Lohoff, T., Xiang, Y., Hanna, C.W., *et al.* (2019). Multi-omics profiling of mouse gastrulation at single-cell resolution. *Nature* 576, 487-491.
- Arimura, Y., Ikura, M., Fujita, R., Noda, M., Kobayashi, W., Horikoshi, N., Sun, J., Shi, L., Kusakabe, M., Harata, M., *et al.* (2018). Cancer-associated mutations of histones H2B, H3.1 and H2A.Z.1 affect the structure and stability of the nucleosome. *Nucleic Acids Res* 46, 10007-10018.
- Ayala, R., Willhoft, O., Aramayo, R.J., Wilkinson, M., McCormack, E.A., Ocloo, L., Wigley, D.B., and Zhang, X. (2018). Structure and regulation of the human INO80-nucleosome complex. *Nature* 556, 391-395.
- Azmi, I.F., Watanabe, S., Maloney, M.F., Kang, S., Belsky, J.A., MacAlpine, D.M., Peterson, C.L., and Bell, S.P. (2017). Nucleosomes influence multiple steps during replication initiation. *Elife* 6.
- Babour, A., Shen, Q., Dos-Santos, J., Murray, S., Gay, A., Challal, D., Fasken, M., Palancade, B., Corbett, A., Libri, D., *et al.* (2016). The Chromatin Remodeler ISW1 Is a Quality Control Factor that Surveys Nuclear mRNP Biogenesis. *Cell* 167, 1201-1214 e1215.
- Bachman, N., Gelbart, M.E., Tsukiyama, T., and Boeke, J.D. (2005). TFIIB subunit Bdp1p is required for periodic integration of the Ty1 retrotransposon and targeting of Isw2p to *S. cerevisiae* tDNAs. *Genes Dev* 19, 955-964.
- Baldi, S., Jain, D.S., Harpprecht, L., Zabel, A., Scheibe, M., Butter, F., Straub, T., and Becker, P.B. (2018a). Genome-wide Rules of Nucleosome Phasing in *Drosophila*. *Mol Cell* 72, 661-672 e664.
- Baldi, S., Korber, P., and Becker, P.B. (2020). Beads on a string-nucleosome array arrangements and folding of the chromatin fiber. *Nat Struct Mol Biol* 27, 109-118.
- Baldi, S., Krebs, S., Blum, H., and Becker, P.B. (2018b). Genome-wide measurement of local nucleosome array regularity and spacing by nanopore sequencing. *Nat Struct Mol Biol* 25, 894-901.
- Bao, Y., Konesky, K., Park, Y.J., Rosu, S., Dyer, P.N., Rangasamy, D., Tremethick, D.J., Laybourn, P.J., and Luger, K. (2004). Nucleosomes containing the histone variant H2A.Bbd organize only 118 base pairs of DNA. *EMBO J* 23, 3314-3324.

- Barisic, D., Stadler, M.B., Iurlaro, M., and Schubeler, D. (2019). Mammalian ISWI and SWI/SNF selectively mediate binding of distinct transcription factors. *Nature* 569, 136-140.
- Barozzi, I., Simonatto, M., Bonifacio, S., Yang, L., Rohs, R., Ghisletti, S., and Natoli, G. (2014). Coregulation of transcription factor binding and nucleosome occupancy through DNA features of mammalian enhancers. *Mol Cell* 54, 844-857.
- Becker, P.B. (2002). Nucleosome sliding: facts and fiction. *EMBO J* 21, 4749-4753.
- Beh, L.Y., Debelouchina, G.T., Clay, D.M., Thompson, R.E., Lindblad, K.A., Hutton, E.R., Bracht, J.R., Sebra, R.P., Muir, T.W., and Landweber, L.F. (2019). Identification of a DNA N6-Adenine Methyltransferase Complex and Its Impact on Chromatin Organization. *Cell* 177, 1781-1796 e1725.
- Berbenetz, N.M., Nislow, C., and Brown, G.W. (2010). Diversity of eukaryotic DNA replication origins revealed by genome-wide analysis of chromatin structure. *PLoS Genet* 6, e1001092.
- Berkowitz, E.M., and Riggs, E.A. (1981). Characterization of rat liver oligonucleosomes enriched in transcriptionally active genes: evidence for altered base composition and a shortened nucleosome repeat. *Biochemistry* 20, 7284-7290.
- Beshnova, D.A., Cherstvy, A.G., Vainshtein, Y., and Teif, V.B. (2014). Regulation of the nucleosome repeat length in vivo by the DNA sequence, protein concentrations and long-range interactions. *PLoS Comput Biol* 10, e1003698.
- Blank, T.A., and Becker, P.B. (1995). Electrostatic mechanism of nucleosome spacing. *J Mol Biol* 252, 305-313.
- Blazeck, J., Garg, R., Reed, B., and Alper, H.S. (2012). Controlling promoter strength and regulation in *Saccharomyces cerevisiae* using synthetic hybrid promoters. *Biotechnol Bioeng* 109, 2884-2895.
- Blosser, T.R., Yang, J.G., Stone, M.D., Narlikar, G.J., and Zhuang, X. (2009). Dynamics of nucleosome remodelling by individual ACF complexes. *Nature* 462, 1022-1027.
- Bonisch, C., and Hake, S.B. (2012). Histone H2A variants in nucleosomes and chromatin: more or less stable? *Nucleic Acids Res* 40, 10719-10741.
- Brahma, S., and Henikoff, S. (2019). RSC-Associated Subnucleosomes Define MNase-Sensitive Promoters in Yeast. *Mol Cell* 73, 238-249 e233.
- Brahma, S., Ngubo, M., Paul, S., Udugama, M., and Bartholomew, B. (2018). The Arp8 and Arp4 module acts as a DNA sensor controlling INO80 chromatin remodeling. *Nat Commun* 9, 3309.
- Brahma, S., Udugama, M.I., Kim, J., Hada, A., Bhardwaj, S.K., Hailu, S.G., Lee, T.H., and Bartholomew, B. (2017). INO80 exchanges H2A.Z for H2A by translocating on DNA proximal to histone dimers. *Nat Commun* 8, 15616.
- Brockwell, P.J., and Davis, R.A. (2013). *Time series : theory and methods* (New York, N.Y.: Springer).
- Brogaard, K., Xi, L., Wang, J.P., and Widom, J. (2012). A map of nucleosome positions in yeast at base-pair resolution. *Nature* 486, 496-501.
- Brunk, C.F., and Martin, W.F. (2019). Archaeal Histone Contributions to the Origin of Eukaryotes. *Trends Microbiol* 27, 703-714.
- Buenrostro, J.D., Giresi, P.G., Zaba, L.C., Chang, H.Y., and Greenleaf, W.J. (2013). Transposition of native chromatin for fast and sensitive epigenomic profiling of open chromatin, DNA-binding proteins and nucleosome position. *Nat Methods* 10, 1213-1218.

- Cakiroglu, A., Clapier, C.R., Ehrensberger, A.H., Darbo, E., Cairns, B.R., Luscombe, N.M., and Svejstrup, J.Q. (2019). Genome-wide reconstitution of chromatin transactions reveals that RSC preferentially disrupts H2AZ-containing nucleosomes. *Genome Res* 29, 988-998.
- Candelli, T., Gros, J., and Libri, D. (2018). Pervasive transcription fine-tunes replication origin activity. *Elife* 7.
- Carey, M., Li, B., and Workman, J.L. (2006). RSC exploits histone acetylation to abrogate the nucleosomal block to RNA polymerase II elongation. *Mol Cell* 24, 481-487.
- Celona, B., Weiner, A., Di Felice, F., Mancuso, F.M., Cesarini, E., Rossi, R.L., Gregory, L., Baban, D., Rossetti, G., Grianti, P., *et al.* (2011). Substantial histone reduction modulates genomewide nucleosomal occupancy and global transcriptional output. *PLoS Biol* 9, e1001086.
- Challal, D., Barucco, M., Kubik, S., Feuerbach, F., Candelli, T., Geoffroy, H., Benaksas, C., Shore, D., and Libri, D. (2018). General Regulatory Factors Control the Fidelity of Transcription by Restricting Non-coding and Ectopic Initiation. *Mol Cell* 72, 955-969 e957.
- Chambers, A.L., Ormerod, G., Durley, S.C., Sing, T.L., Brown, G.W., Kent, N.A., and Downs, J.A. (2012). The INO80 chromatin remodeling complex prevents polyploidy and maintains normal chromatin structure at centromeres. *Genes Dev* 26, 2590-2603.
- Chan, R.K., and Otte, C.A. (1982). Isolation and genetic analysis of *Saccharomyces cerevisiae* mutants supersensitive to G1 arrest by a factor and alpha factor pheromones. *Mol Cell Biol* 2, 11-20.
- Chatterjee, N., Sinha, D., Lemma-Dechassa, M., Tan, S., Shogren-Knaak, M.A., and Bartholomew, B. (2011). Histone H3 tail acetylation modulates ATP-dependent remodeling through multiple mechanisms. *Nucleic Acids Res* 39, 8378-8391.
- Chen, K., Xi, Y., Pan, X., Li, Z., Kaestner, K., Tyler, J., Dent, S., He, X., and Li, W. (2013a). DANPOS: dynamic analysis of nucleosome position and occupancy by sequencing. *Genome Res* 23, 341-351.
- Chen, L., Cai, Y., Jin, J., Florens, L., Swanson, S.K., Washburn, M.P., Conaway, J.W., and Conaway, R.C. (2011). Subunit organization of the human INO80 chromatin remodeling complex: an evolutionarily conserved core complex catalyzes ATP-dependent nucleosome remodeling. *J Biol Chem* 286, 11283-11289.
- Chen, L., Conaway, R.C., and Conaway, J.W. (2013b). Multiple modes of regulation of the human Ino80 SNF2 ATPase by subunits of the INO80 chromatin-remodeling complex. *Proc Natl Acad Sci U S A* 110, 20497-20502.
- Chen, Y.F., Chou, C.C., and Gartenberg, M.R. (2016). Determinants of Sir2-Mediated, Silent Chromatin Cohesion. *Mol Cell Biol* 36, 2039-2050.
- Chereji, R.V., Bryson, T.D., and Henikoff, S. (2019). Quantitative MNase-seq accurately maps nucleosome occupancy levels. *Genome Biol* 20, 198.
- Chereji, R.V., and Clark, D.J. (2018). Major Determinants of Nucleosome Positioning. *Biophys J* 114, 2279-2289.
- Chereji, R.V., Kan, T.W., Grudniewska, M.K., Romashchenko, A.V., Berezikov, E., Zhimulev, I.F., Guryev, V., Morozov, A.V., and Moshkin, Y.M. (2016). Genome-wide profiling of nucleosome sensitivity and chromatin accessibility in *Drosophila melanogaster*. *Nucleic Acids Res* 44, 1036-1051.
- Chereji, R.V., Ocampo, J., and Clark, D.J. (2017). MNase-Sensitive Complexes in Yeast: Nucleosomes and Non-histone Barriers. *Mol Cell* 65, 565-577 e563.
- Chereji, R.V., Ramachandran, S., Bryson, T.D., and Henikoff, S. (2018). Precise genome-wide mapping of single nucleosomes and linkers in vivo. *Genome Biol* 19, 19.

- Churchman, L.S., and Weissman, J.S. (2011). Nascent transcript sequencing visualizes transcription at nucleotide resolution. *Nature* **469**, 368-373.
- Churchman, L.S., and Weissman, J.S. (2012). Native elongating transcript sequencing (NET-seq). *Curr Protoc Mol Biol Chapter 4*, Unit 4 14 11-17.
- Clapier, C.R., and Cairns, B.R. (2012). Regulation of ISWI involves inhibitory modules antagonized by nucleosomal epitopes. *Nature* **492**, 280-284.
- Clapier, C.R., Iwasa, J., Cairns, B.R., and Peterson, C.L. (2017). Mechanisms of action and regulation of ATP-dependent chromatin-remodelling complexes. *Nat Rev Mol Cell Biol* **18**, 407-422.
- Clapier, C.R., Nightingale, K.P., and Becker, P.B. (2002). A critical epitope for substrate recognition by the nucleosome remodeling ATPase ISWI. *Nucleic Acids Res* **30**, 649-655.
- Clark, S.J., Argelaguet, R., Kapourani, C.A., Stubbs, T.M., Lee, H.J., Alda-Catalinas, C., Krueger, F., Sanguinetti, G., Kelsey, G., Marioni, J.C., *et al.* (2018). scNMT-seq enables joint profiling of chromatin accessibility DNA methylation and transcription in single cells. *Nat Commun* **9**, 781.
- Clarkson, C.T., Deeks, E.A., Samarista, R., Mamayusupova, H., Zhurkin, V.B., and Teif, V.B. (2019). CTCF-dependent chromatin boundaries formed by asymmetric nucleosome arrays with decreased linker length. *Nucleic Acids Res* **47**, 11181-11196.
- Claussen, C.A., and Long, E.C. (1999). Nucleic Acid Recognition by Metal Complexes of Bleomycin. *Chemical Reviews* **99**, 2797-2816.
- Cole, H.A., Howard, B.H., and Clark, D.J. (2011). Activation-induced disruption of nucleosome position clusters on the coding regions of Gcn4-dependent genes extends into neighbouring genes. *Nucleic Acids Res* **39**, 9521-9535.
- Cole, H.A., Ocampo, J., Iben, J.R., Chereji, R.V., and Clark, D.J. (2014). Heavy transcription of yeast genes correlates with differential loss of histone H2B relative to H4 and queued RNA polymerases. *Nucleic Acids Res* **42**, 12512-12522.
- Corona, D.F., Eberharter, A., Budde, A., Deuring, R., Ferrari, S., Varga-Weisz, P., Wilm, M., Tamkun, J., and Becker, P.B. (2000). Two histone fold proteins, CHRAC-14 and CHRAC-16, are developmentally regulated subunits of chromatin accessibility complex (CHRAC). *EMBO J* **19**, 3049-3059.
- Correll, S.J., Schubert, M.H., and Grigoryev, S.A. (2012). Short nucleosome repeats impose rotational modulations on chromatin fibre folding. *EMBO J* **31**, 2416-2426.
- Cox, J., Matic, I., Hilger, M., Nagaraj, N., Selbach, M., Olsen, J.V., and Mann, M. (2009). A practical guide to the MaxQuant computational platform for SILAC-based quantitative proteomics. *Nat Protoc* **4**, 698-705.
- Cui, F., Cole, H.A., Clark, D.J., and Zhurkin, V.B. (2012). Transcriptional activation of yeast genes disrupts intragenic nucleosome phasing. *Nucleic Acids Res* **40**, 10753-10764.
- Cuperus, G., and Shore, D. (2002). Restoration of silencing in *Saccharomyces cerevisiae* by tethering of a novel Sir2-interacting protein, Esc8. *Genetics* **162**, 633-645.
- Cutler, S., Lee, L.J., and Tsukiyama, T. (2018). Chromatin Remodeling Factors Isw2 and Ino80 Regulate Chromatin, Replication, and Copy Number of the *Saccharomyces cerevisiae* Ribosomal DNA Locus. *Genetics* **210**, 1543-1556.
- Dacher, M., Tachiwana, H., Horikoshi, N., Kujirai, T., Taguchi, H., Kimura, H., and Kurumizaka, H. (2019). Incorporation and influence of *Leishmania* histone H3 in chromatin. *Nucleic Acids Res* **47**, 11637-11648.

- Dang, W., Kagalwala, M.N., and Bartholomew, B. (2006). Regulation of ISW2 by concerted action of histone H4 tail and extranucleosomal DNA. *Mol Cell Biol* 26, 7388-7396.
- Dann, G.P., Liszczak, G.P., Bagert, J.D., Muller, M.M., Nguyen, U.T.T., Wojcik, F., Brown, Z.Z., Bos, J., Panchenko, T., Pihl, R., *et al.* (2017). ISWI chromatin remodellers sense nucleosome modifications to determine substrate preference. *Nature* 548, 607-611.
- Dao, H.T., Dul, B.E., Dann, G.P., Liszczak, G.P., and Muir, T.W. (2019). A basic motif anchoring ISWI to nucleosome acidic patch regulates nucleosome spacing. *Nat Chem Biol*.
- De Ambrosis, A., Ferrari, N., Bonassi, S., and Vidali, G. (1987). Nucleosomal repeat length in active and inactive genes. *FEBS Letters* 225, 120-122.
- Deindl, S., Hwang, W.L., Hota, S.K., Blosser, T.R., Prasad, P., Bartholomew, B., and Zhuang, X. (2013). ISWI remodelers slide nucleosomes with coordinated multi-base-pair entry steps and single-base-pair exit steps. *Cell* 152, 442-452.
- Deng, C., and Saunders, W.S. (2001). RIM4 encodes a meiotic activator required for early events of meiosis in *Saccharomyces cerevisiae*. *Mol Genet Genomics* 266, 497-504.
- Deniz, O., Flores, O., Aldea, M., Soler-Lopez, M., and Orozco, M. (2016). Nucleosome architecture throughout the cell cycle. *Sci Rep* 6, 19729.
- Dingwall, C., Lomonosoff, G.P., and Laskey, R.A. (1981). High sequence specificity of micrococcal nuclease. *Nucleic Acids Res* 9, 2659-2673.
- Doi, S., Tanabe, K., Watanabe, M., Yamaguchi, M., and Yoshimura, M. (1989). An alpha-specific gene, SAG1 is required for sexual agglutination in *Saccharomyces cerevisiae*. *Curr Genet* 15, 393-398.
- Donovan, D.A., Crandall, J.G., Truong, V.N., Vaaler, A.L., Bailey, T.B., Dinwiddie, D., McKnight, L.E., and McKnight, J.N. (2020). Basis of Specificity for a Conserved and Promiscuous Chromatin Remodeling Protein. *bioRxiv*.
- Dorigo, B., Schalch, T., Kulangara, A., Duda, S., Schroeder, R.R., and Richmond, T.J. (2004). Nucleosome arrays reveal the two-start organization of the chromatin fiber. *Science* 306, 1571-1573.
- Doris, S.M., Chuang, J., Viktorovskaya, O., Murawska, M., Spatt, D., Churchman, L.S., and Winston, F. (2018). Spt6 Is Required for the Fidelity of Promoter Selection. *Mol Cell* 72, 687-699 e686.
- Drew, H.R., and Travers, A.A. (1985). DNA bending and its relation to nucleosome positioning. *Journal of Molecular Biology* 186, 773-790.
- Dunham, M.J., Gartenberg, M.R., and Brown, G.W. (2015). *Methods in Yeast Genetics and Genomics : a Cold Spring Harbor Laboratory course manual* (Cold Spring Harbor, NY: Cold Spring Harbor Laboratory Press).
- Eaton, M.L., Galani, K., Kang, S., Bell, S.P., and MacAlpine, D.M. (2010). Conserved nucleosome positioning defines replication origins. *Genes Dev* 24, 748-753.
- Eberharter, A., Ferrari, S., Langst, G., Straub, T., Imhof, A., Varga-Weisz, P., Wilm, M., and Becker, P.B. (2001). Acf1, the largest subunit of CHRAC, regulates ISWI-induced nucleosome remodelling. *EMBO J* 20, 3781-3788.
- Eberharter, A., Vetter, I., Ferreira, R., and Becker, P.B. (2004). ACF1 improves the effectiveness of nucleosome mobilization by ISWI through PHD-histone contacts. *EMBO J* 23, 4029-4039.
- Ehara, H., Kujirai, T., Fujino, Y., Shirouzu, M., Kurumizaka, H., and Sekine, S.I. (2019). Structural insight into nucleosome transcription by RNA polymerase II with elongation factors. *Science* 363, 744-747.

- Elserafy, M., and El-Khamisy, S.F. (2018). Choose your yeast strain carefully: the RAD5 gene matters. *Nat Rev Mol Cell Biol* 19, 343-344.
- Eltsov, M., Maclellan, K.M., Maeshima, K., Frangakis, A.S., and Dubochet, J. (2008). Analysis of cryo-electron microscopy images does not support the existence of 30-nm chromatin fibers in mitotic chromosomes in situ. *Proc Natl Acad Sci U S A* 105, 19732-19737.
- Ercan, S., and Simpson, R.T. (2004). Global chromatin structure of 45,000 base pairs of chromosome III in a- and alpha-cell yeast and during mating-type switching. *Mol Cell Biol* 24, 10026-10035.
- Eriksson, P.R., and Clark, D.J. (2020). The yeast ISW1b ATP-dependent chromatin remodeler is critical for nucleosome spacing and dinucleosome resolution. *bioRxiv*.
- Eustermann, S., Schall, K., Kostrewa, D., Lakomek, K., Strauss, M., Moldt, M., and Hopfner, K.P. (2018). Structural basis for ATP-dependent chromatin remodelling by the INO80 complex. *Nature* 556, 386-390.
- Fan, J.Y., Gordon, F., Luger, K., Hansen, J.C., and Tremethick, D.J. (2002). The essential histone variant H2A.Z regulates the equilibrium between different chromatin conformational states. *Nat Struct Biol* 9, 172-176.
- Fan, J.Y., Rangasamy, D., Luger, K., and Tremethick, D.J. (2004). H2A.Z alters the nucleosome surface to promote HP1alpha-mediated chromatin fiber folding. *Mol Cell* 16, 655-661.
- Fan, Y., Nikitina, T., Morin-Kensicki, E.M., Zhao, J., Magnuson, T.R., Woodcock, C.L., and Skoultchi, A.I. (2003). H1 linker histones are essential for mouse development and affect nucleosome spacing in vivo. *Mol Cell Biol* 23, 4559-4572.
- Fan, Y., Nikitina, T., Zhao, J., Fleury, T.J., Bhattacharyya, R., Bouhassira, E.E., Stein, A., Woodcock, C.L., and Skoultchi, A.I. (2005). Histone H1 depletion in mammals alters global chromatin structure but causes specific changes in gene regulation. *Cell* 123, 1199-1212.
- Farnung, L., Ochmann, M., Engeholm, M., and Cramer, P. (2020). Structural basis of nucleosome transcription mediated by Chd1 and FACT. *bioRxiv*.
- Farnung, L., Vos, S.M., and Cramer, P. (2018). Structure of transcribing RNA polymerase II-nucleosome complex. *Nat Commun* 9, 5432.
- Farnung, L., Vos, S.M., Wigge, C., and Cramer, P. (2017). Nucleosome-Chd1 structure and implications for chromatin remodelling. *Nature* 550, 539-542.
- Fazio, T.G., Gelbart, M.E., and Tsukiyama, T. (2005). Two distinct mechanisms of chromatin interaction by the Isw2 chromatin remodeling complex in vivo. *Mol Cell Biol* 25, 9165-9174.
- Fazio, T.G., Kooperberg, C., Goldmark, J.P., Neal, C., Basom, R., Delrow, J., and Tsukiyama, T. (2001). Widespread collaboration of Isw2 and Sin3-Rpd3 chromatin remodeling complexes in transcriptional repression. *Mol Cell Biol* 21, 6450-6460.
- Fedor, M.J., Lue, N.F., and Kornberg, R.D. (1988). Statistical positioning of nucleosomes by specific protein-binding to an upstream activating sequence in yeast. *J Mol Biol* 204, 109-127.
- Fennessy, R.T., and Owen-Hughes, T. (2016). Establishment of a promoter-based chromatin architecture on recently replicated DNA can accommodate variable inter-nucleosome spacing. *Nucleic Acids Res* 44, 7189-7203.
- Ferreira, H., Flaus, A., and Owen-Hughes, T. (2007). Histone modifications influence the action of Snf2 family remodelling enzymes by different mechanisms. *J Mol Biol* 374, 563-579.

- Festuccia, N., Owens, N., Papadopoulou, T., Gonzalez, I., Tachtsidi, A., Vandoermel-Pournin, S., Gallego, E., Gutierrez, N., Dubois, A., Cohen-Tannoudji, M., *et al.* (2019). Transcription factor activity and nucleosome organization in mitosis. *Genome Res* 29, 250-260.
- Field, Y., Fondufe-Mittendorf, Y., Moore, I.K., Mieczkowski, P., Kaplan, N., Lubling, Y., Lieb, J.D., Widom, J., and Segal, E. (2009). Gene expression divergence in yeast is coupled to evolution of DNA-encoded nucleosome organization. *Nat Genet* 41, 438-445.
- Field, Y., Kaplan, N., Fondufe-Mittendorf, Y., Moore, I.K., Sharon, E., Lubling, Y., Widom, J., and Segal, E. (2008). Distinct modes of regulation by chromatin encoded through nucleosome positioning signals. *PLoS Comput Biol* 4, e1000216.
- Finch, J.T., and Klug, A. (1976). Solenoidal model for superstructure in chromatin. *Proc Natl Acad Sci U S A* 73, 1897-1901.
- Flaus, A., Martin, D.M., Barton, G.J., and Owen-Hughes, T. (2006). Identification of multiple distinct Snf2 subfamilies with conserved structural motifs. *Nucleic Acids Res* 34, 2887-2905.
- Fu, Y., Sinha, M., Peterson, C.L., and Weng, Z. (2008). The insulator binding protein CTCF positions 20 nucleosomes around its binding sites across the human genome. *PLoS Genet* 4, e1000138.
- Fyodorov, D.V., Blower, M.D., Karpen, G.H., and Kadonaga, J.T. (2004). Acf1 confers unique activities to ACF/CHRAC and promotes the formation rather than disruption of chromatin in vivo. *Genes Dev* 18, 170-183.
- Fyodorov, D.V., and Kadonaga, J.T. (2002a). Binding of Acf1 to DNA involves a WAC motif and is important for ACF-mediated chromatin assembly. *Mol Cell Biol* 22, 6344-6353.
- Fyodorov, D.V., and Kadonaga, J.T. (2002b). Dynamics of ATP-dependent chromatin assembly by ACF. *Nature* 418, 897-900.
- Fyodorov, D.V., Zhou, B.R., Skoultchi, A.I., and Bai, Y. (2018). Emerging roles of linker histones in regulating chromatin structure and function. *Nat Rev Mol Cell Biol* 19, 192-206.
- Galgoczy, D.J., Cassidy-Stone, A., Llinas, M., O'Rourke, S.M., Herskowitz, I., DeRisi, J.L., and Johnson, A.D. (2004). Genomic dissection of the cell-type-specification circuit in *Saccharomyces cerevisiae*. *Proc Natl Acad Sci U S A* 101, 18069-18074.
- Gamarra, N., Johnson, S.L., Trnka, M.J., Burlingame, A.L., and Narlikar, G.J. (2018). The nucleosomal acidic patch relieves auto-inhibition by the ISWI remodeler SNF2h. *Elife* 7.
- Gangaraju, V.K., Prasad, P., Srour, A., Kagalwala, M.N., and Bartholomew, B. (2009). Conformational changes associated with template commitment in ATP-dependent chromatin remodeling by ISW2. *Mol Cell* 35, 58-69.
- Ganguli, D., Chereji, R.V., Iben, J.R., Cole, H.A., and Clark, D.J. (2014). RSC-dependent constructive and destructive interference between opposing arrays of phased nucleosomes in yeast. *Genome Res* 24, 1637-1649.
- Ganter, B., Tan, S., and Richmond, T.J. (1993). Genomic footprinting of the promoter regions of STE2 and STE3 genes in the yeast *Saccharomyces cerevisiae*. *J Mol Biol* 234, 975-987.
- Garcia-Gomez, J.J., Babiano, R., Lebaron, S., Froment, C., Monsarrat, B., Henry, Y., and de la Cruz, J. (2011). Nop6, a component of 90S pre-ribosomal particles, is required for 40S ribosomal subunit biogenesis in *Saccharomyces cerevisiae*. *RNA Biol* 8, 112-124.
- Gavin, A.C., Bosche, M., Krause, R., Grandi, P., Marzioch, M., Bauer, A., Schultz, J., Rick, J.M., Michon, A.M., Cruciat, C.M., *et al.* (2002). Functional organization of the yeast proteome by systematic analysis of protein complexes. *Nature* 415, 141-147.

- Gelbart, M.E., Bachman, N., Delrow, J., Boeke, J.D., and Tsukiyama, T. (2005). Genome-wide identification of Isw2 chromatin-remodeling targets by localization of a catalytically inactive mutant. *Genes Dev* 19, 942-954.
- Gene Ontology, C. (2015). Gene Ontology Consortium: going forward. *Nucleic Acids Res* 43, D1049-1056.
- Gevry, N., Hardy, S., Jacques, P.E., Laflamme, L., Svtelis, A., Robert, F., and Gaudreau, L. (2009). Histone H2A.Z is essential for estrogen receptor signaling. *Genes Dev* 23, 1522-1533.
- Gibson, B.A., Doolittle, L.K., Schneider, M.W.G., Jensen, L.E., Gamarra, N., Henry, L., Gerlich, D.W., Redding, S., and Rosen, M.K. (2019). Organization of Chromatin by Intrinsic and Regulated Phase Separation. *Cell* 179, 470-484 e421.
- Gibson, D.G. (2011). Enzymatic assembly of overlapping DNA fragments. *Methods Enzymol* 498, 349-361.
- Gilchrist, D.A., Dos Santos, G., Fargo, D.C., Xie, B., Gao, Y., Li, L., and Adelman, K. (2010). Pausing of RNA polymerase II disrupts DNA-specified nucleosome organization to enable precise gene regulation. *Cell* 143, 540-551.
- Girardot, C., Scholtalbers, J., Sauer, S., Su, S.Y., and Furlong, E.E. (2016). Je, a versatile suite to handle multiplexed NGS libraries with unique molecular identifiers. *BMC Bioinformatics* 17, 419.
- Gittens, W.H., Johnson, D.J., Allison, R.M., Cooper, T.J., Thomas, H., and Neale, M.J. (2019). A nucleotide resolution map of Top2-linked DNA breaks in the yeast and human genome. *Nat Commun* 10, 4846.
- Gkikopoulos, T., Schofield, P., Singh, V., Pinskaya, M., Mellor, J., Smolle, M., Workman, J.L., Barton, G.J., and Owen-Hughes, T. (2011). A role for Snf2-related nucleosome-spacing enzymes in genome-wide nucleosome organization. *Science* 333, 1758-1760.
- Goldman, J.A., Garlick, J.D., and Kingston, R.E. (2010). Chromatin remodeling by imitation switch (ISWI) class ATP-dependent remodelers is stimulated by histone variant H2A.Z. *J Biol Chem* 285, 4645-4651.
- Goldmark, J.P., Fazio, T.G., Estep, P.W., Church, G.M., and Tsukiyama, T. (2000). The Isw2 Chromatin Remodeling Complex Represses Early Meiotic Genes upon Recruitment by Ume6p. *Cell* 103, 423-433.
- Gossett, A.J., and Lieb, J.D. (2012). In vivo effects of histone H3 depletion on nucleosome occupancy and position in *Saccharomyces cerevisiae*. *PLoS Genet* 8, e1002771.
- Gottschling, D.E., Palen, T.E., and Cech, T.R. (1983). Different nucleosome spacing in transcribed and non-transcribed regions of the ribosomal RNA gene in *Tetrahymena thermophila*. *Nucleic Acids Res* 11, 2093-2109.
- Grava, S., Dumoulin, P., Madania, A., Tarassov, I., and Winsor, B. (2000). Functional analysis of six genes from chromosomes XIV and XV of *Saccharomyces cerevisiae* reveals YOR145c as an essential gene and YNL059c/ARP5 as a strain-dependent essential gene encoding nuclear proteins. *Yeast* 16, 1025-1033.
- Gros, J., Kumar, C., Lynch, G., Yadav, T., Whitehouse, I., and Remus, D. (2015). Post-licensing Specification of Eukaryotic Replication Origins by Facilitated Mcm2-7 Sliding along DNA. *Mol Cell* 60, 797-807.
- Groth, A., Rocha, W., Verreault, A., and Almouzni, G. (2007). Chromatin challenges during DNA replication and repair. *Cell* 128, 721-733.

- Grüne, T., Brzeski, J., Eberharter, A., Clapier, C.R., Corona, D.F.V., Becker, P.B., and Müller, C.W. (2003). Crystal Structure and Functional Analysis of a Nucleosome Recognition Module of the Remodeling Factor ISWI. *Molecular Cell* *12*, 449-460.
- Guldener, U., Heinisch, J., Koehler, G.J., Voss, D., and Hegemann, J.H. (2002). A second set of loxP marker cassettes for Cre-mediated multiple gene knockouts in budding yeast. *Nucleic Acids Res* *30*, e23.
- Guillemette, B., Bataille, A.R., Gevry, N., Adam, M., Blanchette, M., Robert, F., and Gaudreau, L. (2005). Variant histone H2A.Z is globally localized to the promoters of inactive yeast genes and regulates nucleosome positioning. *PLoS Biol* *3*, e384.
- Hafner, M., Landthaler, M., Burger, L., Khorshid, M., Hausser, J., Berninger, P., Rothballer, A., Ascano, M., Jr., Jungkamp, A.C., Munschauer, M., *et al.* (2010). Transcriptome-wide identification of RNA-binding protein and microRNA target sites by PAR-CLIP. *Cell* *141*, 129-141.
- Han, Y., Reyes, A.A., Malik, S., and He, Y. (2020). Cryo-EM structure of SWI/SNF complex bound to a nucleosome. *Nature*.
- Harrer, N., Schindler, C.E.M., Bruetzel, L.K., Forne, I., Ludwigsen, J., Imhof, A., Zacharias, M., Lipfert, J., and Mueller-Planitz, F. (2018). Structural Architecture of the Nucleosome Remodeler ISWI Determined from Cross-Linking, Mass Spectrometry, SAXS, and Modeling. *Structure* *26*, 282-294 e286.
- Hartley, P.D., and Madhani, H.D. (2009). Mechanisms that specify promoter nucleosome location and identity. *Cell* *137*, 445-458.
- Haruki, H., Nishikawa, J., and Laemmli, U.K. (2008). The anchor-away technique: rapid, conditional establishment of yeast mutant phenotypes. *Mol Cell* *31*, 925-932.
- Hauer, M.H., Seeber, A., Singh, V., Thierry, R., Sack, R., Amitai, A., Kryzhanovska, M., Eglinger, J., Holcman, D., Owen-Hughes, T., *et al.* (2017). Histone degradation in response to DNA damage enhances chromatin dynamics and recombination rates. *Nat Struct Mol Biol* *24*, 99-107.
- Hauk, G., McKnight, J.N., Nodelman, I.M., and Bowman, G.D. (2010). The chromodomains of the Chd1 chromatin remodeler regulate DNA access to the ATPase motor. *Mol Cell* *39*, 711-723.
- He, S., Wu, Z., Tian, Y., Yu, Z., Yu, J., Wang, X., Li, J., Liu, B., and Xu, Y. (2020). Structure of nucleosome-bound human BAF complex. *Science* *367*, 875-881.
- Henikoff, J.G., Belsky, J.A., Krassovsky, K., MacAlpine, D.M., and Henikoff, S. (2011). Epigenome characterization at single base-pair resolution. *Proc Natl Acad Sci U S A* *108*, 18318-18323.
- Henikoff, S., Henikoff, J.G., Sakai, A., Loeb, G.B., and Ahmad, K. (2009). Genome-wide profiling of salt fractions maps physical properties of chromatin. *Genome Res* *19*, 460-469.
- Hennig, B.P., Bendrin, K., Zhou, Y., and Fischer, T. (2012). Chd1 chromatin remodelers maintain nucleosome organization and repress cryptic transcription. *EMBO Rep* *13*, 997-1003.
- Hergeth, S.P., and Schneider, R. (2015). The H1 linker histones: multifunctional proteins beyond the nucleosomal core particle. *EMBO Rep* *16*, 1439-1453.
- Herzel, H., Weiss, O., and Trifonov, E.N. (1998). Sequence periodicity in complete genomes of archaea suggests positive supercoiling. *J Biomol Struct Dyn* *16*, 341-345.
- Hocher, A., Rojec, M., Swadling, J.B., Esin, A., and Warnecke, T. (2019). The DNA-binding protein HTa from *Thermoplasma acidophilum* is an archaeal histone analog. *Elife* *8*.

- Hogan, C.J., Aligianni, S., Durand-Dubief, M., Persson, J., Will, W.R., Webster, J., Wheeler, L., Mathews, C.K., Elderkin, S., Oxley, D., *et al.* (2010). Fission yeast *Iec1-ino80*-mediated nucleosome eviction regulates nucleotide and phosphate metabolism. *Mol Cell Biol* *30*, 657-674.
- Hontz, R.D., Niederer, R.O., Johnson, J.M., and Smith, J.S. (2009). Genetic identification of factors that modulate ribosomal DNA transcription in *Saccharomyces cerevisiae*. *Genetics* *182*, 105-119.
- Horz, W., and Altenburger, W. (1981). Sequence specific cleavage of DNA by micrococcal nuclease. *Nucleic Acids Res* *9*, 2643-2658.
- Hota, S.K., Bhardwaj, S.K., Deindl, S., Lin, Y.C., Zhuang, X., and Bartholomew, B. (2013). Nucleosome mobilization by ISW2 requires the concerted action of the ATPase and SLIDE domains. *Nat Struct Mol Biol* *20*, 222-229.
- Hsieh, T.H., Weiner, A., Lajoie, B., Dekker, J., Friedman, N., and Rando, O.J. (2015). Mapping Nucleosome Resolution Chromosome Folding in Yeast by Micro-C. *Cell* *162*, 108-119.
- Hu, Z., Chen, K., Xia, Z., Chavez, M., Pal, S., Seol, J.H., Chen, C.C., Li, W., and Tyler, J.K. (2014). Nucleosome loss leads to global transcriptional up-regulation and genomic instability during yeast aging. *Genes Dev* *28*, 396-408.
- Huff, J.T., and Zilberman, D. (2014). Dnmt1-independent CG methylation contributes to nucleosome positioning in diverse eukaryotes. *Cell* *156*, 1286-1297.
- Hughes, A.L., Jin, Y., Rando, O.J., and Struhl, K. (2012). A functional evolutionary approach to identify determinants of nucleosome positioning: a unifying model for establishing the genome-wide pattern. *Mol Cell* *48*, 5-15.
- Hughes, A.L., and Rando, O.J. (2015). Comparative Genomics Reveals Chd1 as a Determinant of Nucleosome Spacing in Vivo. *G3 (Bethesda)* *5*, 1889-1897.
- Huppertz, I., Attig, J., D'Ambrogio, A., Easton, L.E., Sibley, C.R., Sugimoto, Y., Tajnik, M., Konig, J., and Ule, J. (2014). iCLIP: protein-RNA interactions at nucleotide resolution. *Methods* *65*, 274-287.
- Hwang, W.L., Deindl, S., Harada, B.T., and Zhuang, X. (2014). Histone H4 tail mediates allosteric regulation of nucleosome remodelling by linker DNA. *Nature* *512*, 213-217.
- Ioshikhes, I., Bolshoy, A., Derenshteyn, K., Borodovsky, M., and Trifonov, E.N. (1996). Nucleosome DNA sequence pattern revealed by multiple alignment of experimentally mapped sequences. *J Mol Biol* *262*, 129-139.
- Ioshikhes, I.P., Albert, I., Zanton, S.J., and Pugh, B.F. (2006). Nucleosome positions predicted through comparative genomics. *Nat Genet* *38*, 1210-1215.
- Ito, T., Bulger, M., Pazin, M.J., Kobayashi, R., and Kadonaga, J.T. (1997). ACF, an ISWI-Containing and ATP-Utilizing Chromatin Assembly and Remodeling Factor. *Cell* *90*, 145-155.
- Iyer, V., and Struhl, K. (1995). Poly(dA:dT), a ubiquitous promoter element that stimulates transcription via its intrinsic DNA structure. *The EMBO Journal* *14*, 2570-2579.
- Jeronimo, C., Angel, A., Poitras, C., Collin, P., Mellor, J., and Robert, F. (2020). FACT is recruited to the +1 nucleosome of transcribed genes and spreads in a Chd1-dependent manner.
- Jin, C., and Felsenfeld, G. (2007). Nucleosome stability mediated by histone variants H3.3 and H2A.Z. *Genes Dev* *21*, 1519-1529.
- Jin, J., Cai, Y., Yao, T., Gottschalk, A.J., Florens, L., Swanson, S.K., Gutierrez, J.L., Coleman, M.K., Workman, J.L., Mushegian, A., *et al.* (2005). A mammalian chromatin remodeling complex with similarities to the yeast INO80 complex. *J Biol Chem* *280*, 41207-41212.

- Johnson, S.M., Tan, F.J., McCullough, H.L., Riordan, D.P., and Fire, A.Z. (2006). Flexibility and constraint in the nucleosome core landscape of *Caenorhabditis elegans* chromatin. *Genome Res* 16, 1505-1516.
- Kagalwala, M.N., Glaus, B.J., Dang, W., Zofall, M., and Bartholomew, B. (2004). Topography of the ISW2-nucleosome complex: insights into nucleosome spacing and chromatin remodeling. *EMBO J* 23, 2092-2104.
- Kaplan, C.D., Laprade, L., and Winston, F. (2003). Transcription elongation factors repress transcription initiation from cryptic sites. *Science* 301, 1096-1099.
- Kaplan, N., Moore, I., Fondufe-Mittendorf, Y., Gossett, A.J., Tillo, D., Field, Y., Hughes, T.R., Lieb, J.D., Widom, J., and Segal, E. (2010). Nucleosome sequence preferences influence in vivo nucleosome organization. *Nat Struct Mol Biol* 17, 918-920.
- Kaplan, N., Moore, I.K., Fondufe-Mittendorf, Y., Gossett, A.J., Tillo, D., Field, Y., LeProust, E.M., Hughes, T.R., Lieb, J.D., Widom, J., *et al.* (2009). The DNA-encoded nucleosome organization of a eukaryotic genome. *Nature* 458, 362-366.
- Kato, H., Shimizu, M., and Urano, T. (2019). Chemical map-based prediction of nucleosome positioning using the Bioconductor package nuCpos. *bioRxiv*.
- Keeney, S., Giroux, C.N., and Kleckner, N. (1997). Meiosis-Specific DNA Double-Strand Breaks Are Catalyzed by Spo11, a Member of a Widely Conserved Protein Family. *Cell* 88, 375-384.
- Kelly, T.K., Liu, Y., Lay, F.D., Liang, G., Berman, B.P., and Jones, P.A. (2012). Genome-wide mapping of nucleosome positioning and DNA methylation within individual DNA molecules. *Genome Res* 22, 2497-2506.
- Kent, N.A., Adams, S., Moorhouse, A., and Paszkiewicz, K. (2011). Chromatin particle spectrum analysis: a method for comparative chromatin structure analysis using paired-end mode next-generation DNA sequencing. *Nucleic Acids Res* 39, e26.
- Kim, D., Pertea, G., Trapnell, C., Pimentel, H., Kelley, R., and Salzberg, S.L. (2013). TopHat2: accurate alignment of transcriptomes in the presence of insertions, deletions and gene fusions. *Genome Biol* 14, R36.
- Kingston, R.E., and Narlikar, G.J. (1999). ATP-dependent remodeling and acetylation as regulators of chromatin fluidity. *Genes Dev* 13, 2339-2352.
- Klein-Brill, A., Joseph-Strauss, D., Appleboim, A., and Friedman, N. (2019). Dynamics of Chromatin and Transcription during Transient Depletion of the RSC Chromatin Remodeling Complex. *Cell Rep* 26, 279-292 e275.
- Klinner, U., and Schafer, B. (2004). Genetic aspects of targeted insertion mutagenesis in yeasts. *FEMS Microbiol Rev* 28, 201-223.
- Klymenko, T., Papp, B., Fischle, W., Kocher, T., Schelder, M., Fritsch, C., Wild, B., Wilm, M., and Muller, J. (2006). A Polycomb group protein complex with sequence-specific DNA-binding and selective methyl-lysine-binding activities. *Genes Dev* 20, 1110-1122.
- Knoll, K.R., Eustermann, S., Niebauer, V., Oberbeckmann, E., Stoehr, G., Schall, K., Tosi, A., Schwarz, M., Buchfellner, A., Korber, P., *et al.* (2018). The nuclear actin-containing Arp8 module is a linker DNA sensor driving INO80 chromatin remodeling. *Nat Struct Mol Biol* 25, 823-832.
- Knop, M., Siegers, K., Pereira, G., Zachariae, W., Winsor, B., Nasmyth, K., and Schiebel, E. (1999). Epitope tagging of yeast genes using a PCR-based strategy: more tags and improved practical routines. *Yeast* 15, 963-972.
- Kornberg, R.D., and Lorch, Y. (2020). Primary Role of the Nucleosome. *Mol Cell* 79, 371-375.

- Kornberg, R.D., and Stryer, L. (1988). Statistical distributions of nucleosomes: nonrandom locations by a stochastic mechanism. *Nucleic Acids Res* 16, 6677-6690.
- Krietenstein, N., Wal, M., Watanabe, S., Park, B., Peterson, C.L., Pugh, B.F., and Korber, P. (2016). Genomic Nucleosome Organization Reconstituted with Pure Proteins. *Cell* 167, 709-721 e712.
- Kubik, S., Bruzzone, M.J., Challal, D., Dreos, R., Mattarocci, S., Bucher, P., Libri, D., and Shore, D. (2019). Opposing chromatin remodelers control transcription initiation frequency and start site selection. *Nat Struct Mol Biol* 26, 744-754.
- Kubik, S., Bruzzone, M.J., Jacquet, P., Falcone, J.L., Rougemont, J., and Shore, D. (2015). Nucleosome Stability Distinguishes Two Different Promoter Types at All Protein-Coding Genes in Yeast. *Mol Cell* 60, 422-434.
- Kubik, S., O'Duibhir, E., de Jonge, W.J., Mattarocci, S., Albert, B., Falcone, J.L., Bruzzone, M.J., Holstege, F.C.P., and Shore, D. (2018). Sequence-Directed Action of RSC Remodeler and General Regulatory Factors Modulates +1 Nucleosome Position to Facilitate Transcription. *Mol Cell* 71, 89-102 e105.
- Kubota, T., Nishimura, K., Kanemaki, M.T., and Donaldson, A.D. (2013). The Elg1 replication factor C-like complex functions in PCNA unloading during DNA replication. *Mol Cell* 50, 273-280.
- Kujirai, T., Ehara, H., Fujino, Y., Shirouzu, M., Sekine, S.I., and Kurumizaka, H. (2018). Structural basis of the nucleosome transition during RNA polymerase II passage. *Science* 362, 595-598.
- Kurat, C.F., Yeeles, J.T.P., Patel, H., Early, A., and Diffley, J.F.X. (2017). Chromatin Controls DNA Replication Origin Selection, Lagging-Strand Synthesis, and Replication Fork Rates. *Mol Cell* 65, 117-130.
- Kurihara, L.J., Stewart, B.G., Gammie, A.E., and Rose, M.D. (1996). Kar4p, a karyogamy-specific component of the yeast pheromone response pathway. *Mol Cell Biol* 16, 3990-4002.
- Kusch, T., Florens, L., Macdonald, W.H., Swanson, S.K., Glaser, R.L., Yates, J.R., 3rd, Abmayr, S.M., Washburn, M.P., and Workman, J.L. (2004). Acetylation by Tip60 is required for selective histone variant exchange at DNA lesions. *Science* 306, 2084-2087.
- Lafon, A., Taranum, S., Pietrocola, F., Dingli, F., Loew, D., Brahma, S., Bartholomew, B., and Papamichos-Chronakis, M. (2015). INO80 Chromatin Remodeler Facilitates Release of RNA Polymerase II from Chromatin for Ubiquitin-Mediated Proteasomal Degradation. *Mol Cell* 60, 784-796.
- Lai, B., Gao, W., Cui, K., Xie, W., Tang, Q., Jin, W., Hu, G., Ni, B., and Zhao, K. (2018). Principles of nucleosome organization revealed by single-cell micrococcal nuclease sequencing. *Nature* 562, 281-285.
- Lai, W.K.M., and Pugh, B.F. (2017). Understanding nucleosome dynamics and their links to gene expression and DNA replication. *Nat Rev Mol Cell Biol* 18, 548-562.
- Langmead, B., and Salzberg, S.L. (2012). Fast gapped-read alignment with Bowtie 2. *Nat Methods* 9, 357-359.
- Langmore, J.P., and Paulson, J.R. (1983). Low angle x-ray diffraction studies of chromatin structure in vivo and in isolated nuclei and metaphase chromosomes. *J Cell Biol* 96, 1120-1131.
- Längst, G., Bonte, E.J., Corona, D.F.V., and Becker, P.B. (1999). Nucleosome Movement by CHRAC and ISWI without Disruption or trans-Displacement of the Histone Octamer. *Cell* 97, 843-852.
- Lans, H., Marteiijn, J.A., and Vermeulen, W. (2012). ATP-dependent chromatin remodeling in the DNA-damage response. *Epigenetics Chromatin* 5, 4.

- Larson, K., Sahm, J., Shenkar, R., and Strauss, B. (1985). Methylation-induced blocks to in vitro DNA replication. *Mutat Res* 150, 77-84.
- Lawrence, M., Daujat, S., and Schneider, R. (2016). Lateral Thinking: How Histone Modifications Regulate Gene Expression. *Trends Genet* 32, 42-56.
- Lawrence, M., Gentleman, R., and Carey, V. (2009). rtracklayer: an R package for interfacing with genome browsers. *Bioinformatics* 25, 1841-1842.
- Lawrence, M., Huber, W., Pages, H., Aboyoun, P., Carlson, M., Gentleman, R., Morgan, M.T., and Carey, V.J. (2013). Software for computing and annotating genomic ranges. *PLoS Comput Biol* 9, e1003118.
- Lee, C.H., Holder, M., Grau, D., Saldana-Meyer, R., Yu, J.R., Ganai, R.A., Zhang, J., Wang, M., LeRoy, G., Dobenecker, M.W., *et al.* (2018). Distinct Stimulatory Mechanisms Regulate the Catalytic Activity of Polycomb Repressive Complex 2. *Mol Cell* 70, 435-448 e435.
- Lee, C.H., Wu, J., and Li, B. (2013). Chromatin remodelers fine-tune H3K36me-directed deacetylation of neighbor nucleosomes by Rpd3S. *Mol Cell* 52, 255-263.
- Lee, Y., Park, D., and Iyer, V.R. (2017). The ATP-dependent chromatin remodeler Chd1 is recruited by transcription elongation factors and maintains H3K4me3/H3K36me3 domains at actively transcribed and spliced genes. *Nucleic Acids Res* 45, 7180-7190.
- Leonard, J.D., and Narlikar, G.J. (2015). A nucleotide-driven switch regulates flanking DNA length sensing by a dimeric chromatin remodeler. *Mol Cell* 57, 850-859.
- Levendosky, R.F., and Bowman, G.D. (2019). Asymmetry between the two acidic patches dictates the direction of nucleosome sliding by the ISWI chromatin remodeler. *Elife* 8.
- Levendosky, R.F., Sabantsev, A., Deindl, S., and Bowman, G.D. (2016). The Chd1 chromatin remodeler shifts hexasomes unidirectionally. *Elife* 5.
- Li, H., Handsaker, B., Wysoker, A., Fennell, T., Ruan, J., Homer, N., Marth, G., Abecasis, G., Durbin, R., and Genome Project Data Processing, S. (2009). The Sequence Alignment/Map format and SAMtools. *Bioinformatics* 25, 2078-2079.
- Lieberman-Aiden, E., van Berkum, N.L., Williams, L., Imakaev, M., Ragoczy, T., Telling, A., Amit, I., Lajoie, B.R., Sabo, P.J., Dorschner, M.O., *et al.* (2009). Comprehensive mapping of long-range interactions reveals folding principles of the human genome. *Science* 326, 289-293.
- Lieleg, C., Ketterer, P., Nuebler, J., Ludwigsen, J., Gerland, U., Dietz, H., Mueller-Planitz, F., and Korber, P. (2015a). Nucleosome spacing generated by ISWI and CHD1 remodelers is constant regardless of nucleosome density. *Mol Cell Biol* 35, 1588-1605.
- Lieleg, C., Krietenstein, N., Walker, M., and Korber, P. (2015b). Nucleosome positioning in yeasts: methods, maps, and mechanisms. *Chromosoma* 124, 131-151.
- Lipford, J.R., and Bell, S.P. (2001). Nucleosomes Positioned by ORC Facilitate the Initiation of DNA Replication. *Molecular Cell* 7, 21-30.
- Liu, J.C., Ferreira, C.G., and Yusufzai, T. (2015). Human CHD2 is a chromatin assembly ATPase regulated by its chromo- and DNA-binding domains. *J Biol Chem* 290, 25-34.
- Lohr, D., Tatchell, K., and Van Holde, K.E. (1977). On the occurrence of nucleosome phasing in chromatin. *Cell* 12, 829-836.
- Lorch, Y., Maier-Davis, B., and Kornberg, R.D. (2014). Role of DNA sequence in chromatin remodeling and the formation of nucleosome-free regions. *Genes Dev* 28, 2492-2497.

- Lorch, Y., Maier-Davis, B., and Kornberg, R.D. (2018). Histone Acetylation Inhibits RSC and Stabilizes the +1 Nucleosome. *Mol Cell* 72, 594-600 e592.
- Lowary, P.T., and Widom, J. (1998). New DNA sequence rules for high affinity binding to histone octamer and sequence-directed nucleosome positioning. *J Mol Biol* 276, 19-42.
- Lu, Z., and Lin, Z. (2019). Pervasive and dynamic transcription initiation in *Saccharomyces cerevisiae*. *Genome Res* 29, 1198-1210.
- Ludwigsen, J., Klinker, H., and Mueller-Planitz, F. (2013). No need for a power stroke in ISWI-mediated nucleosome sliding. *EMBO Rep* 14, 1092-1097.
- Ludwigsen, J., Pfennig, S., Singh, A.K., Schindler, C., Harrer, N., Forne, I., Zacharias, M., and Mueller-Planitz, F. (2017). Concerted regulation of ISWI by an autoinhibitory domain and the H4 N-terminal tail. *Elife* 6.
- Luger, K., Mader, A.W., Richmond, R.K., Sargent, D.F., and Richmond, T.J. (1997). Crystal structure of the nucleosome core particle at 2.8 Å resolution. *Nature* 389, 251-260.
- Lundin, C., North, M., Erixon, K., Walters, K., Jenssen, D., Goldman, A.S., and Helleday, T. (2005). Methyl methanesulfonate (MMS) produces heat-labile DNA damage but no detectable in vivo DNA double-strand breaks. *Nucleic Acids Res* 33, 3799-3811.
- Luo, Z., and van Vuuren, H.J.J. (2009). Functional analyses of PAU genes in *Saccharomyces cerevisiae*. *Microbiology* 155, 4036-4049.
- Lusser, A., Urwin, D.L., and Kadonaga, J.T. (2005). Distinct activities of CHD1 and ACF in ATP-dependent chromatin assembly. *Nat Struct Mol Biol* 12, 160-166.
- Maeshima, K., Rogge, R., Tamura, S., Joti, Y., Hikima, T., Szerlong, H., Krause, C., Herman, J., Seidel, E., DeLuca, J., *et al.* (2016). Nucleosomal arrays self-assemble into supramolecular globular structures lacking 30-nm fibers. *EMBO J* 35, 1115-1132.
- Maltby, V.E., Martin, B.J., Schulze, J.M., Johnson, I., Hentrich, T., Sharma, A., Kobor, M.S., and Howe, L. (2012). Histone H3 lysine 36 methylation targets the Isw1b remodeling complex to chromatin. *Mol Cell Biol* 32, 3479-3485.
- Mann, R.K., and Grunstein, M. (1992). Histone H3 N-terminal mutations allow hyperactivation of the yeast GAL1 gene in vivo. *EMBO J* 11, 3297-3306.
- Martin, M. (2011). Cutadapt removes adapter sequences from high-throughput sequencing reads. *EMBnet.journal* 17.
- Mattioli, F., Bhattacharyya, S., Dyer, P.N., White, A.E., Sandman, K., Burkhart, B.W., Byrne, K.R., Lee, T., Ahn, N.G., Santangelo, T.J., *et al.* (2017). Structure of histone-based chromatin in Archaea. *Science* 357, 609-612.
- Mavrigh, T.N., Ioshikhes, I.P., Venters, B.J., Jiang, C., Tomsho, L.P., Qi, J., Schuster, S.C., Albert, I., and Pugh, B.F. (2008a). A barrier nucleosome model for statistical positioning of nucleosomes throughout the yeast genome. *Genome Res* 18, 1073-1083.
- Mavrigh, T.N., Jiang, C., Ioshikhes, I.P., Li, X., Venters, B.J., Zanton, S.J., Tomsho, L.P., Qi, J., Glaser, R.L., Schuster, S.C., *et al.* (2008b). Nucleosome organization in the *Drosophila* genome. *Nature* 453, 358-362.
- McConnell, A.D., Gelbart, M.E., and Tsukiyama, T. (2004). Histone fold protein DIs1p is required for Isw2-dependent chromatin remodeling in vivo. *Mol Cell Biol* 24, 2605-2613.

- McKnight, J.N., Jenkins, K.R., Nodelman, I.M., Escobar, T., and Bowman, G.D. (2011). Extranucleosomal DNA binding directs nucleosome sliding by Chd1. *Mol Cell Biol* 31, 4746-4759.
- McMillan, J., Lu, Z., Rodriguez, J.S., Ahn, T.H., and Lin, Z. (2019). YeastTSS: an integrative web database of yeast transcription start sites. *Database (Oxford)* 2019.
- Michael, A.K., Grand, R.S., Isbel, L., Cavadini, S., Kozicka, Z., Kempf, G., Bunker, R.D., Schenk, A.D., Graff-Meyer, A., Pathare, G.R., *et al.* (2020). Mechanisms of OCT4-SOX2 motif readout on nucleosomes. *Science*.
- Michel, A.H., Hatakeyama, R., Kimmig, P., Arter, M., Peter, M., Matos, J., De Virgilio, C., and Kornmann, B. (2017). Functional mapping of yeast genomes by saturated transposition. *Elife* 6.
- Mieczkowski, J., Cook, A., Bowman, S.K., Mueller, B., Alver, B.H., Kundu, S., Deaton, A.M., Urban, J.A., Larschan, E., Park, P.J., *et al.* (2016). MNase titration reveals differences between nucleosome occupancy and chromatin accessibility. *Nat Commun* 7, 11485.
- Milani, P., Chevereau, G., Vaillant, C., Audit, B., Haftek-Terreau, Z., Marilley, M., Bouvet, P., Argoul, F., and Arneodo, A. (2009). Nucleosome positioning by genomic excluding-energy barriers. *Proc Natl Acad Sci U S A* 106, 22257-22262.
- Mischo, H.E., Chun, Y., Harlen, K.M., Smalec, B.M., Dhir, S., Churchman, L.S., and Buratowski, S. (2018). Cell-Cycle Modulation of Transcription Termination Factor Sen1. *Mol Cell* 70, 312-326 e317.
- Mivelaz, M., Cao, A.M., Kubik, S., Zencir, S., Hovius, R., Boichenko, I., Stachowicz, A.M., Kurat, C.F., Shore, D., and Fierz, B. (2020). Chromatin Fiber Invasion and Nucleosome Displacement by the Rap1 Transcription Factor. *Mol Cell* 77, 488-500 e489.
- Mizuguchi, G., Shen, X., Landry, J., Wu, W.H., Sen, S., and Wu, C. (2004). ATP-driven exchange of histone H2AZ variant catalyzed by SWR1 chromatin remodeling complex. *Science* 303, 343-348.
- Mobius, W., and Gerland, U. (2010). Quantitative test of the barrier nucleosome model for statistical positioning of nucleosomes up- and downstream of transcription start sites. *PLoS Comput Biol* 6.
- Mobius, W., Osberg, B., Tsankov, A.M., Rando, O.J., and Gerland, U. (2013). Toward a unified physical model of nucleosome patterns flanking transcription start sites. *Proc Natl Acad Sci U S A* 110, 5719-5724.
- Morillon, A., Karabetsov, N., O'Sullivan, J., Kent, N., Proudfoot, N., and Mellor, J. (2003). Isw1 chromatin remodeling ATPase coordinates transcription elongation and termination by RNA polymerase II. *Cell* 115, 425-435.
- Morohashi, N., Yamamoto, Y., Kuwana, S., Morita, W., Shindo, H., Mitchell, A.P., and Shimizu, M. (2006). Effect of sequence-directed nucleosome disruption on cell-type-specific repression by alpha2/Mcm1 in the yeast genome. *Eukaryot Cell* 5, 1925-1933.
- Morris, J.H., Knudsen, G.M., Verschueren, E., Johnson, J.R., Cimermanic, P., Greninger, A.L., and Pico, A.R. (2014). Affinity purification-mass spectrometry and network analysis to understand protein-protein interactions. *Nat Protoc* 9, 2539-2554.
- Morrison, A.J., Highland, J., Krogan, N.J., Arbel-Eden, A., Greenblatt, J.F., Haber, J.E., and Shen, X. (2004). INO80 and gamma-H2AX interaction links ATP-dependent chromatin remodeling to DNA damage repair. *Cell* 119, 767-775.
- Moyle-Heyrman, G., Zaichuk, T., Xi, L., Zhang, Q., Uhlenbeck, O.C., Holmgren, R., Widom, J., and Wang, J.P. (2013). Chemical map of *Schizosaccharomyces pombe* reveals species-specific features in nucleosome positioning. *Proc Natl Acad Sci U S A* 110, 20158-20163.

- Mueller, J.E., and Bryk, M. (2007). Isw1 acts independently of the Isw1a and Isw1b complexes in regulating transcriptional silencing at the ribosomal DNA locus in *Saccharomyces cerevisiae*. *J Mol Biol* 371, 1-10.
- Mueller-Planitz, F., Klinker, H., and Becker, P.B. (2013a). Nucleosome sliding mechanisms: new twists in a looped history. *Nat Struct Mol Biol* 20, 1026-1032.
- Mueller-Planitz, F., Klinker, H., Ludwigsen, J., and Becker, P.B. (2013b). The ATPase domain of ISWI is an autonomous nucleosome remodeling machine. *Nat Struct Mol Biol* 20, 82-89.
- Murawska, M., Schauer, T., Matsuda, A., Wilson, M.D., Pysik, T., Wojcik, F., Muir, T.W., Hiraoka, Y., Straub, T., and Ladurner, A.G. (2020). The Chaperone FACT and Histone H2B Ubiquitination Maintain *S. pombe* Genome Architecture through Genic and Subtelomeric Functions. *Mol Cell* 77, 501-513 e507.
- Nacev, B.A., Feng, L., Bagert, J.D., Lemiesz, A.E., Gao, J., Soshnev, A.A., Kundra, R., Schultz, N., Muir, T.W., and Allis, C.D. (2019). The expanding landscape of 'oncohistone' mutations in human cancers. *Nature* 567, 473-478.
- Nagai, S., Davis, R.E., Mattei, P.J., Eagen, K.P., and Kornberg, R.D. (2017). Chromatin potentiates transcription. *Proc Natl Acad Sci U S A* 114, 1536-1541.
- Nagarajavel, V., Iben, J.R., Howard, B.H., Maraia, R.J., and Clark, D.J. (2013). Global 'bootprinting' reveals the elastic architecture of the yeast TFIIB-TFIIC transcription complex in vivo. *Nucleic Acids Res* 41, 8135-8143.
- Nishino, Y., Eltsov, M., Joti, Y., Ito, K., Takata, H., Takahashi, Y., Hihara, S., Frangakis, A.S., Imamoto, N., Ishikawa, T., *et al.* (2012). Human mitotic chromosomes consist predominantly of irregularly folded nucleosome fibres without a 30-nm chromatin structure. *EMBO J* 31, 1644-1653.
- Nitiss, J.L. (2009). DNA topoisomerase II and its growing repertoire of biological functions. *Nat Rev Cancer* 9, 327-337.
- Nizovtseva, E.V., Clauvelin, N., Todolli, S., Polikanov, Y.S., Kulaeva, O.I., Wengrzynek, S., Olson, W.K., and Studitsky, V.M. (2017). Nucleosome-free DNA regions differentially affect distant communication in chromatin. *Nucleic Acids Res* 45, 3059-3067.
- Nodelman, I.M., Bleichert, F., Patel, A., Ren, R., Horvath, K.C., Berger, J.M., and Bowman, G.D. (2017). Interdomain Communication of the Chd1 Chromatin Remodeler across the DNA Gyres of the Nucleosome. *Mol Cell* 65, 447-459 e446.
- Noll, M. (1974). Subunit structure of chromatin. *Nature* 251, 249-251.
- Noll, M., Zimmer, S., Engel, A., and Dubochet, J. (1980). Self-assembly of single and closely spaced nucleosome core particles. *Nucleic Acids Res* 8, 21-42.
- Oberbeckmann, E., Niebauer, V., Watanabe, S., Farnung, L., Moldt, M., Schmid, A., Cramer, P., Peterson, C.L., Eustermann, S., Hopfner, K.-P., *et al.* (2020). Ruler elements in chromatin remodelers set nucleosome array spacing and phasing. *bioRxiv*.
- Oberbeckmann, E., Wolff, M., Krietenstein, N., Heron, M., Ellins, J.L., Schmid, A., Krebs, S., Blum, H., Gerland, U., and Korber, P. (2019). Absolute nucleosome occupancy map for the *Saccharomyces cerevisiae* genome. *Genome Res* 29, 1996-2009.
- Oberg, C., Izzo, A., Schneider, R., Wrangé, O., and Belikov, S. (2012). Linker histone subtypes differ in their effect on nucleosomal spacing in vivo. *J Mol Biol* 419, 183-197.
- Ocampo, J., Chereji, R.V., Eriksson, P.R., and Clark, D.J. (2016). The ISW1 and CHD1 ATP-dependent chromatin remodelers compete to set nucleosome spacing in vivo. *Nucleic Acids Res* 44, 4625-4635.

- Ocampo, J., Chereji, R.V., Eriksson, P.R., and Clark, D.J. (2019). Contrasting roles of the RSC and ISW1/CHD1 chromatin remodelers in RNA polymerase II elongation and termination. *Genome Res* 29, 407-417.
- Ou, H.D., Phan, S., Deerinck, T.J., Thor, A., Ellisman, M.H., and O'Shea, C.C. (2017). ChromEMT: Visualizing 3D chromatin structure and compaction in interphase and mitotic cells. *Science* 357.
- Owens, N., Papadopoulou, T., Festuccia, N., Tachtsidi, A., Gonzalez, I., Dubois, A., Vandormael-Pournin, S., Nora, E.P., Bruneau, B.G., Cohen-Tannoudji, M., *et al.* (2019). CTCF confers local nucleosome resiliency after DNA replication and during mitosis. *Elife* 8.
- Paiva, S., Devaux, F., Barbosa, S., Jacq, C., and Casal, M. (2004). Ady2p is essential for the acetate permease activity in the yeast *Saccharomyces cerevisiae*. *Yeast* 21, 201-210.
- Papamichos-Chronakis, M., Krebs, J.E., and Peterson, C.L. (2006). Interplay between Ino80 and Swr1 chromatin remodeling enzymes regulates cell cycle checkpoint adaptation in response to DNA damage. *Genes Dev* 20, 2437-2449.
- Papamichos-Chronakis, M., and Peterson, C.L. (2008). The Ino80 chromatin-remodeling enzyme regulates replisome function and stability. *Nat Struct Mol Biol* 15, 338-345.
- Papamichos-Chronakis, M., Watanabe, S., Rando, O.J., and Peterson, C.L. (2011). Global regulation of H2A.Z localization by the INO80 chromatin-remodeling enzyme is essential for genome integrity. *Cell* 144, 200-213.
- Park, D., Shivram, H., and Iyer, V.R. (2014). Chd1 co-localizes with early transcription elongation factors independently of H3K36 methylation and releases stalled RNA polymerase II at introns. *Epigenetics Chromatin* 7, 32.
- Partensky, P.D., and Narlikar, G.J. (2009). Chromatin remodelers act globally, sequence positions nucleosomes locally. *J Mol Biol* 391, 12-25.
- Patterton, H.G., Landel, C.C., Landsman, D., Peterson, C.L., and Simpson, R.T. (1998). The biochemical and phenotypic characterization of Hho1p, the putative linker histone H1 of *Saccharomyces cerevisiae*. *J Biol Chem* 273, 7268-7276.
- Pearson, E.C., Bates, D.L., Prospero, T.D., and Thomas, J.O. (1984). Neuronal nuclei and glial nuclei from mammalian cerebral cortex. Nucleosome repeat lengths, DNA contents and H1 contents. *Eur J Biochem* 144, 353-360.
- Pinskaya, M., Nair, A., Clynes, D., Morillon, A., and Mellor, J. (2009). Nucleosome remodeling and transcriptional repression are distinct functions of Isw1 in *Saccharomyces cerevisiae*. *Mol Cell Biol* 29, 2419-2430.
- Pointner, J., Persson, J., Prasad, P., Norman-Axelsson, U., Stralfors, A., Khorosjutina, O., Krietenstein, N., Svensson, J.P., Ekwall, K., and Korber, P. (2012). CHD1 remodelers regulate nucleosome spacing in vitro and align nucleosomal arrays over gene coding regions in *S. pombe*. *EMBO J* 31, 4388-4403.
- Poli, J., Gerhold, C.B., Tosi, A., Hustedt, N., Seeber, A., Sack, R., Herzog, F., Pasero, P., Shimada, K., Hopfner, K.P., *et al.* (2016). Mec1, INO80, and the PAF1 complex cooperate to limit transcription replication conflicts through RNAPII removal during replication stress. *Genes Dev* 30, 337-354.
- Poot, R.A., Dellaire, G., Hulsmann, B.B., Grimaldi, M.A., Corona, D.F., Becker, P.B., Bickmore, W.A., and Varga-Weisz, P.D. (2000). HuCHRAC, a human ISWI chromatin remodelling complex contains hACF1 and two novel histone-fold proteins. *EMBO J* 19, 3377-3387.
- Puig, S., Matallana, E., and Perez-Ortin, J.E. (1999). Stochastic nucleosome positioning in a yeast chromatin region is not dependent on histone H1. *Curr Microbiol* 39, 168-172.

- Qiu, Y., Levandosky, R.F., Chakravarthy, S., Patel, A., Bowman, G.D., and Myong, S. (2017). The Chd1 Chromatin Remodeler Shifts Nucleosomal DNA Bidirectionally as a Monomer. *Mol Cell* **68**, 76-88 e76.
- Racki, L.R., Yang, J.G., Naber, N., Partensky, P.D., Acevedo, A., Purcell, T.J., Cooke, R., Cheng, Y., and Narlikar, G.J. (2009). The chromatin remodeller ACF acts as a dimeric motor to space nucleosomes. *Nature* **462**, 1016-1021.
- Raiber, E.A., Portella, G., Martinez Cuesta, S., Hardisty, R., Murat, P., Li, Z., Iurlaro, M., Dean, W., Spindel, J., Beraldi, D., *et al.* (2018). 5-Formylcytosine organizes nucleosomes and forms Schiff base interactions with histones in mouse embryonic stem cells. *Nat Chem* **10**, 1258-1266.
- Raisner, R.M., Hartley, P.D., Meneghini, M.D., Bao, M.Z., Liu, C.L., Schreiber, S.L., Rando, O.J., and Madhani, H.D. (2005). Histone variant H2A.Z marks the 5' ends of both active and inactive genes in euchromatin. *Cell* **123**, 233-248.
- Raudvere, U., Kolberg, L., Kuzmin, I., Arak, T., Adler, P., Peterson, H., and Vilo, J. (2019). g:Profiler: a web server for functional enrichment analysis and conversions of gene lists (2019 update). *Nucleic Acids Res* **47**, W191-W198.
- Ravindra, A., Weiss, K., and Simpson, R.T. (1999). High-resolution structural analysis of chromatin at specific loci: *Saccharomyces cerevisiae* silent mating-type locus HMRA. *Mol Cell Biol* **19**, 7944-7950.
- Rawal, Y., Chereji, R.V., Qiu, H., Ananthkrishnan, S., Govind, C.K., Clark, D.J., and Hinnebusch, A.G. (2018). SWI/SNF and RSC cooperate to reposition and evict promoter nucleosomes at highly expressed genes in yeast. *Genes Dev* **32**, 695-710.
- Rhodes, D. (1979). Nucleosome cores reconstituted from poly (dA-dT) and the octamer of histones. *Nucleic Acids Res* **6**, 1805-1816.
- Ricci, M.A., Manzo, C., Garcia-Parajo, M.F., Lakadamyali, M., and Cosma, M.P. (2015). Chromatin fibers are formed by heterogeneous groups of nucleosomes in vivo. *Cell* **160**, 1145-1158.
- Richmond, T.J. (2012). Nucleosome recognition and spacing by chromatin remodelling factor ISW1a. *Biochem Soc Trans* **40**, 347-350.
- Rippe, K., Schrader, A., Riede, P., Strohner, R., Lehmann, E., and Langst, G. (2007). DNA sequence- and conformation-directed positioning of nucleosomes by chromatin-remodeling complexes. *Proc Natl Acad Sci U S A* **104**, 15635-15640.
- Risca, V.I., Denny, S.K., Straight, A.F., and Greenleaf, W.J. (2017). Variable chromatin structure revealed by in situ spatially correlated DNA cleavage mapping. *Nature* **541**, 237-241.
- Robinson, J.T., Thorvaldsdottir, H., Winckler, W., Guttman, M., Lander, E.S., Getz, G., and Mesirov, J.P. (2011). Integrative genomics viewer. *Nat Biotechnol* **29**, 24-26.
- Robinson, P.J., Fairall, L., Huynh, V.A., and Rhodes, D. (2006). EM measurements define the dimensions of the "30-nm" chromatin fiber: evidence for a compact, interdigitated structure. *Proc Natl Acad Sci U S A* **103**, 6506-6511.
- Routh, A., Sandin, S., and Rhodes, D. (2008). Nucleosome repeat length and linker histone stoichiometry determine chromatin fiber structure. *Proc Natl Acad Sci U S A* **105**, 8872-8877.
- Rube, H.T., and Song, J.S. (2014). Quantifying the role of steric constraints in nucleosome positioning. *Nucleic Acids Res* **42**, 2147-2158.
- Rubtsov, M.A., Polikanov, Y.S., Bondarenko, V.A., Wang, Y.H., and Studitsky, V.M. (2006). Chromatin structure can strongly facilitate enhancer action over a distance. *Proc Natl Acad Sci U S A* **103**, 17690-17695.

- Ruiz, C., Escribano, V., Morgado, E., Molina, M., and Mazon, M.J. (2003). Cell-type-dependent repression of yeast α -specific genes requires Itc1p, a subunit of the Isw2p-Itc1p chromatin remodelling complex. *Microbiology* *149*, 341-351.
- Ryan, D.P., Sundaramoorthy, R., Martin, D., Singh, V., and Owen-Hughes, T. (2011). The DNA-binding domain of the Chd1 chromatin-remodelling enzyme contains SANT and SLIDE domains. *EMBO J* *30*, 2596-2609.
- Sabantsev, A., Levendosky, R.F., Zhuang, X., Bowman, G.D., and Deindl, S. (2019). Direct observation of coordinated DNA movements on the nucleosome during chromatin remodelling. *Nat Commun* *10*, 1720.
- Sanchez-Molina, S., Mortusewicz, O., Bieber, B., Auer, S., Eckey, M., Leonhardt, H., Friedl, A.A., and Becker, P.B. (2011). Role for hACF1 in the G2/M damage checkpoint. *Nucleic Acids Res* *39*, 8445-8456.
- Santos-Rosa, H., Schneider, R., Bernstein, B.E., Karabetsou, N., Morillon, A., Weise, C., Schreiber, S.L., Mellor, J., and Kouzarides, T. (2018). Methylation of Histone H3 K4 Mediates Association of the Isw1p ATPase with Chromatin. *Mol Cell* *70*, 983.
- Saravanan, M., Wuerges, J., Bose, D., McCormack, E.A., Cook, N.J., Zhang, X., and Wigley, D.B. (2012). Interactions between the nucleosome histone core and Arp8 in the INO80 chromatin remodeling complex. *Proc Natl Acad Sci U S A* *109*, 20883-20888.
- Sardiu, M.E., Gilmore, J.M., Groppe, B., Florens, L., and Washburn, M.P. (2017). Identification of Topological Network Modules in Perturbed Protein Interaction Networks. *Sci Rep* *7*, 43845.
- Satchwell, S.C., Drew, H.R., and Travers, A.A. (1986). Sequence periodicities in chicken nucleosome core DNA. *J Mol Biol* *191*, 659-675.
- Scacchetti, A., Brueckner, L., Jain, D., Schauer, T., Zhang, X., Schnorrer, F., van Steensel, B., Straub, T., and Becker, P.B. (2018). CHRAC/ACF contribute to the repressive ground state of chromatin. *Life Sci Alliance* *1*, e201800024.
- Schalch, T., Duda, S., Sargent, D.F., and Richmond, T.J. (2005). X-ray structure of a tetranucleosome and its implications for the chromatin fibre. *Nature* *436*, 138-141.
- Schep, A.N., Buenrostro, J.D., Denny, S.K., Schwartz, K., Sherlock, G., and Greenleaf, W.J. (2015). Structured nucleosome fingerprints enable high-resolution mapping of chromatin architecture within regulatory regions. *Genome Res* *25*, 1757-1770.
- Schmieder, R., and Edwards, R. (2011). Quality control and preprocessing of metagenomic datasets. *Bioinformatics* *27*, 863-864.
- Schones, D.E., Cui, K., Cuddapah, S., Roh, T.Y., Barski, A., Wang, Z., Wei, G., and Zhao, K. (2008). Dynamic regulation of nucleosome positioning in the human genome. *Cell* *132*, 887-898.
- Schwabish, M.A., and Struhl, K. (2007). The Swi/Snf complex is important for histone eviction during transcriptional activation and RNA polymerase II elongation in vivo. *Mol Cell Biol* *27*, 6987-6995.
- Schwarz, M., Schall, K., Kallis, E., Eustermann, S., Guariento, M., Moldt, M., Hopfner, K.P., and Michaelis, J. (2018). Single-molecule nucleosome remodeling by INO80 and effects of histone tails. *FEBS Lett* *592*, 318-331.
- Seeber, A., Dion, V., and Gasser, S.M. (2013). Checkpoint kinases and the INO80 nucleosome remodeling complex enhance global chromatin mobility in response to DNA damage. *Genes Dev* *27*, 1999-2008.
- Segal, E., Fondufe-Mittendorf, Y., Chen, L., Thastrom, A., Field, Y., Moore, I.K., Wang, J.P., and Widom, J. (2006). A genomic code for nucleosome positioning. *Nature* *442*, 772-778.

- Sekinger, E.A., Moqtaderi, Z., and Struhl, K. (2005). Intrinsic histone-DNA interactions and low nucleosome density are important for preferential accessibility of promoter regions in yeast. *Mol Cell* *18*, 735-748.
- Shen, X., Mizuguchi, G., Hamiche, A., and Wu, C. (2000). A chromatin remodelling complex involved in transcription and DNA processing. *Nature* *406*, 541-544.
- Shen, X., Ranallo, R., Choi, E., and Wu, C. (2003). Involvement of Actin-Related Proteins in ATP-Dependent Chromatin Remodeling. *Molecular Cell* *12*, 147-155.
- Shevchenko, A., Tomas, H., Havlis, J., Olsen, J.V., and Mann, M. (2006). In-gel digestion for mass spectrometric characterization of proteins and proteomes. *Nat Protoc* *1*, 2856-2860.
- Shim, Y.S., Choi, Y., Kang, K., Cho, K., Oh, S., Lee, J., Grewal, S.I., and Lee, D. (2012). Hrp3 controls nucleosome positioning to suppress non-coding transcription in eu- and heterochromatin. *EMBO J* *31*, 4375-4387.
- Shimada, K., Oma, Y., Schleker, T., Kugou, K., Ohta, K., Harata, M., and Gasser, S.M. (2008). Ino80 chromatin remodeling complex promotes recovery of stalled replication forks. *Curr Biol* *18*, 566-575.
- Shimizu, M., Roth, S.Y., Szent-Gyorgyi, C., and Simpson, R.T. (1991). Nucleosomes are positioned with base pair precision adjacent to the alpha 2 operator in *Saccharomyces cerevisiae*. *EMBO J* *10*, 3033-3041.
- Shipony, Z., Marinov, G.K., Swaffer, M.P., Sinnott-Armstrong, N.A., Skotheim, J.M., Kundaje, A., and Greenleaf, W.J. (2020). Long-range single-molecule mapping of chromatin accessibility in eukaryotes. *Nat Methods* *17*, 319-327.
- Shivaswamy, S., Bhinge, A., Zhao, Y., Jones, S., Hirst, M., and Iyer, V.R. (2008). Dynamic remodeling of individual nucleosomes across a eukaryotic genome in response to transcriptional perturbation. *PLoS Biol* *6*, e65.
- Sikorski, R.S., and Hieter, P. (1989). A system of shuttle vectors and yeast host strains designed for efficient manipulation of DNA in *Saccharomyces cerevisiae*. *Genetics* *122*, 19-27.
- Silberhorn, E., Schwartz, U., Loffler, P., Schmitz, S., Symelka, A., de Koning-Ward, T., Merkl, R., and Langst, G. (2016). *Plasmodium falciparum* Nucleosomes Exhibit Reduced Stability and Lost Sequence Dependent Nucleosome Positioning. *PLoS Pathog* *12*, e1006080.
- Simic, R., Lindstrom, D.L., Tran, H.G., Roinick, K.L., Costa, P.J., Johnson, A.D., Hartzog, G.A., and Arndt, K.M. (2003). Chromatin remodeling protein Chd1 interacts with transcription elongation factors and localizes to transcribed genes. *EMBO J* *22*, 1846-1856.
- Simpson, R.T., and Kunzler, P. (1979). Chromatin and core particles formed from the inner histones and synthetic polydeoxyribonucleotides of defined sequence. *Nucleic Acids Res* *6*, 1387-1415.
- Sims, R.J., 3rd, Chen, C.F., Santos-Rosa, H., Kouzarides, T., Patel, S.S., and Reinberg, D. (2005). Human but not yeast CHD1 binds directly and selectively to histone H3 methylated at lysine 4 via its tandem chromodomains. *J Biol Chem* *280*, 41789-41792.
- Skene, P.J., Hernandez, A.E., Groudine, M., and Henikoff, S. (2014). The nucleosomal barrier to promoter escape by RNA polymerase II is overcome by the chromatin remodeler Chd1. *Elife* *3*, e02042.
- Small, E.C., Xi, L., Wang, J.P., Widom, J., and Licht, J.D. (2014). Single-cell nucleosome mapping reveals the molecular basis of gene expression heterogeneity. *Proc Natl Acad Sci U S A* *111*, E2462-2471.
- Smolle, M., Venkatesh, S., Gogol, M.M., Li, H., Zhang, Y., Florens, L., Washburn, M.P., and Workman, J.L. (2012). Chromatin remodelers Isw1 and Chd1 maintain chromatin structure during transcription by preventing histone exchange. *Nat Struct Mol Biol* *19*, 884-892.

- Smolle, M., Workman, J.L., and Venkatesh, S. (2013). reSETting chromatin during transcription elongation. *Epigenetics* 8, 10-15.
- Song, F., Chen, P., Sun, D., Wang, M., Dong, L., Liang, D., Xu, R.M., Zhu, P., and Li, G. (2014). Cryo-EM study of the chromatin fiber reveals a double helix twisted by tetranucleosomal units. *Science* 344, 376-380.
- Soriano, I., Morafraila, E.C., Vazquez, E., Antequera, F., and Segurado, M. (2014). Different nucleosomal architectures at early and late replicating origins in *Saccharomyces cerevisiae*. *BMC Genomics* 15, 791.
- Soudet, J., Gill, J.K., and Stutz, F. (2018). Noncoding transcription influences the replication initiation program through chromatin regulation. *Genome Res* 28, 1882-1893.
- Soushko, M., and Mitchell, A.P. (2000). An RNA-binding protein homologue that promotes sporulation-specific gene expression in *Saccharomyces cerevisiae*. *Yeast* 16, 631-639.
- Soutourina, J., Bordas-Le Floch, V., Gendrel, G., Flores, A., Ducrot, C., Dumay-Odelot, H., Soularue, P., Navarro, F., Cairns, B.R., Lefebvre, O., *et al.* (2006). Rsc4 connects the chromatin remodeler RSC to RNA polymerases. *Mol Cell Biol* 26, 4920-4933.
- Steinmetz, M., Streeck, R.E., and Zachau, H.G. (1978). Closely spaced nucleosome cores in reconstituted histone-DNA complexes and histone-H1-depleted chromatin. *Eur J Biochem* 83, 615-628.
- Stergachis, A.B., Debo, B.M., Haugen, E., Churchman, L.S., and Stamatoyannopoulos, J.A. (2020). Single-molecule regulatory architectures captured by chromatin fiber sequencing. *Science* 368, 1449-1454.
- Stewart-Morgan, K.R., Reveron-Gomez, N., and Groth, A. (2019). Transcription Restart Establishes Chromatin Accessibility after DNA Replication. *Mol Cell* 75, 284-297 e286.
- Stockdale, C., Flaus, A., Ferreira, H., and Owen-Hughes, T. (2006). Analysis of nucleosome repositioning by yeast ISWI and Chd1 chromatin remodeling complexes. *J Biol Chem* 281, 16279-16288.
- Stoddard, C.I., Feng, S., Campbell, M.G., Liu, W., Wang, H., Zhong, X., Bernatavichute, Y., Cheng, Y., Jacobsen, S.E., and Narlikar, G.J. (2019). A Nucleosome Bridging Mechanism for Activation of a Maintenance DNA Methyltransferase. *Mol Cell* 73, 73-83 e76.
- Struhl, K., and Segal, E. (2013). Determinants of nucleosome positioning. *Nat Struct Mol Biol* 20, 267-273.
- Sugiyama, M., and Nikawa, J. (2001). The *Saccharomyces cerevisiae* Isw2p-Itc1p complex represses INO1 expression and maintains cell morphology. *J Bacteriol* 183, 4985-4993.
- Sun, L., Pierrakeas, L., Li, T., and Luk, E. (2020). Thermosensitive Nucleosome Editing Reveals the Role of DNA Sequence in Targeted Histone Variant Deposition. *Cell Rep* 30, 257-268 e255.
- Sundaramoorthy, R., Hughes, A.L., El-Mkami, H., Norman, D.G., Ferreira, H., and Owen-Hughes, T. (2018). Structure of the chromatin remodelling enzyme Chd1 bound to a ubiquitylated nucleosome. *Elife* 7.
- Sundaramoorthy, R., Hughes, A.L., Singh, V., Wiechens, N., Ryan, D.P., El-Mkami, H., Petoukhov, M., Svergun, D.I., Treutlein, B., Quack, S., *et al.* (2017). Structural reorganization of the chromatin remodeling enzyme Chd1 upon engagement with nucleosomes. *Elife* 6.
- Talbert, P.B., and Henikoff, S. (2010). Histone variants--ancient wrap artists of the epigenome. *Nat Rev Mol Cell Biol* 11, 264-275.

- Teng, Y., Yu, S., and Waters, R. (2001). The mapping of nucleosomes and regulatory protein binding sites at the *Saccharomyces cerevisiae* MFA2 gene: a high resolution approach. *Nucleic Acids Res* 29, E64-64.
- Tirosh, I., Sigal, N., and Barkai, N. (2010). Widespread remodeling of mid-coding sequence nucleosomes by *Isw1*. *Genome Biol* 11, R49.
- Topal, S., Vasseur, P., Radman-Livaja, M., and Peterson, C.L. (2019). Distinct transcriptional roles for Histone H3-K56 acetylation during the cell cycle in Yeast. *Nat Commun* 10, 4372.
- Torigoe, S.E., Patel, A., Khuong, M.T., Bowman, G.D., and Kadonaga, J.T. (2013). ATP-dependent chromatin assembly is functionally distinct from chromatin remodeling. *Elife* 2, e00863.
- Tosi, A., Haas, C., Herzog, F., Gilmozzi, A., Berninghausen, O., Ungewickell, C., Gerhold, C.B., Lakomek, K., Aebersold, R., Beckmann, R., *et al.* (2013). Structure and subunit topology of the INO80 chromatin remodeler and its nucleosome complex. *Cell* 154, 1207-1219.
- Trachtulcova, P., Frydlova, I., Janatova, I., and Hasek, J. (2004). The absence of the *Isw2p-Itc1p* chromatin-remodelling complex induces mating type-specific and *Flo11p*-independent invasive growth of *Saccharomyces cerevisiae*. *Yeast* 21, 389-401.
- Tramantano, M., Sun, L., Au, C., Labuz, D., Liu, Z., Chou, M., Shen, C., and Luk, E. (2016). Constitutive turnover of histone H2A.Z at yeast promoters requires the preinitiation complex. *Elife* 5.
- Travers, A., Hiriart, E., Churcher, M., Caserta, M., and Di Mauro, E. (2010). The DNA sequence-dependence of nucleosome positioning in vivo and in vitro. *J Biomol Struct Dyn* 27, 713-724.
- Truong, D.M., and Boeke, J.D. (2017). Resetting the Yeast Epigenome with Human Nucleosomes. *Cell* 171, 1508-1519 e1513.
- Tsankov, A., Yanagisawa, Y., Rhind, N., Regev, A., and Rando, O.J. (2011). Evolutionary divergence of intrinsic and trans-regulated nucleosome positioning sequences reveals plastic rules for chromatin organization. *Genome Res* 21, 1851-1862.
- Tsukiyama, T., Daniel, C., Tamkun, J., and Wu, C. (1995). ISWI, a member of the SWI2/SNF2 ATPase family, encodes the 140 kDa subunit of the nucleosome remodeling factor. *Cell* 83, 1021-1026.
- Tsukiyama, T., Palmer, J., Landel, C.C., Shiloach, J., and Wu, C. (1999). Characterization of the imitation switch subfamily of ATP-dependent chromatin-remodeling factors in *Saccharomyces cerevisiae*. *Genes Dev* 13, 686-697.
- Udugama, M., Sabri, A., and Bartholomew, B. (2011). The INO80 ATP-dependent chromatin remodeling complex is a nucleosome spacing factor. *Mol Cell Biol* 31, 662-673.
- Valouev, A., Johnson, S.M., Boyd, S.D., Smith, C.L., Fire, A.Z., and Sidow, A. (2011). Determinants of nucleosome organization in primary human cells. *Nature* 474, 516-520.
- van Attikum, H., Fritsch, O., Hohn, B., and Gasser, S.M. (2004). Recruitment of the INO80 complex by H2A phosphorylation links ATP-dependent chromatin remodeling with DNA double-strand break repair. *Cell* 119, 777-788.
- van Bakel, H., Tsui, K., Gebbia, M., Mnaimneh, S., Hughes, T.R., and Nislow, C. (2013). A compendium of nucleosome and transcript profiles reveals determinants of chromatin architecture and transcription. *PLoS Genet* 9, e1003479.
- Vary, J.C., Jr., Gangaraju, V.K., Qin, J., Landel, C.C., Kooperberg, C., Bartholomew, B., and Tsukiyama, T. (2003). Yeast *Isw1p* forms two separable complexes in vivo. *Mol Cell Biol* 23, 80-91.

- Vasicova, P., Stradalova, V., Halada, P., Hasek, J., and Malcova, I. (2013). Nuclear import of chromatin remodeler Isw1 is mediated by atypical bipartite cNLS and classical import pathway. *Traffic* *14*, 176-193.
- Vasseur, P., Tonazzini, S., Ziane, R., Camasses, A., Rando, O.J., and Radman-Livaja, M. (2016). Dynamics of Nucleosome Positioning Maturation following Genomic Replication. *Cell Rep* *16*, 2651-2665.
- Venkatesh, S., and Workman, J.L. (2015). Histone exchange, chromatin structure and the regulation of transcription. *Nat Rev Mol Cell Biol* *16*, 178-189.
- Vincent, J.A., Kwong, T.J., and Tsukiyama, T. (2008). ATP-dependent chromatin remodeling shapes the DNA replication landscape. *Nat Struct Mol Biol* *15*, 477-484.
- Viswanathan, M., Muthukumar, G., Cong, Y.-S., and Lenard, J. (1994). Seripauperins of *Saccharomyces cerevisiae*: a new multigene family encoding serine-poor relatives of serine-rich proteins. *Gene* *148*, 149-153.
- Voong, L.N., Xi, L., Sebeson, A.C., Xiong, B., Wang, J.P., and Wang, X. (2016). Insights into Nucleosome Organization in Mouse Embryonic Stem Cells through Chemical Mapping. *Cell* *167*, 1555-1570 e1515.
- Wagner, F.R., Dienemann, C., Wang, H., Stützer, A., Tegunov, D., Urlaub, H., and Cramer, P. (2020). Structure of SWI/SNF chromatin remodeller RSC bound to a nucleosome. *Nature*.
- Wal, M., and Pugh, B.F. (2012). Genome-wide mapping of nucleosome positions in yeast using high-resolution MNase ChIP-Seq. *Methods Enzymol* *513*, 233-250.
- Wang, J., Gao, S., Peng, X., Wu, K., and Yang, S. (2019a). Roles of the INO80 and SWR1 Chromatin Remodeling Complexes in Plants. *Int J Mol Sci* *20*.
- Wang, J., Zhuang, J., Iyer, S., Lin, X., Whitfield, T.W., Greven, M.C., Pierce, B.G., Dong, X., Kundaje, A., Cheng, Y., *et al.* (2012). Sequence features and chromatin structure around the genomic regions bound by 119 human transcription factors. *Genome Res* *22*, 1798-1812.
- Wang, Y., Wang, A., Liu, Z., Thurman, A.L., Powers, L.S., Zou, M., Zhao, Y., Hefel, A., Li, Y., Zabner, J., *et al.* (2019b). Single-molecule long-read sequencing reveals the chromatin basis of gene expression. *Genome Res* *29*, 1329-1342.
- Watanabe, S., Tan, D., Lakshminarasimhan, M., Washburn, M.P., Hong, E.J., Walz, T., and Peterson, C.L. (2015). Structural analyses of the chromatin remodelling enzymes INO80-C and SWR-C. *Nat Commun* *6*, 7108.
- Weber, C.M., Ramachandran, S., and Henikoff, S. (2014). Nucleosomes are context-specific, H2A.Z-modulated barriers to RNA polymerase. *Mol Cell* *53*, 819-830.
- Wedel, C., Forstner, K.U., Derr, R., and Siegel, T.N. (2017). GT-rich promoters can drive RNA pol II transcription and deposition of H2A.Z in African trypanosomes. *EMBO J* *36*, 2581-2594.
- Weiner, A., Hughes, A., Yassour, M., Rando, O.J., and Friedman, N. (2010). High-resolution nucleosome mapping reveals transcription-dependent promoter packaging. *Genome Res* *20*, 90-100.
- Weiss, K., and Simpson, R.T. (1997). Cell type-specific chromatin organization of the region that governs directionality of yeast mating type switching. *EMBO J* *16*, 4352-4360.
- Weiss, K., and Simpson, R.T. (1998). High-resolution structural analysis of chromatin at specific loci: *Saccharomyces cerevisiae* silent mating type locus HML α . *Mol Cell Biol* *18*, 5392-5403.

- Whitehouse, I., Rando, O.J., Delrow, J., and Tsukiyama, T. (2007). Chromatin remodelling at promoters suppresses antisense transcription. *Nature* **450**, 1031-1035.
- Wiechens, N., Singh, V., Gkikopoulos, T., Schofield, P., Rocha, S., and Owen-Hughes, T. (2016). The Chromatin Remodelling Enzymes SNF2H and SNF2L Position Nucleosomes adjacent to CTCF and Other Transcription Factors. *PLoS Genet* **12**, e1005940.
- Willhoft, O., Bythell-Douglas, R., McCormack, E.A., and Wigley, D.B. (2016). Synergy and antagonism in regulation of recombinant human INO80 chromatin remodeling complex. *Nucleic Acids Res* **44**, 8179-8188.
- Willhoft, O., McCormack, E.A., Aramayo, R.J., Bythell-Douglas, R., Ocloo, L., Zhang, X., and Wigley, D.B. (2017). Crosstalk within a functional INO80 complex dimer regulates nucleosome sliding. *Elife* **6**.
- Winger, J., and Bowman, G.D. (2017). The Sequence of Nucleosomal DNA Modulates Sliding by the Chd1 Chromatin Remodeler. *J Mol Biol* **429**, 808-822.
- Winger, J., Nodelman, I.M., Levendosky, R.F., and Bowman, G.D. (2018). A twist defect mechanism for ATP-dependent translocation of nucleosomal DNA. *Elife* **7**.
- Wittschieben, B.O., Fellows, J., Du, W., Stillman, D.J., and Svejstrup, J.Q. (2000). Overlapping roles for the histone acetyltransferase activities of SAGA and elongator in vivo. *EMBO J* **19**, 3060-3068.
- Woodcock, C.L., Frado, L.L., and Rattner, J.B. (1984). The higher-order structure of chromatin: evidence for a helical ribbon arrangement. *J Cell Biol* **99**, 42-52.
- Woodcock, C.L., Skoultchi, A.I., and Fan, Y. (2006). Role of linker histone in chromatin structure and function: H1 stoichiometry and nucleosome repeat length. *Chromosome Res* **14**, 17-25.
- Wu, A.C.K., Patel, H., Chia, M., Moretto, F., Frith, D., Snijders, A.P., and van Werven, F.J. (2018). Repression of Divergent Noncoding Transcription by a Sequence-Specific Transcription Factor. *Mol Cell* **72**, 942-954 e947.
- Yadav, T., and Whitehouse, I. (2016). Replication-Coupled Nucleosome Assembly and Positioning by ATP-Dependent Chromatin-Remodeling Enzymes. *Cell Rep* **15**, 715-723.
- Yadon, A.N., Singh, B.N., Hampsey, M., and Tsukiyama, T. (2013). DNA looping facilitates targeting of a chromatin remodeling enzyme. *Mol Cell* **50**, 93-103.
- Yadon, A.N., and Tsukiyama, T. (2013). DNA looping-dependent targeting of a chromatin remodeling factor. *Cell Cycle* **12**, 1809-1810.
- Yamada, K., Frouws, T.D., Angst, B., Fitzgerald, D.J., DeLuca, C., Schimmele, K., Sargent, D.F., and Richmond, T.J. (2011). Structure and mechanism of the chromatin remodelling factor ISW1a. *Nature* **472**, 448-453.
- Yan, L., Wang, L., Tian, Y., Xia, X., and Chen, Z. (2016). Structure and regulation of the chromatin remodeller ISWI. *Nature* **540**, 466-469.
- Yan, L., Wu, H., Li, X., Gao, N., and Chen, Z. (2019). Structures of the ISWI-nucleosome complex reveal a conserved mechanism of chromatin remodeling. *Nat Struct Mol Biol* **26**, 258-266.
- Yang, J.G., Madrid, T.S., Sevastopoulos, E., and Narlikar, G.J. (2006). The chromatin-remodeling enzyme ACF is an ATP-dependent DNA length sensor that regulates nucleosome spacing. *Nat Struct Mol Biol* **13**, 1078-1083.
- Yao, W., Beckwith, S.L., Zheng, T., Young, T., Dinh, V.T., Ranjan, A., and Morrison, A.J. (2015). Assembly of the Arp5 (Actin-related Protein) Subunit Involved in Distinct INO80 Chromatin Remodeling Activities. *J Biol Chem* **290**, 25700-25709.

- Yao, W., King, D.A., Beckwith, S.L., Gowans, G.J., Yen, K., Zhou, C., and Morrison, A.J. (2016). The INO80 Complex Requires the Arp5-les6 Subcomplex for Chromatin Remodeling and Metabolic Regulation. *Mol Cell Biol* 36, 979-991.
- Ye, Y., Wu, H., Chen, K., Clapier, C.R., Verma, N., Zhang, W., Deng, H., Cairns, B.R., Gao, N., and Chen, Z. (2019). Structure of the RSC complex bound to the nucleosome. *Science* 366, 838-843.
- Yen, K., Vinayachandran, V., Batta, K., Koerber, R.T., and Pugh, B.F. (2012). Genome-wide nucleosome specificity and directionality of chromatin remodelers. *Cell* 149, 1461-1473.
- Yen, K., Vinayachandran, V., and Pugh, B.F. (2013). SWR-C and INO80 chromatin remodelers recognize nucleosome-free regions near +1 nucleosomes. *Cell* 154, 1246-1256.
- Yuan, G.C., Liu, Y.J., Dion, M.F., Slack, M.D., Wu, L.F., Altschuler, S.J., and Rando, O.J. (2005). Genome-scale identification of nucleosome positions in *S. cerevisiae*. *Science* 309, 626-630.
- Zentner, G.E., Tsukiyama, T., and Henikoff, S. (2013). ISWI and CHD chromatin remodelers bind promoters but act in gene bodies. *PLoS Genet* 9, e1003317.
- Zhang, W., Bone, J.R., Edmondson, D.G., Turner, B.M., and Roth, S.Y. (1998). Essential and redundant functions of histone acetylation revealed by mutation of target lysines and loss of the Gcn5p acetyltransferase. *EMBO J* 17, 3155-3167.
- Zhang, X., Wang, X., Zhang, Z., and Cai, G. (2019). Structure and functional interactions of INO80 actin/Arp module. *J Mol Cell Biol* 11, 345-355.
- Zhang, Y., Moqtaderi, Z., Rattner, B.P., Euskirchen, G., Snyder, M., Kadonaga, J.T., Liu, X.S., and Struhl, K. (2009). Intrinsic histone-DNA interactions are not the major determinant of nucleosome positions in vivo. *Nat Struct Mol Biol* 16, 847-852.
- Zhang, Y., Vastenhouw, N.L., Feng, J., Fu, K., Wang, C., Ge, Y., Pauli, A., van Hummelen, P., Schier, A.F., and Liu, X.S. (2014). Canonical nucleosome organization at promoters forms during genome activation. *Genome Res* 24, 260-266.
- Zhang, Z., and Reese, J.C. (2004). Ssn6-Tup1 requires the ISW2 complex to position nucleosomes in *Saccharomyces cerevisiae*. *EMBO J* 23, 2246-2257.
- Zhang, Z., Wippo, C.J., Wal, M., Ward, E., Korber, P., and Pugh, B.F. (2011). A packing mechanism for nucleosome organization reconstituted across a eukaryotic genome. *Science* 332, 977-980.
- Zhou, C.Y., Johnson, S.L., Lee, L.J., Longhurst, A.D., Beckwith, S.L., Johnson, M.J., Morrison, A.J., and Narlikar, G.J. (2018). The Yeast INO80 Complex Operates as a Tunable DNA Length-Sensitive Switch to Regulate Nucleosome Sliding. *Mol Cell* 69, 677-688 e679.
- Zhou, J., Fan, J.Y., Rangasamy, D., and Tremethick, D.J. (2007). The nucleosome surface regulates chromatin compaction and couples it with transcriptional repression. *Nat Struct Mol Biol* 14, 1070-1076.
- Zofall, M., Persinger, J., Kassabov, S.R., and Bartholomew, B. (2006). Chromatin remodeling by ISW2 and SWI/SNF requires DNA translocation inside the nucleosome. *Nat Struct Mol Biol* 13, 339-346.

6. APPENDIX

6.1 List of genes responding at the +1-nucleosome in ISW2 remodeler mutants

List of genes showing a shift in the +1-nucleosome position by at least 10 base pairs in *isw2Δ*, *itc1Δ*, and *itc1^{ΔN}* cells compared to WT. Two biological replicates in the mat a background were considered for this analysis. Mat α replicate was excluded to avoid genes responding in a cell-type specific manner. Cell-type specific genes are listed in Appendix 6.2. Last 9 genes (bold) in the column *itc1^{ΔN}* unique show an upstream +1-nucleosome shift while others show a downstream shift.

<i>isw2Δ</i> , <i>itc1Δ</i> and <i>itc1^{ΔN}</i> common	<i>isw2Δ</i> and <i>itc1Δ</i> common	<i>itc1^{ΔN}</i> unique	<i>isw2Δ</i> unique	<i>itc1Δ</i> unique
YBR085W	YBR038W	YGL248W	YGL133W	YDL022W
YBR297W	YHR137W	YJR130C		YER073W
YDL154W	YIL015W	YHR179W		YBR082C
YDL085W	YJL089W	YGL105W		YOL052C
YDR317W	YJR015W	YHR183W		YOR099W
YDR536W	YLR056W	YOL030W		YAL002W
YER070W	YNR008W	YPL226W		YDR389W
YER095W	YPR071W	YPL131W		
YER096W	YPR119W	YBL088C		
YFL014W	YBL030C	YBR172C		
YFR036W	YBR105C	YBR196C		
YGL039W	YBR177C	YBR245C		
YGR199W	YDR277C	YDR046C		
YHR048W	YER062C	YER036C		
YHR124W	YER137C	YFL045C		
YIL122W	YIR034C	YFL044C		
YIL099W	YJL200C	YFR050C		
YIL072W	YLL046C	YGL056C		
YJL214W	YLR054C	YGR159C		
YJL194W	YNL144C	YHR131C		
YJL159W	YNL058C	YJR016C		
YJL088W	YOL136C	YLR398C		
YJL051W	YOR058C	YNR050C		
YJR092W	YPL112C	YPL199C		
YJR095W	YLR438W	YPR029C		
YPL274W	YPR071W	YPR133C		
YPL200W	YPR119W	YIL121W		
YPL189W	YBL030C	YBR096W		
YPL104W	YBR105C	YGL255W		
YPR009W	YBR177C	YGL220W		
YPR026W	YDR277C	YIL111W		
YPR030W	YER062C	YPL061W		
YAL054C	YER137C	YPR001W		
YBR014C	YIR034C			
YBR182C	YJL200C			
YBR296C	YLL046C			
YCR045C	YLR054C			
YDL101C	YNL144C			
YDR022C	YNL058C			
YDR043C	YOL136C			
YDR256C	YOR058C			
YDR263C	YPL112C			
YDR374C	YLR438W			
YER044C-A	YNL112W			
YFR015C	YGL021W			

YGR067C	YHR160C			
YGR289C	YBR284W			
YHR096C	YLR237W			
YHR153C	YHR005C			
YHR156C	YLR055C			
YHR210C	YHR072W			
YIL160C	YKR058W			
YIL117C	YMR278W			
YIL066C	YPR184W			
YIL057C	YDR368W			
YIL020C	YOR291W			
YIL013C	YIL166C			
YJL153C	YPL121C			
YJR030C	YPR007C			
YJR047C	YPL277C			
YJR150C				
YJR151C				
YKL209C				
YKR005C				
YKR009C				
YLL056C				
YLR058C				
YLR149C				
YLR228C				
YMR006C				
YMR280C				
YNR002C				
YOL104C				
YOR100C				
YPL201C				
YPL017C				
YPR013C				
YPR015C				
YBR021W				
YDL003W				
YDR311W				
YFL052W				
YLR081W				
YOR009W				
YEL039C				
YHR015W				
YNL298W				
YPR028W				
YDL222C				
YBR202W				
YDR272W				
YFL047W				
YGL045W				
YHL028W				
YJR006W				
YJR078W				
YKL045W				
YLR263W				
YMR108W				
YMR144W				
YNL208W				
YNL202W				
YNL102W				
YNR019W				
YOR237W				
YDR522C				
YJL216C				
YOL066C				
YOR028C				

YBR074W				
YJR061W				
YPR192W				
YPR159W				
YPL026C				
YPL021W				
YOR389W				
YOR328W				
YOR255W				
YOL161C				
YNR073C				
YNR071C				
YMR101C				
YLR012C				
YKR102W				
YIR013C				
YGR287C				
YGL251C				
YGL117W				
YGL015C				
YER011W				
YDR501W				
YCL048W				

6.2 List of genes responding in cell-type specific or ISW2 dependent manner

List of genes showing change in nucleosome array regularity in either cell-type specific manner or upon deletion of *ISW2*. Array regularity scores were compared between mat a and α background in WT or cells lacking *Isw2* ATPase. These genes were confirmed manually in genome browser for their predicted change in array regularity.

	WT a	WT α	<i>isw2Δ</i> a	<i>isw2Δ</i> α
<i>ADY2</i>	0.91	0.85	0.73	0.68
<i>AGA2</i>	0.9	0.62	0.77	0.85
<i>BAR1</i>	0.71	0.81	0.55	0.91
<i>CBT1</i>	0.79	0.76	0.39	0.51
<i>DMC1</i>	0.65	0.78	0.8	0.85
<i>GYP8</i>	0.61	0.82	0.78	0.67
<i>HIM1</i>	0.71	0.84	0.91	0.92
<i>KAR4</i>	0.85	0.9	0.66	0.69
<i>LCB3</i>	0.81	0.89	0.76	0.71
<i>LEE1</i>	0.87	0.88	0.85	0.84
<i>MF(ALPHA)1</i>	0.8	0.71	0.84	0.7
<i>MFA1</i>	0.68	0.75	0.66	0.69
<i>NOP6</i>	0.86	0.91	0.63	0.64
<i>PAU20</i>	0.66	0.66	0.58	0.61
<i>PAU5</i>	0.9	0.89	0.4	0.45
<i>POG1</i>	0.84	0.83	0.93	0.88
<i>PRM5</i>	0.86	0.7	0.87	0.86
<i>PRM8</i>	0.53	0.55	0.48	0.41
<i>RIM4</i>	0.93	0.96	0.77	0.66
<i>RRT6</i>	0.91	0.88	0.79	0.73
<i>RSN1</i>	0.79	0.89	0.44	0.6
<i>SAG1</i>	0.9	0.82	0.94	0.8
<i>SCW10</i>	0.82	0.95	0.68	0.68
<i>SKS1</i>	0.69	0.85	0.83	0.91
<i>SNL1</i>	0.41	0.86	0.44	0.5
<i>STE2</i>	0.58	0.94	0.61	0.81
<i>STE3</i>	0.85	0.52	0.83	0.55
<i>STE6</i>	0.7	0.91	0.71	0.87
<i>STL1</i>	0.64	0.8	0.79	0.87
<i>TFB3</i>	0.85	0.88	0.8	0.8
<i>YAP6</i>	0.9	0.83	0.75	0.75
<i>YCR101C</i>	0.73	0.79	0.66	0.55
<i>YFL051C</i>	0.66	0.6	0.92	0.84
<i>YJL218W</i>	0.67	0.89	0.78	0.81
<i>YML131W</i>	0.89	0.92	0.79	0.7
<i>YNL146W</i>	0.4	0.73	0.45	0.65

6.3 List of proteins identified from ISW2-TAP immunoprecipitation

List of proteins identified from Isw2-TAP immunoprecipitation coupled with mass spectrometry in an otherwise WT or *Itc1* lacking cells. Immunoprecipitation was performed under low (150 mM) and high (350 mM) NaCl conditions. Untagged (*Isw2* not TAP-tagged) cells for both WT and *itc1Δ* backgrounds were used as negative controls. Only proteins enriched by 3-fold in the *Isw2*-TAP tagged immunoprecipitation compared to its negative control performed under similar salt concentrations are listed. Experiment was performed only once.

Isw2-TAP 150 mm NaCl	Isw2- TAP 350 mm NaCl	<i>itc1Δ</i> Isw2-TAP 150 mm NaCl	<i>itc1Δ</i> Isw2-TAP 350 mm NaCl	Isw2-TAP 150 mm NaCl	Isw2- TAP 350 mm NaCl	<i>itc1Δ</i> Isw2-TAP 150 mm NaCl	<i>itc1Δ</i> Isw2-TAP 350 mm NaCl
ABF1				CCT3			
ABP1				CCT4	CCT4		
ACC1		ACC1		CCT5		CCT5	
ACO1				CCT6		CCT6	
ACS2				CCT7		CCT7	
ACT1		ACT1		CCT8		CCT8	
ADE3	ADE3			CDC1			
ADE4		ADE4		CDC11	CDC11		
ADE5,7				CDC12			
ADH1		ADH1		CDC19			
AFG2		AFG2		CDC3	CDC3	CDC3	
AHA1	AHA1			CDC33		CDC33	
AHP1				CDC39	CDC39		CDC39
ALA1		ALA1		CDC48			
ALD4				CET1	CET1	CET1	CET1
ALD6	ALD6			CEX1	CEX1	CEX1	
APA1				CFT1			
APE1			APE1	CHC1			
APE3				CHD1		CHD1	
ARB1	ARB1	ARB1		CIC1			
ARC1		ARC1		CKA2			
ARF2	ARF2	ARF2		CLC1			
ARL1		ARL1		CLU1		CLU1	
ARO1		ARO1		COG6	COG6	COG6	
ARO2				COP1		COP1	
ARP4	ARP4			COY1	COY1		COY1
ARP5	ARP5			CPR7	CPR7		
ARP7	ARP7	ARP7		CRM1	CRM1	CRM1	CRM1
ARP8	ARP8			CRN1			
ARP9				CSE1	CSE1	CSE1	CSE1
ARX1				CYC8	CYC8	CYC8	
ASG1	ASG1			CYS4	CYS4		
ASP1	ASP1			DAT1			
ATP1	ATP1			DBP3			
ATP2				DBP5	DBP5	DBP5	
BBC1	BBC1		BBC1	DBP6			
BCY1				DBP8		DBP8	
BFR2				DGP2	DGP2		
BGL2				DED81	DED81		
BMH1		BMH1		DEF1	DEF1		
BRN1	BRN1			DHH1	DHH1	DHH1	
BRO1	BRO1	BRO1		DLD3			
BRX1	BRX1			DLS1	DLS1		
BUR2				DNM1	DNM1	DNM1	
CBF5				DOP1	DOP1	DOP1	DOP1
CCT2				DPB4	DPB4		
DPM1	DPM1	DPM1		HIR2	HIR2	HIR2	HIR2
DSK2				HIR3	HIR3	HIR3	HIR3

Isw2-TAP 150 mm NaCl	Isw2- TAP 350 mm NaCl	<i>itc1Δ</i> Isw2-TAP 150 mm NaCl	<i>itc1Δ</i> Isw2-TAP 350 mm NaCl
DUG2			
DYS1			
EBP2			
ECM29	ECM29	ECM29	ECM29
ECM33			ECM33
EDC3	EDC3		
EDE1			
EFT1			
EIS1	EIS1		EIS1
ELP3		ELP3	
EMP47	EMP47		
ENO2			
ERB1			
ERG1	ERG1	ERG1	
ERG11	ERG11		
ERG26	ERG26	ERG26	
EXG1			
FAA1	FAA1	FAA1	
FAA4	FAA4	FAA4	
FAS1			
FAS2			
FBA1		FBA1	
FET3	FET3	FET3	FET3
FIP1	FIP1		
FKS1			
FOL2		FOL2	
FPR4	FPR4		
FRS1	FRS1		
FUN12			
FUN3	FUN3	FUN3	FUN3
GAS1			
GCD1	GCD1		
GCD11			
GCN1	GCN1	GCN1	
GCN2	GCN2	GCN2	
GDH1			
GET3	GET3	GET3	
GFA1			
GLN4			GLN4
GLO3	GLO3	GLO3	
GLT1			
GND1		GND1	
GPA1	GPA1	GPA1	
GPM1			
GPN2	GPN2		
GPP1			
GSF2	GSF2	GSF2	GSF2
GSP1	GSP1	GSP1	
GSY1			
GSY2			
GUA1	GUA1	GUA1	
GUS1	GUS1		
GVP36			
HAS1			
HCA4	HCA4		
HCR1		HCR1	
HEF3	HEF3	HEF3	
HEK2	HEK2	HEK2	
HEM1			HEM1
HHF1			

Isw2-TAP 150 mm NaCl	Isw2- TAP 350 mm NaCl	<i>itc1Δ</i> Isw2-TAP 150 mm NaCl	<i>itc1Δ</i> Isw2-TAP 350 mm NaCl
HOG1	HOG1	HOG1	
HOM3			
HPC2			
HRP1	HRP1	HRP1	
HSC82			
HSP14	HSP14		
HSP6			
HSP78			
HTA2			
HTB2			
HTS1			
HTZ1	HTZ1		
HXK2		HXK2	
HXT3	HXT3	HXT3	
HXT7	HXT7		
HYP2	HYP2	HYP2	
IDH1	IDH1		
IDH2			
IES1			
IKI3			
ILS1	ILS1	ILS1	
ILV2			
ILV3	ILV3		
ILV6			
IMD3			
IMP4	IMP4		
INO8			INO8
IPI3	IPI3		
IRC22	IRC22		
ISW1			
ISW2	ISW2	ISW2	ISW2
ITC1	ITC1		
IVY1		IVY1	
JSN1			
KAP123	KAP123	KAP123	
KAP14	KAP14	KAP14	
KAP95	KAP95	KAP95	KAP95
KAR2		KAR2	
KEX1	KEX1	KEX1	
KGD1			
KGD2			
KRE33		KRE33	
KRE6	KRE6		
KRI1			
KRS1	KRS1		KRS1
LAT1			
LEO1	LEO1		
LEU1		LEU1	
LOC1			
LOS1	LOS1	LOS1	LOS1
LPD1			
LSG1			
LYS12			
LYS2	LYS2	LYS2	
MAE1			
MCK1	MCK1		
MCM4	MCM4		
MCM5		MCM5	
MCM6	MCM6	MCM6	
MCX1		MCX1	

lsw2-TAP 150 mm NaCl	lsw2-TAP 350 mm NaCl	<i>itc1Δ</i> lsw2-TAP 150 mm NaCl	<i>itc1Δ</i> lsw2-TAP 350 mm NaCl
HHT1	HHT1	HHT1	
HIR1			
MGE1			
MGM11	MGM11		
MIS1			
MKT1	MKT1	MKT1	
MNN9	MNN9		
MOT1		MOT1	
MPM1	MPM1		
MPP1			
MRH1		MRH1	
MRN1		MRN1	
MRP8			
MRPL22		MRPL22	
MRT4			
MSC3	MSC3	MSC3	MSC3
MSC7	MSC7	MSC7	
MSN2			
MSS116		MSS116	
MUM2			
MYO2	MYO2		
NAB6	NAB6	NAB6	
NAM7		NAM7	
NAN1		NAN1	
NAP1			
NFS1			
NHP1			
NIP1	NIP1		
NIP7		NIP7	
NMA1			
NMA111	NMA111		
NMD5	NMD5	NMD5	NMD5
NOC4			
NOG1		NOG1	
NOG2			NOG2
NOP1			
NOP12			
NOP13			
NOP2			
NOP56			
NOP58			
NOP7		NOP7	
NOT3	NOT3		
NOT5			NOT5
NPA3			
NPL3			
NPL6			
NSP1			
NSR1			
NUG1		NUG1	NUG1
NUM1			
NUP188	NUP188	NUP188	NUP188
NUP192	NUP192		
NUP2		NUP2	NUP2
NUP6			
OCA1			
OLA1	OLA1	OLA1	
OLE1	OLE1		
PAA1		PAA1	
PAB1		PAB1	

lsw2-TAP 150 mm NaCl	lsw2-TAP 350 mm NaCl	<i>itc1Δ</i> lsw2-TAP 150 mm NaCl	<i>itc1Δ</i> lsw2-TAP 350 mm NaCl
MDN1	MDN1	MDN1	
MES1	MES1	MES1	
PDI1			
PDR1	PDR1		
PDR5	PDR5	PDR5	
PEP4			
PET9	PET9	PET9	
PFK1			
PFK2	PFK2		
PHO81	PHO81		
PHO86	PHO86	PHO86	
PIL1	PIL1		
PIM1			
PIN4			
PMA1	PMA1	PMA1	PMA1
PMR1	PMR1		
PMT2	PMT2		
PNO1	PNO1	PNO1	PNO1
POB3		POB3	
POL5	POL5	POL5	
POP2	POP2		POP2
PRE9			
PRO1	PRO1	PRO1	
PRO2			
PRO3	PRO3	PRO3	
PRP19	PRP19		
PRP43			
PRS5	PRS5	PRS5	
PRT1	PRT1	PRT1	
PRX1	PRX1		
PSA1		PSA1	
PSO2	PSO2	PSO2	
PST2	PST2	PST2	
PTC2			
PTC3			
PUF4	PUF4	PUF4	
PUF6	PUF6		
PUP2			
PWP1			
PYC2			
RAD51	RAD51	RAD51	
RAP1		RAP1	RAP1
RBG1	RBG1	RBG1	
RET2	RET2	RET2	
RFA2		RFA2	
RHO3	RHO3	RHO3	
RIM1	RIM1		
RIX7	RIX7	RIX7	
RLP24		RLP24	RLP24
RLP7			
RNR1		RNR1	
RPA135	RPA135	RPA135	
RPA19			
RPB2			
RPC34			
RPC4			
RPC82	RPC82		RPC82
RPD3		RPD3	
RPF1	RPF1		RPF1
RPF2		RPF2	

IsW2-TAP 150 mm NaCl	IsW2- TAP 350 mm NaCl	<i>itc1Δ</i> IsW2-TAP 150 mm NaCl	<i>itc1Δ</i> IsW2-TAP 350 mm NaCl
PAN1	PAN1		
PAP1			
PAT1	PAT1		
PDA1			
PDB1		PDB1	
PDC1			
IDH1	IDH1		
RPL21B		RPL21B	
RPL24A	RPL24A		RPL24A
RPL24B		RPL24B	
RPL25		RPL25	
RPL26B			
RPL27A		RPL27A	
RPL28		RPL28	
RPL2B			
RPL2B			
RPL3		RPL3	
RPL3			
RPL31A		RPL31A	
RPL32		RPL32	
RPL33A		RPL33A	
RPL34A			
RPL35B			
RPL36B			
RPL37A			
RPL42B			
RPL43B		RPL43B	
RPL4A			
RPL4B	RPL4B	RPL4B	
RPL4B			
RPL5		RPL5	
RPL6A			
RPL6B			
RPL7A			
RPL7B			
RPL8A		RPL8A	
RPL8B			
RPL9A		RPL9A	
RPN1			
RPN1			
RPN11			
RPN2		RPN2	
RPN3			
RPN5			
RPN6		RPN6	
RPN8			
RPN9			
RPO21	RPO21	RPO21	
RPO31			
RPP			
RPP1B		RPP1B	
RPP2A		RPP2A	
RPP2B			
RPS11B			
RPS12		RPS12	
RPS13			
RPS14A			
RPS15			
RPS16B		RPS16B	
RPS17B		RPS17B	

IsW2-TAP 150 mm NaCl	IsW2- TAP 350 mm NaCl	<i>itc1Δ</i> IsW2-TAP 150 mm NaCl	<i>itc1Δ</i> IsW2-TAP 350 mm NaCl
RPG1	RPG1	RPG1	
RPL1			
RPL11B		RPL11B	
RPL12B			
RPL13A	RPL13A	RPL13A	RPL13A
RPL13B			
RPL21A			
RPS4B			
RPS5		RPS5	RPS5
RPS6B			
RPS7A			
RPS7B			
RPS8B			
RPS9B		RPS9B	
RPSB		RPSB	
RPT1			
RPT2			
RPT3			
RPT4			
RPT5			
RPT6		RPT6	
RRP12	RRP12	RRP12	RRP12
RRP43			
RRP5		RRP5	
RRP9			RRP9
RSC1		RSC1	
RSC2		RSC2	
RSC3	RSC3		
RSC3	RSC3		RSC3
RSC4			
RSC58		RSC58	
RSC6		RSC6	
RSC8		RSC8	
RSC9		RSC9	
RSE1			
RTG2			
RTN1	RTN1		RTN1
RTT16			
RVB1			
RVB2			
RVS167	RVS167		
SAC1			SAC1
SAH1			
SAM1			
SAM2			
SAN1	SAN1		
SAP185		SAP185	SAP185
SAP19	SAP19	SAP19	
SAR1		SAR1	
SBP1			
SCS7	SCS7		
SCW1			
SCW4			
SEC1	SEC1		
SEC13			
SEC16	SEC16	SEC16	
SEC18	SEC18		
SEC21	SEC21	SEC21	
SEC23			
SEC24		SEC24	

Isw2-TAP 150 mm NaCl	Isw2- TAP 350 mm NaCl	<i>itc1Δ</i> Isw2-TAP 150 mm NaCl	<i>itc1Δ</i> Isw2-TAP 350 mm NaCl
RPS19B			
RPS1A		RPS1A	
RPS1B			
RPS2		RPS2	
RPS22B		RPS22B	
RPS23B			
RPS24B			
RPS25A		RPS25A	
RPS26A		RPS26A	
RPS3	RPS3		
RPS3B			
SHM2		SHM2	
SKN7	SKN7		
SKP1		SKP1	
SLA2	SLA2		SLA2
SNF2	SNF2		SNF2
SNF5	SNF5	SNF5	
SNQ2	SNQ2		SNQ2
SNZ2			
SPA2	SPA2	SPA2	
SPC97	SPC97	SPC97	SPC97
SPF1	SPF1	SPF1	SPF1
SPT15	SPT15		SPT15
SPT16			
SPT5	SPT5	SPT5	
SPT6	SPT6		
SRB2		SRB2	
SRB4	SRB4		SRB4
SRO9			
SRP4		SRP4	
SRV2	SRV2		
SSA1			
SSA2			
SSA4	SSA4	SSA4	SSA4
SSB1			
SSB2			
SSC1			
SSD1	SSD1		SSD1
SSE1			
SSE2			
SSO1			
SSQ1	SSQ1		
SSZ1			
STE2	STE2	STE2	STE2
STH1	STH1		
STM1			
SUB2			
SUI2			
SUI3		SUI3	
SUM1		SUM1	
SUN4			
SWC3			
SWI3			SWI3
SWI6			
SXM1	SXM1		SXM1
TAF1			
TAF14			
TAF5	TAF5		
TCB1	TCB1		
TCP1		TCP1	

Isw2-TAP 150 mm NaCl	Isw2- TAP 350 mm NaCl	<i>itc1Δ</i> Isw2-TAP 150 mm NaCl	<i>itc1Δ</i> Isw2-TAP 350 mm NaCl
SEC26	SEC26		
SEC27			
SEC31			
SEC4	SEC4	SEC4	
SEC53		SEC53	
SEC63	SEC63		
SEC7	SEC7	SEC7	
SES1		SES1	SES1
SFH1	SFH1	SFH1	
SGN1			
SHM1		SHM1	
TIF5		TIF5	
TIF6		TIF6	TIF6
TOM1			
TOM22	TOM22		
TOM4	TOM4		
TOM7		TOM7	TOM7
TOP1			
TOP2			
TPD3	TPD3	TPD3	TPD3
TPS1		TPS1	
TRM1		TRM1	
TRP5	TRP5		
TSA1		TSA1	
TSR1			
TUB1		TUB1	
TUB2		TUB2	
TUB3			
TUP1			
TY1B-J	TY1B-J		
TYS1			
UBA1		UBA1	
UBP1	UBP1		UBP1
UBR1		UBR1	
UFD2	UFD2	UFD2	
UFD4	UFD4	UFD4	UFD4
UGP1			
URA2			
URA7			
URB1	URB1		
URE2	URE2		
URK1			
UTP1	UTP1		
UTP13			
UTP15			
UTP21			
UTP6		UTP6	
UTP7			UTP7
UTR1		UTR1	
VAC17			
VAC8	VAC8		
VID27	VID27	VID27	
VMA1			
VMA13	VMA13	VMA13	
VMA2		VMA2	
VMA5			
VMA8	VMA8	VMA8	
VPH1	VPH1	VPH1	
VPS1			
VPS13			

Isw2-TAP 150 mm NaCl	Isw2- TAP 350 mm NaCl	<i>itc1Δ</i> Isw2-TAP 150 mm NaCl	<i>itc1Δ</i> Isw2-TAP 350 mm NaCl
TDH1	TDH1		TDH1
TDH3			
TEF4	TEF4		TEF4
TFC1		TFC1	
TFC3			
TFC4	TFC4		
TFC7		TFC7	
TGL1			
THR1	THR1		
THS1		THS1	
TIF1	TIF1	TIF1	
TIF3			TIF3
TIF34	TIF34	TIF34	
TIF35		TIF35	
TIF463		TIF463	
YNR29		YNR29	
YPK1	YPK1	YPK1	
YPP1			YPP1
YPR89	YPR89		
YPT52	YPT52	YPT52	
YPT7		YPT7	
YRA1			
YTA7			
YTM1			
ZPR1		ZPR1	
	TY1A-J	TY1A-J	
	IPP1		IPP1
	ENO1		
	ILV1	ILV1	
			HSP82
	TEF1		
	DPS1		DPS1
	SUP35	SUP35	
		CDC36	
		SCP16	SCP16
	DED1	DED1	
		SNF1	SNF1
			VAS1
		CAR2	
	MYO1		
	TY1B-M		
	TY1B-P		
	ARF1	ARF1	ARF1
	SST2		
	SUP45	SUP45	
	CPR1		
			STI1
		HSP26	HSP26
			PDX1
		ANB1	ANB1
	SRP54		
		DBP2	
	CHA1	CHA1	
	USO1		
		SYP1	SYP1
	CDC6	CDC6	CDC6
			BUD14
	PSE1	PSE1	

Isw2-TAP 150 mm NaCl	Isw2- TAP 350 mm NaCl	<i>itc1Δ</i> Isw2-TAP 150 mm NaCl	<i>itc1Δ</i> Isw2-TAP 350 mm NaCl
VPS72			
VPS74			
VTC4	VTC4		VTC4
WHI3	WHI3		
WRS1	WRS1	WRS1	
WTM1			WTM1
XRN1			
YDJ1			
YEF3	YEF3		
YGR25		YGR25	
YHB1		YHB1	
YHM2	YHM2	YHM2	
YHR2		YHR2	
YKT6	YKT6	YKT6	
YMR226			
		URA8	
	SRP68	SRP68	
	PRS3		
		IMD2	
	RRP3	RRP3	
		VPS29	VPS29
		PIH1	PIH1
		TRM5	
	GGA2	GGA2	
	APE4		
	LSM12		
			EGD2
			SPT8
	SNU13	SNU13	SNU13
	GEA2		
		MXR1	MXR1
			ALD5
			AIM9
		PEA2	
	NDE1		
	PRE5		
	RFC2		
	NUP159		NUP159
		RPL33B	
	GPD2	GPD2	
			YPI1
	LSB3	LSB3	
			MTR4
		BNA1	
		RNR4	RNR4
		IMD4	
	NUT1		
	PBP1		
	YAP18		YAP18
			YNL247
	NAF1	NAF1	
	SDH1	SDH1	
		RPA49	RPA49
	UBP3		
		MAP1	
		TBF1	
	TIM5	TIM5	
			RAT1
		SRP1	SRP1

Isw2-TAP 150 mm NaCl	Isw2- TAP 350 mm NaCl	<i>itc1Δ</i> Isw2-TAP 150 mm NaCl	<i>itc1Δ</i> Isw2-TAP 350 mm NaCl
	ARO4	ARO4	
			EFB1
		SUA5	
	PUB1	PUB1	
		SEC17	
	GDA1	GDA1	
	KAP122	KAP122	
		NRP1	
			SLA1
	NGR1	NGR1	
	SMY2		
			NIC96
	MDJ1	MDJ1	
		GCS1	
	NUP133		
	GRS1	GRS1	
	NCL1	NCL1	
	YGP1		

Isw2-TAP 150 mm NaCl	Isw2- TAP 350 mm NaCl	<i>itc1Δ</i> Isw2-TAP 150 mm NaCl	<i>itc1Δ</i> Isw2-TAP 350 mm NaCl
		DIG1	
	TY1B-E		
		OYE2	OYE2
	TCB3	TCB3	
	GRX3	GRX3	
	TY1A-G	TY1A-G	
		HMO1	HMO1
			YDR341
			SVF1
	GLO2		
			ADE13
	VAC14	VAC14	
	PBP4		
	PUF3		
			LCL2
	VTS1		
	NEW1	NEW1	
		LYS21	LYS21
	SMT3		

6.4 List of plasmids with galactose-inducible promoters

List of plasmids obtained from Dr. Hal Alper lab. These plasmids are a collection of galactose-inducible hybrid promoters which induces expression of a downstream gene in the presence of galactose (Blazeck et al., 2012). Plasmids are labeled as P1 to P16 in increasing order of expression of a yECitrine gene in synthetic media with galactose as a carbon source.

Plasmid number	Promoter name
P1	Gal4pBS2 - Pleum
P2	Gal4pBS1 - Pleum
P3	Gal4pBS12 - Pleum
P4	Gal4pBS24 - Pleum
P5	UASgal - CU2 - Pcyc
P6	Gal4pBS4 - Pleum
P7	Gal4pBS3 - Pleum
P8	UASgal - CU1 - Pcyc
P9	Gal4pBS13 - Pleum
P10	UASgal - Pcyc
P11	UASgal - A9 - Pcyc
P12	Gal4pBS34 - Pleum
P13	Gal4pBS134 - Pleum
P14	UASgal - Pleum
P15	Pgal
P16	UASgal - Pgal

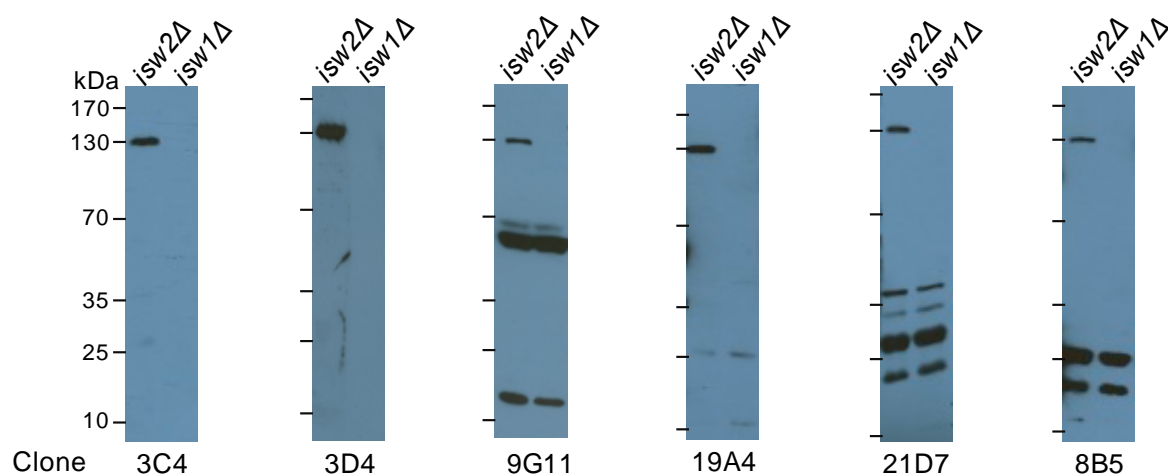
6.5 List of antibodies generated against Isw1.

List of peptides used for generating antibodies against Isw1 and Isw2.

Antigen	Peptide sequence
Isw1-A	SSESTEEDQDKI
Isw1-B	QNRTSLKKKENKADSK
Isw1-C	PHDPESNKKRY
Isw2-A	EWFEQNNSEQDQ
Isw2-B	AIDEYNKPNSEK
Isw2-C	STLDNWRREFLKWTP
Isw2-D	KKGEQKTQELNAKYQ

No specific antibody was found against Isw2. Here is the list of antibodies generated against Isw1.

Antigen	Clone	Species	Specificity	Comments
Isw1-B	3C4	Rat	Isw1	High specificity to Isw1 (used further)
Isw1-A	3D4	Rat	Isw1	High specificity to Isw1
Isw1-A	9G11	Rat	Isw1	Cross-reacts with low molecular weight proteins
Isw1-C	19A4	Rat	Isw1	High specificity to Isw1
Isw1-C	21D7	Rat	Isw1	Cross-reacts with low molecular weight proteins
Isw1-C	8B5	Rat	Isw1	Cross-reacts with low molecular weight proteins



Antibodies were tested against whole cell extracts from cells lacking either Isw1 or Isw2 to test their specificity against two highly similar ATPases. An Isw1 specific antibody shows signal only in Isw2 lacking cells and no signal in Isw1 lacking cells. The predicted molecular weight of the Isw1 ATPase is 131.09 kDa and of the Isw2 ATPase is 130.31 kDa.

7. ACKNOWLEDGEMENTS

First of all, I would like to express my sincere gratitude to my direct supervisor and mentor Prof. Dr. Felix Mueller-Planitz. My time in your laboratory has been an enriching experience both as a scientist and as a person. I am deeply grateful to your valuable guidance, advice, patience, open door and lots of freedom in the lab. You allow young researchers to grow and develop their own questions while challenging their results which has immensely helped to grow as a scientist. I am sure you will be a great influence for my future science and beyond. Thank you very much for the training and lots of fun!

I wish to thank my “Doktorvater” Prof. Dr. Peter B. Becker for agreeing to supervise my thesis, feedback and valuable discussions during my PhD. Moreover, I am grateful to Peter for the excellent environment that you have established in the department. This thesis would not be possible without the support I received at various points from the department. Thanks for the great time and constant support.

Next, I would like to thank my thesis advisory committee, Prof. Dr. Peter B. Becker, PD Dr. Philipp Korber and Dr. Sandro Baldi for their valuable discussions and feedback. I am especially grateful to Philipp and his lab for their immense help and constantly sharing their yeast expertise throughout my time in the department.

I would also like to thank Dr. Tamas Schauer and Dr. Tobias Straub for their help with computational analysis. Tamas has been a constant support and a fruitful collaborator with my projects and bioinformatics analyses. Thank you very much for lots of advice and discussions!

I wish to acknowledge all members of the “Remodeler meeting” for their interest and feedback about my projects. I’m especially grateful to Prof. Dr. Michaela M. Smolle and Dr. Christoph Kurat for their constant help and discussions. I also extend my thank to Dr. Sigurd Braun and Dr. Boris Pfander for sharing equipment, yeast strains and valuable advice.

Next, I would like to thank all present and past members of the Müller-Planitz lab, Johanna, Nadine, Sabrina, Petra, Daan and Kripi for help and discussions. You guys provided a fun and creative atmosphere in the lab which made my time much more pleasant. Special thanks to Petra for amazing discussions for about everything, valuable input from a different perspective and being there in moments of despair. I also thank Silvia Härtel and Madhura Khare for technical support. Thank you for preparing thousands of liters of media!

I’m also grateful to the Molecular biology department, especially Dhawal, Ramona, Stephi, Priyanka and Shibo for their help and discussions in and outside the lab. I’d also like to thank secretaries Edith Müller and Carolin Brieger for their help.

I had a great time working with talented HiWi, Master internship and thesis students, Tea Babushuku, Sarah Schaefer, Arun Kumar Sundaramurthy and Lena Pfaller. It was a great learning experience working with you all. Special thank goes to Lena Pfaller for contributing to the main story. I am also grateful to Jessica Fürtmeir for translating my thesis abstract.

I'd also like to thank my friends in Germany and India, Aditya, Devesh, Annie, Varsha, Ankur and Paras. Thank you very much for always being there when I needed a friend. This would not have been possible without your support!

I am also grateful to the IRTG SFB1064 and Dr. Elizabeth Schroeder-Reiter for coordinating a fantastic graduate program and for support during my PhD.

I also wish to acknowledge the DAAD for funding my PhD studies.

Last but not the least, I would like to express my gratitude to my family who have always supported me and for their unconditional love.